Data reconciliation for mineral and metallurgical processes – Contributions to uncertainty tuning and dynamic balancing – Application to control and optimization

Thèse

Amir Vasebi

Doctorat en génie électrique
Philosophiae Doctor (Ph.D.)

Québec, Canada

Résumé

Pour avoir un fonctionnement de l'usine sûr et bénéfique, des données précises et fiables sont nécessaires. D'une manière générale, une information précise mène à de meilleures décisions et, par conséquent, de meilleures actions pour aboutir aux objectifs visés. Dans un environnement industriel, les données souffrent de nombreux problèmes comme les erreurs de mesures (autant aléatoires que systématiques), l'absence de mesure de variables clés du procédé, ainsi que le manque de consistance entre les données et le modèle du procédé. Pour améliorer la performance de l'usine et maximiser les profits, des données et des informations de qualité doivent être appliquées à l'ensemble du contrôle de l'usine, ainsi qu'aux stratégies de gestion et d'affaires. Comme solution, la réconciliation de données est une technique de filtrage qui réduit l'impact des erreurs aléatoires, produit des estimations cohérentes avec un modèle de procédé, et donne également la possibilité d'estimer les variables non mesurées.

Le but de ce projet de recherche est de traiter des questions liées au développement, la mise en œuvre et l'application des observateurs de réconciliation de données pour les industries minéralurgiques et métallurgiques. Cette thèse explique d'abord l'importance de régler correctement les propriétés statistiques des incertitudes de modélisation et de mesure pour la réconciliation en régime permanent des données d'usine. Ensuite, elle illustre la façon dont les logiciels commerciaux de réconciliation de données à l'état statique peuvent être adaptés pour faire face à la dynamique des procédés. La thèse propose aussi un nouvel observateur de réconciliation dynamique de données basé sur un sous-modèle de conservation de la masse impliquant la fonction d'autocovariance des défauts d'équilibrage aux nœuds du graphe de l'usine. Pour permettre la mise en œuvre d'un filtre de Kalman pour la réconciliation de données dynamiques, ce travail propose une procédure pour obtenir un modèle causal simple pour un circuit de flottation. Un simulateur dynamique basé sur le bilan de masse du circuit de flottation est développé pour tester des observateurs de réconciliation de données et des stratégies de contrôle automatique. La dernière partie de la thèse évalue la valeur économique des outils de réconciliation de données pour deux

applications spécifiques: une d'optimisation en temps réel et l’autre de commande automatique, couplées avec la réconciliation de données.

En résumé, cette recherche révèle que les observateurs de réconciliation de données, avec des modèles de procédé appropriés et des matrices d'incertitude correctement réglées, peuvent améliorer la performance de l'usine en boucle ouverte et en boucle fermée par l'estimation des variables mesurées et non mesurées, en atténuant les variations des variables de sortie et des variables manipulées, et par conséquent, en augmentant la rentabilité de l'usine.

Abstract

To have a beneficial and safe plant operation, accurate and reliable plant data is needed. In a general sense, accurate information leads to better decisions and consequently better actions to achieve the planned objectives. In an industrial environment, data suffers from numerous problems like measurement errors (either random or systematic), unmeasured key process variables, and inconsistency between data and process model. To improve the plant performance and maximize profits, high-quality data must be applied to the plant-wide control, management and business strategies. As a solution, data reconciliation is a filtering technique that reduces impacts of random errors, produces estimates coherent with a process model, and also gives the possibility to estimate unmeasured variables.

The aim of this research project is to deal with issues related to development, implementation, and application of data reconciliation observers for the mineral and metallurgical industries. Therefore, the thesis first presents how much it is important to correctly tune the statistical properties of the model and measurement uncertainties for steady-state data reconciliation. Then, it illustrates how steady-state data reconciliation commercial software packages can be used to deal with process dynamics. Afterward, it proposes a new dynamic data reconciliation observer based on a mass conservation sub-model involving a node imbalance autocovariance function. To support the implementation of Kalman filter for dynamic data reconciliation, a procedure to obtain a simple causal model for a flotation circuit is also proposed. Then a mass balance based dynamic simulator of froth flotation circuit is presented for designing and testing data reconciliation observers and process control schemes. As the last part of the thesis, to show the economic value of data reconciliation, two advanced process control and real-time optimization schemes are developed and coupled with data reconciliation.

In summary, the study reveals that data reconciliation observers with appropriate process models and correctly tuned uncertainty matrices can improve the open and closed loop performance of the plant by estimating the measured and unmeasured process variables, increasing data and model coherency, attenuating the variations in the output and manipulated variables, and consequently increasing the plant profitability.

Table of Contents

List of Tables

List of Figures

Acknowledgements

I would like to express my deepest appreciation and thanks to my advisors Professors Éric Poulin and Daniel Hodouin, for their excellent supervision and priceless guidance during all stages of my work. I would like to thank you for your endless supports and encouragements during these past five years. Working with you was a great honor and experience for me, and I will never forget it.

Moreover, I would like to thank jury members, Dr. Daniel Sbarbaro, Dr. André Desbiens, and Dr. Claude Bazin, for their valuable time that they spent for reviewing my thesis and for their professional comments and insightful guidance. I would also like to thank Dr. Luc Lachance for his professional supports during my Ph.D. project.

A special thanks to my family. Words cannot express how grateful I am to my parents, Gholam and Heshmat, my brothers, Amirabbas and Saeed, and my sister, Mina, for all of the sacrifices that you have made on my behalf. Your supports have been invaluable, and I owe you forever.

I am also very thankful to my great friends and my office mates especially Dr. Massoud Ghasemzadeh-Barvarz, Dr. Ali Vazirizadeh, Alberto Riquelme Diaz, Yanick Beaudoin, Mona Roshani, Mousa Javidani, Mahdi Amiriyan, Asria Afshar Taromi, Ali Shamsaddinlou, Dr. Amir Ghasdi, Saghar Tahmasbi, and Parnian Oktaie for their academic advices and personal supports.

Finally, I would like to express my appreciation to my friend and beloved wife Asra for her patience and kindness. She has always supported me emotionally and mentally when I get stuck or need reclusion. Without her, this project would never have been accomplished.

I dedicate this thesis to my wife and my family.

Foreword

This thesis consists of 9 chapters and two appendices. The first chapter provides a general introduction to data reconciliation techniques, applications, issues, and objective of the study. In Chapter 2, the necessary background to understand and apply the data reconciliation techniques is presented. Chapters 3 to 6 are based on published or submitted articles in international scientific journals and conferences. Chapter 7 presents phenomena based simulator development of flotation circuits. In Chapter 8, value of data reconciliation coupled with advanced process control and real-time optimization schemes are investigated. Chapter 9 contains thesis conclusions and recommendations for future works.

Chapter 3:

Chapter 3 presents the importance of correctly tuning of the statistical properties of the modeling and measurement uncertainties in steady-state data reconciliation. It reveals that neglecting the covariance terms, which is a common industrial practice, and also incorrect tuning of variance terms of the uncertainties matrices can deteriorate the observer performance. In this chapter, using five case-studies taken from mineral and metallurgical industries, the following topics are studied:

- importance of considering the model parameter errors and their correlation terms
- impact of taking into account the correlation of the measurement errors
- importance of involving process dynamic fluctuations in data reconciliation
- linearization of bilinear data reconciliation constraints and correctly tuning of corresponding measurement error covariance matrix
- impact of the variance terms of the uncertainties matrix on data reconciliation performance

This work is presented in:

Amir Vasebi, Éric Poulin & Daniel Hodouin (2014), Selecting proper uncertainty model for steady-state data reconciliation – Application to mineral and metal processing industries. *Minerals Engineering*, 65, p. 130–144.

In this part of the project, I

- reviewed the related literature
- developed simulators for the case-studies in collaboration with my professors
- developed a new technique to calculate the measurement error covariance matrix for bilinear data reconciliation problems
- wrote the necessary MATLAB codes and built Simulink models
- implemented the data reconciliation observers
- defined different simulation scenarios to investigate the effect of uncertainty covariance matrix on the performance of steady-state data reconciliation observer
- analyzed and discussed the results in collaboration with my professors
- wrote the article manuscript in collaboration with my professors

Chapter 4:

Chapter 4 provides several techniques to apply the steady-state data reconciliation commercial software packages for dealing with process dynamics. It proposes three solutions. First, when unit inventories are measured, it is possible to use a sub-optimal implementation of data reconciliation with dynamic mass or energy conservation methods. In the second technique, plant input variables are pre-filtered for synchronizing with other plant variables, in such a way that steady-state reconciliation can be applied. Then, the dynamic process inputs are reconstructed. In the third option, fictitious streams representing the accumulation rate variables (node imbalances) are added to the plant network.

This work is presented in:

Daniel Hodouin, Amir Vasebi & Éric Poulin (2012), How to adequately apply steady-state material or energy balance software to dynamic metallurgical plant data. *IFAC Workshop on Automation in the Mining*, *Mineral and Metal Industries*, Gifu, Japan.

In this chapter, I

- worked on the mathematical development of the solutions in collaboration with my professors
- wrote the necessary MATLAB codes and built Simulink models
- developed simulators for the case-studies
- implemented the data reconciliation observers
- defined different simulation scenarios in collaboration with my professors
- analyzed and discussed the results in collaboration with my professors
- wrote the article manuscript in collaboration with my professors

Chapter 5:

Chapter 5 introduces a new dynamic data reconciliation observer based on a mass conservation sub-model. The observer uses the autocovariance of node imbalances as additional information that improves the estimation precision. For evaluation purpose, two simulated benchmark plants operating in a stationary regime are used, and its performance is compared with classical sub-model based observers and Kalman Filter. The proposed observer provides more precise estimates than steady-state and standard stationary observers, particularly when the process dynamic regime becomes important compared to measurement errors. It exhibits more robust performances against modeling errors compared to Kalman filter. Although Kalman filter leads to optimal performances when perfectly tuned, it is more sensitive to modeling errors than the proposed observer.

This work is presented in:

> Amir Vasebi, Éric Poulin & Daniel Hodouin (2012), Dynamic data reconciliation based on node imbalance autocovariance functions. *Computers and Chemical Engineering*, 43, p. 81–90.

In this study, I

- reviewed the related literature
- carried out the mathematical development of the proposed observer
- developed simulators for the case-studies in collaboration with my professors
- wrote the necessary MATLAB codes and built the Simulink models
- implemented the data reconciliation observer
- defined different tests, simulation scenarios, and performance evaluation indices
- analyzed and discussed the results in collaboration with my professors
- wrote the article manuscript in collaboration with my professors

Chapter 6:

Chapter 6 proposes a procedure to obtain a simple model for a flotation circuit to support the implementation of Kalman filter for dynamic data reconciliation. Using simplifying assumptions, first-order empirical transfer functions obtained from the plant topology, nominal operating conditions, and historical data are used to build the model for Kalman filter. The flotation circuit simulator introduced in Chapter 7 is employed as the case-study. To obtain the model parameters and corresponding uncertainties, practical guidelines are provided. The performance of Kalman filter is compared with two sub-model based observers using the total estimation error variance reduction index and a robustness test. Kalman filter with the empirical model provides more precise estimates than standard and autocovariance based stationary observers. But in the robustness test, sub-model based observers reveal slightly better performance than the implemented Kalman filter.

This work is submitted as:

> Amir Vasebi, Éric Poulin & Daniel Hodouin (2015), Determining a dynamic model for flotation circuits using plant data to implement a Kalman filter for data reconciliation. *Minerals Engineering*, 83, 192-200.

In this chapter, I

- carried out the mathematical development of the modeling error covariance matrix tuning

- proposed guideline to estimate the model parameters and uncertainties using plant data in collaboration with my professors
- wrote the necessary MATLAB codes and built Simulink models
- implemented the data reconciliation observers
- defined different tests, simulation scenarios, and performance evaluation indices
- analyzed and discussed the results in collaboration with my professors
- wrote the article manuscript in collaboration with my professors

Chapter 7:

Chapter 7 develops a dynamic simulator of froth flotation circuit for designing and testing data reconciliation observers and automatic control strategies. This simulator is built based on dynamic mass balance equations and empirical relationships. Collection and froth zones are modeled as the perfect mixer and plug flow reactors. Flotation and entrainment phenomena are considered in the collection zone modeling. Species drainage from the froth zone into the collection zone is also modeled by modifying flotation rate constants. Collector and frother concentrations, collection zone level, and air flowrate are considered as manipulated variables. The performance of a single cell and a flotation circuit are assessed using different test cases and scenarios. The simulator is employed as the case study for data reconciliation observer and advanced controller design in Chapters 6 and 8, respectively.

In this chapter, I

- reviewed the related literature
- carried out the mathematical modeling of the flotation cell in collaboration with my professors
- developed the simulator in MATLAB and Simulink
- defined different tests and simulation scenarios
- tested the simulator performance in collaboration with my professors
- analyzed and discussed the results in collaboration with my professors
- wrote a technical report in collaboration with my professors

Chapter 8:

Two advanced process control and real-time optimization schemes based on receding horizon internal model control are designed in Chapter 8. The aim is coupling dynamic data reconciliation with an advanced controller and a real-time optimizer, and showing its economic value. For this purpose, the flotation circuit simulator developed in Chapter 7 is employed as the benchmark plant. For the advanced controller, a standard quadratic reference tracking objective function is defined while real-time optimizer has an economic based cost function. Then, they are coupled with autocovariance based stationary data reconciliation observer presented in Chapter 5. To assess the effect of involving data reconciliation in closed loop process, several test cases and disturbances are applied. Performance and economic benefits of the advanced control and real-time optimization schemes with and without data reconciliation are investigated using statistical measures and an economic gain function.

In this study, I

- reviewed the related literature
- developed an advanced controller and a real-time optimizer in collaboration with my professors
- applied a mass conserving system identification method to obtain the process model
- developed the necessary MATLAB codes and Simulink models
- implemented and integrated the data reconciliation observer with the plant
- defined different simulation scenarios and tests in collaboration with my professors
- defined the closed loop performance evaluation indices in collaboration with my professors
- tested the closed loop performance in collaboration with my professors
- analyzed and discussed the results in collaboration with my professors
- wrote a technical report in collaboration with my professors

Appendices:

Appendix A provides complementary information about the case-studies used in Chapter 3 while Appendix B presents the mathematical calculations used in Chapter 5 to build the autocovariance based stationary observer.

Chapter 1

Introduction

This chapter first discusses the data reconciliation observers and their effectiveness to improve the accuracy and the reliability of plant data. Issues associated with data reconciliation applications are also presented. Moreover, objectives of this research, original contributions, and a list of publications are given in the following sections.

1.1 Data Reconciliation

Efficient, profitable, and safe plant operations depend on accurate and reliable process data in mineral and metal processing plants. Measurement errors affecting variables such as chemical species concentration and/or particle size distribution are usually important due to sampling errors and material heterogeneity (Gy, 1982). Due costs associated with instrumentation and maintenance and/or technical concerns, direct measurement of such variables using on-line analyzers is faced with many limitations. On the other hand, taking samples with off-line techniques, i.e. laboratory analysis, is also time-consuming and expensive. Therefore, only necessary physicochemical variables and properties are usually measured and evaluated. These issues lead to inconsistency between measurements and process models, and also key properties of the material that are unmeasured.

Data reconciliation is considered as an effective technique to improve the accuracy and reliability of plant data. It is normally formulated as an optimization problem minimizing the measured and estimated variables difference while respecting constraints imposed by the process model. Mass and energy conservation equations are used as process constraints. The technique was first proposed by Kuehn and Davidson (1961) more than fifty years ago. Over time, many improvements and modifications were brought to the technique as

reflected by several reference works (Narasimhan and Jordache, 2000; Romagnoli and Sanchez, 2000; Puigjaner and Heyen, 2006). Data reconciliation has been recently revisited, and interesting mathematical interpretations have been suggested by Mistas (2010) and Maronna and Arcas (2009).

Usually, data reconciliation is coupled with complementary methods that take advantage of improved state estimations. It has been involved in many applications like process monitoring (Martini et al., 2013), plant simulation (Reimers et al., 2008), basic and advanced process control (Bai and Thibault, 2009) or real-time optimization (Manenti et al. 2011). In mineral and metal processing plants, data reconciliation has been widely applied in production accounting, survey analysis, sensor network design and fault detection (Hodouin, 2010; Narasimhan, 2012; Berton and Hodouin, 2003; Berton and Hodouin, 2007).

A wide range of models ranging from simple sub-models like steady-state mass/energy conservation constraints to a complete dynamic causal model has been proposed to handle the plant dynamics for data reconciliation purpose. A model built based on detailed and accurate information about process behavior leads to more precise estimations than those obtained from simple process models. In practice, developing and calibrating such models are demanding tasks. Hodouin (2011) has discussed and presented this point for mineral and metal processing plants.

The simplest approach is to average data to attenuate dynamic variations and apply steady-state data reconciliation (Bagajewicz and Jiang, 2000). Due to its simplicity, this technique is commonly used in numerous industry applications (Bagajewicz, 2010). The approach provides good results when processes have small dynamic variations, but for highly dynamic regimes, estimates could be less precise than measurement themselves (Almasy, 1990; Poulin et al., 2010)

Stationary data reconciliation was proposed by Makni et al. (1995a, 1995b) and Vasebi et al. (2012a) to handle plant dynamics with limited modeling efforts. These techniques consider inventory variations as random variables and rely on the autocovariance function of node imbalances. Other studies have also combined material conservation constraints

with inventory measurements to deal with dynamic variations. These studies can be grouped into two categories: generalized linear dynamic observers (Darouach and Zasadzinski, 1991; Rollins and Devanathan, 1993; Xu and Rong, 2010) and integral linear dynamic observers (Bagajewicz and Jiang, 1997; Tona et al., 2005). However, assuming the availability of inventory measurements is an important limitation. For instance, in the mineral processing industries, measuring of the inventory for a particular species in a separation unit is very difficult or almost impossible.

In the presence of a dynamic causal model of the process, Kalman filter (Kalman, 1960) is largely used to solve dynamic data reconciliation problems (Narasimhan and Jordache, 2000). Approaches inspired by Kalman filter such as the predictor-corrector-based algorithm (Bai et al., 2006) or the generalized Kalman filter (Lachance et al., 2006a) also represent interesting alternatives. However, obtaining the required process models for these algorithms implementation could be difficult and laborious in practice.

In mineral and metal processing industries, data reconciliation is well-established and widely applied. Mass and energy conservation constraints are usually applied as the process model to estimate the underlying steady-state values of process variables. Total material, as well as species flowrates, are estimated leading to bilinear data reconciliation problems. In the Gaussian context, a Maximum-Likelihood estimator is retained. Typically, it is assumed that measurement errors are unbiased and uncorrelated. To characterize the measurement errors, corresponding covariance matrices are often tuned using approximate techniques or trial and error approaches without paying attention to the impacts on the precision of estimated process variables.

1.2 Problem Statement

Data reconciliation is based on a trade-off between modeling effort and estimates precision. In general, model built based on detailed and accurate information of process results in more precise estimations than those that are estimated using the simple description of process models. However, as mentioned before, developing, calibrating, and maintaining such models are challenging tasks in practice (Hodouin, 2011). Using inadequate and inappropriate dynamic models with highly uncertain parameters could also lead to biased

estimates (Dochain, 2003; Özyurt and Pike, 2004). These considerations have often led to the use of simple but reliable sub-models instead of complex and detailed models involving uncertain parameters. The desire of finding a suitable compromise between modeling efforts and estimation performances motivate the development of new observers and development of procedures to obtain appropriate process models used in existing powerful observers like Kalman filter.

Moreover, the performance of data reconciliation observers strongly depends on the covariance matrices used to characterize the model and measurement uncertainties (Bavdekar et al., 2011). In some cases, inappropriate selection can even lead to divergence of the observation algorithm (Willems and Callier, 1992). In steady-state data reconciliation, measurement uncertainties evaluation techniques are generally based on direct methods (that only use measured process variables (Morad et al. 1999)) and indirect methods (which rely on process constraint residuals (Keller et al., 1992; Chen et al., 1997; Darouach, et al., 1989)). A tuning method based on covariance analysis to separate process fluctuations from measurement errors has been proposed by Lachance et al. (2007) for stationary observers. Regarding the evaluation of uncertainties for Kalman filter, several techniques have been introduced in the literature as illustrated by Dunik et al. (2009), Bavdekar et al. (2011), Dunik and Simandl (2008), and Akesson et al. (2008). Determining these covariance matrices is a crucial exercise that has to be carefully addressed to ensure a successful implementation of observers. Besides introducing new tuning techniques, investigation on the effect of uncertainty covariance matrices on the performance of data reconciliation observers is strongly in demand.

High-quality data is essential to make suitable decisions and consequently maximize profits, deal with market changes, and achieve technical objectives. Moreover, to maintain a plant around the optimum point, e.g. for advanced process control, real-time optimization, or plant supervision applications, data quality plays a critical role. Based on the literature, data reconciliation can generally improve the performance of control strategies and real-time optimization by attenuating the measurement noise variance and control action amplitude, estimation of unmeasured variables, updating model parameters, and improving model and data coherency. From an industrial point of view, these improvements can bring

better products quality and more economic revenues. A limited number of papers have coupled data reconciliation with process control (Ramamurthi et al., 1993; Abu-el-zeet et al., 2002; Zhou and Forbes, 2003; Bai et al., 2005a; Bai et al., 2007) and real-time optimization (Naysmith and Douglas, 1995; Zhang and Forbes, 2000; Faber et al., 2006; Hallab, 2010). Most of these studies have evaluated the data reconciliation effectiveness using statistical properties of manipulated and controlled variables, and/or some qualitative measures. They have not investigated the potential economic revenues obtained by applying data reconciliation. Therefore, at least a case-based study is required to reveal how much data reconciliation can be beneficial for a given plant from the economic point of view.

1.3 Objectives of this Work

As reflected by the literature on data reconciliation and as discussed in the problem statement section, there are several issues associated with the development, implementation, and application of data reconciliation observers in practice. To address these points, the aims of this study are:

- Investigating the effect of correctly selecting uncertainty covariance matrices, used for characterizing the modeling and measurement errors, on the data reconciliation performance.
- Developing new dynamic data reconciliation observers based on limited modeling efforts.
- Determining a simple dynamic model for mineral processing plants to support the implementation of a Kalman filter for data reconciliation purpose.
- Developing a simulator of the mineral processing plants for design and test of data reconciliation observers and process control strategies.
- Coupling data reconciliation observers with advanced process control and real-time optimization schemes, and consequently investigating the benefits of using data reconciliation in closed loop plants.

1.4 Original Contributions

Briefly, the main contributions of this thesis are:

- Classification of the data reconciliation observers based on target value estimation: steady-state underlying value versus the true value of variables.
- Proposition of a systematic technique to classify the different source of uncertainties (i.e. modeling errors, process dynamics, and sampling and analysis errors), and also correctly selecting of the uncertainties covariance matrices for steady-state data reconciliation purpose.
- Development of a new technique to calculate the measurement error covariance matrix for bilinear data reconciliation problems, in contrast with existing incorrect practices.
- Proposition of the recommendations and tricks to deal with plant dynamics using the available steady-state data reconciliation software.
- Development of a new stationary data reconciliation observer based on node imbalance autocovariance function.
- Proposition of a procedure to obtain a dynamic empirical model for a flotation circuit based on plant operation and design information for dynamic data reconciliation purpose using Kalman filter.
- Development of the new performance indices for comparing the different data reconciliation observers.
- Development of a phenomenological simulator for a flotation circuit used for design and test of data reconciliation observers and process control schemes.
- Integration of the data reconciliation observers with advanced process control and real-time optimization schemes for illustrating the economic value of using data reconciliation in a simulated flotation plant.

1.5 List of Publications

A list of published and submitted articles in journals and conferences obtained as a result of this research is presented below:

1) Vasebi, A., Poulin, É. & Hodouin, D. (2015), Determining a dynamic model for flotation circuits using plant data to implement a Kalman filter for data reconciliation. *Minerals Engineering*, 83, 192-200.

2) Vasebi, A., Poulin, É. & Hodouin, D. (2014), Selecting proper uncertainty model for steady-state data reconciliation. *Minerals Engineering*, 65, p. 130-144.

3) A Vasebi, A., Poulin, É. & Hodouin, D. (2012), Dynamic data reconciliation in mineral plants. *Annual Reviews in Control*, 36, p. 235-243.

4) Vasebi, A., Poulin, É. & Hodouin, D. (2012), Dynamic Data Reconciliation Based on Node Imbalance Autocovariance Functions. *Computers and Chemical Engineering*, 43, p. 81–90.

5) Vasebi, A., Hodouin, D. & Poulin, É. (2013), The importance of uncertainty covariance tuning for steady-state data reconciliation in mineral and metal processing. *15th IFAC Symposium in MMM*, San Diego, USA.

6) Hodouin, D., Vasebi, A. & Poulin, É. (2012), How to adequately apply steady-state material or energy balance software to dynamic metallurgical plant data. *IFAC MMM 2012*, Gifu, Japan.

7) Vasebi, A., Poulin, É. & Hodouin, D. (2011), Observers for Mass and Energy Balance Calculation in Metallurgical Plants. *18th IFAC World Congress*, Milano, Italy.

8) Vasebi, A., Poulin, É., Hodouin, D. & Desbiens, A. (2015), Coupling dynamic data reconciliation with model predictive control for real-time optimization of a flotation plant simulator. Submitted to XXVIII International Mineral Processing Congress (IMPC 2016), Québec City, Canada.

Chapter 2

Data Reconciliation: Background

This chapter presents the fundamental points that are necessary to understand and apply the data reconciliation techniques. First, accuracy and precision of a measurement are defined based on the different measurement error types. Then, various plant operating regimes are illustrated and discussed. Moreover, the target value of each process variable, i.e. the one that should be estimated by data reconciliation, is clearly stated. Different process models used in the data reconciliation observers, ranging from a simple mass conservation sub-model to a complete causal dynamic model, are also shown in the chapter. Finally, to complete the presentation of process models, measurement equation of the process variables is presented.

2.1 Introduction

Accurate and reliable process data is needed to have an efficient, profitable, and safe plant operation. Plant-wide management and business strategies depend on performance indicators like productivity, material quality and production cost information that combine economic and technical factors. These factors are strictly related to the process variables such as production rate, metal recovery, product grade, and energy consumption. High-quality data is essential to make suitable decisions to maximize profits, deal with market changes, and achieve technical objectives. Moreover, to keep a plant around the optimum point, e.g. for advanced process control, real-time optimization, or plant supervision applications, data quality plays a critical role.

Presence of the random and gross errors in the measurements, infrequent laboratory analyses, and unmeasured strategic variables are the major concerns in most of mineral and metallurgical plants. For these processes, there are many unmeasured flowrates because of technical and economic issues. In contrast, the physical properties and the chemical content of flowing material are analyzed for a large number of streams. However, these analyses are subject to significant measurement errors associated with sampling errors (Pitard, 1993; Holmes, 2004) causing problems for advanced control and optimization applications.

Data reconciliation (DR) is widely applied to improve the reliability and accuracy of data in mineral processing industries. It reduces impacts of random errors by producing estimates coherent with a process model and giving the possibility to estimate the unmeasured variables under favorable observability conditions. For the first time, Kuehn and Davidson (1961) have proposed data reconciliation based on Lagrange multipliers for the steady-state data reconciliation problem. As a proven technique, it has been largely applied to various industrial sectors such as chemical and biochemical processes (Dochain, 2003), pulp and paper industries (Bellec et al., 2007) and mineral and metallurgical processing (Hodouin, 2010). Over the years, many comprehensive books and papers describing fundamental aspects of data reconciliation have been presented (Narasimhan and Jordache, 2000; Romagnoli and Sanchez, 2000; Bagajewicz 2010; Puigjaner and Heyen, 2006; Crowe, 1996; Tamhane and Mah, 1985; Hlavacek, 1977; Mitsas, 2010; Maronna and Arcas, 2009).

For successful implementation of data reconciliation observers, developing a process model is a crucial task. The representation of process model could range from simple noncausal sub-models, e.g. mass conservation constraints, to complete causal dynamic models. In general, more accurate and detailed process model would lead to more precise estimates while using simpler plant description produces less precise estimations. However, in practice, building and calibrating of detailed models is a challenging task (Hodouin, 2011). Updating and maintaining complex models is another point that could be problematic. All these factors have often motivated the use of simple sub-models that have high confidence level rather than complete but uncertain models. The trade-off between estimation performances and modeling efforts has led to different observers regarding the various types of models used to cope with process dynamics.

Plant operating regime is another factor that can affect the development and performance of the observers (Lachance et al., 2006b). Depending on how plant feed varies, the process model and observer structure could be different. Assuming steady-state operating regime, when feed largely fluctuates, could lead to much simpler observers with less precise estimates while developing observers that take into account the feed variations could result in better estimation.

Depending on which part of measured variables should be estimated by data reconciliation, observer design could be different. Each process variable, ignoring the measurement noises, can be represented by two components: a) local/underlying value and b) true value including the underlying value and dynamic variations. Both of these values can be targeted and estimated by data reconciliation observers. Estimation of the underlying value leads to steady-state observers while attempt to estimate the true value is called dynamic DR. Therefore when a data reconciliation observer is developed, the target value should be clearly mentioned.

As the main objective, the points that are necessary to understand and develop data reconciliation observers are presented in this chapter. These concepts are clearly defined for avoiding any confusion in the thesis. Section 2.2 is dedicated to present the various measurement errors, and consequently definition of the measurement accuracy and precision. Then, in Section 2.3, plant operating regimes are illustrated based on the inventory variations. Estimating the averaged underlying value or true dynamic value as the objective of DR is extensively discussed in Section 2.4. Process models applied in DR observers, ranging from a simple mass conservation sub-model to a complete causal dynamic model, are shown in more details in Section 2.5. Finally, to complete the presentation of process models, Section 2.6 provides the measurement equation of the process variables.

2.2 Precision versus Accuracy

Measured data is always affected by errors related to measuring devices. No sensor can be built that is exact and accurate. Also, errors can arise from sampling or sensors positioning caused by the inherent space and time heterogeneity of process variables. About the source of errors in the measurements, a discussion is presented in Chapter 3. Narasimhan and Jordache (2000) have categorized the measurement errors into two main classes:

- Random errors: the random term implies that neither the magnitude nor the sign of the error can be predicted with certainty. In other words, if the measurement is repeated with the same instrument under identical process conditions, different values may be obtained depending on the outcome of the random error. The only possible way that these errors can be characterized is using probability distributions, a property that quantifies measurement precision. These errors can be caused by some different sources such as power supply fluctuations, network transmission and signal conversion noise, changes in ambient conditions, and so on. This error usually corresponds to the high-frequency components of a measured signal and is usually small in magnitude.

- Gross errors, including biases (systematic errors) and outliers, are caused by non-random events such as instrument malfunctioning (due to improper installation of measuring devices), miscalibration, wear or corrosion of sensors, and solid deposits. Therefore, their occurrence and magnitude have not any random distribution. The non-random nature of these errors implies that, at any given time, they have a certain magnitude and sign that are usually unknown.

Based on the presented error classification, the accuracy of a measurement is defined as the closeness to the true value and it includes the effect of both gross and random errors (Miller, 1983). From a mathematical point of view, Mean-Square Error defined as the expected value of the square of the deviation between the estimated and the true value can be a representative for the measurements accuracy. While precision stands for the scattering of samples, i.e. measurements, around the samples mean which could be different from true value. In this sense, standard deviation σ can be an indication of the measurement

precision. The smaller value of σ implies more precision on the measurement and the higher probability that the random error can be close to zero (Benqlilou, 2004). When no bias is present, accuracy and precision are equivalent.

2.3 Plant Operating Regimes

To implement appropriate DR observers, characterization of the process operating regime is an essential factor. The variation of process states mainly depends on the plant dynamics, production rate changes, and the nature of disturbances. Using the node imbalances as a criterion for operating regime classification, four categories could be proposed (Lachance et al., 2006b):

- The steady-state regime: this regime assumes that all process inventories are constant; it implies a zero node imbalance at any time. Based on this definition, flowrates are allowed to fluctuate when equipment related to process nodes have fixed inventories or very fast time response compared to the stream dynamics.
- The stationary operating regime: in practice, a strictly steady-state regime with constant inventory is never met. There are always random or deterministic dynamic variations that can be small or quite significant. The stationary operating regime assumes that, over a long period of time, the process stream properties as well as inventories randomly vary around a constant value with positive and negative values. This operating mode is more realistic than the steady-state regime, and it can be applied to represent a wide range of industrial processes that operate in normal conditions during sufficiently long periods where major deterministic changes do not occur.
- The transient regime: when a process goes from one operating point to another one. On a short time window, to make a distinction between a stationary operating regime and a transient operating condition is a difficult task.
- The quasi-stationary regime: it is a combination of both stationary and transient operating conditions where the stationary intervals are significantly longer than the transient ones. In this mode, the process evolves from one stationary condition to another.

To illustrate the classification, Fig. 2-1 introduces a single node separation unit. The inventory of this process is shown in Fig. 2-2 for different regimes. Local stochastic variations (high frequencies) are mainly caused by input disturbances while trends (low-frequency variations) are the consequences of the deterministic abrupt or slow changes in the input variables. In this thesis, it is assumed that plants always operate in the stationary regime that is a reasonable assumption from the industrial point of view.

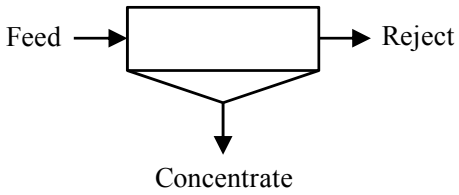

Fig. 2-1: Single node separation unit.

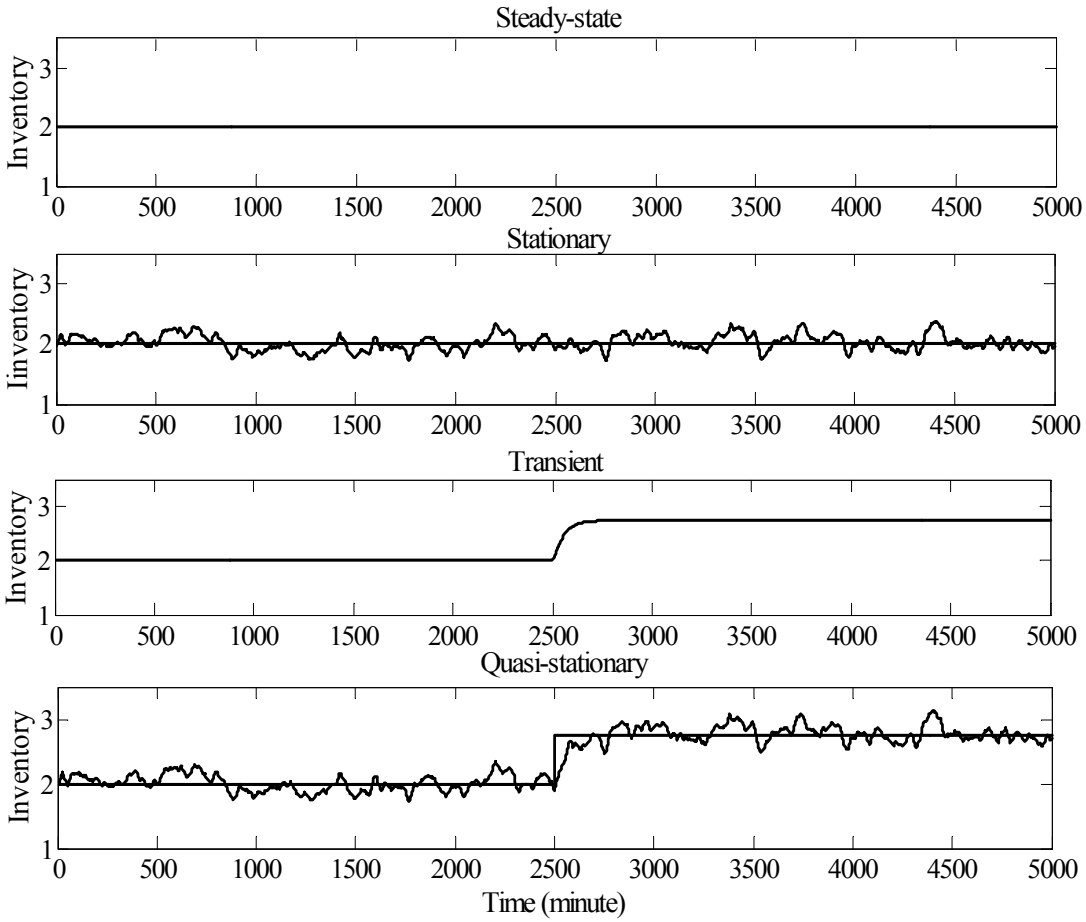

Fig. 2-2: Inventory of a separation unit under different operating regimes (ton).

2.4 Process State Variable versus Steady-State Underlying Value

Feed fluctuations, either random or dynamic, cause dynamic variations in the process states x. Under stationary operating regime assumption, at least for a sufficiently long operating time, each process state x fluctuates around a mean value x_m, therefore allowing to define a dynamic deviation $x_d = x - x_m$ (Fig. 2-3). Defining $\bar{x}_h$ as the averaged value of a process variable x in the time window of h samples, its variation tends to zero when h becomes larger and it has the maximum variance when h=1 . In general, $\bar{x}_h$ does not perfectly obey the steady-state mass or energy conservation law, the deviation becoming smaller for larger h.

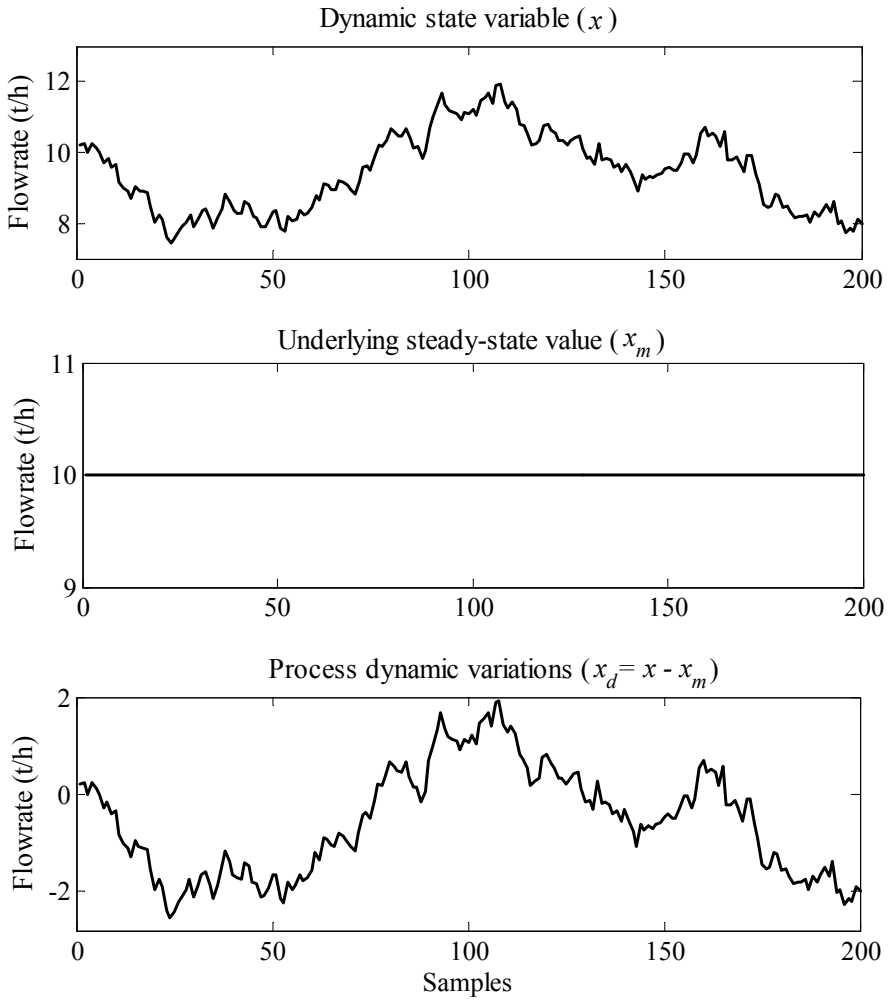

Fig. 2-3: Components of a state variable in stationary regime.

Depending on the application of data reconciliation, x or x_m can be targeted for estimation purpose. For applications like material accounting and auditing, x_m is estimated and the procedure is called steady-state data reconciliation while estimation of the state variable x including mean value and dynamic variations is named dynamic data reconciliation and applied for process control and real-time optimization purposes. When x_m is estimated, data reconciliation observer minimizes the measurement-estimate distance including process dynamic variations x_d and measurement error. In the estimation of x, data reconciliation observer only minimizes the distance induced by measurement error.

In practice, process dynamics are never exactly stationary, and, therefore, the concept of mean x_m estimation is not perfectly adapted to these real situations. It is more convenient to define the steady-state data reconciliation problem as an estimation of a locally underlying steady-state value, i.e. an estimation that exactly satisfies the steady-state mass and energy conservation equations. The current study supposes that the process is locally stationary and Gaussian. Although the process variables may have varying means, assuming fluctuations have reasonably constant variances, Maximum-Likelihood (ML) estimator is used as the optimal choice for data reconciliation purposes in this context. Based on above discussed points, before developing and applying any data reconciliation observer, it should be clearly indicated what is the target value for estimation, i.e. steady-state underlying value or true state variable.

2.5 Process Models

This section reviews most commonly used process models starting with the simple mass conservation sub-model and ending with the complete causal dynamic model. It also presents the unified measurement model associated with the various plant descriptions.

2.5.1 Steady-state conservation model

The simplest model also used by Kuehn and Davidson (1961) is the application of mass and/or energy conservation law in the steady-state situation for data reconciliation purpose. In this context, the process is described through mass and/or energy conservation constraints easily obtained using plant flow sheet. Here, to simplify the presentation, only

mass conservation equations are shown. The model assumes that steady-state mass balance equations are perfectly satisfied at any time, i.e. node imbalances strictly equal to zero. Based on this assumption, the model is expressed by:

$$M\,x(k) = 0 \tag{2-1}$$

where x is the vector of process state variables (e.g. solid and species mass flowrates f), k is the time index, and M is the incidence matrix determined by the plant flow diagram. The elements of each row of M are either +1, -1 or 0, depending on whether the corresponding stream is input, output or not associated with the process unit, respectively. This model is used for processes operating in a near steady-state regime, having limited inventory variations, or in combination with averaged data that attenuates most effects of plant dynamics. When this model is employed for steady-state data reconciliation, i.e. the underlying value is the estimation target value, $x(k)$ should be replaced by x_m in Eq. 2-1.

2.5.2 Stationary conservation model

Despite the attractive simplicity of the steady-state model, when large disturbances happen in the plant feed, because of the plant dynamics, it is no longer representative of the process state variations. In this situation, applying the steady-state model for DR leads to estimates with less precision than measurements (Almasy, 1990). To handle plant dynamics with limited modeling efforts, Makni et al. (1995a) have proposed and applied stationary conservation model. The model supposes that the plant is operating in a stationary mode and it deals with node imbalances as the random variables. Consequently, the mass balance equation is given by:

$$M\,x(k) = \varepsilon(k) \tag{2-2}$$

where ε is a random vector representing node imbalances. They have described the statistical properties of ε using a white noise:

$$\varepsilon(k) \sim N(0, \Sigma_\varepsilon)\ ,\ \mathrm{cov}\{\varepsilon(i), \varepsilon(j)\} = 0 \quad , \quad \forall i \neq j \tag{2-3}$$

Under this assumption, the obtained model is simple but ignores the time correlation of the node imbalances caused by plant dynamics. In Chapter 5, the model is modified so that it takes into account the correlations.

2.5.3 Dynamic conservation model

Another approach to deal with the inventory variations caused by plant dynamics is to directly incorporate the inventory variable in the mass conservation models. This method, named linear dynamic mass conservation model, has been introduced by Darouach and Zasadzinski (1991). Rollins and Devanathan (1993) have proposed improvements to the algorithm to increase computational speed. The method has been also adapted by Xu and Rong (2010) for processes with partial state measurements. The linear dynamic mass conservation concept is expressed by using the inventory variable derivatives. In the discrete time context, the model can be written as:

$$O(k+1) = Mf(k+1) + O(k) \tag{2-4}$$

where O is the selected species inventories divided by the sampling period. To include flowrates f as well as accumulated masses, the vector of states x is defined as:

$$x(k) = \begin{bmatrix} O(k) \\ f(k) \end{bmatrix} \tag{2-5}$$

The model given by Eq. 2-4 can then be rewritten as:

$$-Ex(k+1) + Dx(k) = 0 \tag{2-6}$$

where

$$E = \begin{bmatrix} I & -M \end{bmatrix} \quad , \quad D = \begin{bmatrix} I & 0 \end{bmatrix} \tag{2-7}$$

2.5.4 Complete causal dynamic model

To cope with large process dynamics and feed variations, advanced observers like Kalman filter (Kalman, 1960) need complete causal dynamic models. These models are able to

simulate the process states and outputs from input variables and initial conditions. In practical applications, where a plant operates around steady-state nominal values (i.e. nominal inputs u_n and parameters θ_n), the following linear time invariant approximation can be used:

$$x(k+1) = A(\theta_n)x(k) + B(\theta_n)u_n + w(k) \tag{2-8}$$

where x is the state vector, which may not necessarily represent physical variables of the process. The model coefficients A and B are valid for a local operating regime corresponding to nominal inputs and parameters. Model uncertainties as well as white noise, generating disturbances in the input stream, are included in w. In the present study, it is assumed to obey a normal distribution:

$$w(k) \sim N(0, \Sigma_w) \tag{2-9}$$

Assuming that the plant is operating in stationary regime implies that the states are also randomly distributed:

$$x(k) \sim N(x_n, \Sigma_x) \tag{2-10}$$

where x_n represents the process steady-state nominal value.

It is noticeable that any of the above-mentioned models could be used for data reconciliation purpose regardless of the estimation of target variable x or x_m. However the estimation accuracy is a determinative factor. For example steady-state conservation model can be used for estimation of the true dynamic variable. But it can lead to less accurate estimates than raw measurements especially when the process dynamic variations are larger in comparison with measurement noises.

2.6 Measurement Model

Process models are completed with a measurement equation that indicates which process variables are measured and how they are corrupted by measurement errors. In the linear case, the measurement equation is expressed by:

$$y(k) = Cx(k) + v(k) \tag{2-11}$$

where $y(k)$ and $v(k)$ represent measurements and their corresponding error, respectively. C is a projection matrix that links the model states to the measured process variables. This matrix is useful for complete causal dynamic models where process states may not exactly correspond to physical process variables. In other process models when all states are measured, C is simply an identity matrix. In Eq. 2-11, v is assumed to be a white noise signal with the following characteristics:

$$v(k) \sim N(0, \Sigma_v) \ , \ \mathrm{cov}\{v(i), v(j)\} = 0 \quad , \quad \forall i \neq j \tag{2-12}$$

Measurement error v is assumed to be independent of w and x:

$$\mathrm{cov}\{v(i), w(j)\} = 0 \quad \text{and} \quad \mathrm{cov}\{v(i), x(j)\} = 0 \qquad \forall i, j \tag{2-13}$$

Eq. 2-11 needs slight modification to be applied for estimation of the steady-state underlying value:

$$y(k) = Cx_m + Cx_d(k) + v(k) \tag{2-14}$$

where x_d stands for $x - x_m$. This modification implies that the measurement-estimate distance should contain the process dynamic variations x_d and measurement error v.

2.7 Summary

This chapter has presented the necessary foundations for understanding and using the data reconciliation techniques. It has discussed the accuracy and precision of the measured data based on the various measurement error types. Plant operating regimes have been classified using node imbalance variation of the plant. Estimation target value of process variables has been clearly presented and stated. Different process models applied in data reconciliation observers have also been shown. At the end, the chapter has presented the measurement model used in the data reconciliation observers.

Chapter 3

Selecting Proper Uncertainty Model for Steady-State Data Reconciliation - Application to Mineral and Metal Processing Industries[1]

Résumé

La réconciliation de données est largement appliquée dans les usines de traitement des minéraux et des métaux pour améliorer la qualité de l'information. L'imprécision, le manque de fiabilité et l'incomplétude des mesures sont des problèmes communs qui motivent la mise en œuvre de cette technique. Les pratiques actuelles reposent sur les contraintes de conservation de la masse et de l'énergie pour estimer les valeurs statiques sous-jacentes des variables de procédé. Le contexte est supposé gaussien et un estimateur du maximum de vraisemblance est sélectionné. La performance d'un tel estimateur dépend des matrices de covariance utilisées pour caractériser le modèle et les incertitudes de mesure. Dans la pratique, la détermination de ces matrices de covariance est une tâche difficile qui est souvent négligée. L'utilisation de modèles d'incertitude inappropriés, basés sur des hypothèses simplistes, peut conduire à des sous-performances. L'objectif de ce chapitre est d'illustrer l'impact de la sélection correcte des matrices de covariance des incertitudes à des fins de réconciliation de données pour l'estimation des états permanents sous-jacents. Différentes études de cas impliquant une chambre de combustion, un hydrocyclone, un circuit de flottation, et une unité de séparation sont utilisées pour étudier

[1] Amir Vasebi, Éric Poulin & Daniel Hodouin (2014) Selecting proper uncertainty model for steady-state data reconciliation–Application to mineral and metal processing industries. *Minerals Engineering*, 65, p. 130–144.

la sensibilité de l'algorithme à la structure des matrices de covariance. Un exemple sur la base de simulations de Monte-Carlo est présenté pour évaluer l'importance de l'attribution de valeurs correctes aux termes de la matrice de covariance. Les résultats de simulation montrent que l'ajustement de matrices de covariance a une influence significative sur la précision des estimations et révèlent que certaines pratiques d'optimisation habituelles peuvent avoir des effets néfastes.

Abstract

Data reconciliation is widely applied in mineral and metal processing plants to improve information quality. Imprecision, unreliability and incompleteness of measurements are common problems motivating the implementation of the technique. Current practices rely on mass and energy conservation constraints to estimate the underlying steady-state values of process variables. Typically, the Gaussian context is assumed and a Maximum-Likelihood estimator is selected. The performance of such an estimator depends on the covariance matrices used to characterize model and measurement uncertainties. In practice, determining these covariance matrices is a challenging task that is often overlooked. Using inappropriate uncertainty models, based on simplistic or improper hypotheses, can lead to unexpected underperformances. The objective of this chapter is to illustrate the impact of correctly selecting uncertainty covariance matrices for data reconciliation purpose where steady-state underlying variable states are estimated. Different case-studies involving a combustion chamber, a hydrocyclone, a flotation circuit, and a separation unit are used for investigating the sensitivity of the algorithm to the structure of covariance matrices. An example based on Monte-Carlo simulations is presented to assess the importance of assigning right values to variance terms. Simulation results show that the adjustment of uncertainty covariance matrices has a significant influence on the precision of estimates and reveal that some common tuning practices can have detrimental effects.

3.1 Introduction

Obtaining data of good quality to control critical process variables is a major issue in mineral and metal processing plants. Measurement errors affecting variables such as chemical species concentration or particle size distribution are usually important due to sampling errors and material heterogeneity (Gy, 1982). Direct measurement of such variables with on-line analyzers is also made with parsimony because of instrumentation and maintenance costs or feasibility concerns. Taking samples for laboratory analysis is time-consuming and expensive, so only necessary physicochemical properties are usually evaluated. These issues frequently lead to inconsistent measurements according to process constraints and unmeasured key attributes of the material being processed.

Data reconciliation is an effective method to improve the accuracy and the reliability of plant data. It could be formulated as an optimization problem that minimizes the difference between measured and estimated variables while respecting constraints imposed by the process model. Mass and energy conservation equations are used as process constraints. The technique was introduced more than fifty years ago by Kuehn and Davidson (1961). Over time, many improvements were brought to the technique as reflected by several reference works (Narasimhan and Jordache, 2000; Romagnoli and Sanchez, 2000; Puigjaner and Heyen, 2006). Recently, the method has been revisited, and interesting mathematical interpretations have been suggested by Mistas (2010) and Maronna and Arcas (2009).

Since data reconciliation is not an end in itself, the technique is usually coupled with complementary methods that take advantage of improved state estimations. It can be found in applications like process monitoring (Martini et al., 2013), plant simulation (Reimers et al., 2008), basic and advanced process control (Bai and Thibault, 2009), or real-time optimization (Manenti et al. 2011). In mineral and metal processing plants, data reconciliation plays a central role in production accounting, survey analysis, sensor network design and fault detection (Hodouin, 2010; Narasimhan, 2012). The target use of reconciled data has a strong influence on the model that has to be developed to implement the observer.

A wide range of methods have been proposed to handle plant dynamics. The plant representation could go from simple sub-models like steady-state mass and/or energy conservation constraints to a complete dynamic causal model. In general a model built with detailed and accurate information about the process behavior leads to more accurate estimations than those obtained with a simplified description. However, developing, calibrating, and maintaining such models are demanding tasks in practice. This point has been highlighted for mineral and metal processing plants by Hodouin (2011). Using inadequate dynamic models with highly uncertain parameters could also lead to biased estimates (Dochain, 2003). These considerations have often led to the use of simple but reliable sub-models instead of sophisticated models involving uncertain parameters. The desire of finding a suitable compromise between modeling efforts and estimation performances has motivated the development of different data reconciliation algorithms.

A simple approach consists in averaging data to attenuate dynamic variations and use steady-state data reconciliation (Bagajewicz and Jiang, 2000). This technique is commonly used in numerous industries because of its relatively low complexity. Therefore most data reconciliation software only addresses the steady-steady case (Bagajewicz, 2010). It gives good results when processes present small dynamic variations, but for highly dynamic regimes, estimates could be less precise than measurement themselves as raised by Almasy (1990) and emphasized by Poulin et al. (2010), which is not acceptable from any point of view.

To handle plant dynamics with limited modeling efforts, stationary data reconciliation was proposed by Makni et al. (1995a) and Vasebi et al. (2012a). These algorithms consider inventory variations as random variables and rely on the autocovariance function of node imbalances. Other methods that have combined material conservation constraints with inventory measurements to deal with dynamic variations can be grouped into the categories of generalized linear dynamic observers (Darouach and Zasadzinski, 1991; Rollins and Devanathan, 1993; Xu and Rong, 2010) or integral linear dynamic observers (Bagajewicz and Jiang, 1997; Tona et al., 2005). However, assuming the availability of inventory measurements is an important limitation. For example, in mineral processing, it is almost impossible to measure the inventory of a particular species in a separation unit.

When a complete dynamic causal model of the process is available, Kalman filter (Kalman, 1960) is largely used to solve dynamic data reconciliation problems as illustrated, among others, by Narasimhan and Jordache (2000). Approaches inspired by the Kalman filter such as the predictor-corrector-based algorithm (Bai et al., 2006) or the generalized Kalman filter (Lachance et al., 2006a) also represent interesting alternatives. But obtaining the required models for the implementation of these algorithms in large-scale industrial processes could be difficult and laborious.

The performance of estimators discussed above highly depends on covariance matrices used to characterize model and measurement uncertainties (Bavdekar et al., 2011). Determining these covariance matrices is a crucial exercise that has to be carefully achieved to ensure a successful implementation. In some cases, inappropriate selection can even lead to divergence of the observation algorithm as mentioned by Willems and Callier (1992). For steady-state data reconciliation, measurement uncertainty evaluation techniques are generally gathered into direct methods that only use measured process variables (Morad et al. 1999) or indirect methods which rely on process constraint residuals (Keller et al., 1992; Chen et al., 1997). Other approaches taking advantage of the correlation between process streams are presented by Narasimhan and Shah (2008) and Poulin et al. (2009). For stationary observers, Lachance et al. (2007) have suggested a tuning method based on covariance analysis to separate process fluctuations from measurement errors. Regarding the evaluation of uncertainties for the Kalman filter, the literature is fairly rich as illustrated by Dunik et al. (2009), Bavdekar et al. (2011), Odelson, et al. (2006), and Akesson et al. (2008). Despite the availability of systematic methods for estimating uncertainty covariance matrices, adjustments are frequently carried out by trial and error in the industrial environment, which can impair the benefits of state filtering and estimation.

Data reconciliation is well established in the mineral and metal processing industries. Common practices make use of mass and energy conservation constraints to estimate the underlying steady-state values of process variables. Total material, as well as species flowrates, are estimated which leads to bilinear data reconciliation problems. The hypothesis of Gaussian context is made and a Maximum-Likelihood estimator is retained. Typically, measurement errors are assumed to be unbiased and uncorrelated. Covariance

matrices characterizing measurement errors are often roughly estimated using approximate methods or trial and error approaches without paying attention to the impact they have on the precision of estimated process variables.

The objective of the chapter is to illustrate the effect of correctly selecting uncertainty covariance matrices to characterize modeling and measurement errors. The role of matrix structures and covariance values on the precision of estimates are investigated. The scope is limited to steady-state, linear and bilinear data reconciliation problems to reflect industrial practices because it corresponds to the basic needs of the industry for process performance surveys. Objective of the data reconciliation techniques here is to estimate the steady-state underlying variables states. Analyzes are conducted using various simulated processes: a combustion chamber, a hydrocyclone, a flotation circuit, and a separation unit.

The chapter is organized as follows. Section 3.2 is dedicated to steady-state data reconciliation. The reconciliation problem formulation is reviewed and criteria used for performance assessment are also given. Section 3.3 investigates uncertainty sources and highlights the various ways they affect covariance matrices. Most common methods used to determine covariance matrices are presented in Section 3.4. Finally, Section 3.5 proposes different case studies selected to illustrate the impact of covariance matrices on the performance of steady-state data reconciliation.

3.2 Steady-State Data Reconciliation

Industrial processes are continuously influenced by disturbances and subject to changing operating conditions. A perfect steady-state operation is never reached, and this should be appropriately considered at the data reconciliation stage. The plant operating regimes and the concept of underlying steady-state values have been well addressed in Chapter 2. Here, data reconciliation equations are briefly presented. Evaluation criteria to assess the performance of reconciliation algorithms are suggested. These criteria are used to evaluate the impact of uncertainty covariance matrices for the five case studies presented later. Regarding the definitions presented in Chapter 2, steady-state underlying variables are the target values for estimation in this chapter.

3.2.1 Data reconciliation formulation

The steady-state data reconciliation problem is expressed using constraint equations (process sub-model), measurement equations, and an objective function to be minimized. The process sub-model is written as:

$$f(x_m) = \varepsilon_m \tag{3-1}$$

where f is the set of constraints, x_m represents the state vector of the underlying steady-state variables, and ε_m stands for the modeling error. The latter is assumed to obey a Gaussian statistical distribution:

$$\varepsilon_m \sim N(0, \Sigma_m) \tag{3-2}$$

Eq. 3-1 contains energy and mass balance equations for the whole material and various phases, as well as concentrations of untransformed components or chemical species, and temperatures. It could also contain normalization equations and coherency equations between different variable levels such as total mass and components mass flowrates. In practice, these equations frequently involve flowrates, concentrations, and temperatures.

The measurement equation is formulated as:

$$y = g(x) + v = g(x_m + x_d) + v = g_1(x_m) + g_2(x_d) + v \tag{3-3}$$

where y is the vector of measured variables, g stands for the process observation function, and x is the dynamic state vector at the observation time. In Eq. 3-3, each given measurement y has three components: the underlying steady-state to be estimated $g_1(x_m)$, the uncertainty related to the process dynamic variations $\varepsilon_d = g_2(x_d)$ around x_m, and the measurement error v. g_1 and g_2 are the observation functions corresponding to state underlying value and dynamic variations. For the linear process models which is the case here, $g = g_1 = g_2$. The random measurement error v is assumed to have the following statistical properties:

$$v \sim N(0, \Sigma_v) \tag{3-4}$$

Here, it is assumed that the plant operates in a stationary regime (Lachance et al., 2006b). Therefore, ε_d obeys the following property:

$$\varepsilon_d \sim N(0, \Sigma_d) \tag{3-5}$$

where Σ_d is the covariance of the dynamic fluctuations around x_m. The ML estimator $\hat{x}_m$ is then given, through the minimization of an objective function over the argument x_m, by:

$$\hat{x}_m = \arg \min_{x_m} \left\{ \begin{bmatrix} (y - g_1(x_m)) \\ f(x_m) \end{bmatrix}^T W^{-1} \begin{bmatrix} (y - g_1(x_m)) \\ f(x_m) \end{bmatrix} \right\} \tag{3-6}$$

where W is a weighting matrix. In a Gaussian context, this matrix has the optimal value of:

$$W^* = \mathrm{cov} \begin{pmatrix} \varepsilon_d + v \\ \varepsilon_m \end{pmatrix} \tag{3-7}$$

For steady-steady data reconciliation applications in the mineral and metal processing industries, it is frequently assumed that mass conservation equations are exactly known, and, therefore:

$$\varepsilon_m = 0 \tag{3-8}$$

This assumption is only true when there is no mass leakage or component transformation. This hypothesis could not be valid when more complex models than basic conservation equations are used, especially for energy balance problems. Under this assumption, W only contains covariance terms related to the measurement equation uncertainties. The estimator comes down to:

$$\begin{aligned} \hat{x}_m = \arg \min_{x_m} & \left\{ [y - g_1(x_m)]^T V^{-1} [y - g_1(x_m)] \right\} \\ s.t. \quad & f(x_m) = 0 \end{aligned} \tag{3-9}$$

where

$$V = \mathrm{cov}(\varepsilon_d + v) = \begin{bmatrix} \Sigma_d & \Sigma_{dv} \\ \Sigma_{vd} & \Sigma_v \end{bmatrix} \tag{3-10}$$

and Σ_{dv} represents the covariance between process dynamic fluctuations and measurement errors. Typically, Σ_{dv} is zero for instantaneous sampling. However, in some specific circumstances, the correlation appears and Σ_{dv} should be considered (Hodouin and Ketata, 1994).

The nature of data influences the reconciliation problem. Taking into account total or component flowrates F leads to a 1-level data reconciliation problem. Handling both total mass flowrates (first level variables) and chemical and physical properties of streams z such as species mass fractions, densities, particle sizes, enthalpies, or specific heats (second level variables) generates a 2-level data reconciliation problem. Consequently, the state vector x for 2-level data reconciliation becomes:

$$x_m = \begin{bmatrix} F \\ z \end{bmatrix} \tag{3-11}$$

2-level data reconciliation involves linear conservation equations (conservation of total mass and normalization constraints of mass fractions) and bilinear equations (conservation of minerals or chemical species, conservation of physical properties such as particle size and density, temperature and enthalpy). Considering only total masses brings the problem to linear data reconciliation, while using chemical species and physical properties leads to bilinear data reconciliation where constraints contain cross products of total flowrates and species/properties concentrations. Number of levels could be more than two when a phase is decomposed into sub-phases and sub-phases are analyzed for their compositions (Bellec et al., 2007).

This chapter considers both 1-level linear and 2-level bilinear steady-state data reconciliation problems. The latter one is the most common situation met in the industry. Since the vast majority of commercial data reconciliation software has been designed for 1-level and 2-level data reconciliation, it is frequently proposed to linearize nonlinear and

bilinear problems using the change of variable technique in the literature (Narasimhan and Jordache, 2000). The impact of this approach on uncertainty covariance matrices is illustrated in Section 3.5.4 by a specific case study.

3.2.2 Data reconciliation performance

Different approaches exist to evaluate the performance of an observer. Among others, Poulin et al. (2010) proposed different indices for steady-state data reconciliation. Generally, the performance of the algorithm is expressed in terms of the covariance matrix of the state estimation errors P_x and the measured variables estimation errors P_y defined by:

$$P_x = \mathrm{cov}\left(x_m - \hat{x}_m\right) \tag{3-12}$$

and

$$P_y = \mathrm{cov}\left(g_1(x_m) - g_1(\hat{x}_m)\right) \tag{3-13}$$

where $g_1(x_m)$ is the process observation equation. When all the process state variables are measured, then $P_x = P_y$.

Looking at Eq. 3-6 reveals that estimates and corresponding errors explicitly depend on the weighting matrix W. Obviously, using the exact uncertainty matrix W^* leads to the minimum variance estimates. However, in practice knowing the exact Gaussian behavior of the errors as well as the perfect W tuning is impossible. Therefore, $W \neq W^*$ leads to estimation error covariance values (either P_x or P_y) larger than the optimum theoretical value P^*. The estimation error covariance matrix could be expressed as a function of optimum and applied weighting matrices $P = f(W, W^*)$.

In this chapter, three major aspects are considered for assessing the performance of data reconciliation: the overall uncertainty reduction on the measured variables, the overall state estimation efficiency, and the uncertainty reduction on key process indicators. The first

index evaluates the overall uncertainty reduction on measured process variables y. It compares the estimation error variance of measured variables with the variance induced by both plant dynamics and measurement errors. It is given by:

$$\eta_y = 1 - \frac{\text{trace}(P_y)}{\text{trace}(V)} \tag{3-14}$$

where the "trace" operator stands for summation of the diagonal terms of the covariance matrix, V is the covariance matrix of the measurement equation error including ε_d and v, and P_y is calculated using simulations. The index would be equal to 1 for the fictitious situation of no estimation error. When there is no global variance reduction compared to V, $\eta_y = 0$. A value between 1 and 0 shows the relative improvement brought by the observer while negative values indicate that the observer produces estimates with a larger uncertainty than the measurements themselves.

To assess the efficiency of overall state estimation the following index is proposed (Eldar, 2007; Kay, 1993):

$$\eta_x = \frac{\text{trace}\left(P_x^*\right)}{\text{trace}\left(P_x\right)} \tag{3-15}$$

The index is equal to 1 when the exact uncertainty matrix W^* is used while smaller values mean less precise estimates due to the incorrect description of uncertainties.

Finally, the performance of data reconciliation could be illustrated using key process indicators k calculated using some critical variables expressing the plant performance. The idea consists in comparing the variance of such indicators calculated using raw and reconciled data. Indicators such as mineral species recovery or energy efficiency could be listed as common examples. These performance measures are specific to each plant and are related to production objectives. A general formulation of the index is:

$$\eta_p = 1 - \frac{\sigma^2(\hat{k})}{\sigma^2(k)} \tag{3-16}$$

where $\sigma^2(\hat{k})$ and $\sigma^2(k)$ represent the variances of a given key process indicator k calculated using reconciled and raw data, respectively. The index varies between 0 and 1, larger η_p implies more estimation error variance reduction.

3.3 Uncertainty Sources

As explained above, constraint and measurement equations include uncertainties that are considered through the weighting matrix W of the objective function (Eq. 3-6). Consequently, the data reconciliation performance depends upon the quality of the uncertainty evaluation. They come from various sources and may be systematic, accidental, or randomly distributed around a zero mean. This section investigates the major uncertainty sources while their effects on the reconciliation performance are illustrated in Section 3.5**.** It is worth noticing that the current study only considers random centered normal errors, therefore assuming that systematic and accidental gross errors have previously been detected and corrected, as discussed in Section 3.4 dealing with uncertainty covariance tuning.

3.3.1 Modeling errors

Modeling errors in data reconciliation problems, i.e. uncertainties present in the conservation constraints (Eq. 3-1), may originate from different sources (Hodouin, 2010):

- forgotten or neglected streams in the mass and energy balance network flows (e.g. material leakages or infiltrations, flows due to intermittently activated pumps or valves);
- neglected material transformation reactions;
- inaccuracies in the selection of model parameters (mass or heat transfer coefficients, equilibrium constants, heats of reaction, etc).

One can name a few examples of such model errors induced by neglected phenomena such as heat and gas losses outside the process, water evaporation, solid particle attrition, oxidation of magnetite to hematite, and material overflow. Inaccurate parameters such as

rates of reaction, heat conduction coefficients, and species diffusion coefficients represent common uncertainty sources.

As other errors, they can be systematic or randomly distributed. Modeling errors are frequently systematic, especially when they originate from biased conservation network structures or biased parameter values. They can be randomly distributed, because the dynamic variations of operating conditions may also induce random variations of the model structural coefficients or parameters. While they have been set to constant values by calibration of the model at nominal operating conditions of the plant.

3.3.1 Uncertainty due to process dynamics

As expressed in Eq. 3-3, the first source of randomness in the measured values comes from the fact that no process can strictly operate in a perfect steady-state regime. Due to the dynamic variations of sampled variables, an error ε_d always exists either in the instantaneous or time-averaged measurements. This contribution to the measurement equation error, named integration error, has been extensively studied by Gy (1982), and generalized to multi-stream plant by Hodouin and Ketata (1994). It is valid whether the process variable is numerically sampled (and possibly averaged over a certain time window) or the process variable is measured in a physical sample of the processed material (or possibly in a composite sample accumulated within a given period to attenuate the dynamic contribution to the measurement error and to alleviate the cost of laboratory analytical procedures (Patil, 1995)).

Since measurements at different locations in a plant network are considered, these uncertainties are automatically correlated through the dynamic behavior of the different units (Mirabedini and Hodouin, 1998; Hodouin et al., 1998). Therefore, most of the times, Σ_d is not diagonal, and covariance terms should be considered. For simultaneous instantaneous sampling of input and output streams of a given process, these correlated errors vanish because of pure delays introduced by the process.

3.3.2 Sampling and analysis errors

The second source of randomness in Eq. 3-3 comes from the measurement procedure itself and is represented by v. Several phenomena contribute to this error:

- stream primary sampling;
- fundamental error due to the heterogeneous material structure;
- segregation error due to the spatial distribution of the material properties in the process load to be sampled;
- sample extraction, secondary sampling and sample preparation (drying, grinding, leaching, etc);
- analytical instrument precision;
- miscalibration and ambient conditions;
- raw signal processing;
- data transmission process, etc.

In a real plant, as emphasized by Gy (1982), the sources are many, and their effects should be added up. Depending on the source, this type of error can be systematic or randomly distributed.

In the random error context, the covariance matrix Σ_v is diagonal when all measuring devices are independent (Narasimhan and Jordache, 2000). This is usually the case for total flowrate measurements by in-line instruments. However, concentrations could be measured for various species by the same centralized devices (e.g. sampler and X-ray analyzer). Also, physical properties, such as particle size distributions, could be measured by a single device (e.g. a sieving column or a laser diffraction analyzer). Also, the normalization to a sum of 1 for exhaustive chemical or physical material analysis creates a correlation between data. This point has been illustrated by Bazin and Hodouin (2001) in the case of particle size distribution measurements. These measuring techniques bring correlation between errors for different measured variables and lead to non-diagonal Σ_v.

Measured values of process variables may also contain systematic errors (Narasimhan and Jordache, 2000) caused by non-random events such as:

- loss of water and fines when sampling slurries;
- automatic samplers placed in a segregated material area;
- thermocouples exposed to radiations;
- instrument miscalibration or malfunctioning;
- wear or corrosion of on-line sensors;
- holes in sieving screen, etc.

Accidental gross errors due to either data automatic or manual transmission problems or mistakes in the material sampling or analysis process represent additional sources.

3.4 Determining Covariance Matrices

Data reconciliation for underlying local steady-state estimation requires the determination of uncertainty covariance matrices for both constraint and measurement equations. Typically, the adjustment is performed using a combination of prior process knowledge and experimental data, after the elimination of biased sources of uncertainty. Since tuning methods is a vast topic, that is not the central objective of the present chapter, this section only proposes an overview of most common approaches for characterizing the different uncertainties. Emphasis is rather put on illustrating the impact of covariance matrices on the performance of steady-state data reconciliation through case-studies reflecting industrial practices (Section 3.5).

3.4.1 Prior detection and correction of biases and gross errors

For correct tuning of uncertainty covariance matrices using experimental data, biases must be initially detected and corrected since they do not satisfy assumptions formulated in Eq. 3-4. Several techniques have been proposed for bias detection and compensation before performing data reconciliation (Bagajewicz and Jiang, 1998; Madron, 1985). Statistical analysis of model residuals, calculated by applying measured values to equality constraints of the compressed model, is a valuable approach. A compressed model is obtained through an elimination of the unmeasured variables. The remaining equations are called redundancy equations, and their residuals constitute a parity vector (Berton and Hodouin, 2003) on which the statistical tests could be applied. Posterior statistical analysis of adjustments

brought to the measured variables by reconciliation (i.e. innovation vector) could also be used to detect the presence of systematic biases.

The detection of a systematic or accidental gross error is based on a statistically significant discrepancy between the observed residuals (parity or innovation) and the assumed uncertainty models. For a systematic error, the discrepancy is persistent while, for an accidental gross error, it is not. It must be noted that an anomaly can be detected when the measurement is correct, but the uncertainty model is incorrect. A careful analysis is always recommended in specific cases before deciding whether the process is actually moving to a different state (and, therefore, the model or measurement uncertainty has to be modified) or if there is a true gross error. The problem is usually to correctly locate biases, i.e. pointing out appropriate faulty sensors or model parameters. This is usually a difficult diagnosis task that requires sequential statistical tests and possibly several data sets (Basseville and Nikiforov, 1993).

3.4.2 Covariance of modeling errors

As seen in Section 3.3.1, modeling errors can be difficult to evaluate. They are plant specific and require a careful analysis of either possibly neglected transformations occurring in a process node or neglected small intermittent flows, or parameter uncertainties. This is why, in common industrial practices, modeling error variances are set to zero. This is frequently a reasonable assumption for steady-state data reconciliation based on basic mass conservation constraints. It is sometimes a necessary assumption because commercial reconciliation tools do not consider modeling errors. However, this might be a detrimental assumption, particularly for data reconciliation based on energy conservation equations (as illustrated by the first case-study), and for process models which involve material transformation reactions.

3.4.3 Covariance of measurement uncertainty

Measurement uncertainty, described by Eq. 3-3, can be globally evaluated or decomposed into two contributions: random process dynamics and measurement errors. The simplest method to obtain the covariance matrix is to perform a statistical analysis of historical plant

data (Chen et al., 1997; Almasy and Mah, 1984; Keller et al., 1992). Data embeds both dynamics variations and measurement errors, and this is exactly what is required for underlying steady-state estimation. Obviously, this technique would not be acceptable if the objective were to estimate the true dynamic states for process control purposes, as in dynamic data reconciliation (Bai et al., 2006), or stationary data reconciliation (Vasebi et al., 2012a). For statistical analysis, it is important to select data having a locally stationary behavior with respect to their variances. If variable means seem to be drifting, it is recommended to center the records using moving averages. The width of time window must be selected according to the process time constants as well as time constants related to the reconciled data subsequent application (control, real-time optimization, monitoring, audit, modeling, accountability, etc).

Although this is not compulsory for covariance tuning, it might be informative, for process behavior and measurement error knowledge improvements, to separate dynamic contributions and measurement errors. Techniques such as extraction of the time-uncorrelated part or the high-frequency part of the measured variables could be a useful approach for this separation, as well as signal differencing for eliminating the mean drift.

An alternative to the previous method for characterizing the measurement uncertainty is to systematically analyze the sources described in Sections 3.3.2 and 3.3.3. First, the variations due to process dynamics can be evaluated either by plant modeling using a phenomenological approach (process heat and transport phenomena as well as kinetics of chemical or physical reactions describing transformations occurring at the various plant nodes), or using empirical transfer functions roughly calibrated (with approximate values of gains and time constants deduced from physical understanding of the process nodes dynamic behavior). In both cases, the feed disturbances should be modeled as ARMA or ARIMA random processes used as input variables to the plant simulator. The stochastic models can be obtained from input signal autocovariances or power spectra, after removing the white measurement noise. Afterward, the covariance matrix of the various measured variables can be calculated from Monte-Carlo simulation or directly from the plant state-space model. Then, the measurement error covariance itself can be obtained from the

evaluation of the sampling errors, and the measurement errors of the analytical devices used to measure flowrates or flowing material properties.

3.4.4 Industrial practices

In practice, approaches taken for tuning uncertainty matrices are usually simpler than the above-mentioned approaches (statistical processing of historical data or systematic quantification of uncertainty sources). Covariance terms are ignored and the diagonal elements are usually selected based on a rough evaluation of the measurement accuracies. The assumed quality of the measurement procedure is ranked using discrete values of the relative error standard deviation (e.g. 2.5, 5, 10, or 20%). Dynamic variations are usually ignored. In some cases, the data reconciliation objective function is simply un-weighted, meaning that all errors have the same variance. In other cases, the objective function terms are weighted by the inverse squared value of the measurement value, meaning that all the measured variables have the same relative standard deviation. While the latter practice normalizes the data, the former one is obviously not recommended because variables of the objective function have neither the same units nor the same magnitudes.

3.5 Illustration of the Impact of Covariance Tuning

The impacts of correctly selecting uncertainty covariance matrix structure on steady-state data reconciliation performances are illustrated in the current section. Various plants are simulated using empirical transfer functions or phenomenological models (combustion chamber, hydrocyclone, flotation circuit, and separation unit). Fives case studies are selected to specifically illustrate the following effects:

I. Modeling errors;
II. Correlated measurement error;
III. Dynamic fluctuations;
IV. Linearization by variable change;
V. Overall uncertainty variance magnitudes.

In each case, different tuning strategies are compared using the performance indices proposed in Section 3.2.2.

3.5.1 Case-study I: Modeling error effect

In contrast to mass balance equations, energy conservation equations usually exhibit a larger model uncertainty due to model parameter inaccuracies. A gas burner unit is used to illustrate steady-state data reconciliation with modeling errors in the context of simultaneous mass and energy balances. Combustion chambers are common parts of mineral and metallurgical processes, for instance in drying or conversion processes. Fig. 3-1 depicts the scheme of such a device. This plant has three input streams (fuel gas, pure oxygen, and humid air with respective mass flowrates Q_g, Q_o and Q_a) and one output stream of flowrate Q. The fuel gas contains a mixture of butane and propane where the randomly varying mass fraction of butane in Q_g is expressed by c_b. The input air stream contains oxygen, nitrogen, and water vapor. The water fraction in Q_a frequently varies, and it is expressed by c_h.

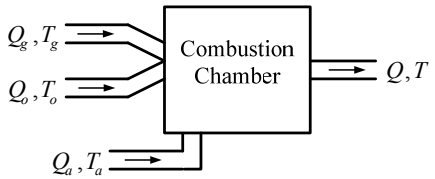

Fig. 3-1: Combustion chamber scheme.

In Fig. 3-1, T_g, T_o, T_a and T stand for input gas, pure oxygen, air, and output gas temperatures. It is assumed that the relative content of oxygen with respect to nitrogen in Q_a is constant. Complete burning reaction is assumed, which implies that the oxygen Q_o is in excess of the required amount for complete gas burning. Therefore, output stream contains vapor, oxygen, nitrogen and carbon dioxide.

For steady-state simulation, the output process variables (flowrates, temperatures, and gas composition) are calculated for a given set of process inputs. Only two input variables c_b and c_h are able to vary. They randomly fluctuate around their nominal values according to a Gaussian distribution law. Their standard deviations are 10% and 30% of c_b and c_h nominal values, respectively.

In this example, balance equations are nonlinear (not bilinear) because of the specific heats dependence on gas compositions and temperatures. Twelve plant process states (four flowrates, four temperatures and four concentrations of output gas) are then supposed to be measured with Gaussian measurement errors that are added to the simulated values. The combustion chamber state vector is:

$$x_m = \left[Q_g \quad Q_o \quad Q_a \quad Q \quad T_g \quad T_o \quad T_a \quad T \quad c_{H2O} \quad c_{O2} \quad c_{N2} \quad c_{CO2}\right]^T \tag{3-17}$$

where c_i is the mass fractions of species *i* at the chamber outlet. Steady-state reconciliation is then performed on the measured data generated by the simulator. For this purpose, the heat and mass balance equations are written under linear and bilinear expressions using the following approximations:

- the specific heats of the species are assumed to be independent of temperature by selecting averaged values in the nominal range of temperature variations;
- the specific heats of the gas mixtures are assumed to be independent of composition variations and tuned for the nominal gas compositions;
- the values of c_b and c_h are set at their nominal values $\overline{c}_b$ and $\overline{c}_h$.

Under these simplifications, the steady-state data reconciliation equations become linear and bilinear, and are presented by using an energy conservation equation:

$$e_1 Q_g + e_2 Q_g T_g + e_3 Q_g T + e_4 Q_g T_o + e_5 Q_a T + e_6 Q_a T_a + e_7 Q_o T_o + e_8 Q_o T = \varepsilon_E \tag{3-18}$$

a total mass balance equation:

$$Q - Q_g - Q_a - Q_o = 0 \tag{3-19}$$

a mass fraction normalization equation:

$$c_{H2O} + c_{O2} + c_{N2} + c_{CO2} = 1 \tag{3-20}$$

and four components conservation equations:

$$c_h Q_a + m_1 Q_g - c_{H2O} Q = \varepsilon_{H2O} \tag{3-21}$$

$$m_2 Q_g - c_{CO2} Q = \varepsilon_{CO2} \tag{3-22}$$

$$m_3 Q_a + Q_o - m_4 Q_g - c_{O2} Q = \varepsilon_{O2} \tag{3-23}$$

$$m_5 Q_a - c_{N2} Q = \varepsilon_{N2} \tag{3-24}$$

In the above equations, e_1 to e_8 and m_1 to m_5 stand for coefficients of energy balance equation (Eq. 3-18) and mass conservation equations (Eqs. 3-21 to 3-24), respectively (see Appendix A.1). Also, ε_E, ε_{H2O}, ε_{CO2}, ε_{O2} and ε_{N2} represent modeling errors ε_m in conservation equations. These uncertainties are induced by simplification and assumptions made for writing the data reconciliation equations. They are correlated Gaussian variables since the variation sources of the simulated data have only two degrees of freedom. In other words, two input variables (c_b and c_h) randomly fluctuate around their nominal value and induce normal stochastic variations on the thirteen parameters of the conservation equations. Because of that, model uncertainties ε_m are strongly correlated. The following matrix illustrates the correlation between model errors:

$$R_{\varepsilon_m} = \begin{array}{c} \begin{matrix} \varepsilon_E & \varepsilon_{H2O} & \varepsilon_{CO2} & \varepsilon_{O2} & \varepsilon_{N2} \end{matrix} \\ \begin{bmatrix} 1.000 & 0.994 & 0.005 & -0.993 & -0.994 \\ 0.994 & 1.000 & -0.012 & -0.997 & -0.997 \\ 0.005 & -0.012 & 1.000 & 0.016 & 0.010 \\ -0.993 & -0.997 & 0.016 & 1.000 & 0.995 \\ -0.994 & -0.996 & 0.010 & 0.995 & 1.000 \end{bmatrix} \end{array} \tag{3-25}$$

Moreover, the measurement error standard deviation is set to 1%, a small value, to only focus on the effects of the modeling error in steady-state data reconciliation.

Three different tuning procedures for steady-state data reconciliation are applied and compared for illustrating the impact of the structure of the model uncertainty matrix:

- *Tuning A*: the process modeling error is assumed to be negligible, in such a way that the measurement noise is the only uncertainty source;

- *Tuning B*: modeling error is considered, but only the diagonal elements of its covariance matrix are used, meaning that the correlation between the modeling errors of the various data reconciliation equations is neglected;
- *Tuning C*: the complete and exact covariance matrix is used.

Simulation results are presented in Table 3-1 using three data reconciliation performance indices: η_y (reduction of error on measured variables), η_x (estimation quality of state variables in comparison to optimal tuning), and η_p (improvement of process performance index calculated using reconciled data rather than raw data). The key metallurgical index *k* used here to calculated η_p (Eq. 3-16) is a burner efficiency index E_b defined as the heat capacity of the chamber output gas per unit mass of consumed fuel gas ($\mathrm{Jg^{-1}K^{-1}}$):

$$E_b = \frac{QC_p}{Q_g} \tag{3-26}$$

where C_p is the gas output heat capacity per unit mass at temperature T, i.e. the sum of the specific heat capacities of the four chemical species weighted by their mass fractions.

According to the results obtained by performance indices from Eqs. 3-14 to 3-16, *Tuning C* (optimal tuning) provides the best estimation of the state variables, as expected since the modeling uncertainty is adequately weighted in the ML estimator. Using modeling errors with the correct variances without consideration to their inherent correlation structure (*Tuning B*), and neglecting the modeling errors (*Tuning A*) are detrimental. The overall uncertainty reduction index η_y for *Tuning B* has a negative value, which implies that data reconciliation deteriorates the estimation compared to the raw measurements. This could not be a general conclusion since it is specific to this case-study where the correlation between modeling errors is quite significant. However in complex industrial plants, the number of mass and energy equations is usually much larger than the number of fluctuation sources in process operating regimes, a situation that brings significant correlation between process variables. Finally, the conclusion is the same for η_p. The data reconciliation

observer tuned with the complete uncertainty matrix more precisely estimates the process performance key variable in comparison with the two other tunings.

Table 3-1: Case-study I: performance indices for various uncertainty matrix tunings.

Indices	*Tuning A*	*Tuning B*	*Tuning C*
η_y	0.190	-0.092	0.297
η_x	0.853	0.610	1.000
η_p	0.832	0.459	0.954

Figs. 3-2 and 3-3 illustrate the variance of estimates for each tuning, variable by variable instead of global presentations (i.e. η_y and η_x). The accuracy of estimates is normalized based on raw data and optimum estimation precisions. In fact, P_{ii}/V_{ii} is the variance ratio of reconciled to the measured value of variable *i*, while P_{ii}^*/P_{ii} represents the variance ratio of optimal to non-optimal estimated value of variable *i.* As seen from Fig. 3-2, both *Tuning A* and *Tuning B* provide estimations that are less precise than raw measurements while *Tuning C* never passes 1.00 line. Fig. 3-3 reveals that except for some variables, *Tuning A* and *Tuning B* show lower estimation performance than *Tuning C*.

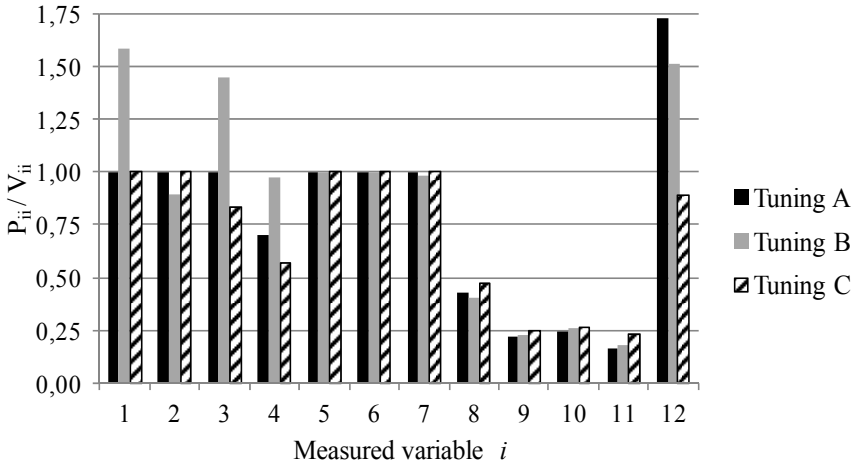

Fig. 3-2: Case-study I: estimates vs. raw measurements.

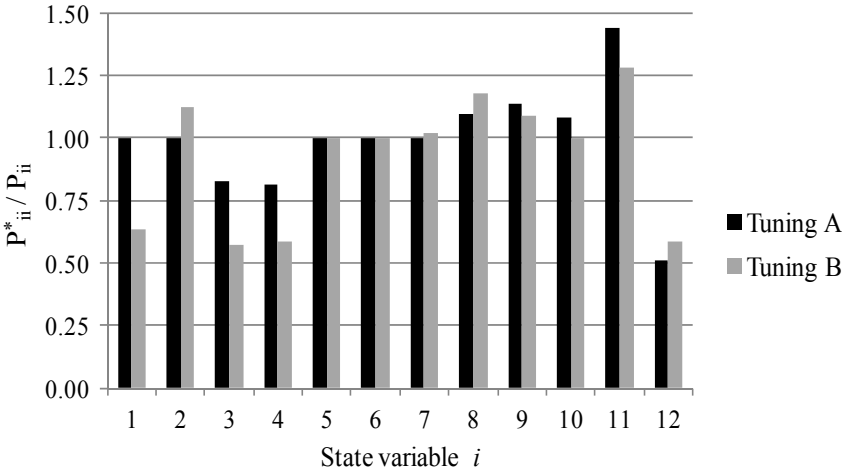

Fig. 3-3: Case-study I: precision of estimated variables vs. optimum estimation.

Based on these simulation results, it could be concluded that taking into account modeling errors improves the accuracy of the state variable estimates. However, neglecting correlation terms between the model parameter errors is severely detrimental.

3.5.2 Case-study II: Correlated measurement error effect

As a second example, a particle size separator (hydrocyclone), where mass fraction measurements are inherently correlated, is selected for illustrating the effect of measurement error correlation in data reconciliation performance. The process has one feed stream and two output streams, underflow and overflow (Fig. 3-4). It is assumed that the hydrocyclone operates in a given constant steady-state regime and measurement noise is the only source of uncertainty. The hydrocyclone behavior is characterized by the separation coefficients (SC) of five size classes (fraction of feed class directed to underflow stream), and the particle size distributions (PSD) are measured by sieving. The nominal value of mass fractions retained on the sieves and SC values are given in Table 3-2. Besides mass fractions of PSD, which are measured, total mass split factor d is an unmeasured state variable that should be estimated by the reconciliation procedure. Therefore the data reconciliation constraints are bilinear and expressed by:

$$f_i - d u_i - (1-d) o_i = 0 \qquad i = 1, \ldots, n \tag{3-27}$$

where f, u and o are the particle size mass fractions, and n stands for the number of particle size classes. i represents the particle size class index.

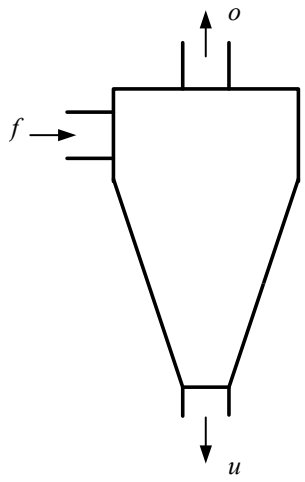

Fig. 3-4: Hydrocyclone scheme.

Table 3-2: Case-study II: feed PSD and SC.

Tyler Mesh	Feed PSD (%)	SC
48	4.64	0.90
100	19.07	0.75
200	24.31	0.60
400	18.01	0.30
-400	33.97	0.15

Repetitive measurements of the 15 state variables (five mass fractions in each stream) are simulated using the following procedure:

- extraction of three samples of constant masses from the three streams;
- sieving of the three samples, with stochastic variations of material retained on the sieves at constant total mass, equal to sample initial value (i.e. no loss of material during sieving).

- weighing of the masses retained on the four sieves and the pan with the addition of a random error;
- calculation of the measured PSDs (i.e. *f*, *o* and *u* mass fractions);
- and data reconciliation.

In this case study, the process state vector consists of:

$$x_m = [f_1 \quad f_2 \quad f_3 \quad f_4 \quad f_5 \quad u_1 \quad u_2 \quad u_3 \quad u_4 \quad u_5 \quad o_1 \quad o_2 \quad o_3 \quad o_4 \quad o_5 \quad d]^T \tag{3-28}$$

Correlation in measurements is generated by two main phenomena: the nature of sieving procedure that brings correlation in the measured masses on the sieve and PSD calculation formula that relates different mass fractions to each other. Therefore, a significant correlation among some measurements is generated (see Appendix A.2). The matrix is dominantly tri-diagonal since the sieving errors are dominant compared to the mass measurement errors of the material retained on the sieve. The correlation between two adjacent sieves is major because obviously missing material on one sieve was retained in the above sieve.

Beside Eq. 3-27, normalization equations could be applied as additional equations to the data reconciliation mass conservation equations. They are:

$$\sum_{i=1}^{n} f_i = \sum_{i=1}^{n} u_i = \sum_{i=1}^{n} o_i = 1 \tag{3-29}$$

For simulation purpose, two data reconciliation scenarios are considered:

- Scenario 1: only Eq. 3-27 is applied as the constraint in data reconciliation;
- Scenario 2: Eq. 3-27 is combined with the normalization constraints of Eq. 3-29.

Two measurement error covariance matrix tunings are defined:

- *Tuning A*: only diagonal elements of measurement error covariance matrix are used;
- *Tuning B*: complete covariance matrix is applied.

Table 3-3 gives the performance indices for the reconciled PSD, and also the standard deviation of estimated mass split factor $\sigma(\hat{d})$. The quality of the reconciled estimates using

the complete matrix tuning is clearly better. Moreover, when *Tuning B* is used, the mass fraction normalization constraint (Eq. 3-29) is not compulsory since the weighting matrix structure warrants it is obeyed. This point shows that even small correlation terms outside the tri-diagonal part of the matrix has a structuring effect on the reconciled data, equivalent to Eq. 3-29. However, as it is impossible to have the exact weighting matrix in practical cases, so Eq. 3-29 must be always applied (Bazin and Hodouin, 2001). Also, smaller standard deviation of $\hat{d}$ for *Tuning B* in both scenarios shows the effectiveness of correctly tuning of the covariance matrix.

Table 3-3: Case-study II: performance indices & standard deviation of estimated *d*.

	Scenario 1		Scenario 2	
Tuning	*A*	*B*	*A*	*B*
η_y	0.346	0.408	0.367	0.408
η_x	0.904	1.000	0.970	1.000
$\sigma_{\hat{d}}$ (%)	8.5	7.5	8.2	7.5

For each variable, the precision of estimates versus measured data is illustrated in Fig. 3-5 for Scenario 2. Moreover, Fig. 3-6 compares the estimate accuracies for the two proposed tunings in Scenario 2. As seen in Fig. 3-5, both tunings bring rather a significant improvement in comparison to raw measurements, and *Tuning B* has slightly better performance (about 3% of η_x). Additionally, to link the reduction of estimation error covariance to improvement in mineral performance indicators, separation coefficients SC for the various size fractions are calculated and used as the metallurgical indices (Table 3-4). Since the hydrocyclone operates in steady-state regime, their mean values are the same for all tunings, but their variances are different. Slightly larger η_p for *Tuning B* suggests the usefulness of applying complete covariance.

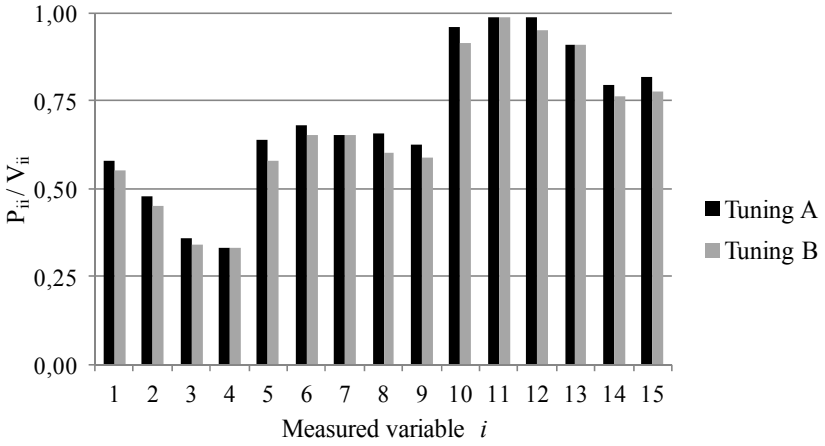

Fig. 3-5: Case-study II: estimates vs. raw measurements (scenario 2).

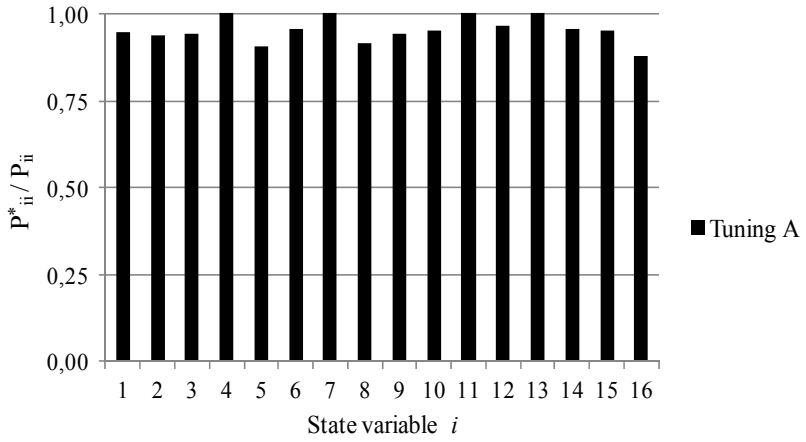

Fig. 3-6: Case-study II: variables estimation precision vs. optimum estimation (scenario 2).

Table 3-4: Case-study II: particle class separation coefficients and the estimation quality indices.

Tyler Mesh	SC	η_p (scenario 1)		η_p (scenario 2)	
		Tuning A	*Tuning B*	*Tuning A*	*Tuning B*
48	0.90	0.98	0.99	0.97	0.99
100	0.75	0.91	0.92	0.91	0.92
200	0.60	0.81	0.83	0.82	0.83
400	0.30	0.50	0.64	0.63	0.64
-400	0.15	0.00	0.00	0.00	0.00

Based on these simulation results, it is concluded that considering the correlation between measured data can improve reconciliation accuracy. Moreover, correlation terms force the data to obey the normalization constraints when they are not considered, therefore they bring some additional information about sampling and measuring procedures that might be not considered in data reconciliation constraints, but still highly recommended.

3.5.3 Case-study III: Dynamic fluctuation effect

The objective of the third example is to illustrate the effect of process dynamic variations on the structure of the error in the measurement equations to estimate the underlying steady-state values by data reconciliation. The flotation plant of Fig. 3-7 is simulated using a dynamic empirical model described by transfer functions and separation coefficients (Vasebi et al., 2012b). The feed stream contains two mineral species, pyrite and chalcopyrite bearing Fe, Cu, and gangue. The plant is assumed to operate in stationary conditions where ore feed rate and composition vary around nominal points. The variance of the measurement noise due to sampling and analysis is perfectly known, and all flowrates and compositions are measured with a relative precision of 5% of corresponding nominal values. The plant feed dynamic fluctuations, responsible for an additional error in the observation equations, are generated using transfer functions driven by Gaussian white noises. The ore feed rate and composition fluctuate with standard deviations equal to 20% and 25% of their nominal values. Moreover, it is assumed that cleaner separation coefficients for both mineral species fluctuate with 1% standard deviation. Here, the process state vector x is composed of ore flowrates f, copper and iron mass fractions:

$$x_m = [f_1, \ \ldots, \ f_8, \ Cu_1, \ \ldots, \ Cu_8, \ Fe_1, \ \ldots, \ Fe_8]^T \tag{3-30}$$

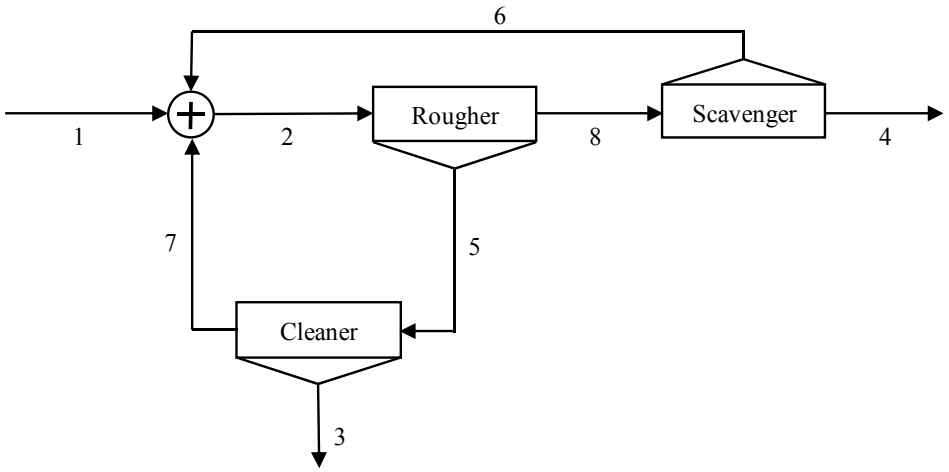

Fig. 3-7: Flotation circuit flow sheet.

The dynamic disturbances of the feed properties and the process parameters generate statistical distributions for 24 states around their nominal values, and these variations are added to the basic measurement errors. Therefore, the variables exhibit variances but also covariances. The below matrix, built for the process variables around the rougher only, illustrates the magnitude of the correlation between variables that include both true dynamic variations and measurement errors:

$$R_{\varepsilon_d+v} = \begin{array}{c} \begin{matrix} f_2 & f_5 & f_8 & Cu_2 & Cu_5 & Cu_8 & Fe_2 & Fe_5 & Fe_8 \end{matrix} \\ \begin{bmatrix} 1.00 & 0.77 & 0.82 & -0.13 & -0.13 & -0.28 & -0.24 & -0.14 & -0.36 \\ 0.77 & 1.00 & 0.85 & -0.04 & -0.04 & -0.10 & -0.10 & -0.14 & -0.24 \\ 0.82 & 0.85 & 1.00 & -0.09 & -0.13 & -0.26 & -0.17 & -0.18 & -0.36 \\ -0.13 & -0.04 & -0.09 & 1.00 & 0.15 & 0.24 & 0.74 & 0.04 & 0.13 \\ -0.13 & -0.04 & -0.13 & 0.15 & 1.00 & 0.43 & 0.12 & 0.12 & 0.25 \\ -0.28 & -0.10 & -0.26 & 0.24 & 0.43 & 1.00 & 0.24 & 0.18 & 0.47 \\ -0.24 & -0.10 & -0.17 & 0.74 & 0.12 & 0.24 & 1.00 & 0.19 & 0.33 \\ -0.14 & -0.14 & -0.18 & 0.04 & 0.12 & 0.18 & 0.19 & 1.00 & 0.40 \\ -0.36 & -0.24 & -0.36 & 0.13 & 0.25 & 0.47 & 0.33 & 0.40 & 1.00 \end{bmatrix} \end{array} \tag{3-31}$$

The following weightings of the reconciliation objective function were tested by simulation:

- *Tuning A*: the process is assumed to operate in truly steady-state, and there is no process dynamics, the only uncertainty source being the uncorrelated measurement noises of variance Σ_v;
- *Tuning B*: the process is assumed to present also dynamic fluctuations, but taking into account only the diagonal elements of the uncertainty covariance matrix;
- *Tuning C*: the complete dynamic uncertainty covariance matrix is considered in addition to the measurement noise variance.

As expected, *Tuning C* provides more precise estimations, i.e. larger η_y and η_x, in comparison to *A* and *B* tunings (Table 3-5). For industrial flotation circuits, recoveries of mineral species are normally used to assess the plant performance. Therefore, the variances of Cu and Fe recoveries calculated from reconciled and measured data in the whole plant and rougher node are used in the calculation of the key variable index η_p. As shown in Table 3-6, variances of mineral recoveries significantly decrease for *Tuning C*. This is obviously due to lower estimation error variances of the reconciled data compared to measured ones, and also to their estimation error covariances induced by the reconciliation procedure (Hodouin and Flament, 1989). Reconciliation with *Tunings A* and *B* lead to negative indices, meaning that reconciliation deteriorates the recovery reliability in comparison to measured data, mainly because of the wrong structure of the covariance matrix. Fig. 3-8 presents the estimation error variances state by state in comparison with raw measured data variance. *Tunings A* and *B* estimate some variables with less precision than raw measurements while optimal tuning estimates are always more accurate than raw data. Fig. 3-9 graphically confirms this observation.

Table 3-5: Case-study III: performance indices for various uncertainty matrix tunings.

Indices	*Tuning A*	*Tuning B*	*Tuning C*
η_y	0.17	0.22	0.31
η_x	0.86	0.89	1.00

Table 3-6: Case-study III: metallurgical performance index calculated using whole plant and rougher recovery (Cu & Fe).

	Species	$\overline{R}$	η_p		
			Tuning A	*Tuning B*	*Tuning C*
Whole plant	Cu	0.95	-0.92	-0.35	0.24
	Fe	0.71	-0.87	-0.52	0.09
Rougher node	Cu	0.77	-0.62	-0.19	0.41
	Fe	0.60	-0.35	-0.07	0.40

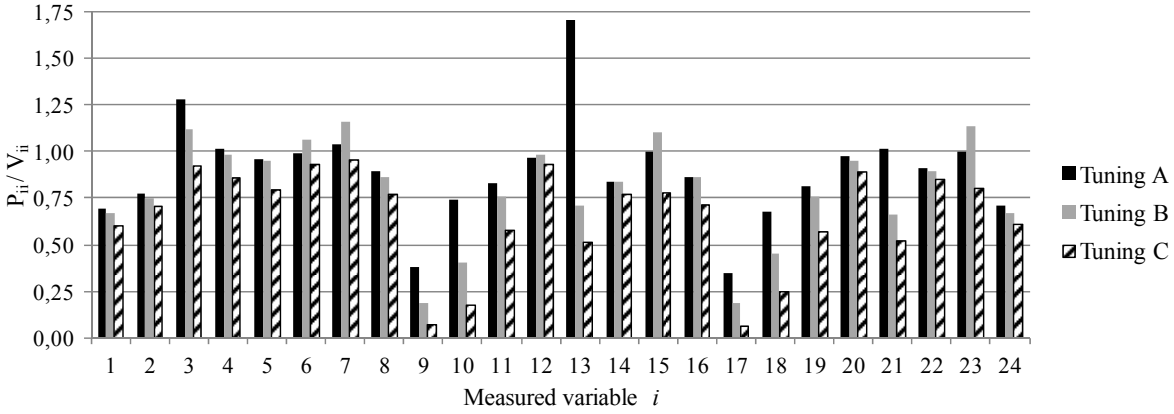

Fig. 3-8: Case-study III: estimates vs. raw measurements.

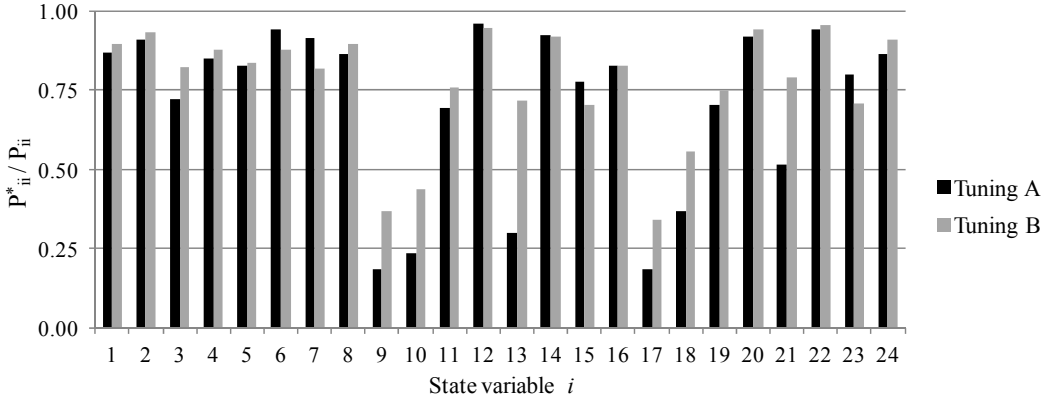

Fig. 3-9: Case-study III: variables estimation precision vs. optimum estimation.

The main conclusion is that neglecting covariance terms induced by process dynamic variations in measurement equation can result in non-optimal and inaccurate estimates. For some process states, the reconciled values could be even less precise than measurements. This problem could become quite serious when performance indices such as mineral species grade or recovery are calculated, because of the amplification of the errors through the calculation process.

3.5.4 Case-study IV: Linearization by variable change

In bilinear data reconciliation problems where the state variable is given by Eq. 3-6 and the observation function $g_1(x_m)$ is linear and written as Cx_m (C is the observation matrix), it is reasonable to transform the ML criterion minimization problem into a linear quadratic problem that has a direct analytical solution by making the following change of variables:

$$X_m = \begin{bmatrix} F \\ \underline{F} \circ z \end{bmatrix} \tag{3-32}$$

where F and z are the mass flowrates and species mass fractions, and $\circ$ is the Hadamard product operator (Ballantine, 1968). Thus $\underline{F} \circ z$ is the vector containing species flowrates. For n number of species, $\underline{F}$ is the flowrate vector defined as:

$$\underline{F} = \left[\underbrace{F^T \quad | \quad F^T \quad | \quad \cdots \quad | \quad F^T}_{n} \right]^T \tag{3-33}$$

Total mass and species conservation equations then become $AX_m = \varepsilon$, where A is the incidence matrix, and ε is equal to zero when modeling errors are negligible. Applying the same change of variables to the observation equation leads to a linear measurement equation:

$$Y = CX_m + C(X_d - X_m) + E \tag{3-34}$$

where E represents the measurement noise for the new variable X_m. Under this change of variable and assuming that all variables are measured (i.e. $C = I$), the analytical solution of Eq. 3-6 for X_m is:

$$\hat{X}_m = \left(I - W^{-1}A^T(AW^{-1}A^T)^{-1}A\right)Y \tag{3-35}$$

where I is an identity matrix with proper dimensions. The weighting matrix W of data reconciliation must be obtained through the calculation of the total measurement error variance of the new variable X_m. In Eq. 3-34, there are two error components: process dynamic fluctuations that are correlated because of the data reconciliation bilinear nature, and the random measurement errors. Here, measurement errors are necessarily correlated because the measurement error of F appear in the product Fz and, obviously, in F itself. As a consequence, for calculating the measurement error of the new variable X, one has to calculate the variance of the cross-products Fz, but also the covariance between the species flowrates Fz and the flowrate F. Furthermore there is a covariance between the component flowrates, particularly on the same stream, since they contain the same variable F. Those covariance terms have been neglected by some authors who used this linearization method (Narasimhan and Jordache, 2000). Appendix A.3 presents the calculation of the new covariance matrix.

To illustrate the importance of considering covariance terms in bilinear data reconciliation where variable change technique is applied, a single node separation plant (Fig. 3-10) is presented in the absence of dynamic fluctuations to focus only on the measurement error itself. The separation unit has one feed and two output streams (reject and concentrate). It is assumed that ore flowrates and concentrations are independently measured with 10% white noise. The process state vector is expressed as:

$$x_m = [f_1 \quad f_2 \quad f_3 \quad z_1 \quad z_2 \quad z_3] \tag{3-36}$$

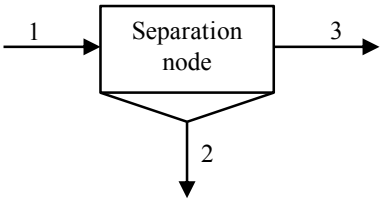

Fig. 3-10: Single node separation unit flow sheet.

Using the variable change technique brings correlation r_Y among fictitious measurements Y of the newly defined variables:

$$r_Y = \begin{array}{c} \begin{matrix} f_1 & f_2 & f_3 & f_1z_1 & f_2z_2 & f_3z_3 \end{matrix} \\ \begin{bmatrix} 1.00 & 0.01 & 0.01 & 0.71 & 0.01 & 0.01 \\ 0.01 & 1.00 & 0.00 & 0.01 & 0.71 & 0.00 \\ 0.01 & 0.00 & 1.00 & 0.01 & 0.00 & 0.71 \\ 0.71 & 0.01 & 0.01 & 1.00 & 0.01 & 0.01 \\ 0.01 & 0.71 & 0.00 & 0.01 & 1.00 & 0.00 \\ 0.01 & 0.00 & 0.71 & 0.01 & 0.00 & 1.00 \end{bmatrix} \end{array} \tag{3-37}$$

To establish a detailed comparison, four steady-state data reconciliation methods are proposed:

- *Technique A*: this method corresponds to optimally solving the bilinear data reconciliation problem by using nonlinear technique (sequential quadratic programming);
- *Technique B*: this technique is based on a linearization of the data reconciliation constraints using a first order Taylor development approximation (Romagnoli and Sanchez, 2000);
- *Technique C*: data reconciliation constraints are linearized by the proposed variable change technique, but using the diagonal approximation of the error covariance matrix of Y (Narasimhan and Jordache, 2000);
- *Technique D*: this method utilizes variable change technique the same *Technique C*, but it takes advantage of the complete error covariance matrix of Y.

Table 3-7 presents the performance indices based on the estimation error indices for different data reconciliation techniques, showing again that *Technique D,* which benefits from correct covariance matrix tuning exhibits the best performance. Figs. 3-11 and 3-12 shows the detailed information about the two first indices for each of the six reconciled process variables. As expected, *Technique D* gives the same performance as the true optimum solution of the bilinear data reconciliation problem (*Technique A*). As a key metallurgical index, the valuable mineral recovery is also considered. Since the plant operates in steady-state regime, the recovery mean value calculated using different data reconciliation techniques has a unique unbiased value: $\overline{R} = 0.90$. Table 3-7 shows η_p index values, which confirm the conclusions drawn from the two other indices. This example illustrates that it is possible to transform a bilinear data reconciliation problem into a linear one by a variable change technique, if the measurement covariance matrix is correctly tuned.

Table 3-7: Case-study IV: performance indices for various bilinear data reconciliation techniques.

Indices	*Technique A*	*Technique B*	*Technique C*	*Technique D*
η_y	0.56	0.55	0.50	0.56
η_x	1.00	0.98	0.87	1.00
η_p	0.52	0.41	0.36	0.52

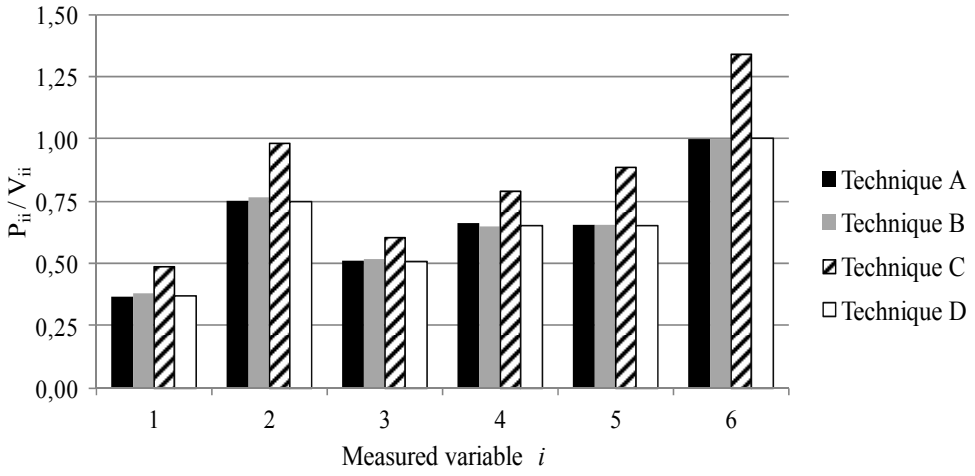

Fig. 3-11: Case study IV: precision of the estimations vs. raw measurements.

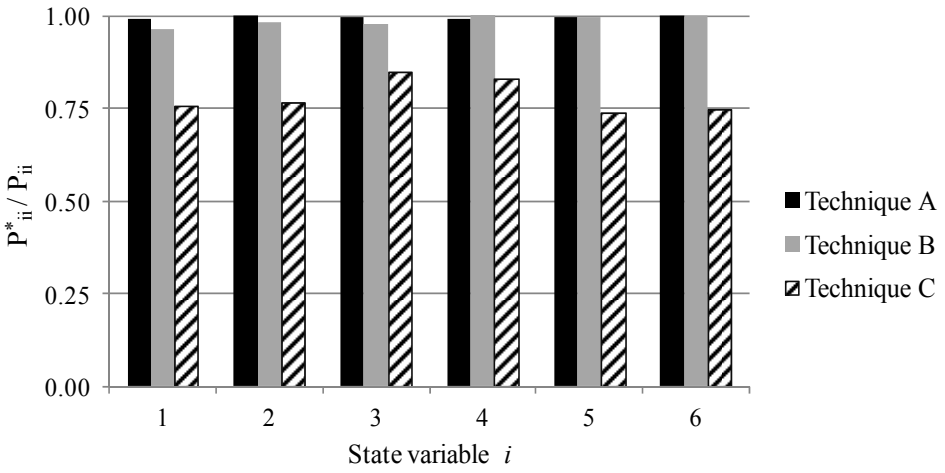

Fig. 3-12: Case study IV: precision of the estimations vs. optimum estimation.

3.5.5 Case-study V: Effect of overall uncertainty variance magnitudes

This section presents a simple example to investigate the impact of correct value assignment to the diagonal elements of the uncertainty covariance matrix. A single node separation unit including one feed and two output streams is considered. It is assumed that only ore feed, concentrate, and tail flowrates are measured with errors of 10%, 8% and 20% of their nominal values. The plant is supposed to operate in true steady-state conditions.

To support the example, Monte-Carlo simulations are applied, and in each simulation run, random values (uniformly distributed) for measured variables variances Σ_v are picked within the intervals that lies from 0.3 to 3 times of their nominal measurement noise variances Σ_v^*, and then η_x is drawn from simulation run results. Fig. 3-13 shows the histogram of η_x index for the different random values of Σ_v. About 45% of simulation runs give η_x larger than 0.95; this implies that in 45% of randomly tuning cases, the estimation error variances are quite acceptable. To confirm the point, the test has been repeated in a shorter range from 0.7 to 1.3 times of nominal variances Σ_v^*. Fig. 3-14 depicts the histogram where 95% of η_x values lies between 0.95 and 1.00. This means that 30% of uncertainty on the diagonal terms of Σ_v is not detrimental to data reconciliation performance, at least in the present case study. These results do not imply that all rough

tuning techniques frequently used in industrial practice can lead to good data reconciliation performance, as it is discussed below.

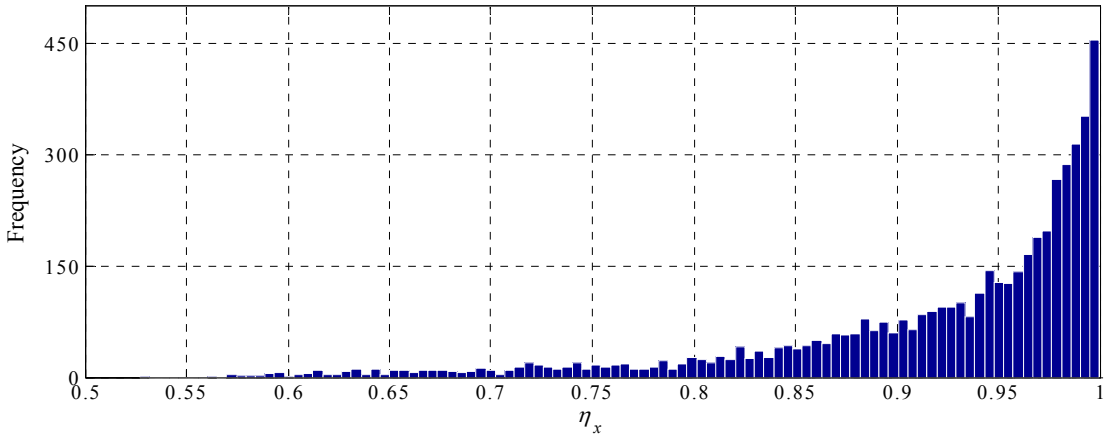

Fig. 3-13: Case-study V: Monte-Carlo simulation results for Σ_v tuning (range 0.3 to 3).

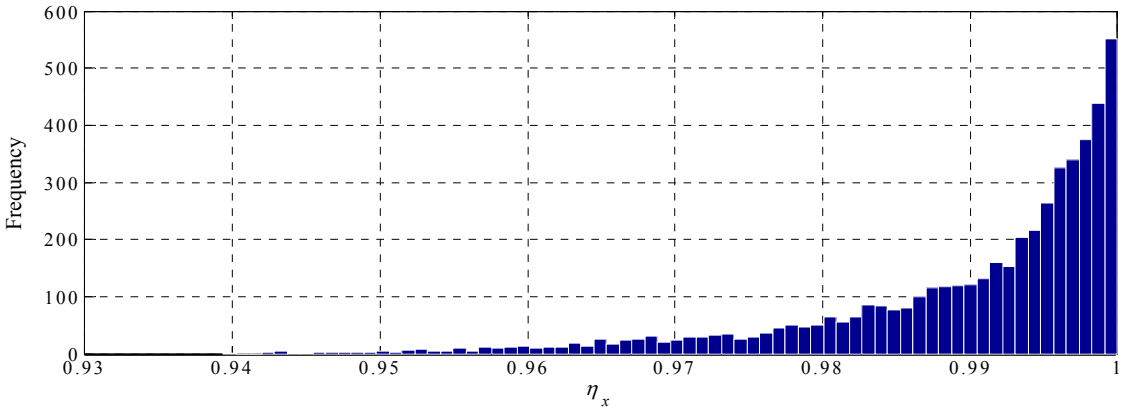

Fig. 3-14: Case-study V: Monte-Carlo simulation results for Σ_v tuning (range 0.7 to 1.3).

To evaluate the effectiveness of common industrial practices for variance tuning, the performance of steady-state data reconciliation is investigated for three different tunings.

- *Tuning A*: uniform weighting (i.e. no weighting);
- *Tuning B*: relative weighting;
- *Tuning C*: qualitative weighting;
- *Tuning D*: optimal weighting.

In the relative weighting practice, it is supposed that measurement error standard deviation is a uniform percentage of the nominal or measured value. In the present simulation, 10% of nominal values is selected. For the qualitative weighting technique, it is assumed that, in the present case feed, tail, and concentration have moderate, bad and good precision, respectively. Good, moderate and bad are here interpreted as 10%, 20%, and 30% measurement error, respectively. Table 3-8 shows the performance indices for these tuning techniques. As expected, uniform weighting gives the worst estimates while relative and qualitative weightings show acceptable performances. Figs. 3-15 and 3-16 confirm this conclusion for each process variable.

Table 3-8: Case-study V: performance indices for various industrial tuning practices.

Indices	*Tuning A*	*Tuning B*	*Tuning C*	*Tuning D*
η_y	0.334	0.385	0.549	0.588
η_x	0.620	0.682	0.930	1.000

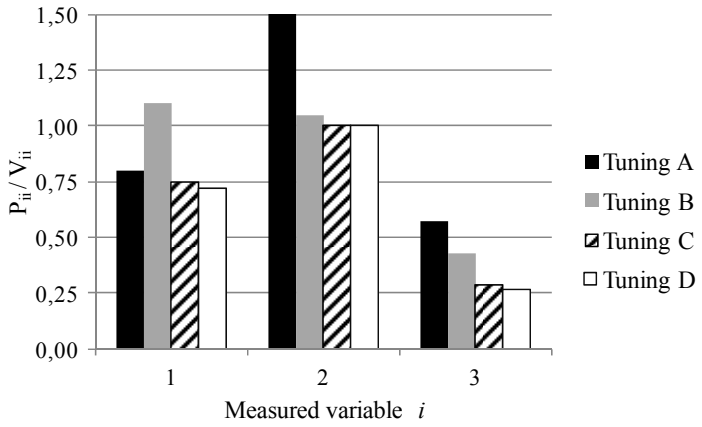

Fig. 3-15: Case study V: precision of the estimations vs. raw measurements.

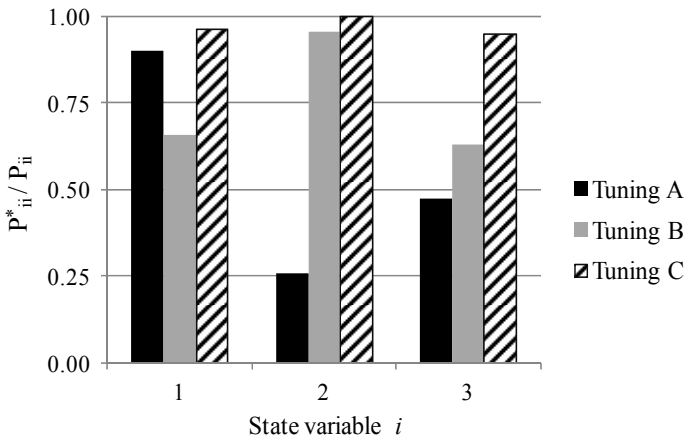

Fig. 3-16: Case study V: precision of the estimations vs. optimum estimation.

To confirm this observation, the procedure was applied to a more complex plant (flotation circuit), and almost the same conclusion was achieved. Obviously, these conclusions are not general and may vary from case to case. However, these examples show that uniform diagonal weighting, i.e. no weighting, is a really bad technique. They also show that uncertainty on variances could be tolerated, and a qualitative analysis of the error magnitudes might be sufficient to benefit from data reconciliation.

3.6 Conclusion

To maximize the precision of mass and energy balances in mineral and metallurgical processes, the statistical properties of the modeling and measurement uncertainties must be carefully tuned when steady-state data reconciliation techniques are applied. This chapter has investigated the detrimental impact of neglecting the covariance terms of the uncertainties, as it is usual industrial practice, and also incorrect tuning of variance terms using five case-studies taken from mineral and metallurgical industries.

In the first case-study, a mass and energy balance for a combustion chamber has been simulated to show how taking into account of model parameter errors, and their correlation terms improves the accuracy of the state variable estimates. This example has illustrated that using model uncertainty in steady-state data reconciliation for relaxing the mass and energy conservation equations, improves the estimation precision when it is applied with correct covariance structure.

The second example, involving particle size classification by a hydrocyclone, has discussed the importance of taking into account the correlation of the measurement errors produced by sieving columns and particle size distributions calculation. Considering correlation between measurements slightly increases data reconciliation precision. Its effect is magnified when normalization equations are not incorporated in the data reconciliation constraints. When the normalization equations are considered, as is usual practice, the correlations of the measurement errors only bring marginal improvement to the data reconciliation performance, at least for the specific studied example.

In the third example, a flotation plant has been used to show that applying measurement errors covariance induced by dynamic fluctuations improves the accuracy of the steady-state mass balance of the plant. The improvement is much more significant when metallurgical indices like metal recovery are utilized for plant performance evaluation.

In case-study four, different data reconciliation techniques based on linearization of the bilinear constraints have been presented. The linearization of mass balance equations by generating pseudo-measurements of components flowrates has been shown to be efficient to simplify the data reconciliation computation; however covariances of the pseudo-measurements should be properly calculated, i.e. without forgetting the correlations induced between the errors of the new state variables generated by the change of process variables.

Finally, an example based on Monte-Carlo simulations has been used to investigate the impact of uncertainties of the variance terms on the data reconciliation performance. The example, limited to the variance terms of the weighting matrix, has shown that random selection of measurement error variances within a reasonable range could provide acceptable process variable estimations, i.e. a reasonable noise reduction on the measured variables. However, some commonly used industrial practice, such as uniform weighting, can be detrimental to data reconciliation performance while sound qualitative evaluation of the measurement error variance may produce quite satisfying results.

As a general conclusion, it must be emphasized that the weighting strategies of the data reconciliation objective function proposed in commercial packages (limitation to diagonal

matrices, and ignoring modeling errors and correlated uncertainties generated by dynamic variations of process variables) may result in poor performance of data reconciliation techniques. Even worse, they may produce additional noises on measured variables and increase the sensitivity of the calculated plant performance indices to measurement errors. The error covariance terms can be extracted from repeated data acquisition campaigns. The correlation terms must be understood as a nonparametric implicit additional model constraint of the process behavior. This is confirmed by the hydrocyclone example where the normalization equation can be replaced by off-diagonal terms in the covariance matrix. This is also the case for the flotation plant where the covariance terms implicitly contain information on the species separation coefficients. Regardless of the mass and energy balance calculation purposes, either auditing, monitoring, modeling, on-line optimization or fault detection, a careful analysis of the structure of uncertainty is a key factor for data reconciliation success.

Chapter 4

How to Adequately Apply Steady-State Material or Energy Balance Software to Dynamic Metallurgical Plant Data[2]

Résumé

La réconciliation de données est une méthode d'observation bien connue qui améliore la précision, c'est-à-dire la justesse et la fiabilité des mesures industrielles. Cette technique utilise des modèles de procédés qui vont de simples équations de conservation de la masse et de l'énergie en régime permanent à des équations complexes de modèles de fonctionnement détaillés. Pour les applications industrielles, plusieurs produits logiciels sont disponibles pour la réconciliation de données, mais la plupart d'entre eux sont basés sur la conservation de la masse et de l'énergie sous l'hypothèse que l'usine fonctionne en régime permanent. Dans les cas réels des perturbations se produisent en continu et produisent des variations dynamiques des états des procédés, incluant les variations des inventaires de matière dans les réacteurs. Ce chapitre propose quelques techniques pour adapter ces produits à l'exploitation des données d'usine réelle, soit pour estimer les états dynamiques ou pour atténuer les effets de la dynamique des processus sur les variables réconciliées. Quatre techniques sont proposées pour utiliser les logiciels de réconciliation en régime permanent dans des conditions de fonctionnement de l'usine en régime dynamique stationnaire. Leurs performances sont comparées aux méthodes dynamiques optimales dérivées du filtre de Kalman.

[2] Daniel Hodouin, Amir Vasebi & Éric Poulin (2012), How to adequately apply steady-state material or energy balance software to dynamic metallurgical plant data. *IFAC Workshop on Automation in the Mining, Mineral and Metal Industries*, Gifu, Japan.

Abstract

Data reconciliation is a well-known observation method that improves accuracy and reliability of plant measurements. This technique uses process models that range from simple mass and energy balance equations to complex detailed models. For industrial applications, several software products have been released for data reconciliation purposes, but most of them are based on mass and energy conservation equations under the assumption that the plant operates in steady-state regime. In real plants, disturbances continuously occur, and a true steady-state operation with constant process inventories is never met. The present chapter proposes some techniques for adapting these products to real plant operation, either for estimating the dynamic states or attenuating process dynamics effects on the reconciled variables. Four techniques that can be cast into steady-state reconciliation computer programs are proposed, and their performance compared to optimal dynamic methods derived from the Kalman filter.

4.1 Introduction

Efficient process supervision using techniques such as fault detection and diagnosis, automatic control, real-time optimization, maximization of either product quality or productivity or economic return, and efficient accountability depend upon reliable estimation of process states (Bagajewicz, 2010). Two types of knowledge are used to estimate process states at the laboratory, pilot, or industrial scales (Romagnoli and Sanchez, 2000). On the one hand, fundamental physicochemical laws or empirical relationships, usually cast into mathematical models, help to predict the process behavior. On the other hand, measurements of process variables bring information on the process states. When these two observation angles of process behavior bring redundant information, inherent discrepancies appear between the process state estimates depending on the type of information used (Narasimhan and Jordache, 2000). The redundancy can come from the measurement data set itself or from the model equations set, but usually the redundancy comes from the whole set of information involving experimental data as well as model equations. When differences are large between the various ways of estimating states, one

might even speak of conflicts, therefore leading to the concept known as data reconciliation (Kuehn and Davidson, 1961; Stanley and Mah, 1977).

In mineral processing or metallurgical plants, conflicts frequently arise when trying to produce material or energy balance of production units. The process knowledge is encapsulated into model equations that express the law of mass and energy conservation while measured values of process variables are simultaneously available. Industrial data suffers from numerous problems, particularly in the harsh environment prevailing in mineral and metal processing industries (Hodouin, 2010). Measurement of properties such as particle size distribution, phase composition, temperature, flow rates, in a context of high capacity plants manipulating heterogeneous and time-varying materials is a difficult and costly task. Measurements are inherently contaminated by errors related to sampling as well as to measurement techniques while models contain unavoidable assumptions leading to prediction uncertainties (Hodouin, 2011).

Commercial software products exist for attenuating the conflicts generated by these two sources of uncertainty, when redundant information is available, and when assumptions can be made about the structure of the uncertainties that corrupt both types of knowledge. Most plants now make use of commercial software packages like Bilmat™ and Metallurgical Accountant™ (Algosys), Bilco™ and Inventeo™ (Caspeo), JKMultibal™ (JKTech), Movazen™ (Banisi), Sigmafine™ (OSIsoft), Datacon™ (IPS), Advisor™ (AspenTech), and VALI™ (Belsim) that are designed to balance chemical species, physical properties and energy conservation equations. These computer programs simultaneously upgrade raw data delivered by on-line sensors or laboratory analyses and estimate unmeasured variables. These packages are based on a network description of the various species or material properties that flow through the plant flow sheet.

The data reconciliation packages available on the market, which are widely used by the minerals and metals processing industries, assume that plants are operating in steady-state (SS) conditions (Bagajewicz and Jiang, 2000; Bagajewicz, 2010). This is obviously never the case, and discrepancy to this hypothesis can sometimes be quite large and thus may generate poorly reliable results (Almasy, 1990). Although there are other sources of model uncertainties, such as neglected species transformations or material leaks or infiltrations, a

major part of the model uncertainty is related to the deviation between the true dynamic behavior of the process and the assumption of steady-state operating regime.

Obviously, to cope with process dynamics, it is possible to develop and implement algorithms that explicitly take account of process dynamics. There are many approaches that have been proposed to deal with data reconciliation in the context of material and energy balance for dynamic plant regimes. For instance, one may refer to data reconciliation techniques such as stationary observers (Makni et al., 1995a; Lachance et al., 2006b; Vasebi et al., 2012a), generalized linear dynamic observers (Darouach and Zasadzinski, 1991; Xu and Rong, 2010), integral linear dynamic observer (Bagajewicz and Jiang, 1997), dynamic data reconciliation method (Bai et al., 2006), and Kalman filter (Stanley and Mah, 1977; Dochain, 2003; Narasimhan and Jordache, 2000; Lachance, 2007). However, it is not the goal to describe here those techniques, although some of them will be used as references to evaluate the results produced in this study.

The objective of this chapter is first to make metallurgical engineers aware of the limits of the application of steady-state commercial data reconciliation packages, and, second, to propose some techniques, or "tricks", to use these products, while properly tuning software parameters, either to partially take account of the process dynamics, or to partially eliminate their effects on the data reconciliation procedure. After a brief description of the plant dynamic properties and models, the following methods are proposed either for estimating the underlying steady-state regime (direct use of instantaneous or averaged dynamic data), or for estimating dynamic states (data synchronization for dynamic behavior attenuation; stationary methods based on node imbalance statistics and methods that involve process inventory measurements). The performance of these methods implemented in steady-state reconciliation (SSR) programs is compared to optimal dynamic reconciliation methods derived from the Kalman filter.

4.2 Properties of Plant Dynamics

In the metallurgical plants, process states that are typically handled consist of extensive properties such as flowrates, and intensive properties such as chemical concentrations and temperatures. They naturally lead to bilinear mass or energy conservation equations

(Hodouin, 2010). For the sake of simplicity, it is considered in the following that process states are species and/or heat flowrates, thus assuming that process states and measurements are obtained through the multiplication of extensive and intensive variables. This fortunately leads to linear balance equations but do not impede the application of the here proposed "tricks" to bilinear problems, although this is neither demonstrated nor illustrated in this chapter.

Different dynamic regimes should be considered. The simplest one is the stationary regime where mean and variances around nominal operating state values are constant (Lachance et al., 2006b). However, this is valid only when set-points are maintained at constant values while disturbances exhibit stationary variations. In practice, a stationary behavior is only observed locally, i.e. for limited periods of time separated by quasi-deterministic changes occurring to disturbances, such as persistent variations of the mean properties of the processed material, and changes to equipment tunings or plant set-points. Finally, equipment stops or start-ups correspond to transient operating regimes where it is generally neither recommended nor useful to perform data reconciliation. In the following, the plant is considered as locally operating in a stationary mode, i.e. during periods stationary disturbances occur in the plant feed.

Usually, metallurgical plants are described as networks where graph branches correspond to streams and nodes to process equipment pieces. Although most commercial packages propose a separation between intensive and extensive states, mass or energy conservation equations, in the context of the present chapter objectives, can be formulated as the following linear steady-state model:

$$\begin{bmatrix} M_1 & \cdots & 0 & \cdots & 0 \\ \vdots & \ddots & & & \vdots \\ 0 & & M_i & & 0 \\ \vdots & & & \ddots & \vdots \\ 0 & \cdots & 0 & \cdots & M_n \end{bmatrix} \begin{bmatrix} x_1 \\ \vdots \\ x_i \\ \vdots \\ x_n \end{bmatrix} = Mx = 0 \quad , \quad i = 1, \cdots, n \tag{4-1}$$

where M_i and x_i stand for the incidence matrix and the extensive property vector of the i^{th} element to be conserved. The corresponding measurement equation is:

$$y = Cx + v \quad , \quad v \sim N(0, \Sigma_v) \tag{4-2}$$

where y is the measured value, C is the measurement matrix and v the measurement error, approximated as belonging to a normal statistical distribution. The solution of the linear quadratic data reconciliation problem is consequently formulated as:

$$\hat{x} = \arg\min_x \left\{ (y - Cx)^T V (y - Cx) \right\} \quad , \quad \text{s.t.} \quad Mx = 0 \tag{4-3}$$

where V is a weighting matrix, which optimally should be Σ_v^{-1}. The solution is the following linear estimator (Kuehn and Davidson, 1961):

$$\begin{aligned} \hat{x} = Ly &= \left[Q^{-1} \left(I - M^T \left(M Q^{-1} M^T \right)^{-1} M Q^{-1} \right) C^T V \right] y \\ Q &= C^T V C \end{aligned} \tag{4-4}$$

where I is the identity matrix. The covariance matrix of the estimation error is:

$$P = L \Sigma_v L^T \tag{4-5}$$

When the optimal weighting matrix is used, P simply becomes:

$$\begin{aligned} P &= Q^{-1} \left(I - M^T \left(M Q^{-1} M^T \right)^{-1} M Q^{-1} \right) \\ Q &= C^T \Sigma_v^{-1} C \end{aligned} \tag{4-6}$$

This method and its modifications proposed in this chapter are supposed to be applicable to separation plants that can be described by the following dynamic model:

$$\begin{aligned} z(k+1) &= Az(k) + Bu_n + w(k) \quad , \quad w \sim N(0, \Sigma_w) \\ x(k) &= Hz(k) \\ y(k) &= Cx(k) + v(k) \end{aligned} \tag{4-7}$$

where x and z are the process and model state variable vectors, respectively. u_n is the nominal value of the input streams and w the vector of white noises that drive flowrate disturbances affecting input streams, as well as those which drive the separation disturbances at the various plant nodes. A, B, C and H are coefficient matrices. The steady-state process variables corresponding to this state equation are:

$$x_n = H\left(I - A\right)^{-1} B u_n \tag{4-8}$$

The autocovariance of the state variable z is obtained through the solution of the following equations:

$$\begin{aligned} \Sigma_z &= A \Sigma_z A^T + \Sigma_w \\ \Sigma_{z,l} &= \Sigma_z \left(A^T\right)^l \end{aligned} \tag{4-9}$$

where Σ_z is the covariance of z and $\Sigma_{z,l}$ is its autocovariance for a time lag of l sampling periods. The corresponding variances of the process variables x are then:

$$\Sigma_{x,l} = H \Sigma_{z,l} H^T \tag{4-10}$$

4.3 Direct Use of Instantaneous or Averaged Data

The simplest way to use a steady-state data reconciliation computer program is to estimate x at time k by directly applying Eq. 4-3 and using the measurements at time k. The usual practice is to select as weighting factor the inverse of the measurement error variance Σ_v. As the plant is in a dynamic state, it is rather difficult to appreciate the real meaning of this kind of estimate. It could be either said that this is an estimate of a fictitious steady-state plant regime which is close to the measurements obtained at time *k* or an estimate of a fictitious local underlying steady-state at time *k*.

Another point of view is that the real objective of this approach is to estimate the true mean value of process states, i.e. x_n given by Eq. 4-8, assuming that the process exhibit a stationary behavior as described by Eq. 4-7. If this is the true objective of the reconciliation procedure, as it should be, the correct weighting factor in Eq. 4-3 must be the inverse of

total variance of y (Σ_y), i.e. a variance which includes both the dynamic variance of x and measurement error variance Σ_v:

$$\Sigma_y = C\Sigma_z C^T + \Sigma_v \tag{4-11}$$

The accuracy of this estimation method is obviously decreasing when the amplitudes of the process dynamic variations are increasing in comparison to the experimental measurement error standard deviation. To improve the reliability of the method, it is possible to pre-filter the measured variables by averaging in a sliding window containing *h* subsequent values of the process variables. This is partially cancel the process dynamics, and at the same time decrease the measurement error. Again, the procedure of Eq. 4-3 can be directly applied by substituting the averaged measurement $\bar{y}_h$ to y, and tuning the weighting matrix V as the inverse of the total variance Σ_{v_h}:

$$\Sigma_{v_h} = C\Sigma_{\bar{x}_h} C^T + \frac{\Sigma_v}{h} \tag{4-12}$$

where $\Sigma_{\bar{x}_h}$ is the dynamic variance of the averaged value of x in the window of size *h*. It is given by:

$$\begin{aligned} \Sigma_{\bar{x}_h} &= E\left[(\bar{x}_h - x_n)(\bar{x}_h - x_n)^T\right] \\ &= \frac{1}{h^2}\left[h\Sigma_x + \sum_{i=1}^{h-1}(h-1)\left(\Sigma_{x,i} + \Sigma_{x,i}^T\right)\right] \end{aligned} \tag{4-13}$$

The estimate of x_n and its variance are therefore obtained using Eqs. 4-4 and 4-6 with the correct variable substitutions. When *h*=1, the method is in fact applied to the instantaneous measurements at time *k*.

4.4 A Method when Inventories are Measured

Dynamic variations of plant stream properties do not disqualify steady-state reconciliation problems when the processing equipment exhibits zero dynamics. This is the case for instance for particle size classification by hydrocyclones. The residence time within the reactor is so small that the instantaneous measurements on the input and output streams still obey the steady-state balance equations. The source of problems of applying steady-state reconciliation computer programs to dynamic data comes from process inertia that generates equipment inventory variations. However, if it is possible to measure the content of a reactor, one may cast the reconciliation problem into the same formulation as a steady-state data reconciliation problem. The discretized mass or energy dynamic conservation equation for each species or component i can be written as (Darouach and Zasadzinski, 1991):

$$M_i x_i(k) = \frac{1}{\Delta t}\left(O_i(k) - O_i(k-1)\right) \tag{4-14}$$

where $O_i(k)$ is the vector containing the amount of species i accumulated in the plant nodes, and Δt the sampling period. In a matrix form, this is expressed as:

$$\left[M_i \;\mid -I \mid +I\right]\begin{bmatrix} x_i(k) \\ O_i(k)/\Delta t \\ O_i(k-1)/\Delta t \end{bmatrix} = 0 \tag{4-15}$$

for the component i. For the whole set of components, one has:

$$\mathrm{MX}(k) = 0 \tag{4-16}$$

In terms of the plant network used for defining the data reconciliation problem, this is equivalent to add one input stream with flowrate $O_i(k-1)/\Delta t$ and one output stream with flowrate $O_i(k)/\Delta t$ at each node of the oriented graph. For this case, the reconciliation problem is solved as Eq. 4-3, substituting X to x and using the inverse of flowrates and inventories measurement error variances as the weighting matrix. A large weighting factor

is applied to $O_i(k-1)$, to freeze its value to the previously estimated one, if this is required for the industrial application of the method. Otherwise, it could be set to the inverse value of the previously estimated variance. This method leads in fact to a suboptimal version of the optimal generalized linear dynamic (GLD) method proposed by Darouach and Zasadzinski (1991). The estimate and its variance are obtained by applying Eqs. 4-4 and 4-6 after substitution of the appropriate values of the measurements, incidence matrix, and variance matrix.

4.5 Data Synchronization Method

Averaging, as presented in Section 4-3, is a method to cancel process dynamics, and estimate an underlying steady-state regime. In the present method, the objective is to estimate the true dynamic state value. In order to cope with the dynamic effect generated by process nodes, it is proposed to reconstruct the properties of the plant feed streams in such a way that they match with the other streams at time *k*. This synchronization of the input streams with the behavior observed at time k on the process states can be performed if, at least, some rough approximation of the process dynamics can be identified. The simplest way to approximate the dynamic behavior of a process would be to assume linear gains and pure delays between the plant node input and outputs. However, more complex transfer functions may also be used. For the sake of simplicity, the presentation will be limited to plants consisting of a single node.

Let us consider the process unit of Fig. 4-1, where x_1, x_2 and x_3 are the flowrates of a selected species. The process dynamics are represented by the transfer functions G_2 and G_3 and their corresponding pure delays d_2 and d_3:

$$\begin{cases} x_2(k) = G_2(z^{-1}) z^{-d_2} x_1(k) \\ x_3(k) = G_3(z^{-1}) z^{-d_3} x_1(k) \end{cases} \tag{4-17}$$

where *z* is the discrete time domain operator, and z^{-1} represents one sample delay.

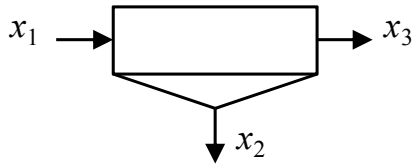

Fig. 4-1: A single node plant.

Depending upon the method of dynamic model identification, transfer functions can be as well replaced by polynomials or truncated impulse responses. Then, by creating the synchronized input:

$$x_1^s(k) = \left(G_2(z^{-1})z^{-d_2} + G_3(z^{-1})z^{-d_3}\right)x_1(k) \tag{4-18}$$

the reconciliation constraint becomes a steady-state conservation equation:

$$x_1^s(k) - x_2(k) - x_3(k) = 0 \tag{4-19}$$

The reconciliation problem can then be solved as Eq. 4-3, where y_1 must be replaced by its synchronized measurement y_1^s, and its corresponding variance. The estimates $\hat{x}_2(k)$ and $\hat{x}_3(k)$ are obtained with Eq. 4-4, allowing the reconstruction of the reconciled value of x_1 by solving:

$$\hat{x}_1(k-d_1) = \left(G_2(z^{-1})z^{-(d_2-d_1)} + G_3(z^{-1})z^{-(d_3-d_1)}\right)\hat{x}_1^s(k) \tag{4-20}$$

where $d_1 = \min(d_2, d_3)$. There are two ways to calculate y_1^s and its variance $\Sigma_{y_1^s}$: 1) if the reconciliation is infrequently performed, y_1^s and its corresponding variance are calculated from the past measurements of x_1, and their variances by application of Eq. 4-19 to the measured values of x_1; 2) if the reconciliation is performed at each sampling time, it is then possible to replace the past measured values of x_1 by the recent estimate of x_1, as schematically shown in Fig. 4-2. The error variance of y_1^s must be changed accordingly. The proposed method is, in fact, a suboptimal implementation of a Kalman filter with input uncertainty, which could be optimally solved by a generalized Kalman filter algorithm.

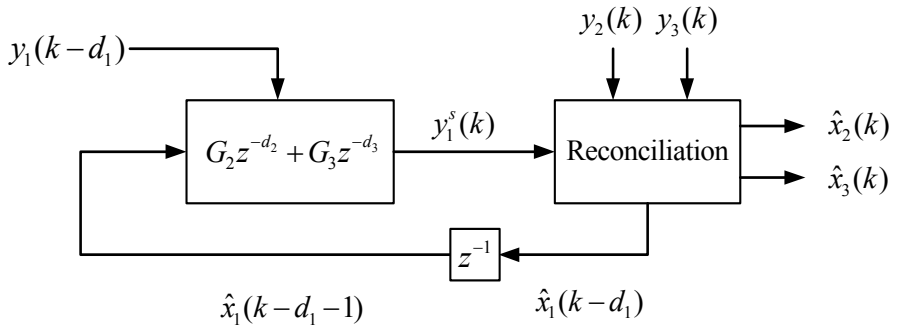

Fig. 4-2: Data preprocessing for dynamic data reconciliation by steady-state reconciliation software (data synchronization method).

4.6 Accumulation Rate Method

The dynamic conservation equation given by Eq. 4-14 can be rewritten as:

$$M_i\, x_i(k) = \varepsilon_i(k) \tag{4-21}$$

where ε_i is the accumulation rate vector for species *i*, i.e. the rates of inventory variations at the various nodes, alternatively named node imbalances. For a stationary plant, as supposed here, ε_i is a zero-centered random variable, leading to a dynamic reconciliation method already introduced as the stationary data reconciliation or node imbalance method (Hodouin, 2010). For applying a steady-state reconciliation package, Eq. 4-21 can be rewritten as the following steady-state conservation equation:

$$\left[M_i \;\middle|\; -I\right]\begin{bmatrix} x_i(k) \\ \varepsilon_i(k) \end{bmatrix} = 0 \tag{4-22}$$

The dynamic conservation equation for the whole set of components to be conserved is, therefore:

$$\mathrm{M}_{\varepsilon}\,\mathrm{X}_{\varepsilon}(k) = 0 \tag{4-23}$$

Graphically, this procedure is equivalent to adding an additional output stream to every node of the plant oriented graph. This additional stream brings the vector of the various component accumulation flowrates.

Again, the reconciliation problem solution is given by Eq. 4-3 where x is replaced by X_ε, y by the measured values of x augmented by the expected value of ε, i.e. zero. The variance of ε in the new weighting factor must be estimated using the plant model of Eq. 4-7. For this purpose, the new process variable ε which is a linear combination of x variables (e.g. $\varepsilon = Fx$) should be added to the vector of process states x. The associated variance is $F\Sigma_x F^T$. Moreover, Matrix C is to be accordingly modified. The estimated values of the augmented process states and their variances are obtained using Eq. 4-4 and Eq. 4-6 by changing accordingly the variables in these expressions.

4.7 Numerical Illustration for a Single Node Plant

The above-proposed methods are tested on the single node plant of Fig. 4-1 simulated through the approach of Eq. 4-7 applied to a single species. Two versions of Eq. 4-7 are used: one where all flowrates are measured and another one where, in addition, the species inventory is measured. Table 4-1 gives the numerical values of the model parameters. In Table 4-2, transfer functions of the plant are given in Laplace domain where time constants are expressed in minutes, and $\mathcal{L}$ represents the Laplace operator. For simulation purposes, discrete transfer functions are obtained with a sampling period of 1 minute.

Table 4-1: Nominal values and standard deviations (STD) of model parameters.

Process states	$x_1\,(t/h)$	$x_2\,(t/h)$	$x_3\,(t/h)$	$O(t)$
Nominal value (x_n)	10.00	8.00	2.00	2.00
STD of state dynamic variation	2.00	1.49	0.37	0.08
Measurement error STD	0.50	0.40	0.10	0.20

Table 4-2: Transfer functions of the process model.

Stream No.	Transfer function
1	$G_1(s) = \frac{\mathcal{L}(x_1)}{\mathcal{L}(u_n + \xi)} = \frac{1}{50s+1}$
2	$G_2(s) = \frac{\mathcal{L}(x_2)}{\mathcal{L}(x_1)} = \frac{0.8}{8s+1}$
3	$G_3(s) = \frac{\mathcal{L}(x_3)}{\mathcal{L}(x_1)} = \frac{0.2}{10s+1}$

Table 4-3 gives the estimation error standard deviations obtained by the method that estimates the underlying steady-state regime. The estimation accuracy of x_n increases as the number of samples for averaging increases, as expected. Since, in this example, the degree of redundancy is quite low, the reconciled estimate $\hat{x}_h$ is not significantly better than the raw estimate $\bar{y}_h$ obtained by averaging. For instance, for h=10, the reconciled, and raw relative standard deviations for x_1 are respectively 18.6 and 19.5 %. Also, it must be noticed that the variance remaining in $\bar{y}_h$ is mainly due to process dynamics, since the measurement error contribution has almost vanished (the total standard deviation is 20.6 %, and the standard deviation due to dynamics is 20%). It must be also observed that there exist a steady-state regime of the system which can be obtained by very few adjustments of the dynamic variables, and therefore which is far from the nominal state. This again is related to the very low information redundancy for this system.

It is repeated that usually steady-state reconciliation is applied to dynamic data with the hope to improve the estimation of the dynamic data while using a weighting matrix that incorporates only the measurement errors (Bagajewicz, 2010). This may generate reconciled values that are less reliable than the measurements. In the present example, this practice would, for instance, lead to a standard deviation of 5.8 % though the measurement error is only 5%.

Table 4-3: Results for the estimation of nominal values with different window widths

Window width h	Standard deviation of estimation error (%)		
	x_1	x_2	x_3
1	19.02	19.31	18.97
10	18.58	18.59	18.27
100	15.06	15.06	14.99
500	8.37	8.38	8.37

Table 4-4 gives the estimation error standard deviations obtained by the three data reconciliation methods proposed for estimating the dynamic states x. The GLD method implemented through a steady-state reconciliation algorithm produces sub-optimal results compared to its optimal implementation. This is clearly noticeable for the inventory estimation, since the method is not able to improve the flowrate estimation, because of the inherently low redundancy degree of the GLD method, and of the relative values of the measurement errors in inventory and flowrates. The inventory measurement is largely less accurate than the flowrate ones and, therefore, exhibits room for improvement.

Data synchronization is applied here without using the implementation of Fig. 4-2, i.e. in the case of its infrequent use. The results compared to those of the generalized Kalman filter applied to the model of Eq. 4-7 (without inventory measurement) clearly show that the steady-state reconciliation implementation produces a loss of optimality. In the present case, it is, however, better than the accumulation rate method of Section 4-6, which implemented in a steady-state reconciliation package gives exactly the same optimal results than the original algorithm (already called stationary method). There is no loss of optimality using its steady-state reconciliation implementation.

Table 4-4: Estimation results of the dynamic process states.

DR Method	Standard deviation of estimation error (%)			
	x_1	x_2	x_3	O
GLD (optimal)	5.00	5.00	5.00	2.29
GLD-implemented by SSR (proposed in Section 4-4)	5.00	5.00	5.00	7.08
Generalized Kalman filter	5.00	1.06	0.92	NA
Data synchronization (proposed in section 4-5)	4.80	1.83	4.86	NA
Accumulation rate (original stationary method)	4.38	4.61	4.98	NA
Accumulation rate (SSR implementation of section 4-6)	4.38	4.61	4.98	NA

4.8 Conclusion

Data reconciliation methods for dynamic process information can be sub-optimally implemented in commercial software products based on steady-state mass and energy conservation equations. Steady-state processing can be directly applied to dynamic plant data, in as much as the measurement errors dominate the plant unit dynamic variations. However, in a strongly disturbed environment steady-state reconciliation may produce poor results unless process variability is attenuated by averaging techniques. It must be recognized that forcing steady-state mass and energy conservation equations requires that measurement variances be adjusted to take account of the dynamic variances, including the process state autocovariances when averaged measurements are used. Another approach consists in using steady-state data reconciliation computer programs to estimate or filter dynamic process variables. Three methods are proposed. When unit process inventories are measured, it is possible to use a sub-optimal implementation of data reconciliation with dynamic mass or energy conservation methods. Plant input process variables may also be

pre-filtered for synchronization with other plant variables, in such a way that steady-state reconciliation can subsequently be applied, and followed by a reconstruction of the dynamic process inputs. The third option is to implement fictitious streams in the plant network that take account of the accumulation rate variables (node imbalances). When the variance of these variables is correctly evaluated, the steady-state implementation produces the same optimal results as the stationary data reconciliation method.

Chapter 5

Dynamic Data Reconciliation Based on Node Imbalance Autocovariance Functions[3]

Résumé

Pour réduire l'impact des erreurs de mesure sur les variables des usines, la réconciliation de données est largement appliquée dans les industries. Des mesures réconciliées sont utilisées dans des applications telles que le suivi de performances, le contrôle des processus, ou l'optimisation en temps réel. Toutefois, l'estimation précise se fonde généralement sur des modèles de procédés détaillés et précis qui pourraient être difficiles à construire dans la pratique. Le compromis entre la précision des estimations et la complexité du modèle est un défi pertinent motivant le développement d'observateurs efficaces avec des efforts de modélisation limités. Ce chapitre propose une méthode de réconciliation de données basée sur un sous-modèle simple de conservation de la masse et/ou de l'énergie qui considère la fonction d'autocovariance des déséquilibres de bilan aux nœuds du graphe d'écoulement de la matière dans l'usine. L'observateur est appliqué à des usines de référence simulées et sa performance est évaluée en termes de réduction de la variance d'estimation et de la robustesse face aux erreurs de modélisation. Les résultats montrent une performance supérieure par rapport aux méthodes classiques à base de sous-modèle et moins de dégradation des performances que le filtre de Kalman en présence d'incertitudes de modèle.

[3] Amir Vasebi, Éric Poulin & Daniel Hodouin (2012), Dynamic data reconciliation based on node imbalance autocovariance functions. *Computers and Chemical Engineering*, 43, p. 81–90.

Abstract

To reduce impacts of measurement errors on plant variables, data reconciliation is widely applied in process industries. Reconciled measurements are used in applications such as performance monitoring, process control, or real-time optimization. However, precise estimation relies on accurate and detailed process models that could be difficult to build in practice. The trade-off between estimate precision and model complexity is a relevant challenge motivating the development of effective observers with limited modeling efforts. This chapter proposes a data reconciliation method based on a simple mass and/or energy conservation sub-model that also considers the autocovariance function of plant node imbalances. The observer is applied to simulated benchmark plants, and its performance is evaluated in terms of variance reduction and robustness against modeling errors. Results show a superior performance in comparison with classical sub-model based methods and reveal less performance degradation than the Kalman filter in the presence of model uncertainties.

5.1 Introduction

Reliable and accurate process measurements are crucial for the improvement of plant operations. The decision-making to achieve planned objectives strongly depends on data collected from the plant instrumentation and laboratory analyzers. Critical actions to increase plant performances also rely on process models, estimation of indicators, and advanced control and optimization applications that require accurate data. To maximize profits and reduce environmental impacts of industrial processes, high-quality data, and information must be applied to plant-wide management and business strategies. In many cases, advanced measurement methods incorporating appropriate filtering or estimation techniques would generate significant benefits in comparison with their implementation and maintenance costs (Bagajewicz, 2010).

Multiple errors, arising from different sources such as measuring devices, sampling equipment, sensor positioning, or signal conversion, always affect measurements and consequently reduce the reliability of gathered data. Measurement errors are classified as random or systematic (Narasimhan and Jordache, 2000). Random errors are due to

stochastic events related to instrumentation (sampling and measurement devices), fluctuation of material properties, and external disturbances. These errors are characterized by statistics such as standard deviation, a parameter that quantifies measurement precision. Occurrence and magnitude of systematic errors, also called biases, are linked to deficient instrumentation or inexact calibration. This kind of error should be treated in early filtering stages before any further data processing. As defined by Miller (1983), the accuracy of a measurement is the closeness to the true value and it includes the effect of both systematic and random errors. In the present chapter, only random errors are considered, and thus, accuracy and precision are equivalent.

Data reconciliation (DR), first introduced by Kuehn and Davidson (1961), is a model-based filtering method that applies simple process models to improve the reliability and precision of measured variables. Under favorable observability conditions, DR also allows the estimation of unmeasured process variables. These abilities are valuable for process industries since, in many practical cases, strategic variables are only measured with limited precision or simply not measured because of technical or economic constraints. DR has been applied to a large number of processes including petrochemical, chemical, biochemical, mineral, and metallurgical processes as summarized by Mah (1990), Crowe (1996), Narasimhan and Jordache (2000), Romagnoli and Sanchez (2000), and Hodouin (2010).

Different DR techniques have been proposed based on various assumptions regarding process dynamics and depending on the subsequent application of reconciled data. On the one hand, steady-state DR is largely used to estimate the underlying average regime of a plant in applications such as production accounting, process audit, or survey analysis. On the other hand, advanced process control, fault detection algorithms, and real-time optimization require the estimation of true dynamic states of a process, and are generally coupled to dynamic DR. Different approaches could be taken for dynamic DR. The filtering algorithm complexity depends on the selected process model. It could range from a simple mass conservation constraint sub-model to a complete causal dynamic model. The selection of the most appropriate algorithm should result from a compromise between modeling efforts, required to develop and adapt the observer, and improvement of estimate precision.

Tamhane and Mah (1985), Crowe (1996), Puigjaner and Heyen (2006), and Moreno (2010) have discussed the properties of steady-state observers and related problems such as steady-state detection, observability and redundancy analysis, and gross error detection. Poulin et al. (2010) have studied steady-state DR applied on a real-time basis. They have concluded that, despite the attractive simplicity of this solution, the estimate precision could be less than measurement precision itself depending on plant dynamics, which is not acceptable from the practical point of view. In order to cope with process dynamics, which can be interpreted as inventory variations, Makni et al., (1995a, 1995b) have introduced a stationary observer which offers an interesting compromise between estimate precision and model complexity. They have considered process node imbalances as normally distributed random variables. Also, Lachance et al. (2006a, 2006b) and Hodouin et al. (2007) have investigated other practical aspects of this observer such as tuning, robustness and non-linear cases found in mineral and metallurgical processing. Vasebi et al. (2011) have proposed a modified stationary observer that takes advantage of the correlation of node imbalances to improve estimation performances. However, only two successive time lags were considered.

Darouach and Zasadzinski (1991) have proposed a generalized linear dynamic observer (GLD) to handle mass conversation constraints incorporating accumulation terms. This technique benefits from dynamic mass conservation equations, and it assumes that node accumulations are measurable. As a main drawback of this technique, it can be mentioned that measurement of species accumulation is difficult or impossible to achieve in most practical cases. Recently, Xu and Rong (2010) have modified this method for partial measurement situations. Bagajewicz and Jiang (1997) have also developed an observer based on dynamic mass balance equations named integral linear dynamic observer. This observer is close to the GLD concept, but it uses models of process accumulations and flowrates to avoid dealing with singular systems. Bagajewicz and Jiang (2000) have applied this observer to averaged plant data and have compared its performance with steady-state observers. Bai et al. (2006) have proposed a sub-model based observer, called dynamic data reconciliation filter. They have used a simple one-step-ahead prediction as process model and they have concluded that, in asymptotic conditions, this method and the Kalman filter

converge to the same results, but they have discussed neither tuning of the proposed model nor its sensitivity against modeling error.

Definitively, the Kalman filter is the most important and commonly used dynamic observer. It can be said that other dynamic observers have been originated from the Kalman filter directly or are strongly related to it. These techniques use a complete dynamic model for estimation purposes. In the literature, it has extensively been applied to dynamic DR problems (Stanley and Mah, 1977; Almasy, 1990; Narasimhan and Jordache, 2000; Dochain, 2003; Bai et al., 2006). Also, Lachance (2007) has investigated the application of a generalized Kalman filter for DR purposes.

The objective of this chapter is to propose a DR observer based on a simple mass and/or energy conservation sub-model that estimates process dynamic states and also includes the autocovariance function of node imbalances as supplementary information. The observer is compared to classical sub-model based DR methods (the steady-state and standard stationary observers) and to the Kalman filter that serves as a reference. Performances are evaluated by considering both the capability of reducing the estimation variance and the robustness in the presence of process modeling uncertainties. Comparisons are carried out in simulation using two benchmark plants commonly used in the mineral and metallurgical industries: a single node separation unit and a flotation circuit.

The chapter is organized as follows. Section 5.2 presents process models used for DR are. The principles of the proposed observer and details mathematical relations are explained in Section 5.3. Other observers employed for comparison purposes are briefly reviewed. Methods selected for performance evaluation are discussed in Section 5.4. Finally, Section 5.5 presents benchmark plants and discusses simulation results.

5.2 Plant Model and Constraints

The precision of reconciled data strongly depends on measurement errors, model constraints, and the optimization criterion used to solve conflicts between the model and measurements. For a given level of raw data precision, increasing the information contained in the model, either in the complexity of its structure or the quality of its parameters, leads

to more precise estimation of variables. Therefore, the design of a DR observer necessarily requires a suitable trade-off between modeling efforts and precision of reconciled data.

The best model structure should be able to predict the process states from the values of externally applied process variables (manipulated variables and disturbances). This is called a complete causal dynamic model in what follows. Obviously, for a given level of model complexity, the amount of information it contains increases with the accuracy of its parameters. As the number of parameters to be calibrated increases with model complexity, it may happen that the accuracy of parameters decreases unless they came from fundamental knowledge. Thus, it is important to find the right balance between model complexity and parameter reliability, in such a way to end with an observer that optimizes estimate precision at a reasonable level of modeling efforts. In this section, model structures are discussed starting with the complete causal dynamic model and then, introducing the mass conservation sub-model.

5.2.1 *Complete causal dynamic model*

This model is able to simulate the process states and outputs from input variables and initial states. In the general nonlinear and time variant case, it can be expressed by:

$$x(k+1) = f(x(k), u(k), \theta(k)) \tag{5-1}$$

$$y(k) = g(x(k), u(k), \theta(k)) \tag{5-2}$$

where $x(k)$, $y(k)$, and $\theta(k)$ respectively stand for states, measured variables, and model parameters vectors at time k. Functions $f(\cdot)$ and $g(\cdot)$ represent process dynamics and observation relationships that link process states to external process variables $u(k)$.

For most practical DR applications, where a plant can be assumed to operate in a stationary regime, the following linear and time invariant approximation can be used:

$$x(k+1) = Ax(k) + Bu_n + w(k) \tag{5-3}$$

$$y(k) = Cx(k) + v(k) \tag{5-4}$$

where A, B and C are model coefficients valid for a local operating regime corresponding to nominal inputs u_n and parameters θ_n. Modeling uncertainties and measurement errors estimated at the nominal operating point are $w(k)$ and $v(k)$ respectively. In present study, these are assumed to obey a normal distribution:

$$w(k) \sim N(0, \Sigma_w) \tag{5-5}$$

$$v(k) \sim N(0, \Sigma_v) \tag{5-6}$$

$$\mathrm{cov}\{w(i), v(j)\} = 0 \quad , \quad \forall i, j \tag{5-7}$$

Assuming the plant operating in a stationary regime implies that:

$$x(k) \sim N(x_n, \Sigma_x) \tag{5-8}$$

$$\mathrm{cov}\{x(i), v(j)\} = 0 \quad , \quad \forall i, j \tag{5-9}$$

where x_n represents the process steady-state nominal value.

Flow diagram of a single node separation unit is presented in Fig. 5-1, and its corresponding causal model structure is illustrated in Fig. 5-2. The plant feed rate $x_1(k)$ is composed of the nominal feed rate u_n disturbed by a random fluctuation, which is generated by a white noise $\xi(k)$ subsequently filtered by the transfer function $F_1(z)$. The transfer functions $F_2(z)$ and $F_3(z)$ are linear approximations of the local behavior of the process operating in a stationary regime defined by x_n and u_n. Here, $x_2(k)$ and $x_3(k)$ are respectively plant concentrate and reject flowrates.

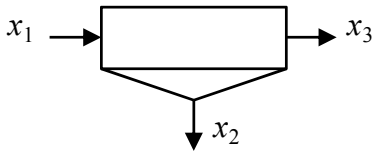

Fig. 5-1: Single node separation unit.

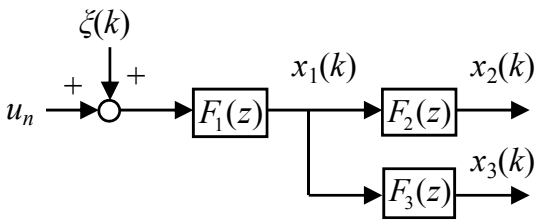

Fig. 5-2: Complete causal dynamic model of the single node separation unit.

5.2.1 Mass conservation sub-model

As previously discussed, it could be more suitable for DR to use simpler models involving fewer parameters with higher accuracy. Parameters of a complex model can be very sensitive to the changing nature of operating conditions and consequently might require sophisticated updating procedures. Simple models with precisely known parameters may offer better information than complex models with highly uncertain parameters. For industrial DR applications, simple but reliable models like deterministic natural laws of conservation of mass or energy are frequently preferred to causal models. These models are typically applied as constraints for DR since they are easily obtained from the process flow sheet.

The general mass conservation equation can be expressed by

$$\frac{dO}{dt} = Mx^f + P_r - \delta \tag{5-10}$$

where O represents the total mass accumulation and/or accumulation of a given material or chemical species in the process. The vector x^f represents the mass flowrate, M is the incidence matrix determined by flowrate directions around each plant node where conservation laws are applied. The vector P_r stands for species production rate (P_r is zero when the total mass is considered or when no reaction occurs). The uncertainty vector δ represents structural errors such as forgotten secondary or intermittent streams, or errors in the production rates evaluation.

For the sake of simplicity, it is assumed that O and x^f correspond to inventory and flowrate of total material or a given species. In the latter case, process states and

measurements are obtained through the multiplication of the concentrations and the total masses or flowrates. This fortunately leads to linear mass balance equations (instead of bilinear equations), giving the possibility of deriving analytical solutions for estimates and estimation error covariance matrices.

For process operating under stationary regime and assuming $P_r = 0$, the mass balance equation can be rewritten in discrete form as:

$$Mx^f(k) = \varepsilon(k) \tag{5-11}$$

where $\varepsilon(k)$ represents process accumulation rates, also named node imbalances, and it is assumed to be a random variable with the following statistical properties:

$$\varepsilon(k) \sim N(0, \Sigma_\varepsilon) \tag{5-12}$$

The observation equation for this model is:

$$y(k) = C^f x^f(k) + v(k) \tag{5-13}$$

and it is assumed that

$$\mathrm{cov}\{\varepsilon(i), v(j)\} = 0 \quad , \quad \forall i, j \tag{5-14}$$

Process dynamics implies that the node imbalances $\varepsilon(k)$ are time correlated. Fig. 5-3 illustrates the process node imbalance autocovariance function obtained for a single node separation unit operating in a stationary regime defined in Chapter 2. This statistical property can be injected into the observer model to improve the estimation precision for DR. This is the main topic of the next section.

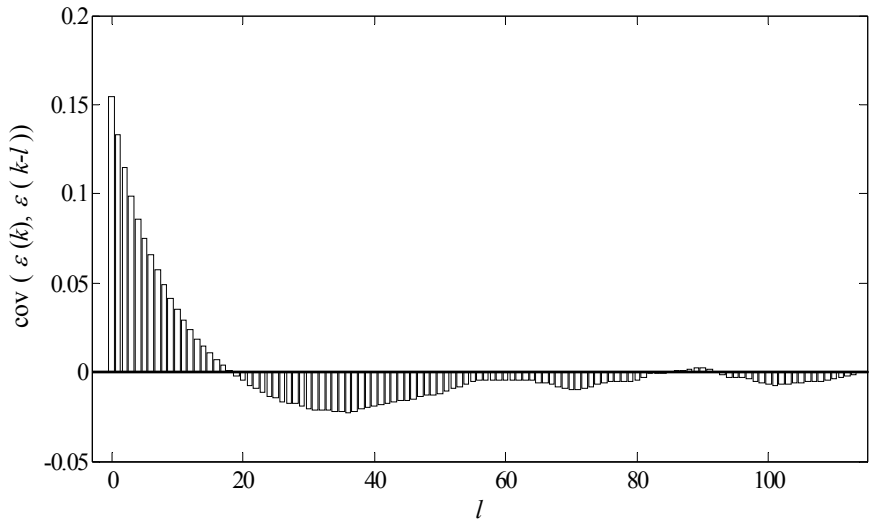

Fig. 5-3: Node imbalance autocovariance function of the separation unit.

5.3 Observer Equations

This section presents the development of a DR observer, fundamentally based on a mass conservation sub-model, which includes the node imbalance autocovariance properties as supplementary information to improve estimate precision. It also briefly reviews concepts and equations of classical observers used for comparison purposes in Section 5.5.

5.3.1 Autocovariance based stationary observer

The sub-model presented in Eq. 5-11 can be completed by the node imbalance autocovariance function to improve DR performances since it contains valuable information about process dynamics. The autocovariance based stationary (ABS) observer uses the existing autocovariance between l successive time lags of process node imbalances. Modifying Eq. 5-11 to incorporate material balance constraints along a period of time running from k to $k-l$ leads to

$$\underline{M}\,\underline{x}^{f}(k) = \underline{\varepsilon}(k) \tag{5-15}$$

where

$$\underline{x}^{f}(k) = \left[x^{f}(k) \quad x^{f}(k-1) \quad \cdots \quad x^{f}(k-l)\right]^{T} \tag{5-16}$$

$$\underline{\varepsilon}(k) = \left[\varepsilon(k) \quad \varepsilon(k-1) \quad \cdots \quad \varepsilon(k-l)\right]^T \tag{5-17}$$

$$\underline{M} = I_{l+1} \otimes M \tag{5-18}$$

Here, I_{l+1} is an identity matrix of size *l*+1. The standard stationary observer (Makni et al., 1995a) is a particular case of the ABS observer that does not consider the time correlation of node imbalances and only uses its covariance function at time *k*. The measurement equation for the ABS observer is expressed by

$$\underline{y}(k) = \underline{C}^f \, \underline{x}^f(k) + \underline{v}(k) \tag{5-19}$$

where

$$\underline{y}(k) = \left[y(k) \quad y(k-1) \quad \cdots \quad y(k-l)\right]^T \tag{5-20}$$

$$\underline{v}(k) = \left[v(k) \quad v(k-1) \quad \cdots \quad v(k-l)\right]^T \tag{5-21}$$

and

$$\underline{C}^f = I_{l+1} \otimes C^f \tag{5-22}$$

Assuming that measurement errors and node imbalances behave as independent Gaussian stochastic phenomena, the maximum likelihood solution of this DR problem is

$$\hat{\underline{x}}^f(k) = \underset{\underline{x}^f(k)}{\arg\min} \left\{ \left(\underline{y}(k) - \underline{C}^f \, \underline{x}^f(k) \right)^T \underline{\Sigma}_v^{-1} \left(\underline{y}(k) - \underline{C}^f \, \underline{x}^f(k) \right) + \underline{\varepsilon}^T(k) \underline{\Sigma}_\varepsilon^{-1} \underline{\varepsilon}(k) \right\} \tag{5-23}$$

where the measurement errors are assumed unbiased and of constant variance given by:

$$\underline{\Sigma}_v = I_{l+1} \otimes \Sigma_v \tag{5-24}$$

Since process dynamics is assumed stationary, the covariance matrix of node imbalances in the time window $[k-1,\ k]$ is:

$$\underline{\Sigma}_{\varepsilon} = \begin{bmatrix} \Sigma_{\varepsilon} & \Sigma_{\varepsilon,1} & \cdots & \Sigma_{\varepsilon,l} \\ \Sigma_{\varepsilon,1} & \Sigma_{\varepsilon} & \cdots & \Sigma_{\varepsilon,l-1} \\ \vdots & \vdots & & \vdots \\ \Sigma_{\varepsilon,l} & \Sigma_{\varepsilon,l-1} & \cdots & \Sigma_{\varepsilon} \end{bmatrix} \tag{5-25}$$

where

$$\Sigma_{\varepsilon,i} = \mathrm{cov}\{\varepsilon(k), \varepsilon(k-i)\} \tag{5-26}$$

Eq. 5-23 minimizes the sum of two weighted terms. The first term considers the difference between measurements and estimated values (innovations) while the second term considers process node imbalances over the selected time window. Both terms are appropriately weighted according to their respective covariance matrices $\underline{\Sigma}_v$ and $\underline{\Sigma}_{\varepsilon}$. Eq. 5-23 attempts to satisfy the process mass conservation for a sequence of time lags by taking into account the correlation of node imbalances. Therefore, by using this concept, the ABS observer is able to deal with process dynamics.

The solution of Eq. 5-23 can be formulated as (see Appendix B for a complete demonstration)

$$\underline{\hat{x}}^f(k) = \left(\underline{\alpha} - \underline{\alpha}\,\underline{M}^T(\underline{\Sigma}_{\varepsilon} + \underline{M}\,\underline{\alpha}\,\underline{M}^T)^{-1}\underline{M}\,\underline{\alpha}\right)(\underline{C}^f)^T\underline{\Sigma}_v^{-1}\,\underline{y}(k) \tag{5-27}$$

where

$$\underline{\alpha} = \left((\underline{C}^f)^T\,\underline{\Sigma}_v^{-1}\underline{C}^f\right)^{-1} \tag{5-28}$$

The estimation error covariance matrix under stationary operating regime is given by (see Appendix B for a complete demonstration)

$$\underline{P} = \mathrm{cov}\left(\hat{x}^f(k) - x^f(k)\right) = \underline{\alpha} - \underline{\alpha}\,\underline{M}^T(\underline{\Sigma}_{\varepsilon} + \underline{M}\,\underline{\alpha}\,\underline{M}^T)^{-1}\underline{M}\,\underline{\alpha} \tag{5-29}$$

The selection of an appropriate time lag l can be done on the basis of the confidence interval of the estimated autocovariance function using plant data. The impact of l is investigated in Section 5-5.

5.3.2 Observers used for comparison

Three DR observers are selected to evaluate the performance of the ABS observer: the steady-state observer (SS), the standard stationary observer (ST), and the Kalman filter (KF). These techniques rely on process models with a different level of complexity. The expression of variable estimates and their estimation error covariance matrix are presented in this section. Since the ST observer neglects the time correlation of node imbalances, its properties can be obtained directly from ABS observer expressions by selecting l=0. Consequently, its corresponding equations are not presented here.

5.3.2.1 Steady-state observer

The SS observer assumes that the mass conservation equation is strictly satisfied at any time. Therefore, in Eq. 5-11 which expresses the process model, the node imbalances term is zero. By minimizing the sum of the weighted squared innovations at time k, subject to the constraint that node imbalances are zero, state estimates are given by (Kuehn and Davidson, 1961):

$$\hat{x}^f(k) = \left(I - \Sigma_v M^T (M \Sigma_v M^T)^{-1} M\right) y(k) \tag{5-30}$$

This expression assumes that all variables are measured (i.e. $C^f = I$). For a process operating in a stationary regime, implying that true states satisfy $Mx^f(k) = \varepsilon(k)$, the estimation error covariance matrix is (Almasy, 1990):

$$P = \mathrm{cov}\left(\hat{x}^f(k) - x^f(k)\right) = P_0 + \Sigma_v M^T (M \Sigma_v M^T)^{-1} \Sigma_\varepsilon (M \Sigma_v M^T)^{-1} M \Sigma_v \tag{5-31}$$

where

$$P_0 = \Sigma_v - \Sigma_v M^T (M \Sigma_v M^T)^{-1} M \Sigma_v \tag{5-32}$$

Eq. 5-31 shows that under a true steady-state operating regime, i.e. $\Sigma_\varepsilon = 0$, the minimum variance of estimates is P_0. This variance is increased by the second term, related to node imbalances, as the deviation from steady-state conditions becomes more significant.

5.3.2.2 Kalman filter

In the context of involving linear models and Gaussian errors, KF is considered as an optimal observer minimizing the variance of estimates. When a dynamic causal model (Eqs. 5-3 and 5-4) is available; KF recursive estimation equations are given by:

$$P(k \mid k-1) = AP(k-1 \mid k-1)A^T + \Sigma_w \tag{5-33}$$

$$K(k) = P(k \mid k-1)C^T \left(CP(k \mid k-1)C^T + \Sigma_v\right)^{-1} \tag{5-34}$$

$$\hat{x}(k \mid k-1) = A\hat{x}(k-1 \mid k-1) + Bu(k-1) \tag{5-35}$$

where $K(k)$ is the observer gain. The state estimate $\hat{x}(k \mid k)$ and the covariance $P(k \mid k)$ at time *k*, based on the knowledge of measurements up to time *k*, are given by:

$$\hat{x}(k \mid k) = \hat{x}(k \mid k-1) + K(k)\left(y(k) - C\hat{x}(k \mid k-1)\right) \tag{5-36}$$

$$P(k \mid k) = \left(I - K(k)\right)P(k \mid k-1) \tag{5-37}$$

In the present study, the KF observer is based on a complete causal model that has a structure identical to the simulated process. So, it serves as a reference method to assess the performance of other observers.

5.4 Evaluation Methods of the Performance of Observers

The proposed observer performance is assessed from two points of view. First, the variance reduction is considered. Different indices are given to compare the estimation error covariance matrix P with the covariance matrix of measurement errors Σ_v. Second, the observer robustness in the presence of modeling errors is investigated.

5.4.1 Reduction of estimation error covariance

Several techniques could be applied to compare P and Σ_v. One possibility is to directly compare diagonal elements of P with Σ_v. The following variance reduction index can be used for this purpose:

$$\eta_{i,i} = \frac{\Sigma_{vi,i} - P_{i,i}}{\Sigma_{vi,i}} \tag{5-38}$$

where, $\Sigma_{vi,i}$ and $P_{i,i}$ are diagonal elements of Σ_v and P respectively. Although this method gives a rapid state by state indication of the precision improvement or degradation, it is not able to completely assess the observer performance. It neglects the correlation between estimates induced by DR, a property that has been shown as a positive factor when using simultaneously various state estimates to calculate performance indices (Hodouin and Flament, 1991).

To assess the overall performance of observers, Poulin et al. (2010) have suggested some performance indices that deal with the comparison of covariance matrices. In the present chapter, two performance indices are selected: the trace index (or total variance index) and the user-defined index that is related to variables involved in the calculation of a key performance indicator (KPI) of a plant. These indices are given by

$$\eta_t = \frac{\text{trace}\, P}{\text{trace}\, \Sigma_v} \tag{5-39}$$

$$\eta_u = \frac{\text{trace}\, z^T P z}{\text{trace}\, z^T \Sigma_v z^T} \tag{5-40}$$

Eq. 5-40 assumes that a KPI is calculated as a linear combination of process states, i.e. $\beta = z x^f$. This combination is obtained either by linearization of β or by directly formulating an economic indicator as a weighted sum of the process flowrates. Mazzour and Hodouin (2008) have investigated cases where β is a non-linear function of x^f.

5.4.2 Robustness to modeling errors

To verify the robustness of observers against modeling error, tuning is achieved for a specific condition, and then observers are applied to non-ideal conditions where model parameters vary randomly around nominal values. Trace and user-defined indices given by Eqs. 5-39 and 5-40 are used to illustrate the performances of DR observers under these conditions.

5.5 Benchmark Plants, Results, and Discussion

Two benchmark plants are used for comparing observer performances. Simulated plants are taken from the mineral and metallurgical processing industries and consist of a single node separation unit and a typical flotation circuit. In both cases, it is assumed that the plant operates under a stationary regime, and all process variables are measured. Also, the feed rate has a stationary behavior centered on a constant nominal value. For testing purposes, five simulation scenarios are defined. They are generated by increasing feed rate fluctuations to induce more important dynamic variations. The testing scenarios are gathered in Table 5-1. In this table, σ_{x_1} refers to the standard deviation of the feed rate stream normalized by its nominal value. Achieved simulation results for each plant are presented and discussed separately in the following sections.

Table 5-1: Different simulation scenarios.

Scenario No.	1	2	3	4	5
σ_{x_1} (%)	0	2	10	20	30

5.5.1 Single node separation unit

Fig. 5-1 illustrates the flow diagram of a separation unit which can be single equipment, a processing circuit or an overall plant. It has one input stream x_1 (feed) and two output streams x_2 and x_3 that respectively refers to concentrate and tailings. According to the notation introduced in Fig. 3, the transfer functions of the plant are presented in Table 5-2. They are given in Laplace domain and time constants are expressed in minutes. In the table, $\mathcal{L}$ represents the Laplace operator. For simulation purposes, discrete transfer functions are obtained with a sampling period of 1 minute. As indicated by the transfer function gains, valuable material flowrates (obtained by multiplying the concentration and total flowrates) are considered in this case study.

Table 5-2: Transfer functions of the separation unit.

Input Filter	Concentrate	Reject
$F_1(s)=\frac{\mathcal{L}(x_1)}{\mathcal{L}(u_n+\xi)}=\frac{1}{50s+1}$	$F_2(s)=\frac{\mathcal{L}(x_2)}{\mathcal{L}(x_1)}=\frac{0.8}{8s+1}$	$F_3(s)=\frac{\mathcal{L}(x_3)}{\mathcal{L}(x_1)}=\frac{0.2}{10s+1}$

It is assumed that process variables are measured with a relative precision of 5 % of their nominal values $x_n=[10 \;\; 8 \;\; 2]^T$ in tons per hour. The plant recovery is considered as the KPI. It is obtained by linearization of the relation $\beta=x_2/(x_2+x_3)$ at nominal values. The value of z is then

$$z=[0 \quad 0.02 \quad -0.08] \tag{5-41}$$

Table 5-3 shows performances of the ABS observer for different time lags when the feed rate fluctuates with a standard deviation equal to 30 % of its nominal value (Scenario 5). Each column shows the diagonal elements of P for a specific time lag ranging from 0 (ST observer) to 20. The last column gives the variance of measurement errors. Achieved results show that generally, increasing of time lag improves the estimation precision, but for this case, the improvement is not significant for l larger than 5.

Table 5-3: $P_{i,i}$ for the ABS observer with different time lags l in Scenario 5 (separation unit).

Variable	ABS-0 (ST)	ABS-1	ABS-2	ABS-5	ABS-10	ABS-20	$\Sigma_{vi,i}$
x_1	0.217	0.189	0.186	0.187	0.187	0.187	0.250
x_2	0.146	0.134	0.133	0.133	0.133	0.133	0.160
x_3	0.010	0.010	0.010	0.010	0.010	0.010	0.010

To assess ABS observer performances, results are compared to those obtained with SS, ST, and KF observers using the variance reduction index (Eq. 5-38). Results are given in Table 5-4 for Scenario 5. The ABS observer, with a time lag larger than one, shows a significant

improvement in comparison with SS and ST observers when process dynamic is relatively high. Negative values for the SS observer imply that it provides less precise estimates than measurements. Therefore, it is unable to handle highly dynamic operating regimes. Also, Table 5-4 reveals that the ABS observer almost does not improve the precision of the reject flowrate x_3. This problem is due to the small measurement error variance of x_3 in comparison with the variance induced by process dynamics. Variables which their measurement error level is comparable with process dynamic variations are subjected to more adjustments by the ABS observer.

Table 5-4: Variance reduction for SS, ABS and KF observers (separation unit).

Variables	$\eta_{i,i}$ (%)							
	ABS-0 (ST)	ABS-1	ABS-2	ABS-5	ABS-10	ABS-20	SS	KF
x_1	13.2	24.4	25.7	25.9	25.9	26.0	-145.8	32.9
x_2	8.5	15.6	16.5	16.6	16.6	16.6	-93.3	95.9
x_3	0.5	1.0	1.0	1.0	1.0	1.0	-5.8	96.9

Fig. 5-4 shows values of η_t and η_u as a function of time lag l in Scenario 5. This figure confirms results of Tables 5-3 and 5-4 that there is no improvement for l larger than 5 because the autocovariance function becomes relatively small for large time lags as depicted in Fig. 5-3.

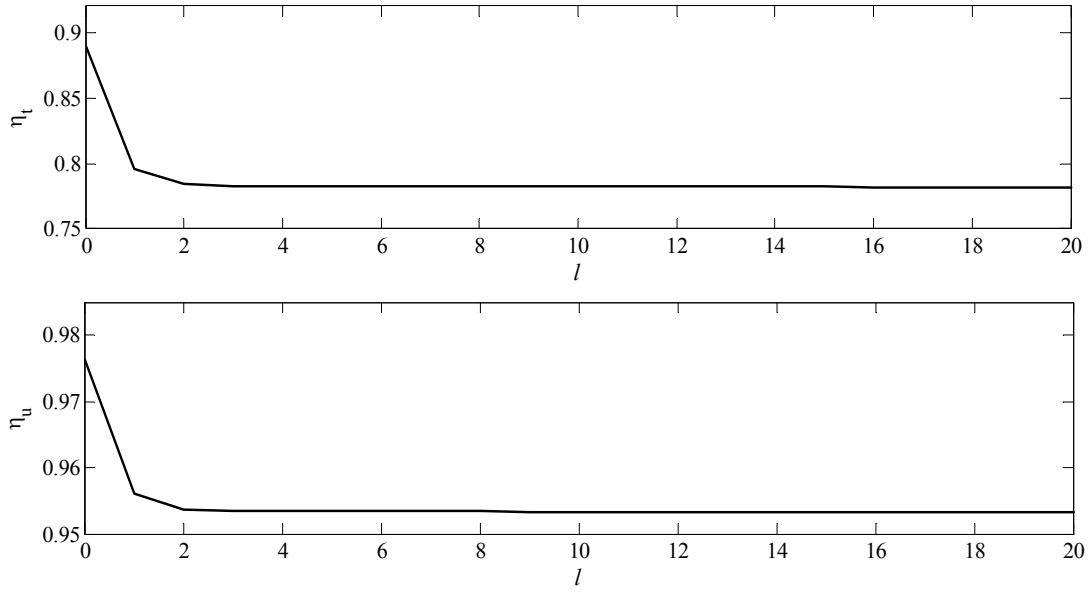

Fig. 5-4: Performance indices as a function of l in Scenario 5 (separation unit).

To investigate performances for different levels of process dynamics, Table 5-5 presents η_t and η_u for the five evaluation scenarios. All observers show growing indices for increasing value of σ_{x_1}. Generally, ABS observer exhibits better performance than SS and ST observers, and the improvement is more significant for large values of σ_{x_1}. Again, SS observer in Scenarios 4 and 5 shows performance indices larger than one, which implies that it provides estimates with precision less than measurements. In all scenarios, KF serves as a reference and gives the best performance. As already mentioned, it benefits from an exact and complete plant model. Generally, observers show a similar behavior for both indices, but η_u emphasizes improvement for some streams more than others.

Table 5-5: η_t and η_u for SS, ABS and KF observers in different scenarios (separation unit).

Scenario No.	η_t				η_u			
	ABS-0 (ST)	ABS-5	SS	KF	ABS-0 (ST)	ABS-5	SS	KF
1	0.500	0.500	0.500	0.000	0.893	0.893	0893	0.000
2	0.508	0.508	0.508	0.042	0.895	0.895	0895	0.000
3	0.640	0.600	0.692	0.196	0.923	0.914	0.934	0.000
4	0.805	0.706	1.266	0.330	0.958	0.937	1.057	0.001
5	0.890	0.782	2.224	0.416	0.976	0.953	1.262	0.001

5.5.2 Flotation circuit

To evaluate the performance of the proposed observer with a more complex and realistic plant, a flotation circuit is considered (Fig. 5-5). The plant has seven streams and three nodes. Transfer functions of the different units as well as the input stream filter that manages feed rate dynamics is given in Table 5-6 in the Laplace domain. Time constants are expressed in minute unit. A sampling period of 1 minute is selected to obtain the discrete transfer functions for simulation. Similar to the single node separation unit, valuable material flowrates are considered.

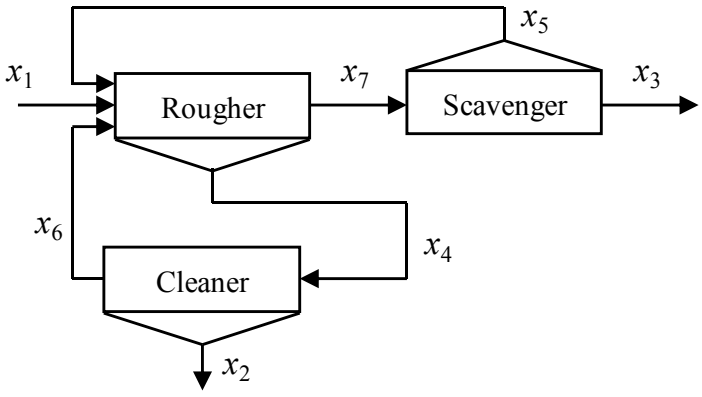

Fig. 5-5: Flotation circuit flow diagram.

Table 5-6: Transfer functions of the flotation circuit.

Unit Name	Concentrate	Reject
Rougher	$G_{rc}(s) = \frac{\mathcal{L}(x_4)}{\mathcal{L}(x_1 + x_5 + x_6)} = \frac{0.77}{10s+1}$	$G_{rr}(s) = \frac{\mathcal{L}(x_7)}{\mathcal{L}(x_1 + x_5 + x_6)} = \frac{0.23}{8s+1}$
Scavenger	$G_{sc}(s) = \frac{\mathcal{L}(x_5)}{\mathcal{L}(x_7)} = \frac{0.82}{12s+1}$	$G_{sr}(s) = \frac{\mathcal{L}(x_3)}{\mathcal{L}(x_7)} = \frac{0.18}{10s+1}$
Cleaner	$G_{cc}(s) = \frac{\mathcal{L}(x_2)}{\mathcal{L}(x_4)} = \frac{0.93}{8s+1}$	$G_{cr}(s) = \frac{\mathcal{L}(x_6)}{\mathcal{L}(x_4)} = \frac{0.07}{6s+1}$
Input Filter	$G_{if}(s) = \frac{\mathcal{L}(x_1)}{\mathcal{L}(u_n + \xi)} = \frac{1}{50s+1}$	

It is assumed that process variables are measured with a relative precision of 10 % of the following nominal values (in tons per hour):

$$x_n = \begin{bmatrix} 12.8 & 12.1 & 0.7 & 13.0 & 3.2 & 0.9 & 3.9 \end{bmatrix}^T \tag{5-42}$$

The parameter z, which corresponds KPI (i.e. $\beta = zx^f$) is defined as:

$$z = \begin{bmatrix} -1.0 & 2.0 & -3.0 & 0 & -1.5 & -1 & 0 \end{bmatrix} \tag{5-43}$$

This indicator assigns profits to the concentrate x_2, processing costs to streams x_1, x_5, and x_6, and decontamination costs to x_3.

The performance of the ABS observer for this circuit is evaluated using the same procedure as the one applied to the single node separation unit. First, its performance with different time lags is investigated in Scenario 5. Table 5-7 gives the diagonal elements of P for specific time lags. These results show that the estimation precision improves with increasing time lags. Again, this improvement is not significant for l larger than 5.

Table 5-7: $P_{i,i}$ for the ABS observer with different time lags l in Scenario 5 (flotation circuit).

Variables	ABS-0 (ST)	ABS-1	ABS-2	ABS-5	ABS-10	ABS-20	$\Sigma_{vi,i}$
x_1	1.196	0.995	0.945	0.935	0.937	0.937	1.638
x_2	0.832	0.728	0.694	0.673	0.672	0.671	1.464
x_3	0.005	0.005	0.005	0.005	0.005	0.005	0.005
x_4	0.669	0.650	0.647	0.647	0.646	0.646	1.690
x_5	0.070	0.068	0.067	0.066	0.066	0.066	0.103
x_6	0.008	0.008	0.008	0.008	0.008	0.008	0.008
x_7	0.080	0.076	0.074	0.072	0.071	0.071	0.152

The variance reduction achieved by the ABS observer in comparison with SS and ST observers is illustrated in Table 5-8. It shows that the ABS observer improves the estimation precision more than SS and ST observers, especially for x_1, x_2 and x_7. The SS observer gives a negative value that confirms that this observer provides less precise estimates than measurements for large inventory variations. Results also reveal that the ABS observer does not significantly improves the precision of x_3 and x_6. As for the separation unit case study, this problem is due to their small measurement error variances compared to node imbalance variances. Fig. 5-6 shows that the global indices η_t and η_u decrease as the time lag increases in scenario 5. This confirms the detailed results presented in Tables 5-7 and 5-8. For l larger than 5, there is almost no improvement of DR performances. In the remaining simulation runs, only 5 time lags are considered for the ABS observer.

Table 5-8: Variance reduction for SS, ABS and KF observers (flotation circuit).

Variable	$\eta_{i,i}$ (%)							
	ABS-0 (ST)	ABS-1	ABS-2	ABS-5	ABS-10	ABS-20	SS	KF
x_1	27.0	39.3	42.3	43.0	43.0	42.9	-78.4	56.8
x_2	43.2	50.3	52.6	54.1	54.1	54.2	-13.6	99.2
x_3	1.4	1.6	1.7	1.8	1.8	1.8	0.0	99.2
x_4	60.4	61.6	61.8	61.8	61.8	61.8	57.2	98.1
x_5	31.9	33.7	34.6	35.6	35.9	35.9	24.1	99.4
x_6	0.3	0.3	0.3	0.3	0.3	0.3	0.3	99.1
x_7	47.3	50.1	51.5	52.9	53.3	53.3	35.7	97.5

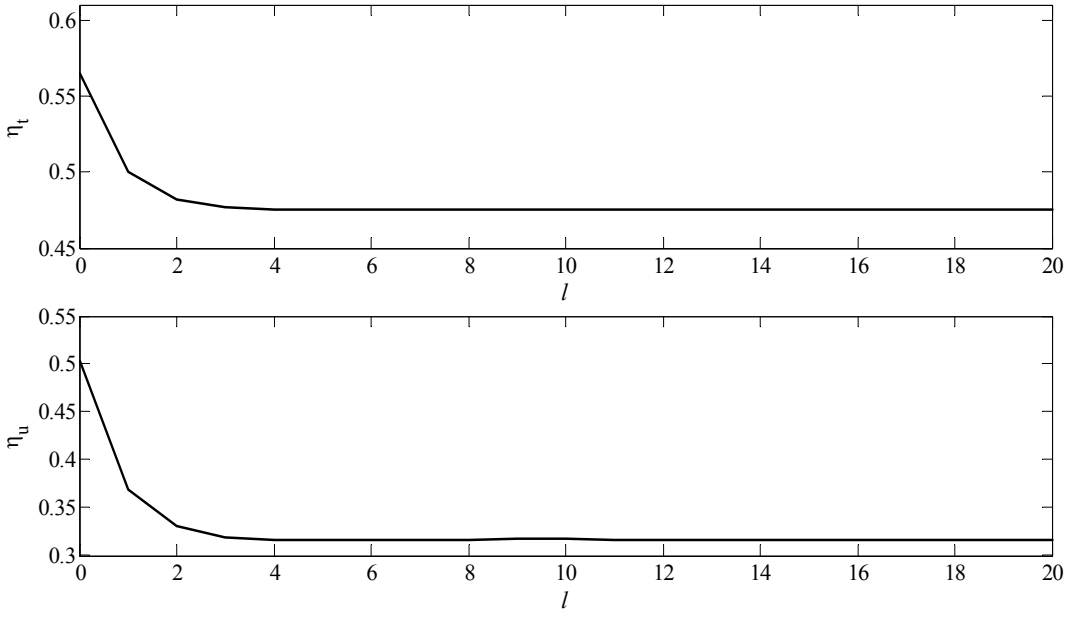

Fig. 5-6: Performance indices as a function of l in Scenario 5 (flotation circuit).

Table 5-9 gives values of η_t and η_u for all testing scenarios. Although the flotation circuit is more complex than the single node separation unit, similar conclusions can be drawn. The main difference is that the SS observer produces estimates that are more precise than the measurements for a wider range of regimes (Scenarios 1 to 4). This is caused by the higher filtering effect induced by circulating streams that reduces inventory fluctuations.

Table 5-9: η_t and η_u for SS, ABS and KF observers (flotation circuit).

Scenario No.	η_t				η_u			
	ABS-0 (ST)	ABS-5	SS	KF	ABS-0 (ST)	ABS-5	SS	KF
1	0.343	0.343	0.343	0.000	0.096	0.096	0.096	0.000
2	0.346	0.346	0.346	0.011	0.102	0.102	0.103	0.003
3	0.401	0.382	0.433	0.061	0.209	0.170	0.282	0.031
4	0.495	0.430	0.727	0.111	0.385	0.248	0.893	0.066
5	0.565	0.475	1.180	0.153	0.503	0.316	1.830	0.093

To test the robustness of the ABS observer in the presence of modeling uncertainties, it is assumed that the separation coefficients of the flotation circuit fluctuate randomly around their nominal values with various standard deviations. Five cases corresponding to the different level of variation of the separation coefficients of the rougher, scavenger, and cleaner units (α_r, α_s, and α_c) are proposed as presented in Table 5-10. In each case, the standard deviation of feed rate fluctuations is 15 %. All observers are tuned for case 3. Other cases thus illustrate observer performances with inappropriate tunings. The SS observer, which has no tuning parameter for model uncertainty, is omitted in this comparison. Values of η_t and η_u obtained for the five test cases are given in Table 5-10. Roughly, the ABS observer demonstrates a superior robustness against modeling errors than the KF observer.

Table 5-10: η_t and η_u for the robustness test (σ_{x_1} = 15 %).

Case	σ_{α_r} %	σ_{α_s} %	σ_{α_c} %	η_t			η_u		
				ABS-0 (ST)	ABS-5	KF	ABS-0 (ST)	ABS-5	KF
1	0	0	0	0.458	0.408	0.103	0.325	0.213	0.065
2	2	2	1	0.460	0.409	0.112	0.328	0.214	0.082
3	**5**	**2**	**1**	**0.467**	**0.412**	**0.143**	**0.335**	**0.217**	**0.103**
4	5	5	2	0.470	0.413	0.154	0.338	0.218	0.136
5	10	5	2	0.494	0.421	0.273	0.359	0.227	0.216

To emphasize the performance degradation of an incorrectly tuned observer, the following normalized index is proposed:

$$q_i = \frac{\eta(3,i) - \eta(i,i)}{\eta(i,i)} \qquad i = 1, 2, \cdots, 5 \tag{5-44}$$

where $\eta(3,i)$ is the performance index (trace or user-defined index) for test case i when the observer is tuned for case 3. Therefore, $\eta(i,i)$ is the performance index for test case i for a correctly tuned observer.

Table 5-11 presents normalized trace and user-defined indices $q_{t,i}$ and $q_{u,i}$. In general, all observers show growing indices when model parameters depart from tuned conditions. In comparison with the KF observer, the ABS-5 observer shows a superior performance and its maximum deviation from the well-tuned situation is less than 1 %. Also, the ST observer shows good performances with a deviation slightly larger than the ABS-5 observer one. Although the KF observer still has better results in term of variance reduction (Table 5-10), it demonstrates the most degraded performance (Table 5-11). In case 5, the deviation values for KF are 43 % and 68.7 % for $q_{t,5}$ and $q_{u,5}$, respectively. These results reveal that, although the well-tuned KF gives optimal performances, it is very sensitive to modeling

uncertainty, while ABS-5 observer shows encouraging performances in the presence of modeling errors.

Table 5-11. Normalized indices for the robustness test (σ_{x_1} = 15 %).

Case	σ_{α_r} %	σ_{α_s} %	σ_{α_c} %	$q_{t,i}$ (%)			$q_{u,i}$ (%)		
				ABS-0 (ST)	ABS-5	KF	ABS-0 (ST)	ABS-5	KF
1	0	0	0	0.3	0.3	19.5	1.9	1.9	31.0
2	2	2	1	0.1	0.2	2.8	1.0	1.4	2.0
3	**5**	**2**	**1**	**0.0**	**0.0**	**0.0**	**0.0**	**0.0**	**0.0**
4	5	5	2	0.5	0.2	6.2	0.2	0.3	20.0
5	10	5	2	1.7	0.6	43.0	0.6	0.4	68.7

5.6 Conclusion

Efficient and safe plant operation can only be achieved by an accurate measurement of process variables. Data reconciliation is a useful technique to provide a precise estimation of measured or unmeasured variables. From a practical point of view, the trade-off between modeling effort and estimate precision is important for a successful implementation of such a technique. To estimate the process dynamic states, this chapter has proposed an observer based on a simple mass conservation sub-model including the autocovariance of node imbalances as additional information that improves the estimation precision. The observer has been evaluated using two simulated benchmark plants operating in a stationary regime. Comparisons with classical sub-model based observers and the Kalman Filter have been performed to assess its performance and robustness.

The proposed observer has provided more precise estimates than steady-state and standard stationary observers, particularly when the dynamic regime of the process becomes important compared to measurement errors. It has exhibited more robust performances against modeling errors compared to the Kalman filter. Although the Kalman filter has led

to optimal performances when perfectly tuned, it is more sensitive to modeling errors than the proposed observer. Also, it has been observed that autocovariance function could be truncated after few time lags, thus limiting the modeling effort. In this study, 5 time lags were sufficient to obtain a satisfactory precision improvement. Linear balance equations were considered in order to give analytical expressions for estimates and covariance matrices and, also, to simplify comparisons. However, the proposed method could be extended to bilinear cases following an approach similar to the one suggested by Makni et al. (1995a) applied to standard stationary observers. It can be concluded that the proposed observer is able to cope with process dynamics, offers interesting estimation performances, is robust against plant variations and requires reasonable modeling efforts.

Chapter 6

Determining a Dynamic Model for Flotation Circuits Using Plant Data to Implement a Kalman Filter for Data Reconciliation[4]

Résumé

La réconciliation de données est largement appliquée pour améliorer la précision et la fiabilité des mesures des usines. Elle repose sur des modèles de procédé allant des simples équations de conservation de la masse et de l'énergie jusqu'aux modèles causaux. La précision des données réconciliées dépend principalement de la complexité et de la qualité des modèles des usines utilisés pour développer les observateurs utilisés pour la réconciliation des données. En pratique, la difficulté d'obtenir des modèles détaillés handicape l'application d'observateurs puissants comme le filtre de Kalman. L'objectif de cette étude est de proposer une méthodologie afin de construire un modèle simple pour un circuit de flottation qui permet la mise en œuvre d'un filtre de Kalman pour la réconciliation de données dynamiques. Cette approche de modélisation est essentiellement basée sur les informations de la topologie de l'usine, les conditions nominales de fonctionnement, et les données historiques. Les résultats de simulation montrent que l'application du filtre de Kalman basé sur un modèle empirique grossier, mais correctement réglé, donne de meilleures estimations que celles obtenues avec les observateurs basés sur de simples sous-modèles.

[4] Amir Vasebi, Éric Poulin & Daniel Hodouin (2015), Determining a dynamic model for flotation circuits using plant data to implement a Kalman filter for data reconciliation. Submitted to *Minerals Engineering*, 83, 192-200.

Abstract

Data reconciliation is extensively applied to improve the accuracy and reliability of plant measurements. It relies on process models ranging from simple mass and energy conservation equations to complete causal models. The precision of reconciled data mainly depends on the complexity and quality of plant models used to develop data reconciliation observers. In practice, the difficulty of obtaining detailed models prevents the application of powerful observers like the Kalman filter. The objective of this study is to propose a methodology to build a model for a flotation circuit to support the implementation of a Kalman filter for dynamic data reconciliation. This modeling approach extracts essential information from the plant topology, nominal operating conditions, and historical data. Simulation results illustrate that applying a Kalman filter based on a rough empirical model that has been correctly tuned gives better estimates than those obtained with sub-model based observers.

6.1 Introduction

Data reconciliation is widely employed in the mineral processing industry. The method was introduced by Kuehn and Davidson (1961), and many refinements were proposed over the years as illustrated, among others, by Bagajewicz (2010). Data reconciliation aims at improving the accuracy and the reliability of plant data. It attenuates the effect of measurement errors and allows the estimation of unmeasured variables under favorable conditions while ensuring that reconciled values satisfy the constraints imposed by the process model. Several applications such as plant monitoring, process control or real-time optimization take advantage of improved state estimations (Narasimhan, 2012).

Depending on the target use of reconciled data, different algorithms could be selected. Steady-state data reconciliation is well suited for the estimation of underlying steady-state operating conditions. It generally relies on static mass and energy conservation constraints that could be extracted from plant flow diagrams. For slow dynamic regimes, stationary observers (Makni et al., 1995; Vasebi et al., 2012a), generalized dynamic observers (Darouach and Zasadzinski, 1991; Rollins and Devanathan, 1993; Xu and Rong, 2010) and integral linear dynamic observers (Bagajewicz and Jiang, 1997; Tona et al., 2005) are

valuable options. In addition to mass conservation constraints, these observers require inventory variations to be either modeled or measured. Finally, the Kalman filter (Kalman, 1960), which is based on a dynamic causal model of the plant, is able to effectively cope with highly dynamic regimes. A survey on dynamic data reconciliation observers and their performances have been presented by Vasebi et al. (2012b).

The Kalman filter being the general representation of most observers based on sub-models of a plant (Lachance et al., 2006a), one may think this algorithm is widely implemented for a large class of data reconciliation problems in the mineral processing industry. Surprisingly, this is not the case as reflected by the relatively few number of applications reported in the literature. Moreover, the vast majority of data reconciliation software offered on the market only considers the steady-state case (Bagajewicz, 2010). The difficulty of developing a reliable dynamic causal model is generally evoked as the main explanation of this situation.

The objective of this chapter is to propose a simple method to build a model of a flotation circuit to support the implementation of a Kalman filter for dynamic data reconciliation. The necessary information is extracted from the plant topology, nominal operating conditions and historical data. Simulation results support that assumptions introduced during the model elaboration does not impair the reconciliation performances while greatly simplifying the development.

Section 6.2 begins with a description of the plant model. To simplify the presentation, equations are given for a single separation unit even though the approach is general and is applicable to more complex circuits. Extraction of parameters for a single separation unit is detailed in Section 6.3. Section 6.4 first assesses the assumptions made in the modeling phase and then compares the data reconciliation performances of the Kalman filter with the ones obtained from stationary observers. Evaluations are performed through simulation of a flotation circuit based on a phenomenological model. Concluding remarks are given in Section 6.5.

6.2 Plant Model

This section describes the plant model used for designing the Kalman filter. For this purpose, a flotation unit is modeled using few low order transfer functions. For the Kalman filter implementation, this model adds deterministic aspects (i.e. gains and time constants) which create additional information increasing the observer efficiency while it decreases the role of the stochastic elements which, in the sub-model observers, embeds the missing deterministic information of causal models. Although it may seem ambitious to properly model a complex flotation plant using such transfer functions, this approach lead to better estimates than other sub-model based observers for data reconciliation, as illustrated later.

The plant is assumed to operate in stationary regime implying that, over a long period of time, the process stream properties, as well as inventories, randomly fluctuate around a constant value. In practice, this is a representative description of a wide range of industrial processes. To seek simplicity and bring the problem to a linear case, only the valuable mineral flowrates are here considered as process variables. This assumption does not compromise the generality of the proposed technique, since literature has already introduced some innovative methods to transform the bilinear data reconciliation problem to a linear one (Crowe, 1989; Vasebi et al., 2014). Therefore, it could easily be applied to chemical/physical species flowrates as well as total flowrates. In the following paragraphs, the basic idea and formulation of the model is detailed for a single node separation unit. In Section 6.4, which presents simulation results, the approach is extended to a flotation circuit with three separation nodes.

The flow sheet of the separation unit, involving three streams (feed, concentrate and reject), is presented in Fig. 6-1. The main idea is to model this unit using three empirical models and assign corresponding uncertainties. The structure of such a model is illustrated in Fig. 6-2. Only the state variations x_d around the operating point are considered and, therefore, nominal values x_n should be added if global values are desired. It is assumed that feed variations x_{d_1} are generated by filtering a zero-mean normally distributed white noise ξ via a transfer function G_f where the corresponding time constant T_f represents the dynamics of feed disturbances induced by the material itself or generated by previous

processing stages. In this process model, the gain of concentrate and reject transfer functions are constrained so that steady-state mass conservation is obeyed for each species.

The parametric representation of transfer functions in discrete time form and their corresponding poles are shown in Table 6-1, where T_s stands for the process sampling time, and T_c and T_r are time constants that can be obtained based on the selected species residence time toward the concentrate and reject streams, respectively, and α represents the valuable mineral separation coefficient. When several species are considered, additional transfer functions with corresponding separation coefficients and time constants can be added. It is worth noticing that these parameters, i.e. time constants, poles, and separation coefficients could be time variant. In Table 6-1, b_i is only used to compact the model presentation and is defined as:

$$b_i = 1 - a_i \qquad i = 1,2,3 \tag{6-1}$$

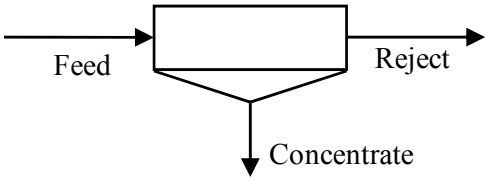

Fig. 6-1: Separation unit flow diagram.

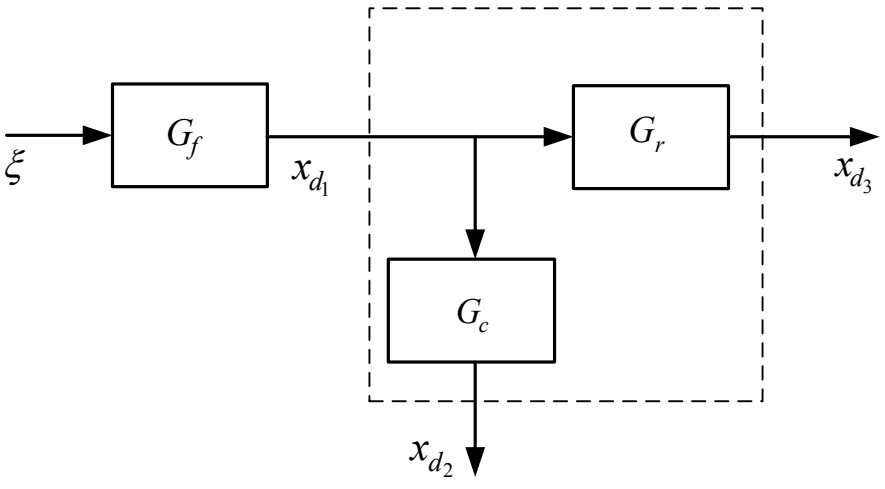

Fig. 6-2: Separation unit model.

Table 6-1: Transfer functions of the separation unit model.

	Input Filter	Concentrate	Reject
Discrete time transfer functions	$G_f(z^{-1}) = \frac{b_1 z^{-1}}{1 - a_1 z^{-1}}$	$G_c(z^{-1}) = \alpha \frac{b_2 z^{-1}}{1 - a_2 z^{-1}}$	$G_r(z^{-1}) = (1-\alpha) \times \frac{b_3 z^{-1}}{1 - a_3 z^{-1}}$
Poles	$a_1 = e^{-\left(\frac{T_s}{T_f}\right)}$	$a_2 = e^{-\left(\frac{T_s}{T_c}\right)}$	$a_3 = e^{-\left(\frac{T_s}{T_r}\right)}$

Since first-order transfer functions cannot perfectly describe the complex behavior of the valuable mineral flow inside the flotation cell, uncertainty is introduced to represent the model imperfection. This uncertainty is characterized using a covariance matrix. The separation unit model can be presented in the following state-space format:

$$x_d(k+1) = A(k)x_d(k) + B(k)\xi(k) \tag{6-2}$$

where x_d stands for the state vector representing the flowrate variations:

$$x_d(k) = \begin{bmatrix} x_{d_1}(k) & x_{d_2}(k) & x_{d_3}(k) \end{bmatrix}^T \tag{6-3}$$

The coefficient matrices are given by

$$A(k) = \begin{bmatrix} a_1(k) & 0 & 0 \\ \alpha(k)b_2(k) & a_2(k) & 0 \\ (1-\alpha(k))b_3(k) & 0 & a_3(k) \end{bmatrix} \tag{6-4}$$

$$B(k) = \begin{bmatrix} b_1(k) & 0 & 0 \end{bmatrix}^T \tag{6-5}$$

In the present case, it is assumed that any variation in the feed (either in terms of flowrate or composition) under a stationary operating regime leads to normally distributed variations in the states and parameters. Therefore,

$$x_{d_i}(k) \sim N(0, \Sigma_{x_i}) \tag{6-6}$$

where Σ_{x_i} is the variance of the process state x_{d_i} that is strongly cross and autocorrelated. The assumption of normally distributed parameter variations is investigated and supported in the simulation and results section.

In a plant, the variation of feed, process states, and parameters are dependent, i.e. changing one of them affects the others. For instance, increasing the valuable mineral feed can change the material residence time inside the cell. Moreover, these variables and parameters are time correlated. In the current study, as mentioned before, the objective is to facilitate the development of the plant model used for data reconciliation purposes. Therefore, several assumptions are made that might not perfectly reflect all observed phenomena. Here, it is assumed that the model parameters, a_i and α, are white noises with the following properties, although they are obviously colored by the process dynamics:

$$a_i(k) = a_{i_n} + \tilde{a}_i(k) \quad , \quad \tilde{a}_i(k) \sim N(0, \Sigma_{a_i}) \tag{6-7}$$

$$\alpha(k) = \alpha_n + \tilde{\alpha}(k) \quad , \quad \tilde{\alpha}(k) \sim N(0, \Sigma_{\alpha}) \tag{6-8}$$

where the subscript *n* stands for the nominal value and ~ represents the variation. Using Eq. 6-1,

$$\tilde{b}_i(k) = -\tilde{a}_i(k) \quad , \quad \tilde{b}_i(k) \sim N(0, \Sigma_{a_i}) \tag{6-9}$$

so these variables, taking into account the appropriate sign, can easily be interchanged in the upcoming developments for convenience. Regarding model parameter variations, the process model (Eq. 6-2) can alternatively be written as:

$$x_d(k+1) = A_n x_d(k) + \tilde{A}(k) x_d(k) + \left(B_n + \tilde{B}(k)\right)\xi(k) = A_n x_d(k) + w(k) \tag{6-10}$$

where

$$A_n = \begin{bmatrix} a_{1n} & 0 & 0 \\ \alpha_n b_{2_n} & a_{2n} & 0 \\ (1-\alpha_n) b_{3_n} & 0 & a_{3n} \end{bmatrix} \quad , \quad B_n = \begin{bmatrix} b_{1_n} & 0 & 0 \end{bmatrix}^T \tag{6-11}$$

and w is the stochastic part of the model representing modeling uncertainty and feed variation. Here, $\widetilde{A}$ and $\widetilde{B}$ stand for

$$\widetilde{A}(k)=\begin{bmatrix} \widetilde{a}_1(k) & 0 & 0 \\ -\alpha_n\,\widetilde{a}_2(k)+\widetilde{\alpha}(k)b_{2_n}-\widetilde{\alpha}(k)\widetilde{a}_2(k) & \widetilde{a}_2(k) & 0 \\ -(1-\alpha_n)\,\widetilde{a}_3(k)-\widetilde{\alpha}(k)b_{3_n}+\widetilde{\alpha}(k)\,\widetilde{a}_3(k) & 0 & \widetilde{a}_3(k) \end{bmatrix},\ \widetilde{B}(k)=\begin{bmatrix}-\widetilde{a}_1(k) & 0 & 0\end{bmatrix}^T \quad (6\text{-}12)$$

In expanded format, w can be expressed by:

$$w(k)=\begin{bmatrix} w_1(k) \\ w_2(k) \\ w_3(k) \end{bmatrix}=\begin{bmatrix} \widetilde{a}_1(k)x_{d_1}(k)+\left(1-a_{1_n}-\widetilde{a}_1(k)\right)\xi(k) \\ \left(-\alpha_n\,\widetilde{a}_2(k)+\widetilde{\alpha}(k)b_{2_n}-\widetilde{\alpha}(k)\widetilde{a}_2(k)\right)x_{d_1}(k)+\widetilde{a}_2(k)\,x_{d_2}(k) \\ \left(-(1-\alpha_n)\,\widetilde{a}_3(k)-\widetilde{\alpha}(k)b_{3_n}+\widetilde{\alpha}(k)\widetilde{a}_3(k)\right)x_{d_1}(k)+\widetilde{a}_3(k)\,x_{d_3}(k) \end{bmatrix} \quad (6\text{-}13)$$

As the uncertainty, w can be characterized using statistical properties like covariance matrix. The covariance of w can be calculated using variance and covariance of the product of random variables as proposed by Goodman (1960) and Bohrnstedt and Goldberger (1967), respectively.

$$\mathrm{cov}(w)=\begin{bmatrix} \Sigma_{11} & \Sigma_{12} & \Sigma_{13} \\ \Sigma_{21} & \Sigma_{22} & \Sigma_{23} \\ \Sigma_{31} & \Sigma_{32} & \Sigma_{33} \end{bmatrix} \quad (6\text{-}14)$$

Considering the autocorrelation of x_{d_1} and using the properties of geometric progression series, one can obtain:

$$\begin{cases} \Sigma_{11}=\mathrm{var}(w_1)=\Sigma_{a_1}\Sigma_{x_1}+b_{1_n}^2\Sigma_\xi+\Sigma_{a_1}\Sigma_\xi \\ \Sigma_{22}=\mathrm{var}(w_2)=\left(\alpha_n^2\Sigma_{a_2}+b_{2_n}^2\Sigma_\alpha+\Sigma_{a_2}\Sigma_\alpha+2\alpha_n^2 b_{2_n}\dfrac{a_{2_n}}{1-a_{2_n}^2}\Sigma_{a_2}\right)\Sigma_{x_1}+\Sigma_{a_2}\Sigma_{x_2} \\ \Sigma_{33}=\mathrm{var}(w_3)=\left((1-\alpha_n)^2\Sigma_{a_3}+b_{3_n}^2\Sigma_\alpha+\Sigma_{a_3}\Sigma_\alpha+2(1-\alpha_n)^2 b_{3_n}\dfrac{a_{3_n}}{1-a_{3_n}^2}\Sigma_{a_3}\right)\Sigma_{x_1}+\Sigma_{a_3}\Sigma_{x_3} \end{cases} \quad (6\text{-}15)$$

and

$$\Sigma_{ij} = \mathrm{cov}(w_i, w_j) = \begin{cases} -b_{i_n} b_{j_n} \Sigma_\alpha \Sigma_{x_1} & i, j \in \{2,3\} \,\&\, i \neq j \\ 0 & \text{otherwise} \end{cases} \tag{6-16}$$

For the transfer function of the input filter G_f given in Table 6-1, a unit gain has been assigned. This implies that the uncertainty on Σ_ξ has been neglected and not considered in the development of Eqs. 6-15 and 6-16. When the process state and parameter uncertainties covariances are known, the overall model uncertainty could easily be evaluated using Eqs. 6-15 and 6-16. To calculate $\mathrm{cov}(w)$, Σ_{x_i} can be obtained from the state-space model of Eq. 6-10:

$$\begin{cases} \Sigma_{x_1} = \left(a_{1_n}^2 + \Sigma_{a_1}\right)\Sigma_{x_1} + b_{1_n}^2 \Sigma_\xi + \Sigma_{a_1}\Sigma_\xi \\ \Sigma_{x_2} = \left(\alpha_n^2 b_{2_n}^2 + 2\alpha_n^2 b_{2_n}^2 \dfrac{a_{2_n}^2}{1-a_{2_n}^2} + \alpha_n^2 \Sigma_{a_2} + b_{2_n}^2 \Sigma_\alpha + \Sigma_{a_2}\Sigma_\alpha + 2\alpha_n^2 b_{2_n} \dfrac{a_{2_n}}{1-a_{2_n}^2}\Sigma_{a_2} \right)\Sigma_{x_1} + \left(a_{2_n}^2 + \Sigma_{a_2}\right)\Sigma_{x_2} \\ \Sigma_{x_3} = \left((1-\alpha_n)^2 b_{3_n}^2 + 2(1-\alpha_n)^2 b_{3_n}^2 \dfrac{a_{3_n}^2}{1-a_{3_n}^2} + (1-\alpha_n)^2 \Sigma_{a_3} + b_{3_n}^2 \Sigma_\alpha + \Sigma_{a_3}\Sigma_\alpha + 2(1-\alpha_n)^2 b_{3_n} \dfrac{a_{3_n}}{1-a_{3_n}^2}\Sigma_{a_3} \right)\Sigma_{x_1} \\ \qquad + \left(a_{3_n}^2 + \Sigma_{a_3}\right)\Sigma_{x_3} \end{cases} \tag{6-17}$$

Using the first relation in Eq. 6-17, Σ_{x_1} can be calculated and then substituted in the next two equations to get Σ_{x_2} and Σ_{x_3}, therefore allowing the evaluation of $\mathrm{cov}(w)$ from the model parameter nominal values and uncertainties. In Section 6.3, the way of obtaining these parameters and their associated uncertainties in practice is discussed.

The following measurement equation is coupled with Eq. 6-2 to build the observer model:

$$y(k) = Cx(k) + v(k) = Cx_d(k) + Cx_n + v(k) \tag{6-18}$$

where $x(k)$ is the true process state including dynamic variation and nominal value, and

$$y(k) = \begin{bmatrix} y_1(k) & y_2(k) & y_3(k) \end{bmatrix}^T \tag{6-19}$$

and x_n stands for the vector of the process states nominal value,

$$x_n = \begin{bmatrix} x_{n_1} & x_{n_1} & x_{n_3} \end{bmatrix}^T = \begin{bmatrix} x_{n_1} & \alpha_n x_{n_1} & (1-\alpha_n) x_{n_1} \end{bmatrix}^T \tag{6-20}$$

The vector of white noises $v(k)$, which represents the random measurement errors, is characterized by:

$$v(k) \sim N(0, \Sigma_v) \tag{6-21}$$

In the present study, it is assumed that all process variables x are measured, so the observation matrix C comes down to an identity matrix.

6.3 Evaluation of Model Parameters and Uncertainties

This section proposes a procedure to estimate the parameters of the model presented in Eq. 6-10 and uncertainties introduced in Eqs. 6-15, 6-16, and 6-17. A list of model parameters and uncertainties that should be estimated is summarized in Table 6-2. To estimate them, it is assumed that a set of historical data is available (at least, for an operation period of one month). In the case that continuous measurements are not available for some of the flowrates, either the nominal operating states or plant design information can be used to establish the model. The nominal operating states can be evaluated, from time to time, by carefully planned sampling campaigns, without permanent installation of flowmeters on all the streams. Moreover, when some flowrates are unmeasured, bilinear steady-state data reconciliation can be employed to estimate the steady-state value of flowrates using redundant information obtained from the concentration of species in the collected samples during sampling campaigns. So unavailability of continuous measurements for a number of streams does not impair the generality and applicability of the proposed approach.

Table 6-2: Model parameters and uncertainties to be estimated.

Parameters	Uncertainties
α_n	Σ_α
a_{i_n} , $i = 1,2,3$	Σ_{a_i} , $i = 1,2,3$
	Σ_ξ
	Σ_v

6.3.1 Separation coefficient

To find a suitable value for the nominal separation coefficient α_n and its corresponding uncertainty Σ_α, different techniques could be applied. The simplest way is to use the average value of measurements $\bar{y}_i$:

$$\alpha_n = \frac{\bar{y}_2}{\bar{y}_2 + \bar{y}_3} \tag{6-22}$$

The nominal values of process variables x_i, taken from plant design information or steady-state reconciled values, can also be used to estimate α_n. To calculate Σ_α, measured values are selected,

$$\Sigma_\alpha = \mathrm{var}\left(\alpha(k)\right) = \mathrm{var}\left(\frac{y_2(k)}{y_2(k) + y_3(k)}\right) \tag{6-23}$$

6.3.2 Time constants of the separation unit

Regarding the discrete time representation of the process, poles a_i can be obtained from reasonable estimates of the time constants calculated from plant information and historical measured data. In the present case-study, it is assumed that time constants T_c and T_r can be represented by the valuable mineral mean residence times toward concentrate and reject streams:

$$T_r(k) = \frac{m(k)}{F_R(k)} \tag{6-24}$$

$$T_c(k) = \frac{m(k) + m_c(k)}{F_C(k)} \tag{6-25}$$

where m and m_c are respectively the valuable mineral masses in the pulp and froth phases, and F_R and F_C stands for mass mineral flowrates in the reject and concentrate streams. The slurry phase behaves as a perfect mixer while the froth phase behavior is close to a plug flow reactor. These are the modeling hypotheses used for simulating the plant in

Section 6.4. However for simplifying the estimation of both time constants for the Kalman Filter, perfect mixing conditions are assumed in the two phases. Therefore *m* and m_c can be estimated from the measurement of the concentrate and reject mineral concentrations, and estimation of the slurry volumes and solid percent of the two phases. When continuous measurements are available, the time constants can be updated at time *k*. If they are not, historical data can be used. The poles $a_2(k)$ and $a_3(k)$ are then estimated:

$$\begin{cases} a_2(k) = e^{-\left(\frac{T_s}{T_c(k)}\right)} \\ a_3(k) = e^{-\left(\frac{T_s}{T_r(k)}\right)} \end{cases} \tag{6-26}$$

Nominal values a_{2_n} and a_{3_n} can be calculated by averaging of a_2 and a_3 signals. In Section 6.4, it is shown that when the feed has normally distributed stationary variations, T_c and T_r almost follow a log-normal distributions and so normal distributions can be assigned to a_2 and a_3. This idea is supported by simulation results. The variance of the poles is estimated by usual statistical techniques.

6.3.3 Parameters and uncertainties of the feed transfer function

To estimate the parameters of the feed transfer function, the autocovariance of measurement y_1 with l time lags, i.e. $C_{y_1}(l)$, calculated from historical data can be used. Using Eq. 6-18,

$$y_1(k) = x_{d_1}(k) + x_{n_1} + v_1(k) \tag{6-27}$$

Since v_1 is a white noise, it only contributes to $C_{y_1}(0)$. This fact can be utilized to separate Σ_{v_1} and Σ_{x_1}, and consequently estimate a_{1_n}, Σ_{a_1} and Σ_{ξ}. For a given y_1, a typical autocovariance function is shown in Fig. 6-3. For lag zero,

$$C_{y_1}(0) = \Sigma_{x_1} + \Sigma_{v_1} \tag{6-28}$$

while for other time lags, the assumption of a first-order autoregressive system leads to:

$$C_{y_1}(l) = (a_{1_n})^l \Sigma_{x_1} \tag{6-29}$$

Moreover, the input transfer function implies that:

$$\Sigma_\xi = \left(\frac{1 - a_{1_n}{}^2}{(1 - a_{1_n})^2} \right) \times \Sigma_{x_1} \tag{6-30}$$

These relations can be used to estimate a_{1_n} and Σ_{x_1}, and then calculate Σ_ξ. For this purpose, an estimation technique based on autocovariance function fitting is applied. In other words, a_{1_n}, Σ_{x_1} and Σ_{v_1} are adjusted to produce an autocovariance function that fits the one calculated using measurements. To select the appropriate number of time lags used in Eq. 6-29, a reasonable solution is to choose the number of lags *h* over which the value of the autocovariance function is significant according to the 95% confidence intervals. Fig. 6-3 illustrates the autocovariance function including 95% confidence interval line (dash-line).

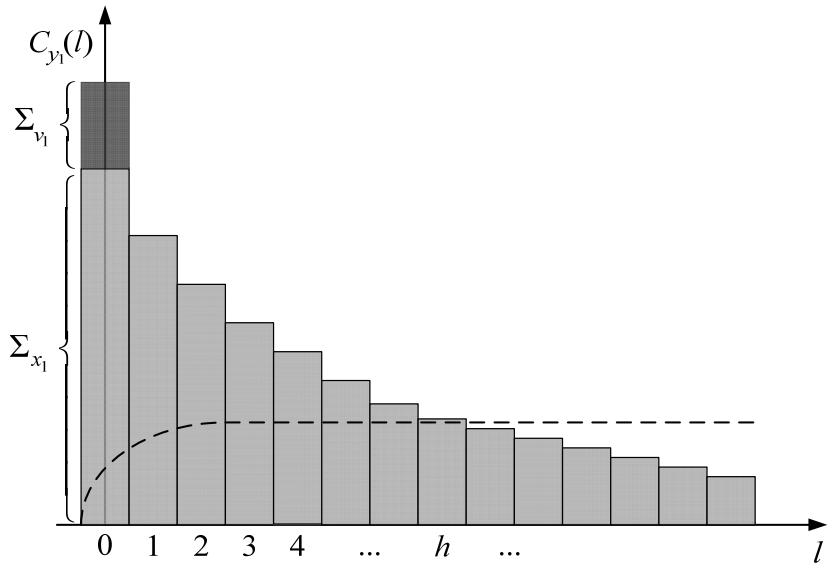

Fig. 6-3: Measurement autocovariance function.

An iterative estimation approach is applied that minimizes the least square criterion (see Fig. 6-4):

$$J = \sum_{l=0}^{h} \left(C_{y_1}(l) - \hat{C}_{y_1}(l) \right)^2 \tag{6-33}$$

where $\hat{C}_{y_1}$ is the estimated autocovariance function that satisfies Eqs. 6-28 to 6-30. Lachance et al. (2007) presented an alternative method that uses two successive time lags of the autocovariance function to formulate the estimation problem and then apply the simple least squares solution.

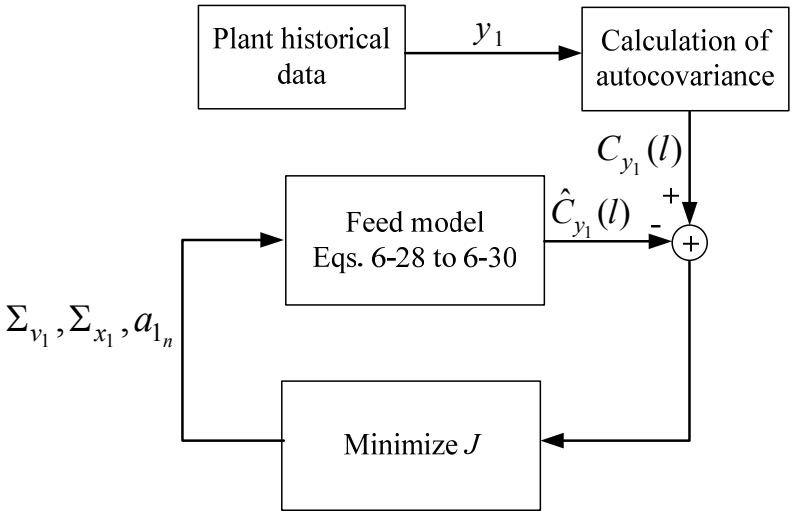

Fig. 6-4: Iterative approach to estimate the feed model parameters and corresponding uncertainties.

The proposed approach provides an estimation of Σ_{v_1}, Σ_{x_1}, a_{1_n} and Σ_{ξ}. To find Σ_{a_1}, it is necessary to generate several a_1 and then calculate the variance of them. For this purpose, the whole historical data set is fractioned into smaller sets and then the above-mentioned algorithm is repeated to produce a set of a_1 and calculate its variance Σ_{a_1}.

6.3.4 Measurement uncertainty

To apply the Kalman filter, the measurement error variance Σ_v is required. Using Eq. 6-18 when $C = I$, it can simply be calculated by:

$$\Sigma_y = \text{var}(y) = \text{var}(x + v) \tag{6-32}$$

where Σ_y is the variance of the measurements. Since *x* and *v* are independent,

$$\Sigma_v = \Sigma_y - \Sigma_x \tag{6-33}$$

where Σ_x is calculated using Eq. 6-17. Eq. 6-33 implies that any incorrect estimation of Σ_x is compensated by Σ_v and the total variance observed in the measured data is preserved.

6.4 Simulation Results and Discussion

A phenomenological simulator of a flotation circuit is used as the case study. The simulator is developed based on mass conservation equations, and a first-order kinetic is assumed to model the flotation process. For the collection zone, a perfect mixing model is considered while the froth zone is simulated using a plug flow model. The simulator takes into account the particle size/volume distributions while bubble size distribution is neglected, i.e. it only employs the air volume inside the tank. Entrainment that brings water and non-floatable particles into the concentrate is also considered. In order to simulate the particle drainage, it is assumed that the flotation rate constant is inversely affected by froth depth. The effect of several manipulated variables, including collector and frother concentrations, air flow, and interface level, are modeled. Complete details of the simulator are available in Chapter 7. The flotation circuit flow sheet is depicted in Fig. 6-5. The circuit consists of three stages, i.e. rougher, cleaner, and scavenger, and eight streams.

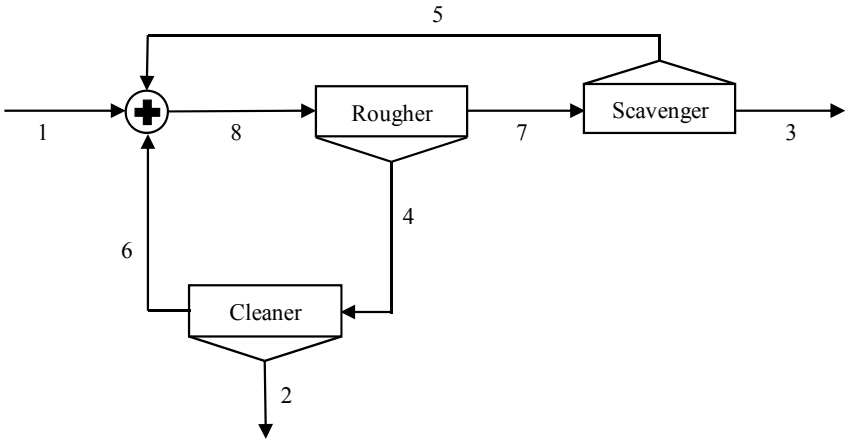

Fig. 6-5: Flotation circuit flow sheet.

6.4.1 Distribution of model parameters uncertainties

As already mentioned, only flowrates of one valuable mineral have been considered as the process variables, but the approach can be extended to multi-mineral systems. In the above sections, it has been assumed that a_i and α are normally distributed around a mean value when feed properties exhibit normally distributed stationary variations. Fig. 6-6 shows the stationary variation of the valuable mineral in the feed rate. This fluctuation results from stationary variations of the feed flow and grade generated by filtering normally distributed white noises with suitable time constants. Probability density functions of time constants, poles and separation coefficient for the rougher cell are presented in Fig. 6-7 to support the assumption of normal distribution. Although a log-normal distribution roughly fits the time constants variations, their corresponding poles acceptably fit a normal distribution. Obviously these fits are not perfect, but they are good enough to make the assumption reasonable. For separation coefficients, the normal distribution shows almost a perfect match.

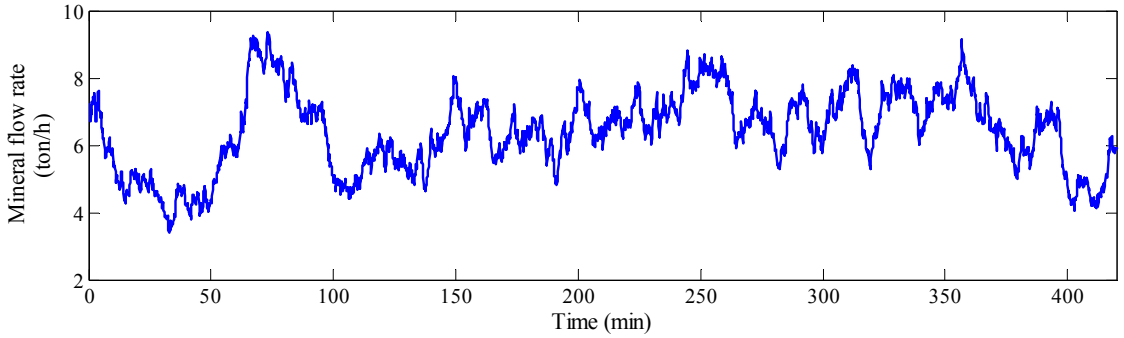

Fig. 6-6: Stationary variation of the valuable mineral feed rate.

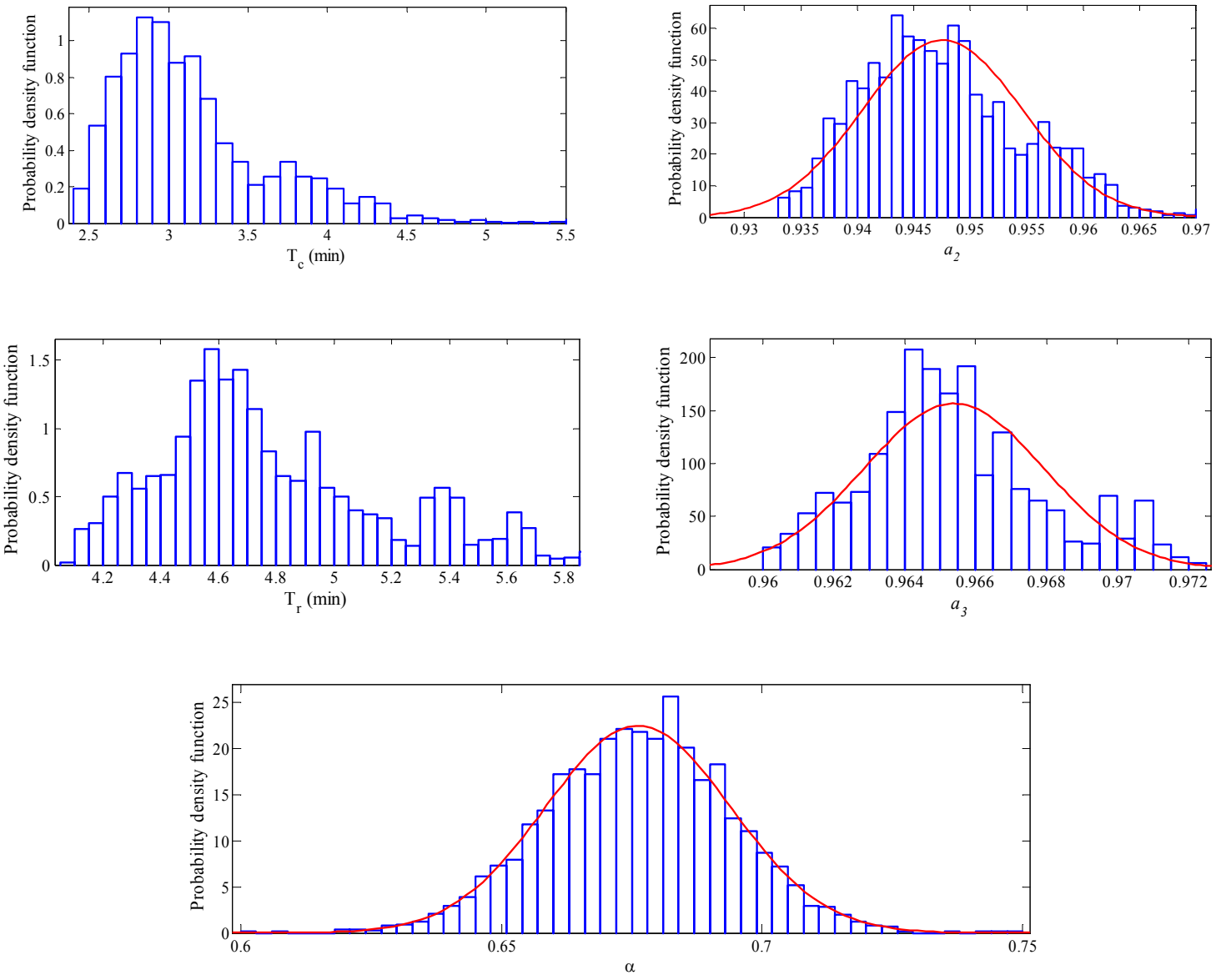

Fig. 6-7: Distribution of time constants (T_c, T_r), poles (a_2, a_3) and separation coefficient (α).

6.4.2 Estimation of model parameters and uncertainties

In this section, the proposed estimation approach is applied to the flotation circuit simulator, and results are presented. The procedure has been performed when feed rate and grade vary with standard deviations of 10% and 15% of their nominal values respectively, i.e. 100 t/h and 6.48%. Data is collected from 30 days simulation with a sampling time of 10 seconds, although slightly longer sampling period could have been selected. Here it is assumed that all of the valuable mineral flowrates (as the true process states x) are

measured, and they contain random errors with a standard deviation of 5% of their nominal values:

$$x = \begin{bmatrix} x_1 & x_2 & \dots & x_8 \end{bmatrix}^T \tag{6-34}$$

$$y_i = x_i + v_i \qquad i = 1,\dots,8 \tag{6-35}$$

Model parameters and their corresponding uncertainties are estimated using the procedure described in Section 6.3. For simulation, a sampling time T_s of 10 seconds has been used. The estimated process model parameters and their uncertainties are presented in Table 6-3 while the feed model characteristics are illustrated in Table 6-4.

Table 6-3: List of the estimated model parameters and uncertainties.

Unit	Mean residence time (min)		Poles		Separation coefficient
	Concentrate (T_c)	Reject (T_r)	Concentrate (a_c)	Reject (a_r)	α
Rougher	3.17	4.80	0.949±0.007	0.966±0.002	0.670±0.030
Cleaner	3.35	12.18	0.952±0.008	0.986±0.003	0.800±0.020
Scavenger	12.25	6.63	0.987±0.001	0.975±0.002	0.400±0.018

Table 6-4: Estimation of feed model characteristics.

Feed Model Elements	Value
T_f (min)	14.6
a_f	0.987±0.004
Σ_ξ	205.2

To simplify the calculation of the residence time in the froth zone, it is assumed that gas hold-up inside the froth is constant. In practice, gas hold-up is measurable using conductivity or ultrasonic sensors (Shean & Cilliers, 2011). Large value of valuable

mineral residence inside cleaner toward the reject as well as scavenger toward concentrate in comparison with other residence times come from the fact that only a small amount of valuable minerals exists in the reject and concentrate streams of cleaner and scavenger, respectively. So the residence time calculation from Eqs. 6-24 and 6-25 leads to large values. This point complies with what is observed in practice.

6.4.3 Observer performance evaluation

For comparing the performance of data reconciliation, three observers are considered:

- Standard stationary observer (ST) proposed by Makni et al.(1995a);
- Autocovariance based stationary observer (ABS) presented by Vasebi et al., (2012a);
- Kalman filter (KF) with the approximate model as previously described.

All of these observers estimate the instantaneous value of the variables rather than their steady-state underlying value. As a brief recall, the ABS observer uses sub-model taken from mass conservation law and plant flow sheet. It applies the autocovariance function of node imbalances to estimate the dynamic value of the process states. The ST observer is a particular case of ABS where only the node imbalances variance is utilized. The process model used in ABS and ST observers is expressed as:

$$M x(k) = \varepsilon(k) \tag{6-36}$$

where M is the process incidence matrix, and ε stands for the plant node imbalances. For the present case-study, both sides of Eq. 6-32 are multiplied by *M* to estimate the variance of ε :

$$My(k) = \varepsilon(k) + Mv(k) \tag{6-37}$$

and consequently,

$$\Sigma_{\varepsilon} = M\Sigma_{y}M^{T} - M\Sigma_{v}M^{T} \tag{6-38}$$

where Σ_v is estimated using Eq. 6-33. Also, autocovariance of ε can easily be extracted from simulation data. More details about ABS tuning and application are available in Vasebi et al. (2012a).

Two indices are selected to evaluate the performance of the observers in terms of noise reduction. The first one quantifies the total estimation error variance reduction. The covariance of the estimation error is expressed by:

$$P = \mathrm{cov}(x - \hat{x}) \tag{6-39}$$

where $\hat{x}$ is the reconciled value. The total variance reduction index is:

$$\eta_t = 1 - \frac{\mathrm{trace}(P)}{\mathrm{trace}(\Sigma_v)} \tag{6-40}$$

A value of 1 means that all noises have been filtered, while smaller index shows less noise reduction. To present the noise reduction for each valuable mineral flowrate, the second performance index is defined as:

$$\eta_{x_i} = 1 - \frac{P_{ii}}{\Sigma_{v_{ii}}} \qquad i = 1,2,\ldots,8 \tag{6-41}$$

where $\Sigma_{v_{ii}}$ and P_{ii} stand for i^{th} diagonal element of Σ_v and P, respectively.

For simulation purposes, a stationary variation with a standard deviation of 16% of the nominal value has been applied to the valuable mineral feed rate. Simulation results are given in Table 6-5. For ABS observer, 15 time lags were selected. KF observer with the proposed empirical model shows much better estimates than the two others. This illustrates that, by doing some limited modeling efforts, better reconciliation could be achieved. In the stream by stream evaluation, the KF also has better performance except for the fourth flowrate that is rougher concentrate. To illustrate the performance of observers, reconciled value of the concentrate and reject flowrates is presented in comparison with true and measured value of variables in Fig. 6-8. In this figure, the estimates are presented in a short two-hour time window for illustration purposes. As shown in Fig. 6-8, the KF with dynamic empirical model provides more precise estimates than the ST observer.

Table 6-5: Performance indices (%) for ST, ABS, and KF observers.

Indices (%)	ST	ABS	KF
η_t	58.1	63.0	72.9
η_{x_1}	50.6	59.0	68.3
η_{x_2}	32.4	44.4	62.1
η_{x_3}	20.0	23.5	79.6
η_{x_4}	58.3	61.5	46.0
η_{x_5}	8.4	8.9	37.9
η_{x_6}	2.6	2.8	46.1
η_{x_7}	60.1	64.3	71.9
η_{x8}	73.2	77.3	81.1

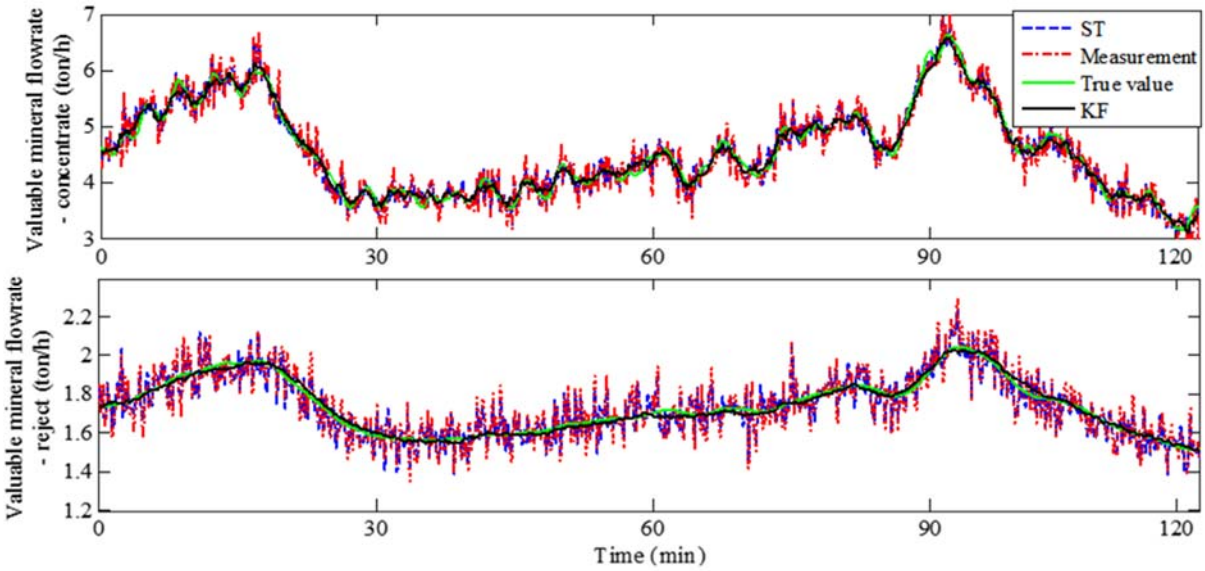

Fig. 6-8: KF and ST estimates vs. true and measured values (concentrate and reject flowrates).

For testing the robustness of KF observer, i.e. its sensitivity to the tuning of the covariance matrices that corresponds to the uncertainties of model parameters, multiple stationary disturbances with different variances are applied to the mineral feed rate. Observers are tuned for a specific disturbance while they are facing disturbances having different characteristics. Four test cases involving amplitude variation of the valuable mineral feed rate have been considered. To quantify the robustness, the following index is proposed:

$$q_j = \frac{\eta_t(3,j) - \eta_t(j,j)}{\eta_t(j,j)} \qquad j = 1, 2, \cdots, 4 \tag{6-42}$$

where j is the test index, and $\eta_t(3,j)$ is the performance index of test j when the observer is tuned for case 3. By this definition, $\eta_t(j,j)$ stands for the performance index of test j with the correctly tuned observer. Results presented in Table 6-6 reveal that all observers show increasing indices when model parameters depart from well-tuned conditions. Sub-model based observers, i.e. ST and ABS, reveal better robustness in comparison with the proposed KF observer. The maximum deviation for KF from the reference situation is about 12% while this value for ABS and ST is smaller. This point can be explained by the fact that the Kalman filter relies on a more detailed and complex model than two other observers. So it is more sensitive to plant operating conditions. However, it still gives better estimates than ABS and ST even in the presence of the worst feed disturbances.

Table 6-6: Performance indices (%) of ST, ABS, and KF in the robustness test.

Test case (j)	Mineral feed var. (%)	ST			ABS			KF		
		$\eta_t(j,j)$	$\eta_t(3,j)$	q_j	$\eta_t(j,j)$	$\eta_t(3,j)$	q_j	$\eta_t(j,j)$	$\eta_t(3,j)$	q_j
1	0	75.0	70.0	6.4	75.0	71.0	5.0	100	89.0	11.0
2	9.0	71.0	69.0	2.8	72.0	70.0	2.8	88.0	85.0	3.4
3	**16.0**	**58.0**	**58.0**	**0.0**	**63.0**	**63.0**	**0.0**	**73.0**	**73.0**	**0.0**
4	28.0	45.0	43.0	4.4	49.0	47.0	4.1	57.0	50.0	12.2

6.5 Conclusion

Precise measurement of process variables is vital for efficient and safe process operation. In industrial plants, data reconciliation is widely applied to provide a precise estimation of measured or unmeasured variables. Successful implementation of data reconciliation relies on a compromise between modeling effort and estimate precision. Although many powerful observers have been developed in the literature, they have not been frequently applied in the mineral processing industry. As a main reason, these observers need complex and detailed models that are not available or difficult to build in practice. Therefore, besides developing any observer, a procedure for obtaining the corresponding model should also be established.

In that sense, this chapter has proposed a procedure to get a simple model for a flotation circuit to support the implementation of a Kalman filter for dynamic data reconciliation purposes. Useful assumptions have been formulated to simply and facilitate the model elaboration. Empirical first-order transfer functions obtained from the plant topology, nominal operating conditions, and historical data were used to build the model.

A phenomenological flotation circuit simulator operating in a stationary regime has been used as case-study. To simplify and linearize the data reconciliation problem, only the valuable mineral flowrates have been considered as process variables. To obtain the parameters and uncertainties of the causal model, the chapter has provided practical guidelines. For instance, the mean residence time of the valuable mineral inside the different units has been selected as the time constant of the transfer functions, while the gains have been estimated using separation coefficients calculated from historical data. To model the feed fluctuations, the autocovariance function has been used.

The performance of the Kalman filter has been compared with two sub-model based observers: the standard and autocovariance based stationary observers. To assess the performances, indices based on estimation error variance reduction and robustness tests have been used. The Kalman filter with the empirical model has provided more precise estimates than standard and autocovariance based stationary observers in all scenarios. Regarding the robustness tests, sub-model based observers have been slightly better than

the Kalman filter. The high sensitivity of the Kalman filter to the plant operational conditions can be explained by the fact that the Kalman filter relies on a more detailed model than two other observers that use a simple description of the process. Despite its slightly higher sensitivity, the Kalman filter has produced better estimates even in the presence of important feed disturbances.

Although many assumptions have been used in the modeling stage, simulations results have revealed that these assumptions do not degrade reconciliation performances while greatly simplify the model development. As a general conclusion, although all dynamic behaviors of a complex plant like flotation circuits cannot completely be captured by few first-order empirical transfer functions, such models are beneficial for data reconciliation purposes if the model uncertainties are correctly represented. Therefore, a dynamic causal model with well-tuned uncertainties can be considered as an alternative for sub-models in the data reconciliation context. Doing some limited modeling efforts can facilitate the application of advanced observers like the Kalman filter in the mineral processing industry.

Chapter 7

Froth Flotation Circuit: Model and Dynamic Simulator

In this chapter, a dynamic simulator of a froth flotation circuit is presented for designing and testing data reconciliation observers (Chapter 6), and automatic control and real-time optimization schemes (Chapter 8). The simulator is derived from phenomenological and empirical relationships. To develop the simulator, several assumptions are made to simplify the model while its performance is kept reasonably close to a real process behavior. First, a single flotation unit is modeled, and its performance is evaluated using different tests. Then a flotation circuit simulator consisting of three cells is presented, and its behavior is discussed.

7.1 Flotation Circuit Modeling: A Review

Flotation plants are dynamic processes, and their performance is always affected by disturbances, strong interactions, and large and variable time delays (Pérez-Correa et al., 1998). On the one hand, flotation units are faced with disturbances in feed characteristics, e.g. flowrate, grade, and particle size distribution. On the other hand, changes in the manipulated variables affect the particles and air bubbles behavior inside the cell. To correctly understand the behavior of the cell, dynamic models are extremely beneficial, especially for automatic control practices.

In the steady-state situation where plant transients are not considered, several models and simulators have been developed (Arbiter and Harris, 1962; Mika and Fuerstenau, 1969; Jamsa-Jounela and Lattila, 1995). As a pioneer, Arbiter and Harris (1962) have proposed a two-phase model that conserves the mass in steady-state conditions. They have assumed that froth and pulp phases are perfect mixers, and then considered the interaction between

these two phases. Harris has extended the steady-state model to multiphase flotation cells (Harris, 1978). However, to study the transient effects of disturbances and sampling systems design, and also to develop automatic control systems, dynamic models are required.

In the literature, a limited number of dynamic flotation models have been presented, mainly based on Bascur and Hebst (1982). They have developed a phenomenological model to describe the dynamic behavior of a flotation cell. Their model represents the behavior of three types of particles (free valuable mineral, free gangue and locked mineral) in four possible states in the cell (free in the pulp, attached in the pulp, free in the froth and attached in the froth). A population balance model is applied to each state. Aeration rate, froth addition, and impeller speed have been considered as manipulated variables. Bascur (2000) has generalized the model by modifying the pulp/air and particle/bubble interactions and introducing new manipulated variables such as wash water flowrate.

To study the transient and time responses, Williams and Meloy (1983) have introduced a lumped-parameter dynamic model for continuous flotation circuits. Assuming a single mineral class, they have proposed a model based on dynamic mass balance equations. Pérez-Correa et al. (1998) have developed a dynamic model taken from mass balances and empirical relationships. Then based on the proposed model, they have applied different rule based and predictive control strategies.

Casali et al. (2002) have presented a flotation unit model specifically for control practices, process performance evaluation, and training applications. The dynamic model has been developed using phenomenological and empirical relationships. As the main core of the model, mass conservation law has been applied while two empirical sub-models have been used for modeling of feed composition, and bubble saturation. The model has been built based on the following major assumptions: one slurry phase, perfect mixing condition, no water flotation model, and constant airflow. The main advantage of the study is the calibration of model parameters using plant data and comparing the simulator performance with the plant behavior. Neglecting the froth zone model is the main weakness of the work.

A flotation circuit coupled to a grinding circuit has been modeled and simulated by Ruel (2010). The model has been developed based on dynamic mass conservation equations of

the particles and water. A perfect mixer model has been assumed for the collection zone. In the simulator, twelve particles in 3 size and 4 composition classes have been considered, and the corresponding first-order flotation and entrainment relations have been applied. As the strength of the work, Ruel (2010) has coupled the flotation simulator with a grinding circuit to present a more realistic case. However, he has not modeled the froth zone and effect of the plant operational variables on the simulator performance. These points could be considered as the drawbacks of the study.

Yianatos et al. (2012) have presented a procedure for modeling and simulating rougher flotation banks based on operating variables and parameters fitted using empirical data from plant measurements. They have first modeled mineral recovery in the collection and froth zones, and then expressed the total recovery in the term of recovery of zones. The recovery in the collection zone has been described as a function of residence time and flotation rate distributions. To characterize the cleaning zone behavior, they have applied a plug flow model leading to an exponential expression in terms of the maximum recovery of froth zone, froth stability, and the gas mean residence time. As a key point, the paper has proposed a sensitivity analysis for the effect of different operating conditions such as particle size distribution, froth depth, feed tonnage, feed grade and solid percentage. The simulator has not considered the effect of chemical reagents, i.e. collector and frother dosages, as manipulated variables. Based on the developed simulator, Bergh and Yianatos (2013) have investigated the control problem of rougher flotation circuits.

Pietila et al. (2015) have developed a flotation circuit simulator running in parallel with the copper plant in Finland. The simulator has been designed based on mass conservation of particles. A three-component first-order kinetic rate model, where the paritcles are defined as fast, slow and non-floating particles, has been considered. The simulator parameters have been tuned through a laboratory flotation test work. Although the simulator has not taken into account water and air dynamic mass conservation and froth zone model, its main advantage is the online updating of the model parameters based on the plant-model output differences.

This chapter presents a dynamic simulator for froth flotation circuit. The simulator is developed for designing and testing data reconciliation observers and automatic control

strategies. In fact, the aim of this section is not to develop a complex and perfect simulator but to build a simulator that reasonably behaves in transients and is suitable for process control and data reconciliation studies. The core of simulator is derived from mass conservation laws and flotation phenomena while empirical relationships are applied to model the effects of manipulated variables on hydrodynamics and flotation rates. To simplify the model, different assumptions are used while trying to keep its performance reasonably close to the behavior of flotation plant. First, a single flotation cell is modeled and discussed, and then a flotation circuit simulator that consists of three cells is presented.

Section 7.2 provides the basics and definitions needed to build a flotation cell model. Then, in Section 7.3, assumptions used to model the process are presented and justified. Collection zone model and effects of process operational variables are extensively discussed in Section 7.4 where empirical relations and mass balance equations are combined to build the dynamic model. Modeling of froth zone and froth depth effect on the material drainage are shown in Section 7.5. In Section 7.6, more details about the plant simulation procedure are provided. Sections 7.7 and 7.8 are devoted to investigate the single cell and the flotation circuit performances.

7.2 Basics and Definitions

This section gives preliminary information and defines variables that are used for flotation cell modeling. Fig. 7-1 shows the scheme of a flotation cell. To simplify the problem, froth and collection zones are separated. In other words, two separate phases are assumed: pulp phase and froth phase. In the collection zone, the interactions between particles, water, and air are modeled using two phenomena: flotation and entrainment. A particle can be carried into the froth by attachment to an air bubble (true flotation), or it can be suspended in the water trapped between the bubbles (entrainment). While true flotation is selective between hydrophobic and hydrophilic particles, entrainment is non-selective. So entrained particles are just as likely to be gangue as they are to be the valuable mineral. Drainage, i.e. returning particles from froth zone in collection zone, is embedded into the flotation rate constant model. Table 7-1 presents the notation and corresponding units of the process variables.

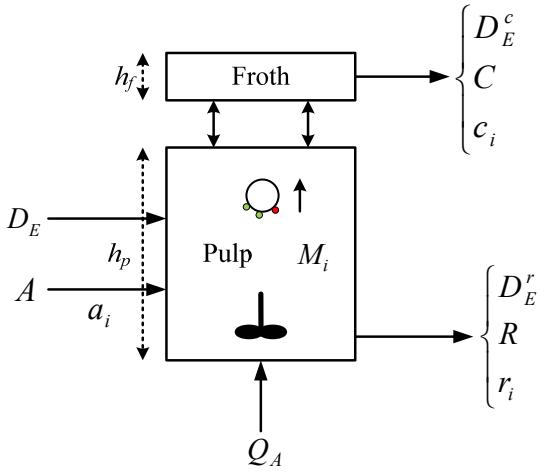

Fig. 7-1: Flotation cell scheme.

Table 7-1: Process variables notations and units.

Variable notation	Variable description	Unit	Variable notation	Variable description	Unit
h	cell total height	m	D_E^c	water flowrate in concentrate	t/h
h_f	froth zone height	m	D_E^r	water flowrate in reject	t/h
h_p	collection zone height	m	C	total solid flowrate in concentrate	t/h
S	tank sectional area	m^2	R	total solid flowrate in reject	t/h
i	species index	-----	C_i	species *i* flowrate in concentrate	t/h
ρ_i	species *i* density	g/cm^3	R_i	species *i* flowrate in reject	t/h
ρ_E	water density	g/cm^3	c_i	species *i* grade in concentrate	
A	solid flowrate in feed	t/h	r_i	species *i* grade in reject	
D_E	water flowrate in feed	t/h	a_i	species *i* grade in feed	
V_S	solid volume in pulp zone	m^3	M_i	species *i* mass inventory in pulp zone	t
M_S	total solid inventory in pulp zone	t	M_E	water mass in pulp zone	t
U_C	collector concentration	l/t	F_i	species *i* attachment flowrate	t/h
C_F	frother concentration	ppm	E_i	species *i* entrainment flowrate	t/h
Q_A	air feedrate	l/s	R_s	reject valve resistance	-----
S_b	bubble surface area flux	s^{-1}			

7.3 Assumptions

Although a flotation cell is a complex system, applying some assumptions can simplify its modeling for control and reconciliation purposes. These simplifications are selected to keep the realistic behavior of the cell. Assumptions applied in the current study are discussed in more details in the following sections.

7.3.1 Two phases

Here, two phases are considered for flotation cell modeling: the pulp and froth phases. It is assumed that collection zone obeys a perfect mixing condition while a plug flow model is considered for the froth zone. A perfect mixing condition implies that the concentration of each particle in the pulp phase is equal to its concentration in the tailing.

7.3.2 Limited number of mineral classes

The flotation process should be considered as a distributed system where many mineralogical species with different characteristics are involved. To keep the model simple, the different classes have been grouped into a reduced number of classes that are representative enough to describe the flotation behavior. In this study, it is assumed that the solid feed contains a single valuable mineral like chalcopyrite, gangue, and their mixture. Three size classes for solid particles are considered where each one has four different compositions. In fact, twelve particles with different size and composition classes are involved in the model (Table 7-2). In the table, particle grade stands for the chalcopyrite percentage in each particle size class.

7.3.3 No bubble size distribution

Size distribution of air bubbles is not considered. Only an averaged bubble size as well as total air volume is used in the modeling approach.

Table 7-2: Particles distribution in the feed.

Particle size	Species (*i*)	Particle grade
Large	1	100 %
	2	70 %
	3	30 %
	4	0 %
Medium	5	100 %
	6	70 %
	7	30 %
	8	0 %
Fine	9	100 %
	10	70 %
	11	30 %
	12	0 %

7.3.4 Net flotation and entrainment

As mentioned above, a particle can be carried into concentrate either by flotation or by entrainment phenomena. At the interface of the phases, Fig. 7-1 shows that both of these phenomena can act in forward and reverse directions, i.e. detachment and drainage could happen. In the current research, only net flotation and entrainment are used. This means that only particles entering the final concentrate stream are considered, and interaction between two phases is not explicitly taken into account. However, it is notable that particle drainage from the froth zone has been implicitly modeled by modifying the flotation rate constant when froth characteristics are changing.

7.4 Collection Zone Model

This section presents a model for the collection zone where a perfect mixing condition is assumed. For modeling purpose, different phenomena and laws are applied ranging from dynamic mass conservation equations to empirical relationships between the flotation rate constant and the manipulated variables.

7.4.1 Mass conservation equations

The core of the simulator is based on mass conservation equations of the particles and water. For the mineral particles, mass balance equation is:

$$\frac{dM_i}{dt} = Aa_i - C_i - R_i \qquad i = 1,\ldots,12 \tag{7-1}$$

where a_i, M_i, C_i, and R_i stand for the i^{th} particle mass fraction in the feed, mass inventory, flowrate in the concentrate, and flowrate in the reject, respectively. A is the ore feed rate. The water balance is expressed by:

$$\frac{dM_E}{dt} = D_E - D_E^r - D_E^c \tag{7-2}$$

where D_E, D_E^c, and D_E^r are water flowrate in the feed, concentrate, and reject, respectively. M_E is water inventory mass. Considering flotation and entrainment phenomena, the particle flowrate toward the concentrate is given by:

$$C_i = F_i + E_i \qquad i = 1,\ldots,12 \tag{7-3}$$

where F_i, and E_i are the i^{th} particle flotation and entrainment flowrates.

7.4.2 Overall mass transfer to reject

Bernoulli law can be employed to find a relationship between tank content volume and discharge flowrates. Local linearization of Bernoulli law gives a relation between the reject flowrates, total mass inside tank, and resistance of the reject valve R_s:

$$\frac{D_E^r}{\rho_E} + \sum_{i=1}^{12} \frac{R_i}{\rho_i} = \frac{M_E}{R_s} + \frac{M_S}{R_s} \tag{7-4}$$

where ρ_E and ρ_i stand for water and i^{th} particle density, and

$$M_S = \sum_{i=1}^{12} M_i \tag{7-5}$$

7.4.3 Flotation kinetics

Assuming a first-order kinetics for the flotation mechanism, i.e. particles attachment into bubbles, gives:

$$F_i = k_i M_i \qquad i = 1,\ldots,12 \tag{7-6}$$

where k_i (min^{-1}) is the flotation rate constant of particle *i*. Eq. 7-6 describes the particle flowrate into concentrate stream caused by flotation phenomenon. The flotation rate constant plays an important role in modeling of the cell behaviors. Many operational and process variables and parameters can affect k_i and consequently the plant performance. To have a reasonable simulator, the relations between the manipulated variables and k_i should be precisely addressed and modeled. The flotation rate constant of a particle depends on:

- the particle size (d_i): large particles are difficult to float because they are easily detached from bubbles, but their probability of being collided is higher. On the other hand, small particles are well attached to bubbles. However their collision probability with bubbles are lower.
- the hydrophobicity of the mineral (H): when more collector is absorbed on the mineral surface, its hydrophobicity gets higher and consequently its ability to be floated is increased.
- the particle composition (c_i): particles containing more hydrophobic minerals are more likely to be floated.

- the amonut of free surface available on the bubble: a parameter that depends on the bubble size distribution and air flowrate. It is mainly expressed as the bubble surface area flux S_b (min^{-1}).

Therefore, k_i can be expressed as:

$$k_i = \lambda g(d_i, c_i) H S_b \tag{7-7}$$

where H stands for the mineral hydrophobicity, and $g(d_i, c_i)$ is a function expressing the probability of being floated as a function of particle size and composition. λ is a constant coefficient. For the selected 12 particle classes presented in Table 7-2, the pure mineral average size particle (i.e. class 5) is chosen to be the class that has the highest flotation rate k_0. This class is used as the reference rate constant. Then the function $g(d_i, c_i)$ is numerically selected to represent a realistic situation. Table 7-3 gives the value of $g(d_i, c_i)$ for each particle, where

$$g(d_5, c_5) = 1 \tag{7-8}$$

and so

$$k_5 = k_0 = \lambda H S_b \tag{7-9}$$

$$k_i = g(d_i, c_i) k_0 \tag{7-10}$$

As mentioned before, H is mainly affected by the collector concentration while S_b depends on the air flowrate Q_A and the bubble size distribution influenced by the frother concentration C_F (Gorain et al., 1998a; Ofori et al., 2014).

Table 7-3: Value of $g(d_i, c_i)$ function (Eq. 7-7) representing the distribution of the kinetic constant based on the particle size and composition.

Species (*i*)	$g(d_i, c_i)$
1	0.8
2	0.4
3	0.010
4	0.0004
5	1
6	0.5
7	0.02
8	0.0005
9	0.7
10	0.35
11	0.014
12	0.00035

7.4.3.1 Evaluation of hydrophobicity

The collector reagent can change the characteristics of the particle surface and consequently affects the attachment mechanism. The collector concentration U_C (l/t) is the amount of collector (l) per ton of feed ore added into the cell. Finch and Dobby (1990) have shown that the mineral hydrophobicity and collector concentration are directly related. Their experiments have revealed that increasing U_C increases the mineral hydrophobicity. However, the trend is not linear; very high dosages of the collector can adversely affect the hydrophobicity, and consequently the particle flotability. For low and moderate collector dosages, which is assumed to be the case here, an exponential relationship with saturation has been observed (Song et al., 2000; Song et al., 2001):

$$H = b_1 + b_2 e^{-b_3 U_c} \tag{7-11}$$

where b_1, b_2, and b_3 are constant values obtained from empirical tests. This relationship depends on the collector type and changes from one collector to another one. It has been observed for some of the collectors like kerosene and #2 fuel oil. Fig. 7-2 shows the model used in the current research. The model coefficients are taken from experiments shown in the literature. Moreover, to model the evolution of collector inside the tank, a linear dynamic behavior with a 4-minute time constant (equal to the liquid residence time inside the tank) is considered. This is the time that collector needs to be uniformly speared inside the tank.

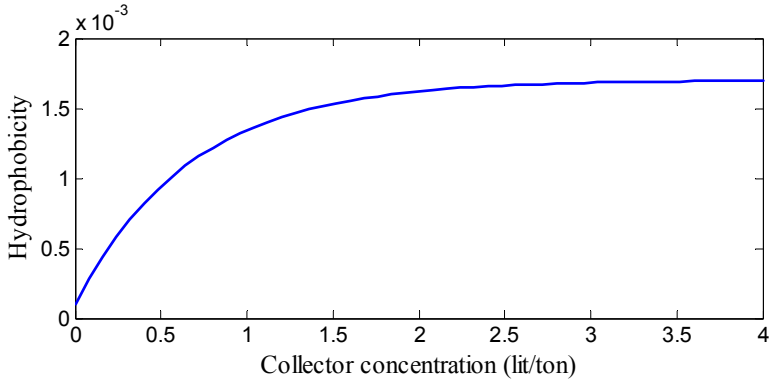

Fig. 7-2: Mineral hydrophobicity and collector concentration relationship.

7.4.3.2 Evaluation of bubble surface area flux S_b

S_b is formally defined as the surface area of bubbles per unit cross-sectional area of the flotation cell per unit time (Xu et al., 1991; Finch et al., 1999). Since both C_F and Q_A affect the flotation rate constant through S_b, so their effects are simultaneously modeled. S_b is expressed as (Finch and Dobby, 1990):

$$S_b = \frac{6J_g}{D_{32}} \tag{7-12}$$

where J_g is the superficial gas velocity ($\mathrm{cm/s}$) defined by:

$$J_g = \frac{Q_A}{S} \tag{7-13}$$

and D_{32}, called Sauter mean diameter, is an average value for bubble size, i.e. bubble diameter. It is defined as the diameter of a sphere that has the same volume/surface area ratio as a bubble and here, it is used to represent the bubble size distribution. In Eq. 7-13, *S* stands for the tank sectional area that is a constant value, so Q_A and J_g can be considered as the interchangeable variables in the text.

For a constant C_F, Nesset et al. (2006) have proposed a linear relationship between D_{32} and J_g:

$$D_{32} = D_0 + qJ_g \tag{7-14}$$

where D_0 and q are constant values that can be estimated from experimental tests. D_0 represents the minimum bubble size D_{32} that can be inside the tank. Using Eq. 7-12 gives:

$$S_b = \frac{6J_g}{D_0 + qJ_g} \tag{7-15}$$

In another case, when J_g is constant, D_{32} could be expressed in term of C_F as (Finch, et al., 2008):

$$D_{32} = D_0 + D_1 e^{-\beta C_F} \tag{7-16}$$

where D_1 and β are constant values. So Eq. 7-12 comes down to:

$$S_b = \frac{6J_g}{D_0 + D_1 e^{-\beta C_F}} \tag{7-17}$$

In practice, C_F and J_g can be simultaneously changed, so Eqs. 7-14 and 7-16 should be properly combined. Maldonado (2010) presented a new equation for D_{32} that takes into account the variations of both variables:

$$D_{32} = D_0(J_g) + D_1(J_g)e^{-\beta C_F} \tag{7-18}$$

where parameter D_0 and D_1 are functions of J_g :

$$\begin{cases} D_0(J_g) = d_1 + q_1 J_g \\ D_1(J_g) = d_2 + q_2 J_g \end{cases} \tag{7-19}$$

here d_1, d_2, q_1 and q_2 are constant values and should be identified using curve fitting from experimental tests. Fig. 7-3 illustrates the effect of J_g and C_F on D_{32}. Using Eqs. 7-12 and 7-18, S_b can be easily modeled based on C_F and J_g. To model the evolution of the frother as a chemical reagent, inside the tank, a first-order transfer function with 4 minutes time constant (equal to the liquid residence time inside tank) is considered. Since air flowrate shows a fast response, so no dynamic is considered for it.

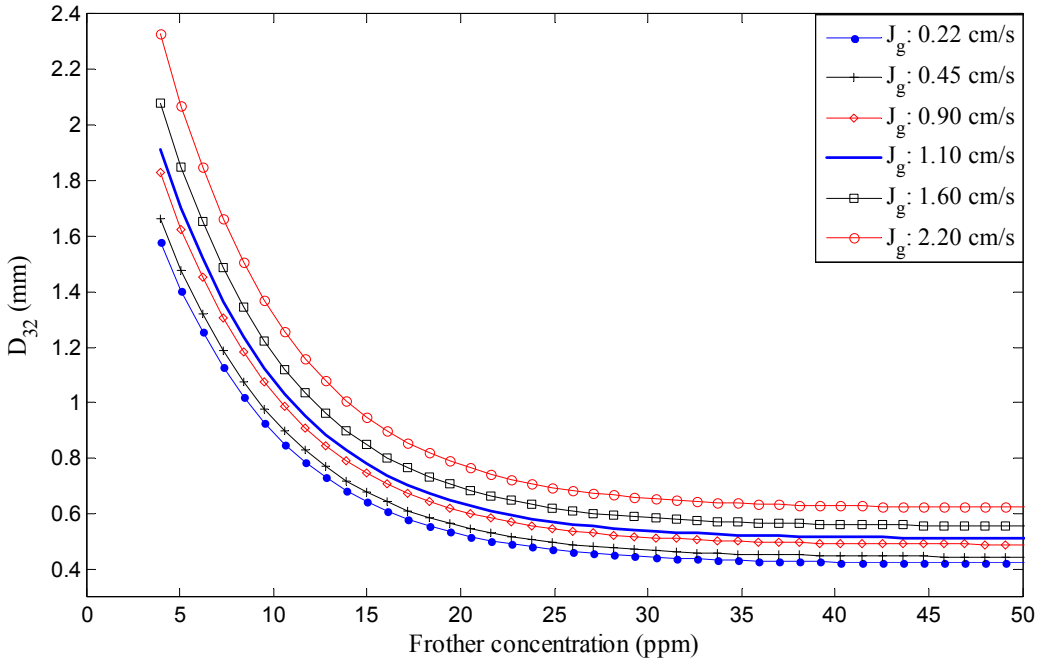

Fig. 7-3: D_{32} and frother concentration relationship.

7.4.4 Mixing properties

The perfect mixing assumption in the collection zone leads to:

$$\frac{R_i}{D_E^r} = \frac{M_i}{M_E} \tag{7-20}$$

It means that reject flowrate and collection zone have the same pulp composition.

7.4.5 Collection zone height and hold-up

Changes in the feed properties and process operational variables, i.e. U_C, J_g and C_F, affect the collection zone volume and height h_p, and consequently froth depth that is an important variable influencing the cell behavior. Therefore, it is valuable to find a relationship expressing h_p dynamics and variations. The collection zone volume V_C could be expressed as:

$$V_C = V_P + V_A \tag{7-21}$$

where V_P and V_A are pulp and air volume inside the collection zone, respectively. Using the reject stream composition and Bernoulli law that led to Eq. 7-4, V_P value can be easily calculated. To find the air volume inside the collection zone, other relationships are needed. C_F and J_g variations change S_b, i.e. the bubble size distribution, and consequently the bubble rising velocity is modified. This causes variation in the air resistance time and volume inside the collection zone. In other words, C_F and J_g variations also affect the air volume V_A. Therefore, as an alternative, V_A could be expressed in terms of S_b variations. Using experiments, it has been observed that S_b and gas holdup E_g are related through a linear relationship (Finch et al., 2000):

$$S_b = \gamma E_g \tag{7-22}$$

where γ is a constant value, and E_g (%) is defined as:

$$E_g = 100\frac{V_A}{V_A + V_P} \tag{7-23}$$

Combining Eqs. 7-22 and 7-23 provides an equation that expresses the air volume variations inside the collection zone as function of S_b variations resulting from C_F and J_g changes:

$$V_A = \frac{S_b V_P}{100\gamma - S_b} \tag{7-24}$$

where V_P can be obtained from the reject composition and flowrate (under the perfect mixing condition), and linearized Bernoulli law. Using Eq. 7-21 and tank cross-sectional area *S*, dynamic value of h_p can be calculated by:

$$h_p = \frac{V_A + V_P}{S} \tag{7-25}$$

Because of the important effect of h_p on the plant behavior, its set-point value can be used as a manipulated variable to change the plant performance. To bring h_p value to the desired value, a simple PI controller could be designed where the reject valve resistance R_s acts as a manipulated variable. For this purpose, a PI controller using pole cancelation technique has been designed and applied in the current chapter. This controller adjusts h_p by changing R_s. In all the following sections, the simulator performance is always illustrated in the presence of the level controller.

Table 7-4 summarizes the empirical relationships and equations expressed in the above sections. In the current study, model coefficients presented in the table have been obtained by curve fitting from the experiments that reported in the above-mentioned literature. Fig. 7-4 shows how the variables affect the flotation rate constant and E_g.

Table 7-4: Summary of empirical relationships.

Equations	Coefficients
$k_0 = \lambda H S_b$	$\lambda = 1$
$H = b_1 + b_2 e^{-b_3 U_c}$	b_1, b_2, b_3
$S_b = \frac{6 J_g}{D_{32}}$	-------
$D_{32} = D_0(J_g) + D_1(J_g) e^{-\beta C_F}$ $D_0(J_g) = d_1 + q_1 J_g$ $D_1(J_g) = d_2 + q_2 J_g$	D_0, D_1, d_1, d_2 q_1, q_2, β
$S_b = \gamma E_g$ $V_A = \frac{S_b V_P}{100\gamma - S_b}$	γ

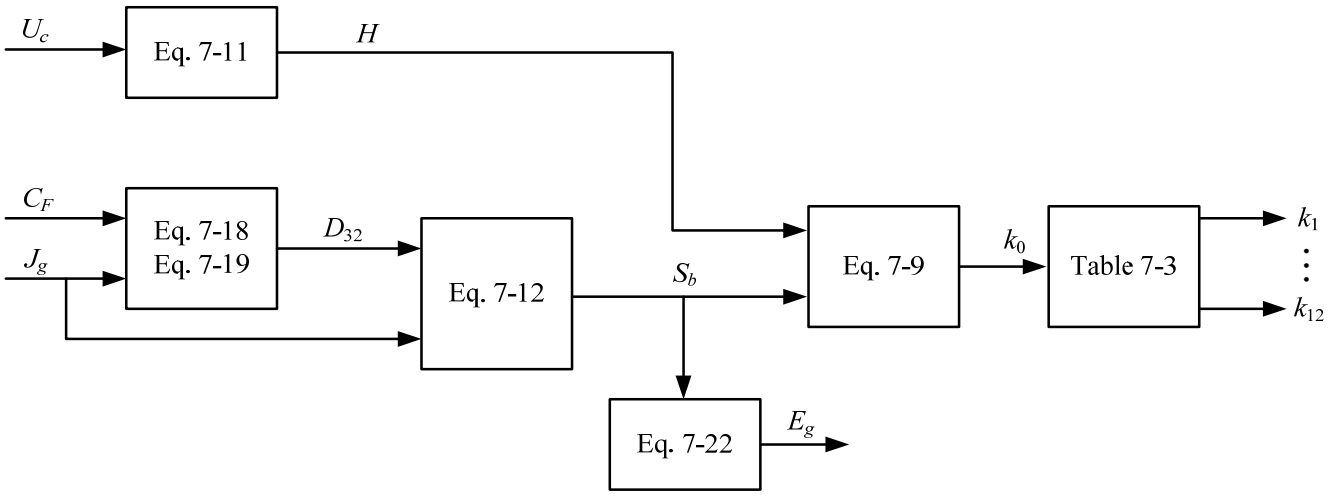

Fig. 7-4: Schematic of operational variables effect on the flotation rate constant and gas hold-up.

7.4.6 Entrainment

Entrained water is supposed to be proportional to the mineral flotation, so:

$$D_E^c = k_e \sum_{i=1}^{12} F_i \tag{7-26}$$

where k_e is the water entrainment coefficient (a dimensionless parameter). Since solid particles are entrained by water, the entrainment flowrate can be modeled as:

$$E_i = \alpha_i \, D_E^c \frac{M_i}{M_E} \qquad i = 1, \ldots, 12 \tag{7-27}$$

where α_i is the particle *i* entrainment coefficient (a dimensionless parameter). Based on the particle weight (size and density), a distribution can be assigned to the entrainment constants (Table 7-5). Lighter particles have more chance to be entrained. Therefore, fine particles have larger α in comparison to other size classes. In this table, entrainment coefficient of the lightest particle (12^{th} species) is considered as the reference entrainment coefficient α_0.

Table 7-5: Distribution of entrainment constants.

Species (i)	α_i / α_0
1	0.3
2	0.35
3	0.45
4	0.5
5	0.54
6	0.65
7	0.8
8	0.9
9	0.6
10	0.7
11	0.9
12	1

7.5 Froth Zone Model

For froth zone, a plug flow model with a pure time delay is considered. Value of the delay depends on the froth depth h_f. Gorain et al. (1998b) have investigated the effect of froth residence time, alternatively froth depth, on the kinetics of flotation. They have observed that an increase in the froth depth exponentially decreases the flotation rate. This conclusion could be applied to model the particle drainage from the froth zone into the collection zone. They have proposed that the net effect of drainage and flotation can be modeled as:

$$k = k_0 e^{-\theta T_d} \tag{7-28}$$

where k_0 is the reference flotation rate constant in the collection zone, i.e. when the froth depth effect is not taken into account, while k stands for the reference flotation rate

constant for the whole cell including the collection and froth zones. θ is a constant value and T_d is the pulp residence time inside the froth zone calculated by:

$$T_d = \frac{(1-\frac{E_{g_f}}{100})Sh_f}{C} \tag{7-29}$$

where E_{g_f} (%) is the gas holdup inside the froth zone. Here, it is assumed to be constant and set to 90% (Yianatos et al., 2008). *C* represents the volumetric flow rate of pulp into the concentrate. To involve the nominal operating conditions, Eq. 7-28 should be slightly modified as:

$$k = k_0 e^{-\theta(T_d - T_0)} \tag{7-30}$$

where T_0 is the time delay resulting from the nominal froth depth and concentrate flowrate. Therefore, Eq. 7-10 can be modified as $k_i = g(d_i, c_i)k$, and then, the flotation rate distribution can be obtained using Table 7-3.

7.6 Simulation Algorithm

The simulation algorithm for the flotation cell is presented in Fig. 7-5. The plant model is simulated using an explicit fixed-step continuous solver in Simulink (ode3) where the step size is 1 second. If the empirical equations representing the manipulated variables (MV) effects on the flotation rate constant are excluded from equations shown in Section 7.4, 52 differential-algebraic equations (DAE) remain. This equation set contains 13 differential equations for the dynamic mass balance of 12 species and water, and 39 algebraic equations for the flotation, entrainment, mixing condition, etc. To facilitate the simulator implementation, 52 DAEs are reduced to 13 compact differential equations by substituting variables and equations using Maple software. Water and species masses in the collection zone are considered as the process states. The algorithm is iterative, and process states and outputs in each step *i* are used as the initial value for the next step. As a key point, it is worthwhile to say that since the simulator and equations are dynamic, the simulator is run for about 1 hour to reach the nominal and steady-state situation. Table 7-6 precisely describes each stage of the simulation algorithm.

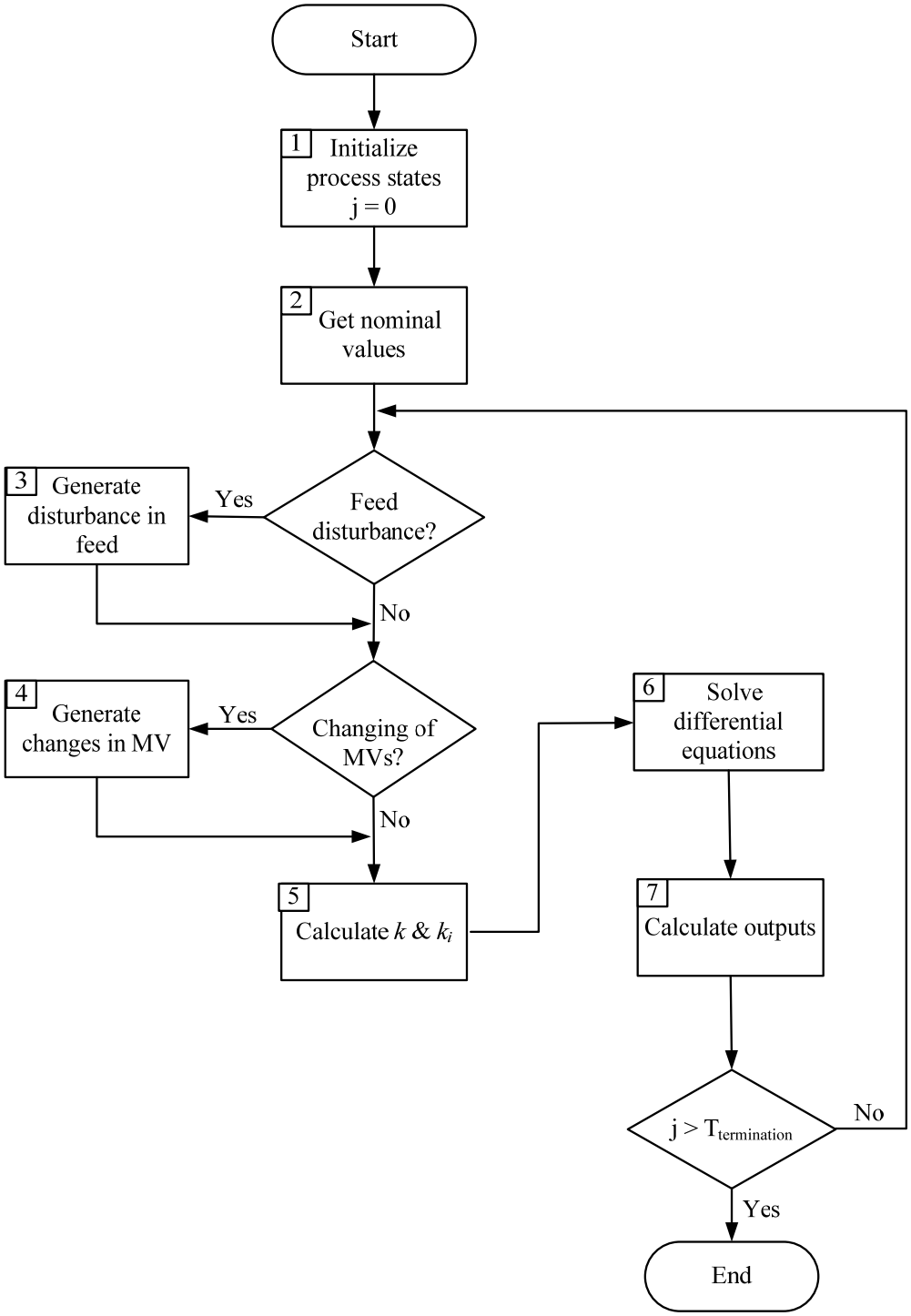

Fig. 7-5: Flotation cell simulation algorithm.

Table 7-6: Simulation algorithm details.

Stage No.	Description
1	Process states, i.e. water and species masses in the collection zone, are initialized using the values that are close to the steady-state values (this reduces the plant start-up time).
2	Nominal value of MVs (i.e. collector concentration, air flow rate, frother concentration, and collection zone level), feed characteristics, froth depth, reject valve resistance, simulation duration ($T_{termination}$) are fed.
3	If feed should be disturbed, a procedure generates the desired disturbances in feed characteristics, i.e. composition and flowrate. These stationary disturbances in ore flowrate and composition are generated by filtering of whine noises.
4	If necessary, MV values are changed by operator or controller.
5	Based on MV values and the froth depth, k is calculated, and the corresponding distribution k_i is generated.
6	Compact 13 differential equations are solved, and water and species masses are obtained.
7	Using masses obtained in the previous step and 39 algebraic equations, the plant outputs, flowrates, grades, collection zone level, froth depth, and recovery are calculated.

7.7 Flotation Cell Performance Test

This section presents the performance of the flotation cell simulator based on the above-mentioned models. First the nominal value of variables and feed characteristics are shown. Then steady-state performance, maximum theoretical recovery-grade curve, and cell batch test are presented. The behavior of the cell, when multiple disturbances affect the manipulated variables and feed characteristics, is also illustrated.

7.7.1 Nominal values and characteristics of process variables and feed

Table 7-7 presents the nominal value of cell dimensions, feed characteristics, and manipulated variables. In this table, *a* stands for chalcopyrite grade in the feed. Nominal characteristics of the particle distribution in the feed are depicted in Table 7-8 where middling grade is the average grade of particles containing both gangue and valuable

mineral, and liberation degree is defined as the percentage of valuable mineral that is fully liberated. The table provides each size class grade, mass fraction, middling grade, liberation degree as well as each particle mass fraction in the total feed.

Table 7-7: Nominal value of cell dimensions, feed characteristics, and manipulated variables.

Cell dimensions	Nominal value	Feed characteristics	Nominal value	Manipulated variables	Nominal value
h	3.0 m	A	100 ton/h	Q_A	50 l/s
S	4.5 m^2	a	6.5 %	U_c	0.5 l/t
		D_E	100 t/h	C_f	11 ppm
				h_p	2.7 m

Table 7-8: Characteristics of particles distribution in the cell feed.

Ore grade	Particle size	Species (i)	Particle grade	Class grade	Class mass fraction	Particle mass fraction in class	Middling grade	Liberation degree	Particle mass fraction in feed-a_i
6.48%	Large	1	100 %	5.0 %	25 %	0.15%	31%	3%	0.0375 %
		2	70 %			0.5			0.125 %
		3	30 %			15			3.75 %
		4	0 %			84.35			21.0875 %
	Medium	5	100 %	6.35 %	35 %	1.8	43%	28%	0.63 %
		6	70 %			3.5			1.225 %
		7	30 %			7.0			2.45 %
		8	0 %			87.7			30.695 %
	Fine	9	100 %	7.52 %	40 %	6.5	57%	86%	2.60 %
		10	70 %			1.2			0.48 %
		11	30 %			0.6			0.24 %
		12	0 %			91.7			36.68 %

7.7.2 Cell nominal performance in steady-state

The simulator performance is first evaluated in steady-state regime when there is no fluctuation in feed rate and manipulated variables. Value of plant outputs and flotation rate constant are illustrated in Table 7-9 for nominal conditions where τ_{pulp} stand for pulp residence time inside the collection zone calculated based on the reject stream. ρ is the cell recovery calculated based on output streams.

Table 7-9: Steady-state value of plant variables at the nominal operating regime.

Variable	Steady-state value
ρ	68.8 %
C	10.45 t/h
c	42.7 %
R	89.55 t/h
r	2.3 %
τ_{pulp}	5.8 min
k_0	2.5 min^{-1}
T_0	43 s

7.7.3 Maximum theoretical recovery-grade curve

To generate a maximum theoretical recovery-grade curve, first it is assumed that all feed content passes to the concentrate, so the recovery is 100% and the concentrate grade is 6.48% (equal to feed grade). Then feed species illustrated in Table 7-8 are eliminated from the concentrate one by one and transferred to the reject, and corresponding recovery-grade points are drawn. The order of species elimination from the concentrate is based on their chalcopyrite content, less chalcopyrite content, sooner elimination. Table 7-10 shows the elimination order used in this study. Fig. 7-6 presents the obtained maximum theoretical recovery-grade curve for the designed cell based on the nominal feed composition distribution. The plant nominal recovery-grade point is also illustrated (red point). The nominal point is far from the curve boundary. It can be improved by changing design and

modeling parameters such as tank dimensions, nominal value of manipulated variables, entrainment coefficient, and flotation rate constant distributions. Since the objective of the thesis is to use the simulator for testing data reconciliation observers and control schemes, this chapter is not involved in the cell designing issues. Therefore, the nominal recovery and grade are considered as acceptable.

Table 7-10: Maximum theoretical recovery-grade: species elimination order and recovery-grade calculation.

Eliminated specie no. (based on Table 7-8)	Particle size	Particle grade (%)	Recovery (%)	Grade (%)
All species in	---	----	100	6.48
12	Fine	0	100	10.2
8	Medium	0	100	19.9
4	Large	0	100	56.2
3	Large	30	82.6	68.7
7	Medium	30	71.3	86.5
11	Fine	30	70.2	89.2
6	Medium	70	57	95.24
10	Fine	70	51.8	98.8
2	Large	70	50.4	99.9
1	Large	100	49.8	100
5	Medium	100	40.1	100
9	Fine	100	0	100

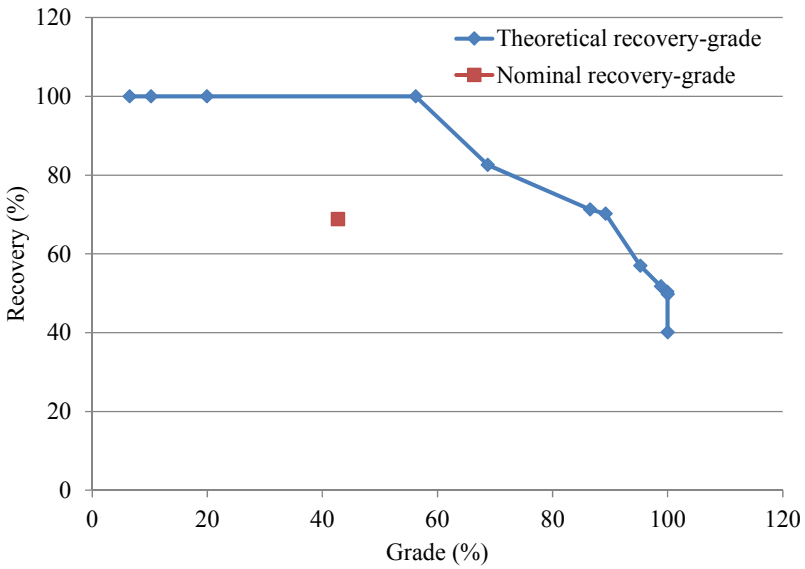

Fig. 7-6: Flotation cell maximum theoretical recovery-grade curve.

7.7.4 Flotation cell batch simulation test

A batch test can be used to monitor the flotation conditions, and it provides a lot of valuable information about the flotation cell performance such as particles residence time, flotation time response, verification of tank sizing, etc. Here, the test is performed to show that behaviors and features of the designed cell are acceptable and not far from real cases. For running the test, the tank is filled with pulp that has the nominal feed composition. Then flotation starts with the nominal value of manipulated variables while the feed and reject streams are turned off. Here, only flotation time response and residence time are presented (Fig. 7-7). The figure reveals:

- at the end of the test, all particles that contain chalcopyrite have been floated. This is reasonable because there is no trapped chalcopyrite in the feed particle distribution.
- 95% of minerals containing chalcopyrite have been floated in 40 min showing acceptable time response of the cell. Recovery reaches to 69%, i.e. nominal recovery, in about 5 minutes.
- two fast and slow parts of flotation behavior frequently reported in the flotation modeling literature.

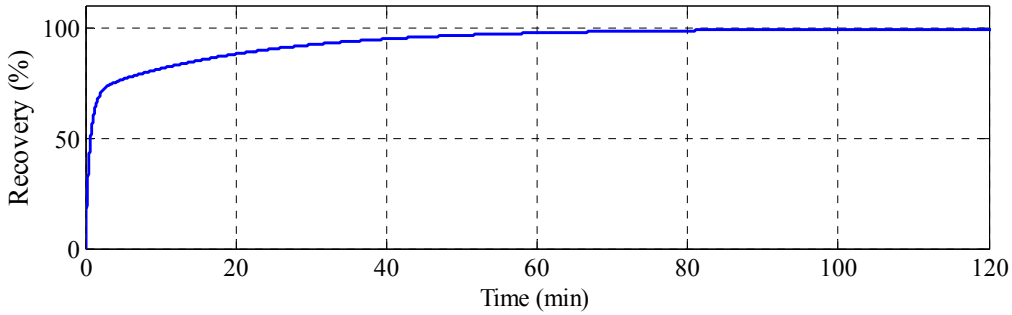

Fig. 7-7: Cell recovery during the batch test.

7.7.5 Cell steady-state outputs for disturbed feed characteristics

In Section 7.7.3, cell recovery and grade have been presented for nominal feed characteristics. Here its recovery and grade are shown when feed characteristics are changing. Therefore, twelve scenarios are defined (Table 7-11), and the corresponding recoveries and grades are illustrated in the recovery-grade plot (Fig. 7-8). In this figure, the cell behavior for all scenarios can be easily explained using three factors: feed particles composition and size, residence time inside the collection zone, and residence time inside the froth zone. When more liberated and smaller valuable mineral is injected, the flotation is enhanced, and consequently recoveries and grades increase. More pulp flowrate means less residence time inside collection and froth zones leading to less recovery and higher grade. More feed solid percentage reduces the selectivity and increases the entrainment, so it leads to higher recovery with a lower grade. In the current case, variation in the liberation degree causes the largest variation in the recovery-grade plot. Based on the illustrated results, the designed cell behavior is reasonably close to a real flotation plant performance.

Table 7-11: Disturbances in the feed characteristics used to investigate cell steady-state performance.

Scenario No.	Scenario index in Fig. 7-8	Description
0	Nominal	Table 7-8
1	+ Size	Class mass fraction is increased for **large** particles while the particle mass fraction in each size class is constant.
2	- Size	Class mass fraction is increased for **fine** particles while the particle mass fraction in each size class is constant.
3	+ Grade	Feed **grade** is increased while size class mass fractions are constant. To generate this scenario, ratio of the valuable mineral to the gangue inside each size classes is increased (size class mass fractions is constant).
4	- Grade	Feed **grade** is decreased while size class mass fractions are constant (the same procedure as + Grade, but the ratio is decreased).
5	+ Lib	Valuable mineral **liberation degree** is increased while class mass fractions are constant. In this scenario, the ratio of the particles containing the full liberated valuable mineral to the other particles inside each size classes is increased (size class mass fractions is constant).
6	- Lib	Valuable mineral **liberation degree** is decreased while class mass fractions are constant (the same procedure as + Lib, but the ratio is decreased).
7	+ Pulp	**Pulp** flowrate is increased.
8	- Pulp	**Pulp** flowrate is decreased.
9	+ Solid(S)	Increase feed **solid percentage** while water flowrate is constant.
10	- Solid(S)	Decrease feed **solid percentage** while water flowrate is constant.
11	+ Solid(W)	Increase feed **solid percentage** while solid flowrate is constant.
12	- Solid(W)	Decrease feed **solid percentage** while solid flowrate is constant.

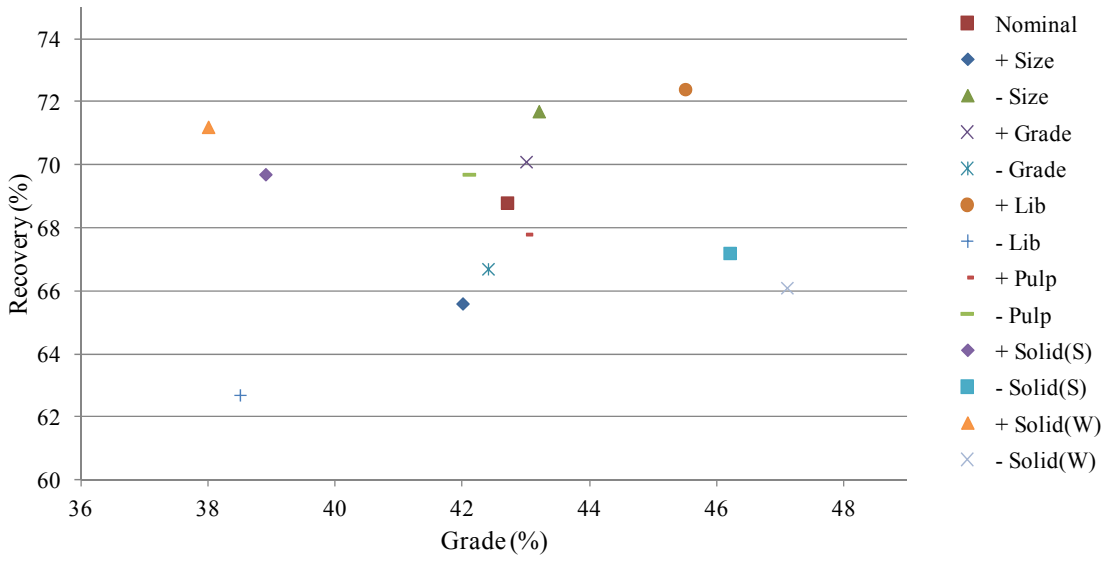

Fig. 7-8: Cell steady-state recovery-grade for different feed disturbances.

7.7.6 Flotation cell performance: manipulated variable changes

In this section, performance of the continuous cell is investigated when step changes are applied to the manipulated variables. The plant time responses including transient and steady-state behaviors are presented and discussed. Based on the variations of manipulated variables, twelve scenarios are defined. Table 7-12 summarizes the simulation scenarios. In this table, each scenario is presented as a transition from one stage to another stage as shown in Fig. 7-9. Stage 0 stands for nominal operating conditions of the plant where all manipulated variables and feed stream are set to nominal values.

Table 7-12: Different simulation scenarios based on the manipulated variables variations.

Scenario	S_1	S_2	S_3	S_4	S_5	S_6	S_7	S_8	S_9	S_{10}	S_{11}	S_{12}
From stage	0	1	2	3	4	5	6	7	8	9	10	11
To stage	1	2	3	4	5	6	7	8	9	10	11	12
ΔU_c (lit/ton)	**+0.5**	**-0.8**	**+0.3**	0.0	0.0	0.0	0.0	0.0	0.0	0.0	0.0	0.0
ΔC_F (ppm)	0.0	0.0	0.0	**+7.0**	**-13.0**	**+6.0**	0.0	0.0	0.0	0.0	0.0	0.0
ΔQ_A (lit/s)	0.0	0.0	0.0	0.0	0.0	0.0	**+25.0**	**-50.0**	**+25.0**	0.0	0.0	0.0
ΔL_r (m)	0.0	0.0	0.0	0.0	0.0	0.0	0.0	0.0	0.0	**+0.25**	**-0.45**	**+0.20**

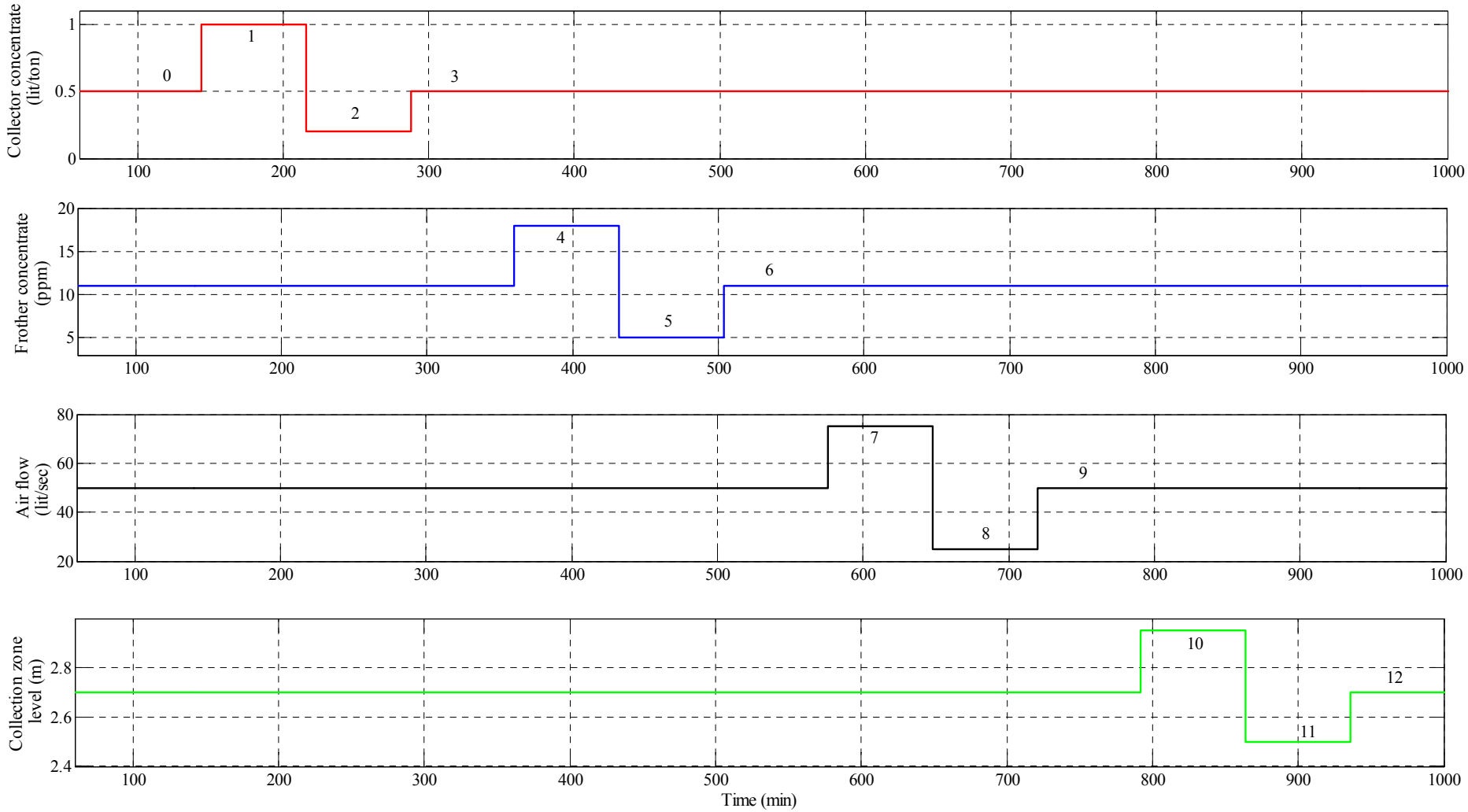

Fig. 7-9: Flotation cell: variations of the manipulated variables.

7.7.6.1 Flotation cell performance: collector concentration changes

First three scenarios in Table 7-12 are devoted to present the effects of the collector concentration on the cell behavior. Fig. 7-10 depicts how collector concentration variation changes the flotation rate constant. Increasing the collector raises k, and consequently enhances the material flotation. Because of the dynamic considered for the evolution of the collector inside the tank, a first-order behavior is observed in the transients. The plant output variables are illustrated in Fig. 7-11. When collector concentration and consequently k increase, more hydrophobic particles including mixed particles and chalcopyrite are floated toward the concentrate stream, and so concentrate flowrate increases while the concentrate grade decreases. Based on the mass conservation of the solid and chalcopyrite, the reject flowrate and grade decrease. The effects are reversed when the collector concentrate decreases.

It is worthwhile to say that transients in the outputs are affected by several players like collector concentration, collection zone level, particle composition inside the tank, etc. In other words, k is nonlinearly manipulated by the collector concentration and froth depth; so depending on the direction and amplitude of step changes, the cell behavior is different. This could be one of the reasons for the transient seen around 300 minute in the concentrate flowrate time response. Time response of the froth depth as representative of the level controller performance is illustrated in Fig. 7-12. As seen, the controller appropriately keeps the level constant. However there are some smooth transients. Plant recovery and grade calculated using output variables are shown in Fig. 7-13 where the variation of recovery and grade comply with all other results, i.e. increasing collector improves the recovery while decreases the grade.

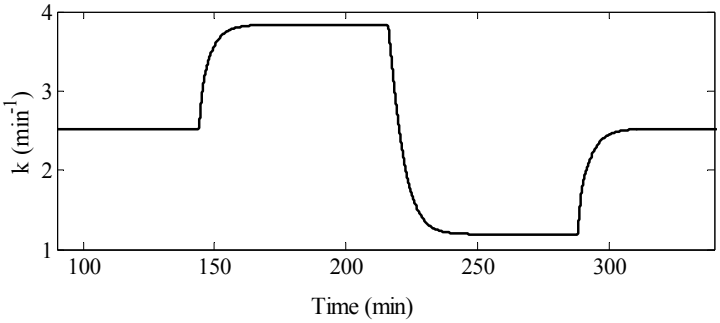

Fig. 7-10: Cell performance: effect of the collector concentration on the flotation rate constant.

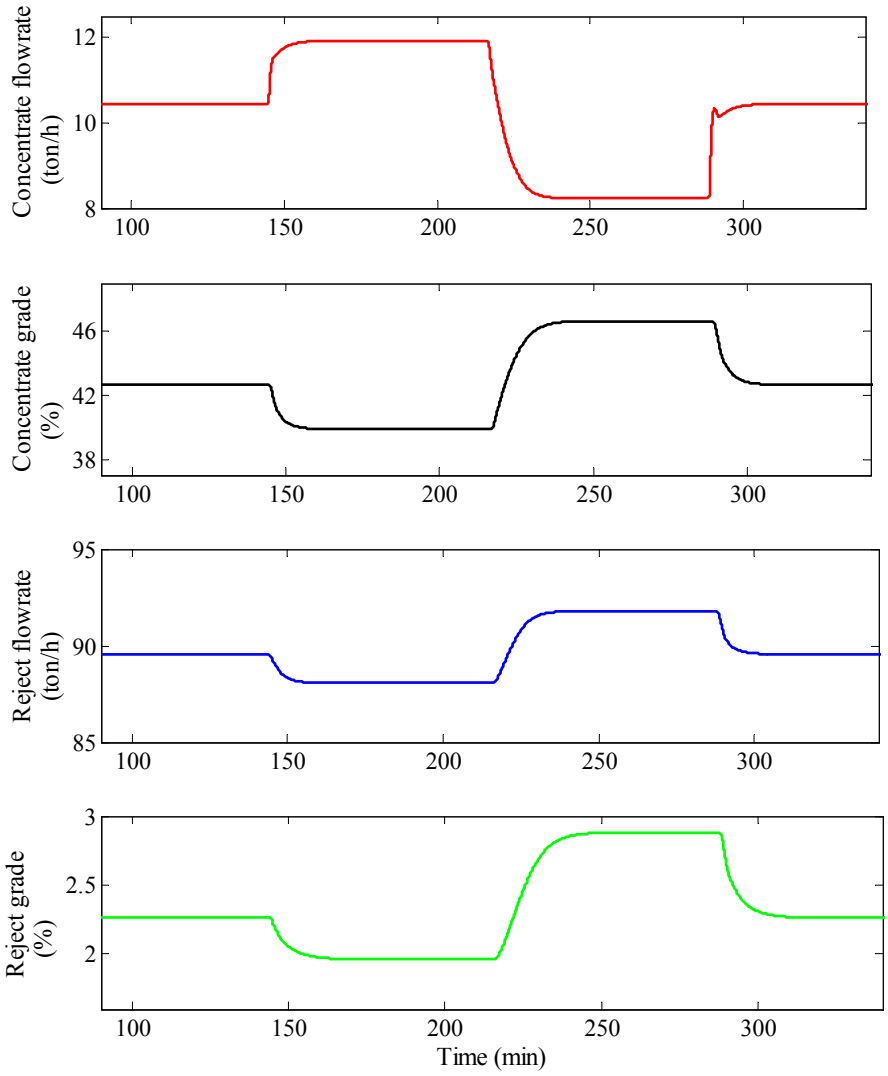

Fig. 7-11: Cell performance: the collector concentration effect on the output variables.

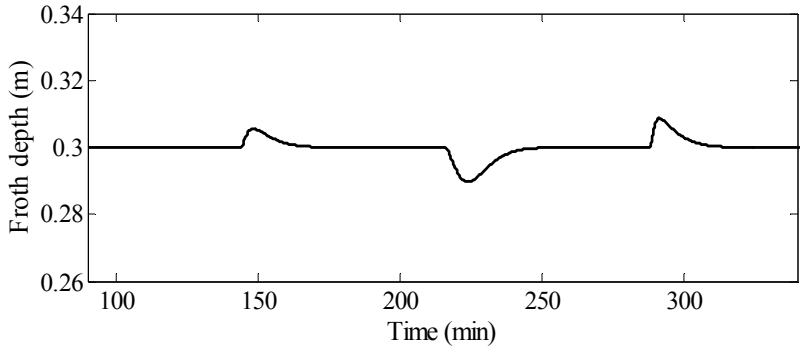

Fig. 7-12: Cell performance: froth depth when the collector concentration varies.

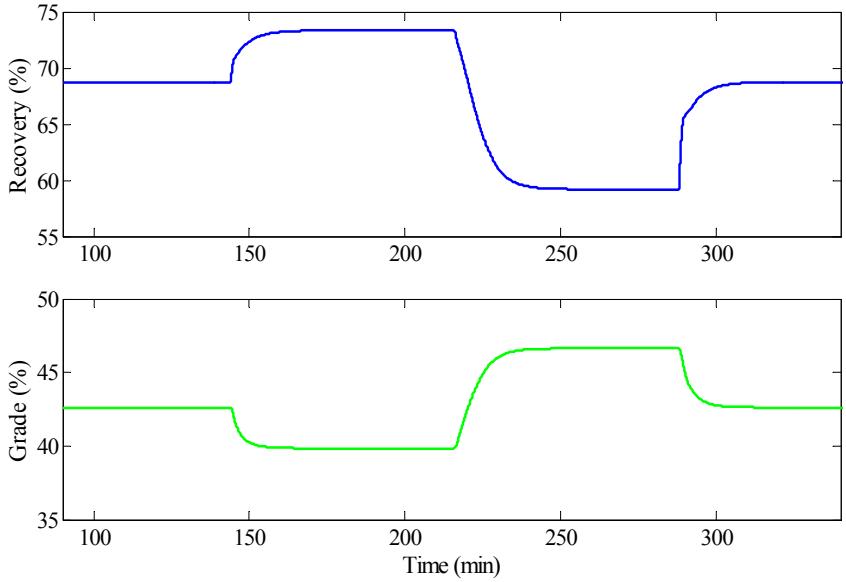

Fig. 7-13: Cell performance: plant recovery and grade when collector concentration varies.

7.7.6.2 Flotation cell performance: frother concentration changes

Scenarios S_4, S_5 and S_6 in Table 7-12 present the effects of the frother concentration on the cell behavior. The effect of frother variation on the flotation rate constant k is depicted in Fig. 7-14. According to Eqs. 7-18 and 7-12, increasing C_F at a constant J_g reduces D_{32} and consequently increases S_b and k. This exactly complies with the conclusion taken from Fig. 7-14. Again, because of the evolution dynamic considered for the frother inside the tank, a first-order behavior is observed in the transients.

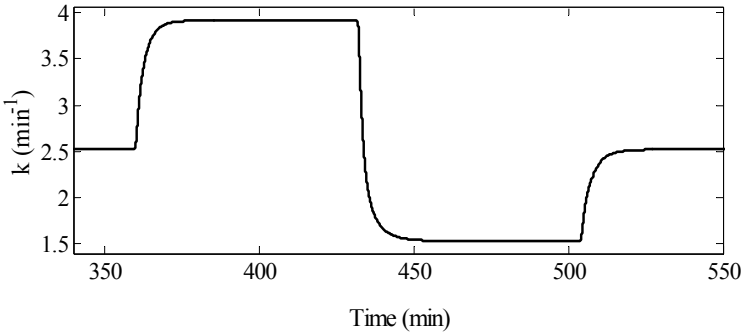

Fig. 7-14: Cell performance: frother concentration effect on the flotation rate constant.

The behavior of the plant output variables are illustrated in Fig. 7-15. An increase of k enhances the material flotation and consequently increases the concentrate flowrate and decreases the grade. Although based on mass conservation law, the reject flowrate should decrease, but a kind of non-minimum phase behavior in transient is observed. At the beginning, R has an overshoot and then converges to the steady-state value. In the current case, i.e. frother variation, two factors are determinative: flotation rate constant and air volume percentage inside the tank E_g. Effect of C_F on k has been already discussed and shown in Fig. 7-14. Regarding the effect of E_g, increasing frother concentration reduces the bubble size D_{32} and rising velocity of the bubbles. This means that more air volume is trapped inside the tank causing an increase in the collection zone level (interchangeably a decrease in froth depth – Fig. 7-16). In this situation, the controller acts to reduce the level by the reject valve opening that temporarily increases the reject flowrate. When the level is controlled, R comes back to the steady-state value that is smaller than the nominal one.

Plant recovery and grade are shown in Fig. 7-17 where an increase of the frother concentration improves the recovery and reduces the plant grade. The presented effects and behaviors are reversed when the frother concentration decreases. It is also noticeable that because of the nonlinear models utilized in the simulator, the plant performance and response depend on the direction and amplitude of step changes applied to the manipulated variables.

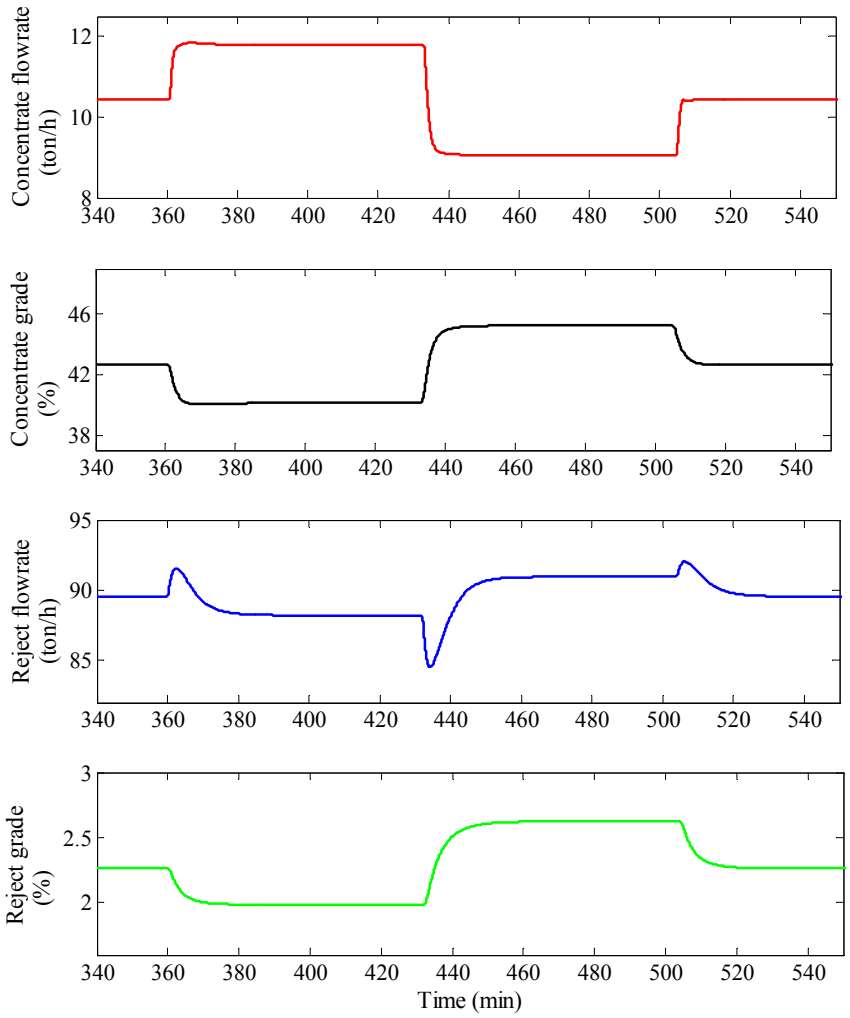

Fig. 7-15: Cell performance: frother concentration effect on the output variables.

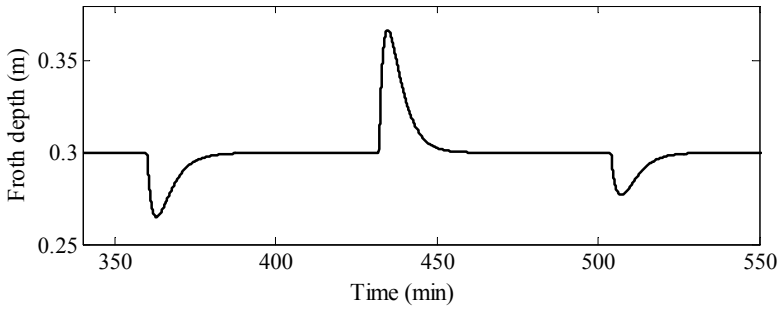

Fig. 7-16: Cell performance: froth depth when frother concentration varies.

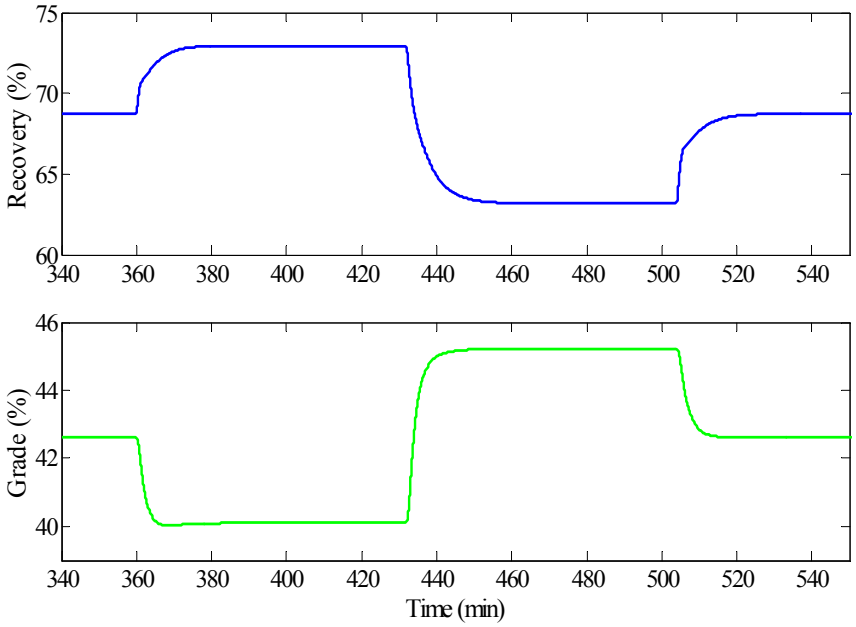

Fig. 7-17: Cell performance: plant recovery and grade when frother concentration varies.

7.7.6.3 Flotation cell performance: air flowrate changes

This subsection investigates the effect of air flowrate Q_A on the cell performance, i.e. S_7, S_8 and S_9 in Table 7-12. Q_A can modify the behavior of the cell by changing the flotation rate constant *k* and air volume inside the tank i.e. the collection zone level. As a key point, it should be noticed that Q_A has very fast response to affect *k* and level, and so it has a very fast transient. Influence of Q_A on *k* is more complex than C_F, because air flow participates in both nominator and dominator of Eq. 7-12. In other words, an increase of Q_A increases both the bubble size D_{32} and J_g, but the amplitude of the change in J_g is larger. This point results in an increase of S_b and *k*. Fig. 7-18 illustrates *k* variation when air flowrate changes. Overshoot in *k* is caused by the fact that when Q_A suddenly increases the volume of air inside the collection zone rapidly increases, and froth depth consequently decreases. In this situation, based on Eq. 7-30, large overshoot is observed in *k*. After this overshoot, the level controller tries to bring down the level and so *k* is settled down.

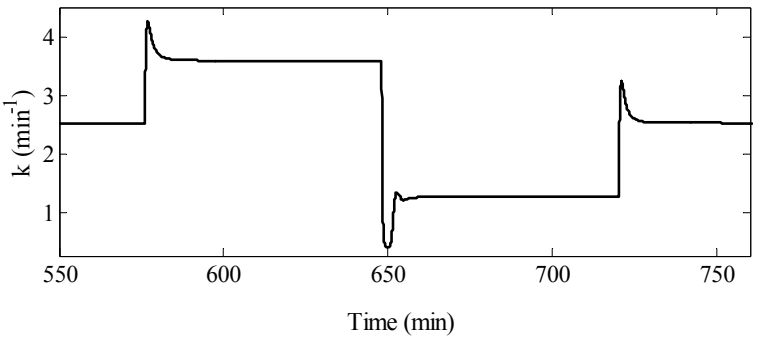

Fig. 7-18: Cell performance: air flowrate effect on the flotation rate constant.

The behavior of the plant output variables is depicted in Fig. 7-19 when air flowrate changes. Increasing of Q_A improves the flotation of particles and consequently increases the solid flowrate in the concentrate stream. Therefore, chalcopyrite percentage in the concentrate and solid flowrate in the reject decrease. In the transients, the time response of the output variables has two parts: fast and slow responses. The fast part comes from the immediate increase of the air volume that pushes the pulp toward the reject and concentrate streams. The flotation phenomenon is responsible for the slow dynamics. The presented behaviors are reversed when the air flow drops. However, some oscillations observed in the transients could originate from nonlinearity of the models. Fig. 7-20 illustrates the froth depth behavior. It shows immediate changes at the beginning, and then a slow dynamic transition. Plant recovery and grade calculated based on the output variables are shown in Fig. 7-21.

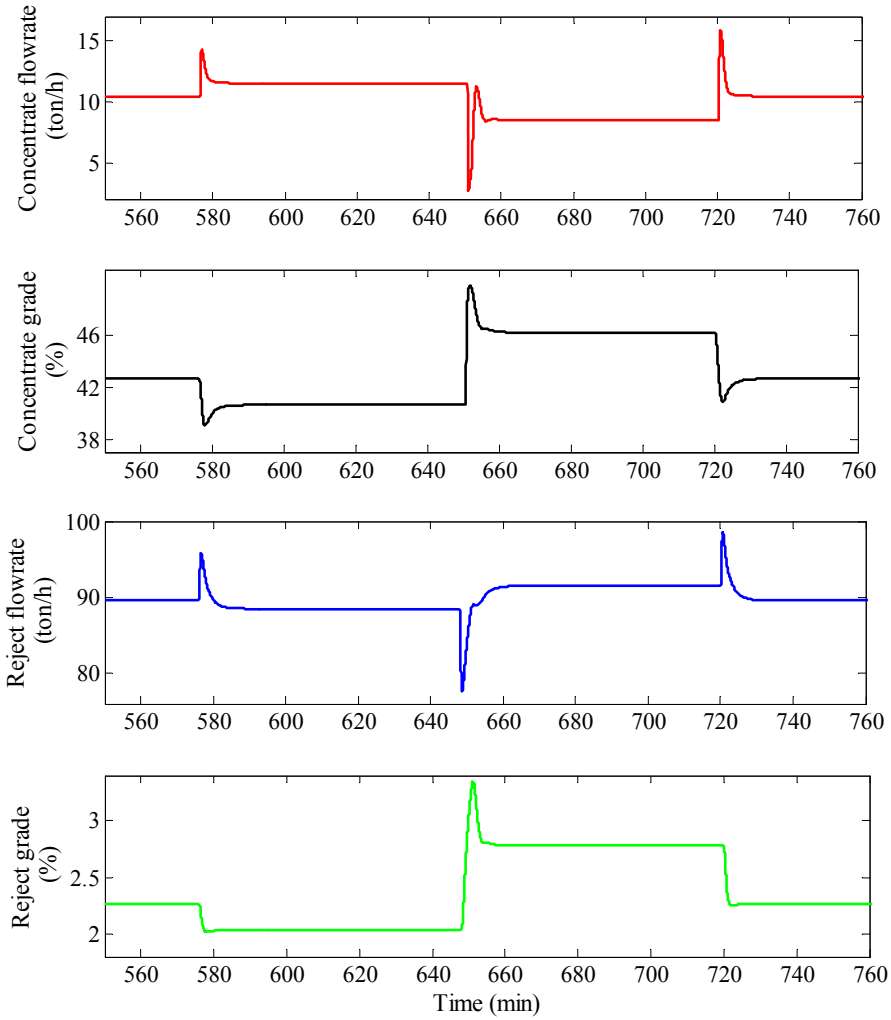

Fig. 7-19: Cell performance: air flowrate effect on the output variables.

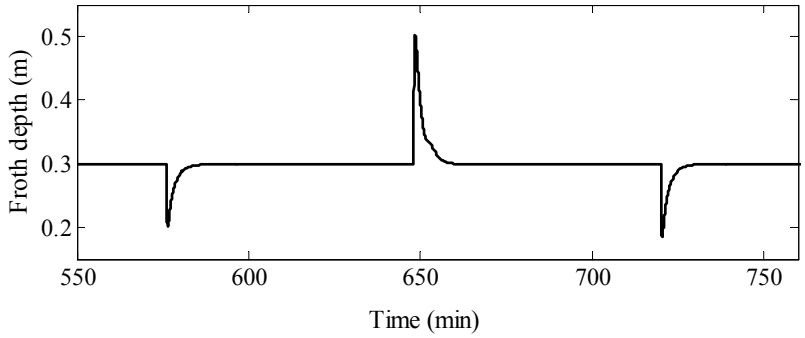

Fig. 7-20: Cell performance: froth depth when air flowrate varies.

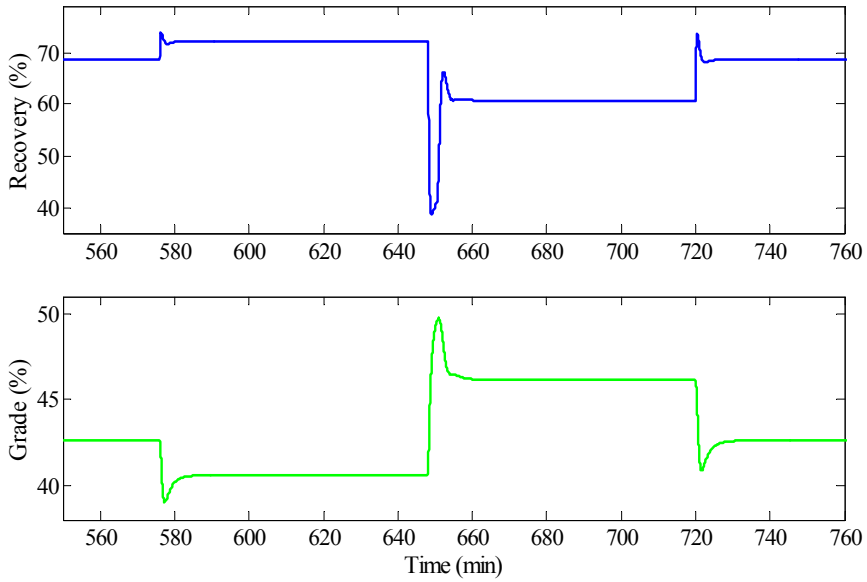

Fig. 7-21: Cell performance: plant recovery and grade when air flowrate varies.

7.7.6.4 Flotation cell performance: collection zone level changes

In the section, the presented results correspond to S_{10}, S_{11} and S_{12} in Table 7-12 where the collection zone level changes. Increase of level decreases the froth depth h_f and, based on Eqs. 7-30 and 7-29, it increases the net flotation rate constant. In fact, it decreases the material drainage from froth zone into collection zone. This point explains why k and h_f have the same transients as shown in Figs. 7-22 and 7-23. Therefore, an increase of level enhances the net material flotation; it consequently increases the solid flowrate in the concentrate and reduces its chalcopyrite concentration (Figs. 7-24). For the reject flowrate, the situation is different. When the level set-point suddenly rises; the level controller turns off the reject valve to fill the tank. So a large drop happens in the reject flowrate at the beginning. When the augmented volume of collection zone is compensated, the reject flowrate tends to the steady-state value which, based on the mass conservation law, is smaller than its nominal value. Plant recovery and grade calculated based on the output variables are shown in Fig. 7-25 where an increase of level enhances the recovery and reduces the plant grade. Despite the model nonlinearities, behaviors of the output variables are reversed when the level drops.

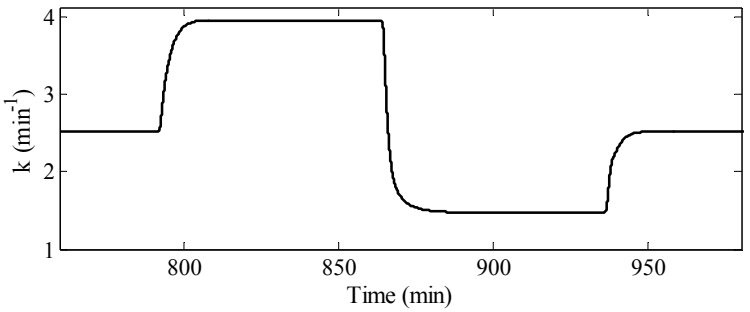

Fig. 7-22: Cell performance: the collection zone level effect on the flotation rate constant.

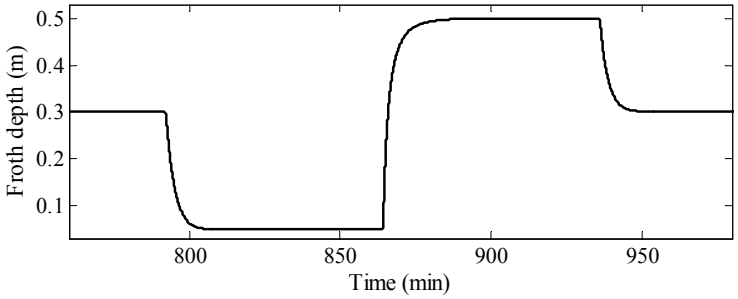

Fig. 7-23: Cell performance: froth depth when the collection zone level varies.

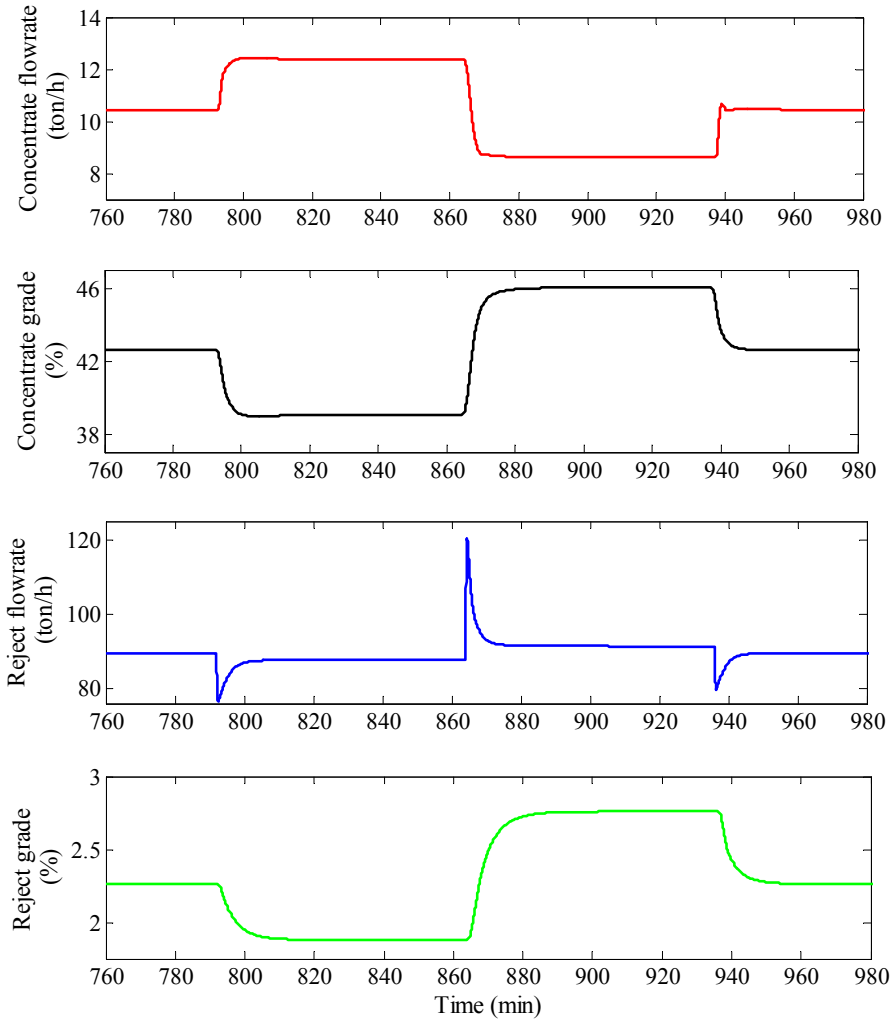

Fig. 7-24: Cell performance: the collection zone level effect on the output variables.

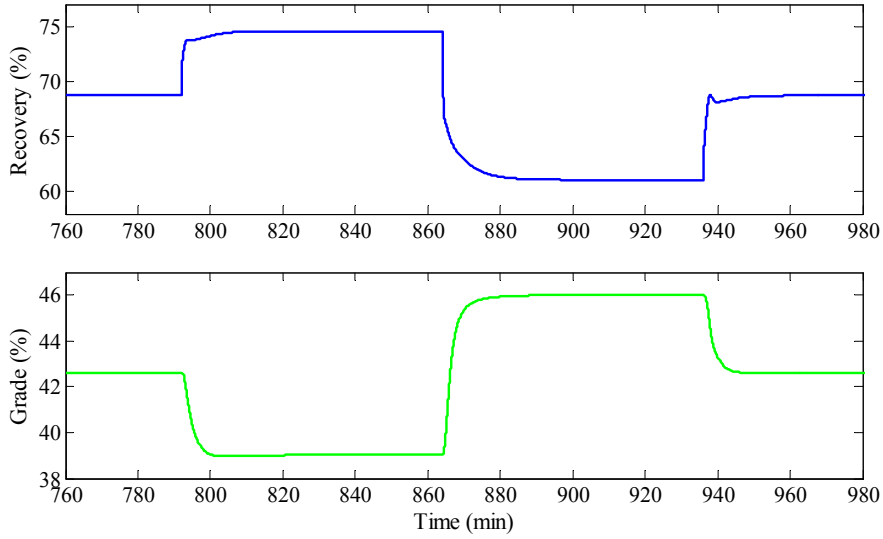

Fig. 7-25: Cell performance: plant recovery and grade when the collection zone level varies.

7.7.7 Flotation cell performance: feed characteristics changes

In this section, the dynamic performance of the cell is investigated when different types of disturbances are applied to the plant feed. In the first part, step changes in feed rate and grade are applied, and the plant time responses are investigated. Then, the plant behavior under the stochastic disturbances is shown and assessed.

7.7.7.1 Flotation cell performance: step changes in the feed

In this case, it is assumed that all the manipulated variables are set to their nominal values, and only feed characteristics are changing. Based on the variations of the feed rate and grade, six scenarios are defined. Table 7-13 summarizes the simulation scenarios. Each scenario is presented as a transition from one stage to another as shown in Fig. 7-26. Stage 0 stands for nominal operating conditions of the plant where feed stream and all manipulated variables are set to the nominal values.

Table 7-13: Different simulation scenarios based on the feed characteristics variations.

Scenario	S_1	S_2	S_3	S_4	S_5	S_6
From stage	0	1	2	3	4	5
To stage	1	2	3	4	5	6
ΔA (ton/h)	**+10**	**-20**	**+10**	0.0	0.0	0.0
Δa (%)	0.0	0.0	0.0	**+0.7**	**-1.2**	**+0.5**

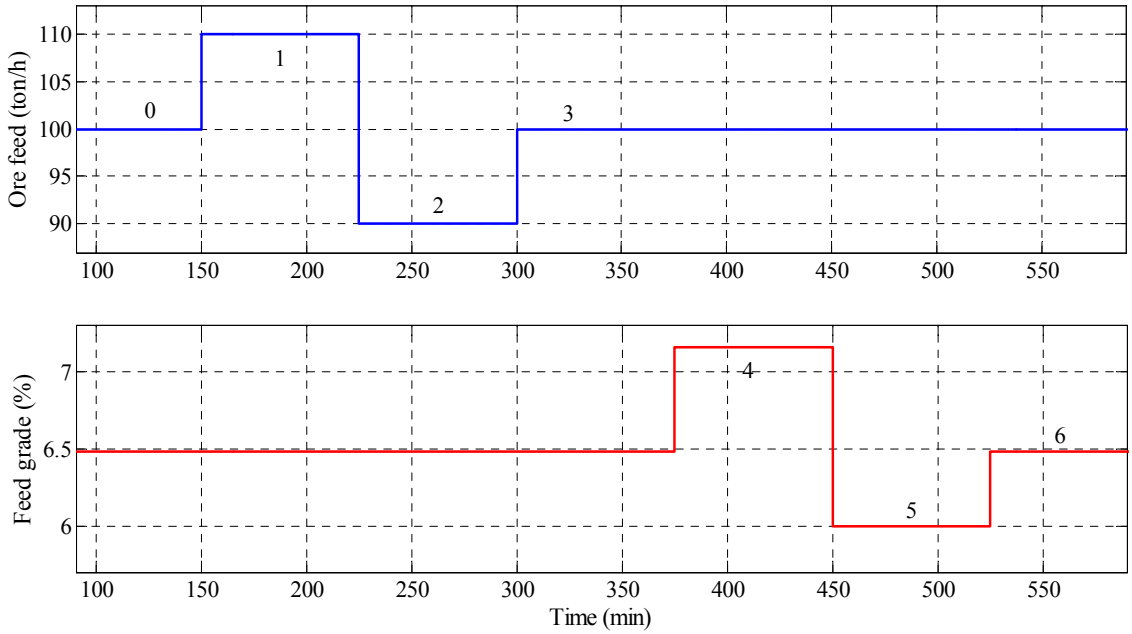

Fig. 7-26: Flotation cell: variations of the feed characteristics.

a) *Feed rate change*

Scenarios S_1, S_2 and S_3 in Table 7-13 present the effect of the feed rate changes on the cell behavior. As it is expected, increasing the feed enhances both the concentrate and reject flowrates (Fig. 7-27). It decreases the material residence time inside the collection zone. So the plant recovery decreases while the grade slightly increases (Fig. 7-28). In the transient, two different dynamics are observed: fast and slow variations. When feed rate suddenly increases, at the beginning, it immediately pushes the material toward the outputs. This causes an overshoot in the flowrates and grades. When the feed strike passed, the slow dynamic is revealed. Increase of the feed reduces the froth depth (Fig. 7-29). In this situation, level controller starts to bring back the level. Therefore, the concentrate flowrate decreases while the grade is compensated.

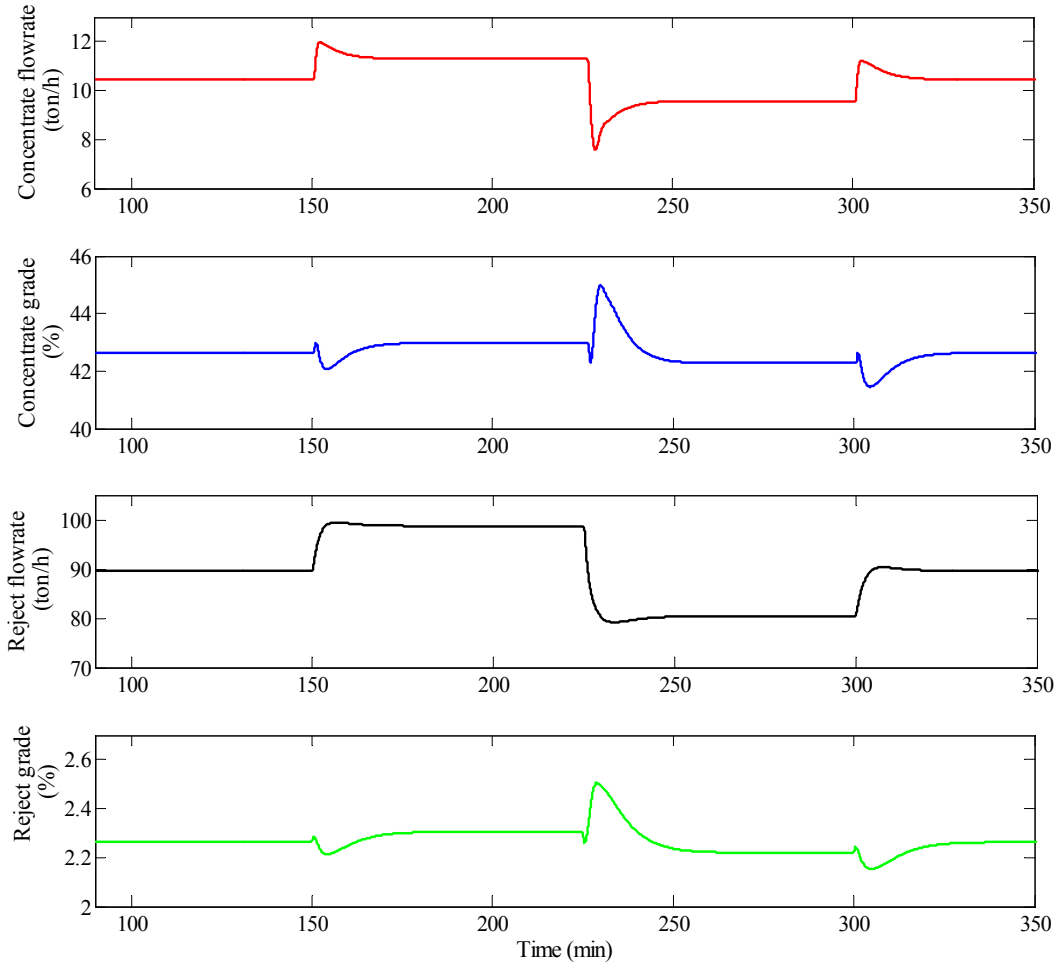

Fig. 7-27: Cell performance: feed rate changes effect on the output variables.

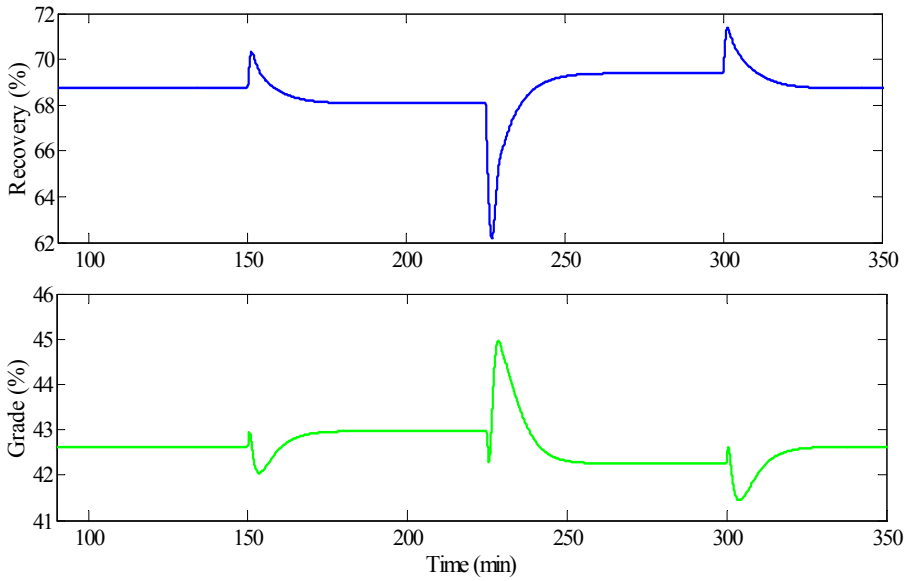

Fig. 7-28: Cell performance: plant recovery and grade when feed rate changes.

In this test, although the manipulated variables are constant, some variations are observed in k (Fig. 7-30). Constant manipulated variables guarantee that k_0 is constant, but the variations of C change the residence time of material inside froth T_d calculated from Eq. 7-29 and consequently change k. This could be explained by the fact that the smaller residence time inside froth means less material drainage from the froth zone into the collection zone, and therefore producing more floated material.

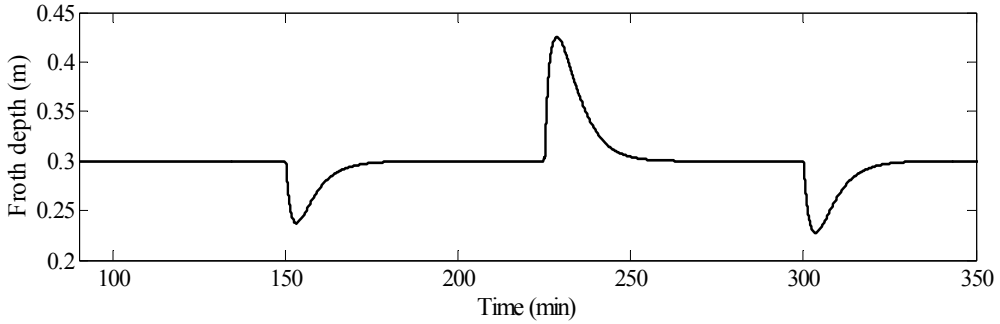

Fig. 7-29: Cell performance: froth depth when feed rate changes.

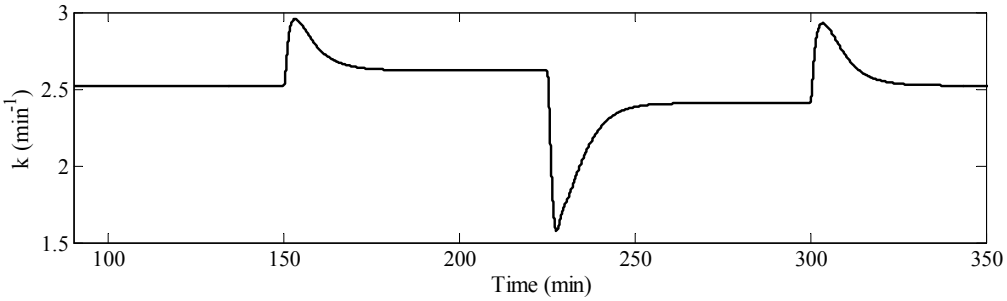

Fig. 7-30: Cell performance: feed rate changes effect on flotation rate constant.

b) *Feed grade change*

The effect of feed grade changes on the cell behavior is investigated using Scenarios S_4, S_5 and S_6 of Table 7-13. This study is more complex than feed rate effect because twelve particles classes contribute to the feed grade variations. Depending on which particle class has more contribution, the plant performance could be different. Here, to generate the disturbance, the mass fraction of particle classes is changed while the liberation degrees, the particle size and composition classes are free to change. This disturbance generating procedure is more representative for the disturbances in a real situation. So, as a starting point, the distribution of the feed particle classes in each stage is presented in Table 7-14.

Table 7-14: Characteristics of feed particles distribution for the grade variation scenarios.

Particle size	Species (*i*)	Particle grade (%)	**Feed grade: 6.48%** Stage 3 – **nominal**	**Feed grade: 7.15%** Stage 4	**Feed grade: 6.00%** Stage 5
			Particle mass fraction (%)	Particle mass fraction (%)	Particle mass fraction (%)
Large	1	100	0.0375	0.040	0.040
	2	70	0.125	0.150	0.100
	3	30	3.75	4.25	3.390
	4	0	21.0875	20.79	21.230
Medium	5	100	0.63	0.51	0.47
	6	70	1.225	1.51	1.22
	7	30	2.45	3.00	2.34
	8	0	30.695	29.98	30.89
Fine	9	100	2.60	2.62	2.34
	10	70	0.48	0.71	0.52
	11	30	0.24	0.49	0.36
	12	0	36.68	35.95	37.01

The output variable variations are illustrated in Fig. 7-31. As seen, when feed grade increases (Fig. 7-26), the concentrate flowrate and reject grade increase while the two other output variables decrease. Degradation of the reject flowrate can be explained by mass conservation law, but decrease in the concentrate grade needs clarification. The explanation could be found in Table 7-14 showing that although the feed grade increases in stage 4, the total liberation degree decreases. It means that a larger amount of chalcopyrite is fed to the plant, mostly through the mixed particle classes. In other words, the plant receives more valuable mineral, but with less floatable particles. This point also justifies the reduction of the plant recovery (Fig. 7-32).

In scenario 5, where the grade comes down as illustrated in Fig. 7-26, both feed grade and liberation degree decrease, so the concentrate flowrate decreases. Therefore, recovery comes down. In this case, the mass fractions of pure gangue particles have also increased in comparison to the previous scenario. In other words, the feed grade reduction partly comes from the injection of pure gangue particles which are almost non-floatable. This point explains the slight improvement of concentrate grade in comparison with the previous scenario.

Here again, some variations are observed in k (Fig. 7-33) while the manipulated variables are constant. These variations come from the particle residence time T_d variations inside the froth zone. They originate from concentrate flowrate variation. This is why k and C have similar trends. As a complementary result, the froth depth variation is depicted in Fig. 7-34 that could be beneficial for the explanation of some transients.

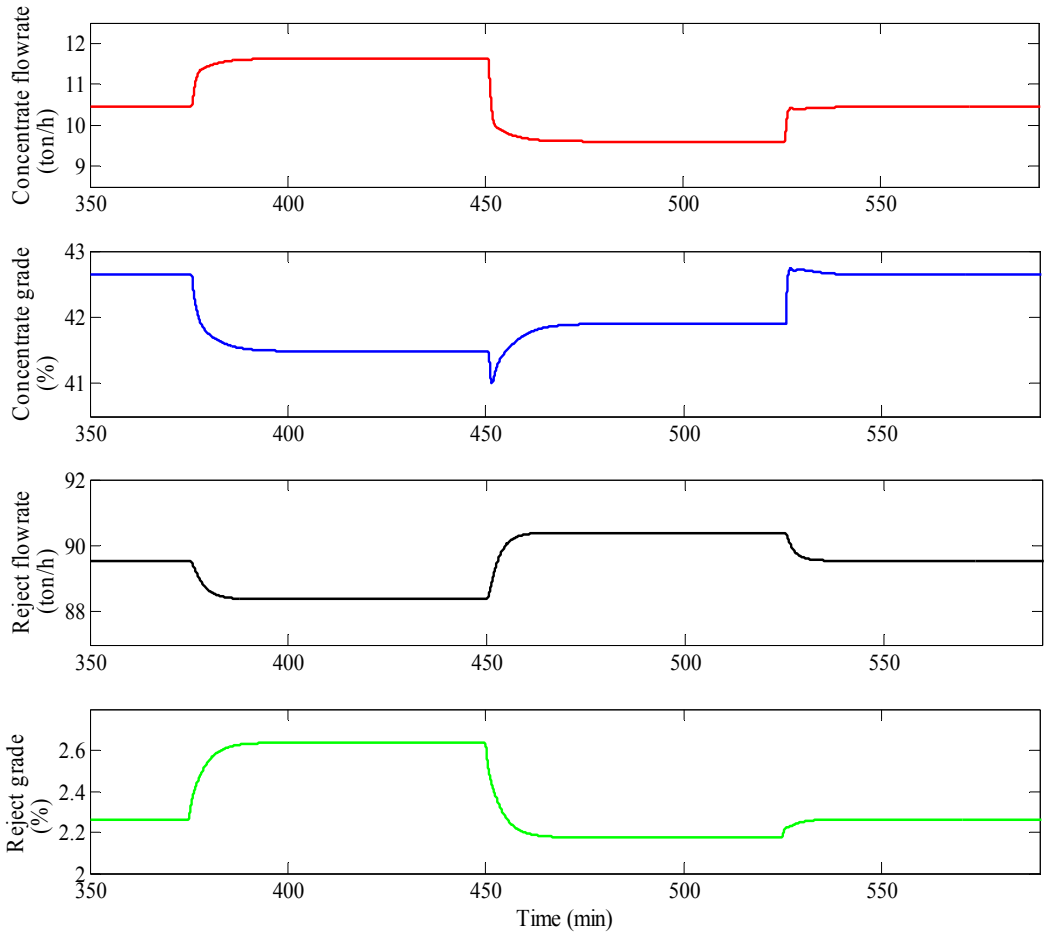

Fig. 7-31: Cell performance: feed grade changes effect on the output variables.

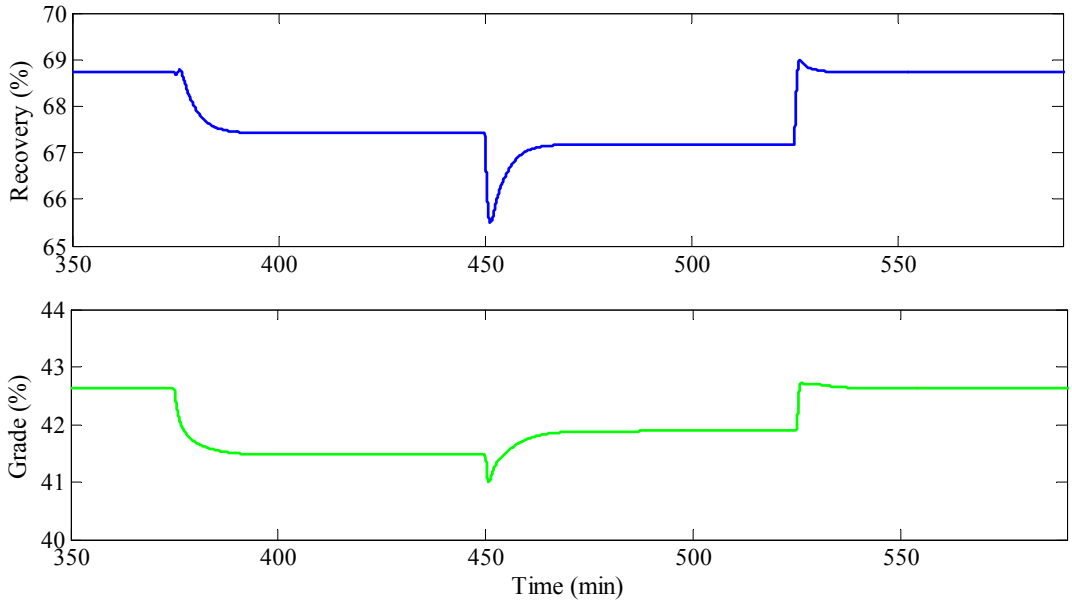

Fig. 7-32: Cell performance: plant recovery and grade when feed grade changes.

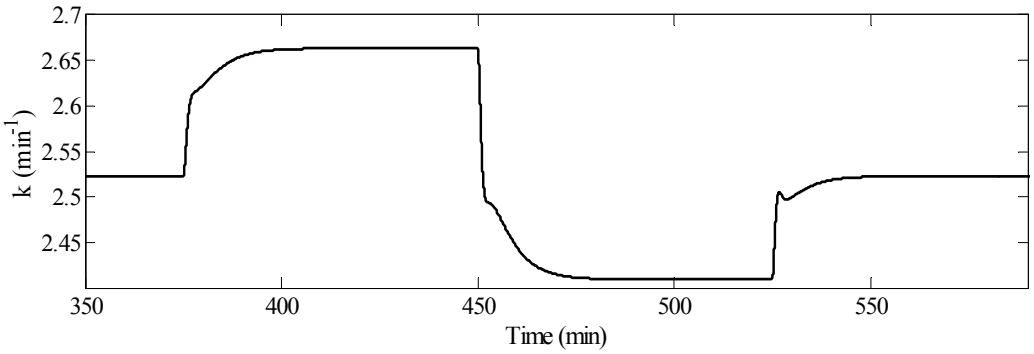

Fig. 7-33: Cell performance: feed grade changes effect on flotation rate constant.

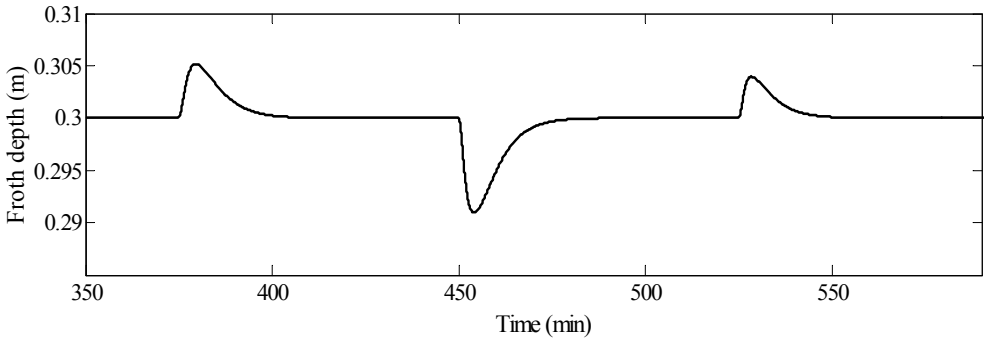

Fig. 7-34: Cell performance: froth depth when feed grade changes.

7.7.7.2 Flotation cell performance: stochastic disturbances in the feed

This section presents the performance of the cell when stationary disturbances affect both feed rate and grade. Although it is hard to interpret the behavior of the plant under stationary disturbances, it gives an idea of how plant reasonably operates. Applied disturbances in the feed are shown in Fig. 7-35 where the feed rate and grade vary with a standard deviation of 10% and 6% of their nominal value. To generate the disturbances, random fluctuation of pulp flowrate and particles mass fractions are filtered using a low-pass filter while sum of the particles mass fraction is always 1.

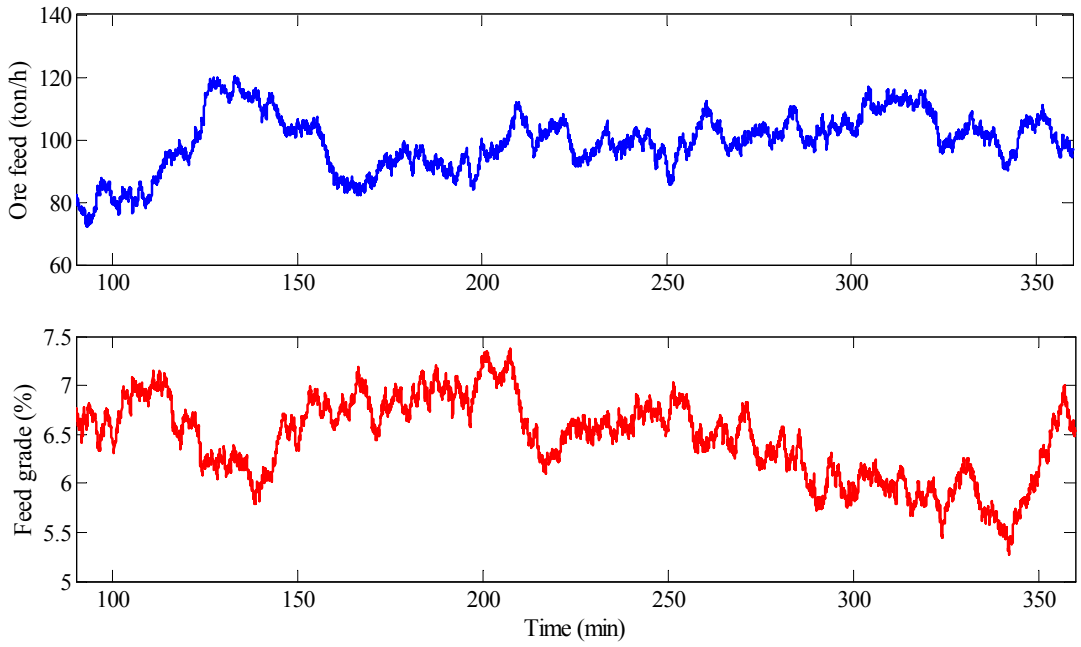

Fig. 7-35: Flotation cell: stationary variations of the feed characteristics.

Variations of the plant outputs are illustrated in Fig. 7-36 where the manipulated variables are constant. The variations could be explained by the facts presented in the previous sections. In comparison to feed fluctuations, high-frequency variations in the outputs are filtered by the plant nature. Calculated plant recovery and grade are depicted in Fig. 7-37.

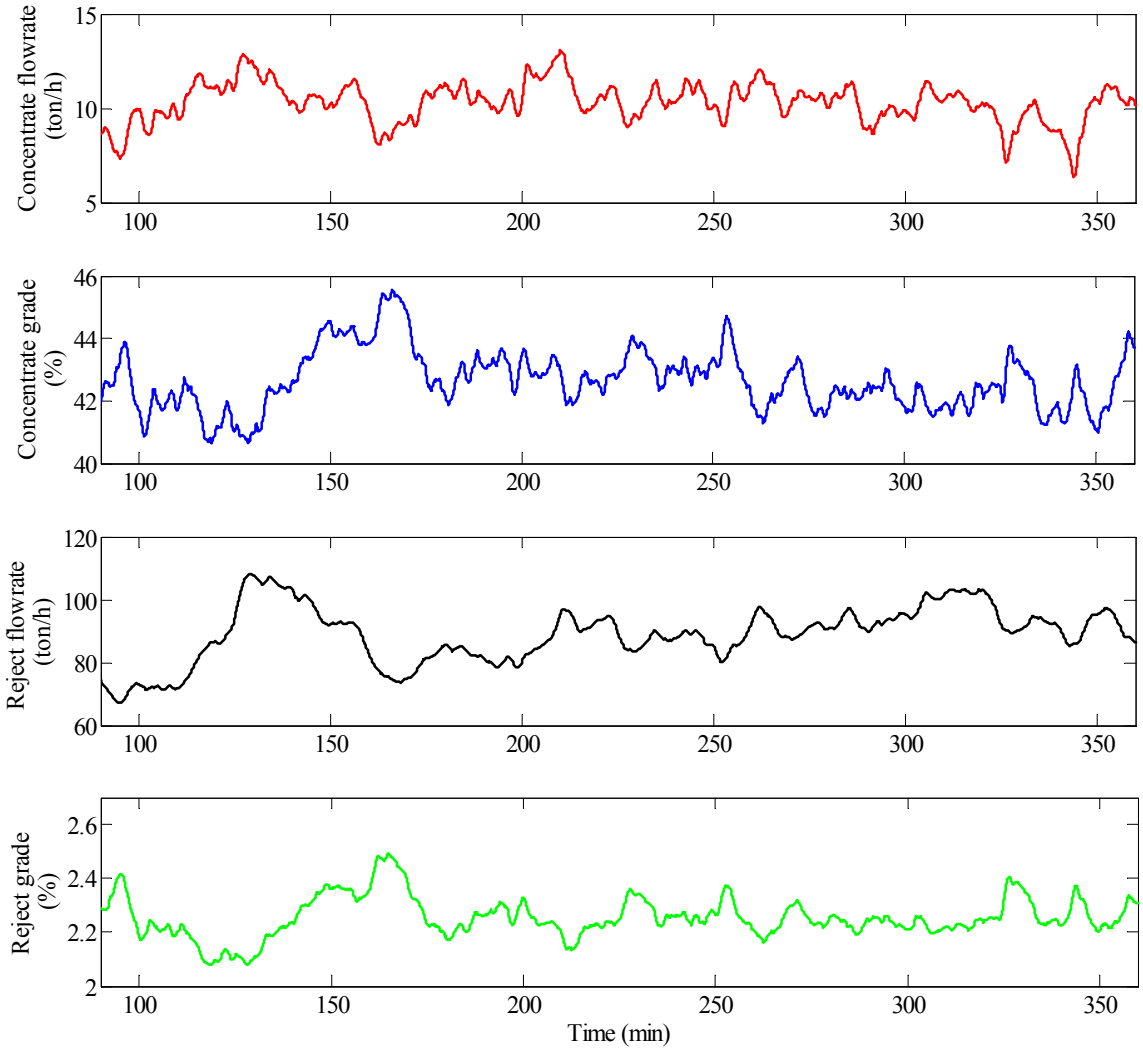

Fig. 7-36: Cell performance: stationary variation of the feed characteristics effect on the output variables.

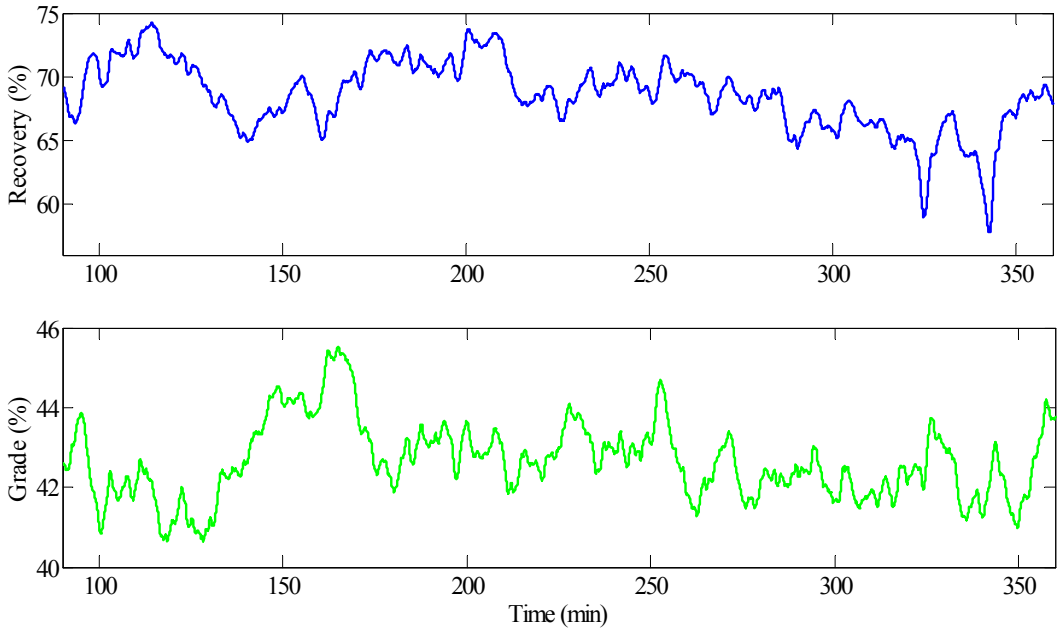

Fig. 7-37: Cell performance: plant recovery and grade when the feed characteristics stationary change.

In the current case, fluctuations in the rate constant k (Fig. 7-38) come from the variation of C that changes the material residence time inside froth T_d (Eq. 7-29). In fact, a smaller residence time inside the froth means less material drainage from the froth zone into the collection zone and so more floated material. This leads to a larger recovery and a smaller grade. To illustrate how the level controller acts, the froth depth variation is shown in Fig. 7-39.

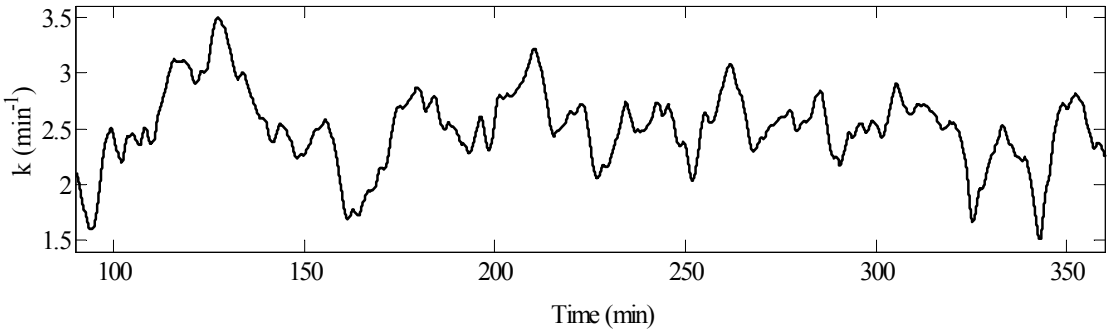

Fig. 7-38: Cell performance: stationary variation of the feed characteristics effect on the flotation rate constant.

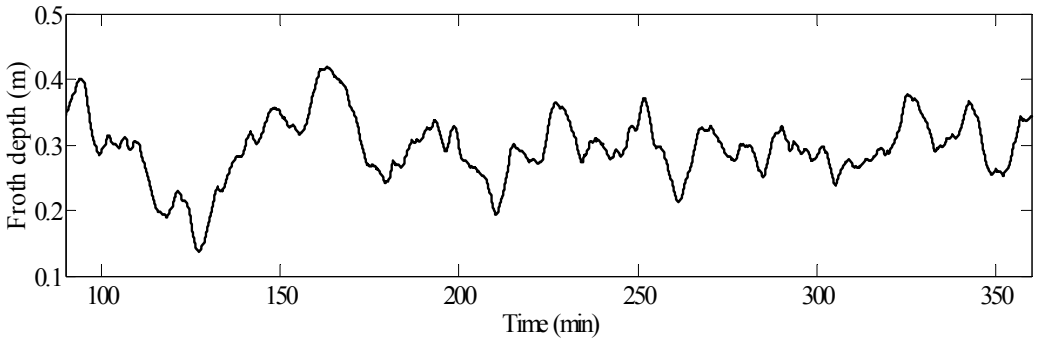

Fig. 7-39: Cell performance: froth depth when stationary changes occur in the feed characteristics.

7.8 Flotation circuit: features and performance

In the previous sections, the model and performance of a single flotation cell have been presented. Here, a flotation circuit consisting of three cells is considered. The circuit flow diagram is shown in Fig. 7-40. In this topology, the rougher cell is mainly responsible for the valuable mineral recovery while the cleaner increases the grade. The scavenger cell helps the rougher to recover more valuable minerals. To achieve these goals, each cell is designed with specific characteristics. Table 7-15 presents the dimensions of each cell.

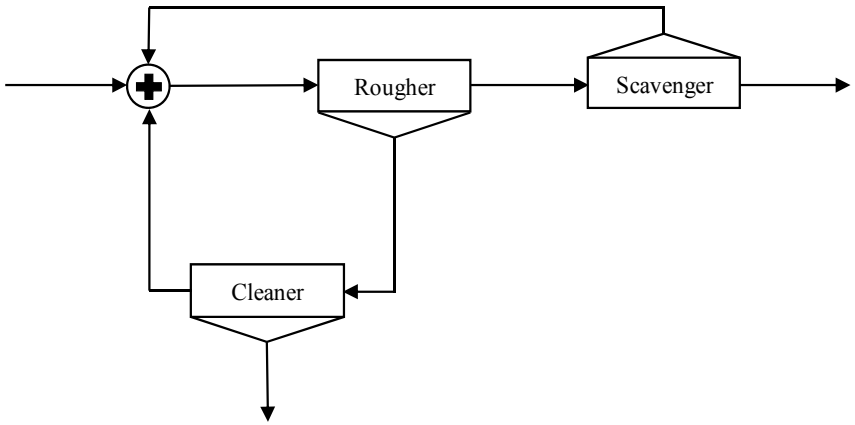

Fig. 7-40: Flotation circuit flow diagram.

Table 7-15: Flotation circuit - cell dimensions.

Dimension	Rougher	Cleaner	Scavenger
h (m)	3.0	1.0	3.0
S (m^2)	4.5	1.0	6.0

In the flotation circuit, as for the single cell, four types of manipulated variables are considered: air flowrate, collection zone level, collector concentration, and frother concentration. The two former manipulated variables are cell specific while the two later ones are for the whole plant. In other words, chemical reagents, i.e. collector and frother, are added to the plant feed, not to each cell feed. Therefore, a propagation model should be considered for chemical reagents inside the circuit. In this study, it is assumed that the reagents follow the water behavior in nominal operating conditions. Precisely, added reagents in the plant first pass through the rougher with the appropriate dynamic discussed in Section 7.4.3. At the rougher outputs that are also the cleaner and scavenger feeds, the reagent amounts are proportional to water separation coefficient in the rougher. Then, the chemical reagents pass through the cleaner and scavenger cells with corresponding dynamics obtained from water residence time. Since most water finally goes to the plant reject (about 90%), it is assumed that no chemical reagent is re-circulated.

7.8.1 Flotation circuit: steady-state performance

To present steady-state performance of the plant, it is essential to provide the nominal value of the feed characteristics and manipulated variables of each cell (Table 7-16). Detailed feed composition at nominal conditions has been already presented in Table 7-8. When the plant operates in the nominal conditions, the steady-state performance of the different cells is illustrated in Table 7-17 where τ_{pulp} stands for pulp residence time toward the reject stream. In order to have an acceptable solid percentage in the cleaner feed, i.e. about 50%, 4.5 t/h water is added to its input stream. This variable could be also used as a manipulated variable to affect the plant behavior. In comparison with the performance of the single cell shown in Table 7-9, the circuit improves both grade and recovery by 20% and 4%, respectively. If more recovery and grade improvements are desired, a grinding unit should be added to the circuit. But, according to the objective of the current study, such a unit is not needed.

Table 7-16: Nominal value of feed characteristics and manipulated variables.

Feed		Rougher cell		Cleaner cell		Scavenger cell	
A	100 t/h	U_c	0.5 l/t	U_c	0.5 l/t	U_c	0.5 l/t
a	6.5 %	Q_A	50 l/s	Q_A	11 l/s	Q_A	67 l/s
D_E	100 t/h	C_f	11 ppm	C_f	11 ppm	C_f	11 ppm
		h_p	2.7 m	h_p	0.7 m	h_p	2.7 m
		h_f	0.3 m	h_f	0.3 m	h_f	0.3 m

Table 7-17: Steady-state value of flotation circuit variables in the nominal operating regime.

	Whole plant	Rougher cell	Cleaner cell	Scavenger cell
Recovery (%)	72.7	66.8	80.3	39.5
Concentrate flowrate (ton/h)	7.76	13.9	7.76	5.35
Concentrate grade (%)	60.8	42.1	60.8	21.5
Reject flowrate (ton/h)	92.24	97.60	6.15	92.24
Reject grade (%)	1.92	3.00	18.75	1.92
τ_{pulp} (min)	-----	4.7	3.6	6.5
k (min^{-1})	-----	2.8	2.4	2.8
T_0 (s)	-----	43.0	10.0	120.0

7.8.2 Flotation circuit performance: manipulated variables changes

In this section, performance of the circuit is assessed when step changes are applied to the manipulated variables. In the simulator, several variables are available as the manipulated variables. To keep the investigation concise, only variables that are used in Chapter 8 are considered. These variables are: collector concentration, added water to the cleaner feed, and collection zone level in rougher, cleaner, and scavenger. Based on the variations of these variables, fifteen scenarios are defined (Table 7-18). Manipulated variable changes are illustrated in Fig. 7-41.

Table 7-18: Flotation circuit: different simulation scenarios based on the manipulated variables variations.

Scenario	S_1	S_2	S_3	S_4	S_5	S_6	S_7	S_8	S_9	S_{10}	S_{11}	S_{12}	S_{13}	S_{14}	S_{15}
From stage	0	1	2	3	4	5	6	7	8	9	10	11	12	13	14
To stage	1	2	3	4	5	6	7	8	9	10	11	12	13	14	15
ΔU_c (l/t)	**+0.5**	**-0.8**	**+0.3**	0.0	0.0	0.0	0.0	0.0	0.0	0.0	0.0	0.0	0.0	0.0	0.0
ΔL_r (m)	0.0	0.0	0.0	**+0.2**	**-0.4**	**+0.2**	0.0	0.0	0.0	0.0	0.0	0.0	0.0	0.0	0.0
ΔL_c (m)	0.0	0.0	0.0	0.0	0.0	0.0	**+0.2**	**-0.4**	**+0.2**	0.0	0.0	0.0	0.0	0.0	0.0
ΔL_s (m)	0.0	0.0	0.0	0.0	0.0	0.0	0.0	0.0	0.0	**+0.2**	**-0.4**	**+0.2**	0.0	0.0	0.0
ΔA_w (t/h)	0.0	0.0	0.0	0.0	0.0	0.0	0.0	0.0	0.0	0.0	0.0	0.0	**+3.0**	**-6.0**	**+3.0**

Similar to the manipulated variables, there are many candidates for the output variables. Here, only solid flowrate and grade of the plant concentrate and reject streams are considered. In the following subsections, the plant responses to each manipulated variable variations are investigated. Since the transient behavior of the plant is complex and difficult to be exactly explained, steady-state responses are mainly discussed.

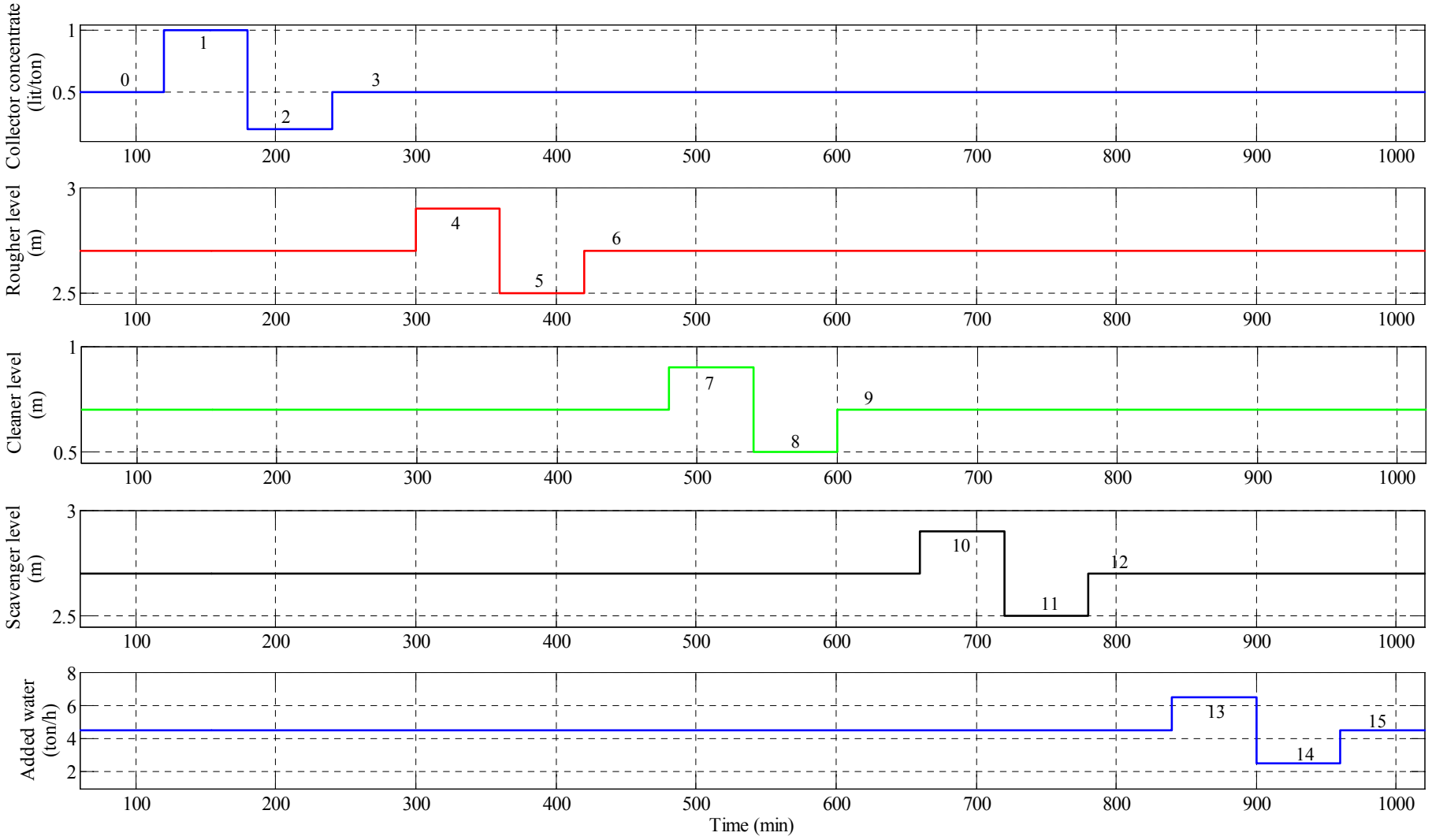

Fig. 7-41: Flotation circuit: variations of the manipulated variables.

7.8.2.1 Flotation circuit performance: changes of the collector concentration

Increase of the collector concentration increases the flotation rate constant and consequently valuable mineral recovery while valuable mineral grade decreases in the plant concentrate stream. Figs. 7-42 and 7-43 present the plant outputs and recovery-grade.

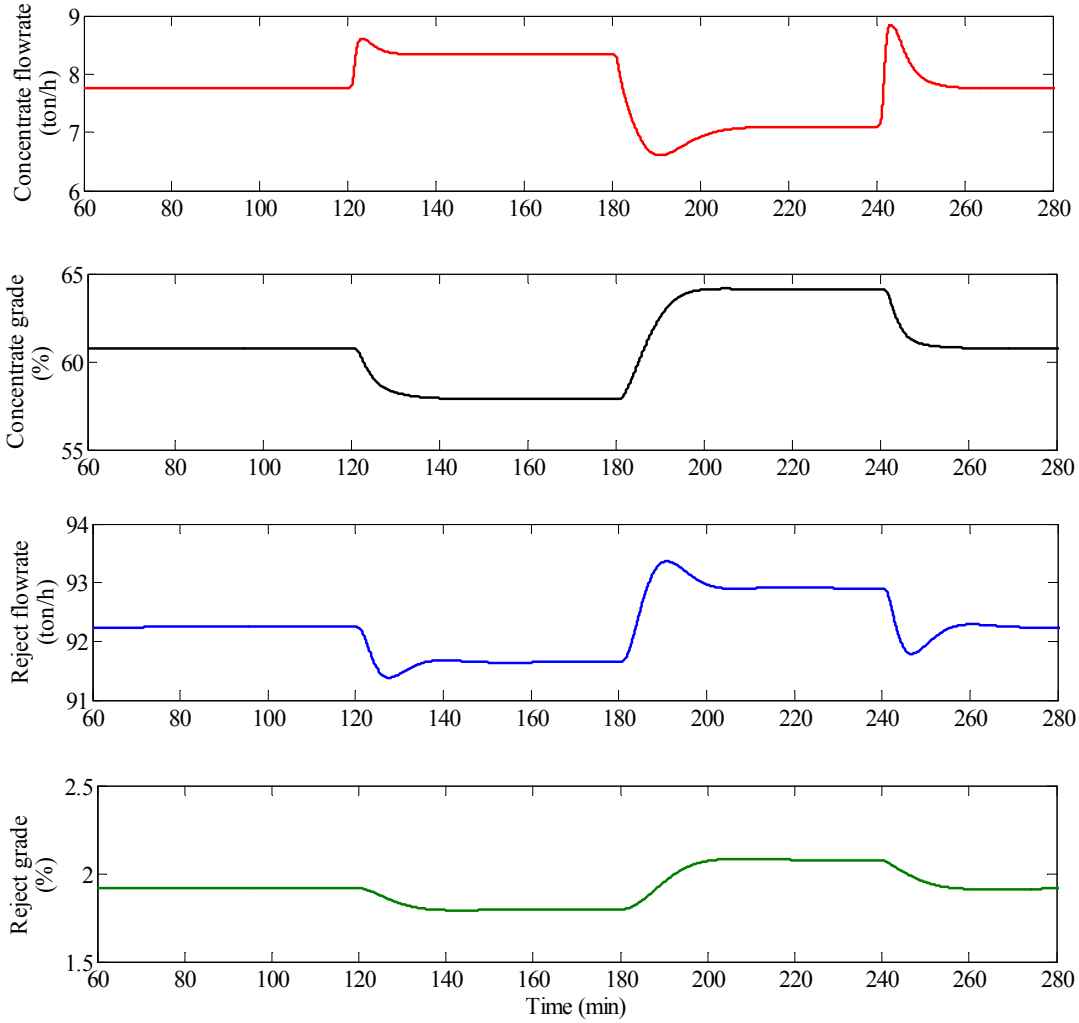

Fig. 7-42: Circuit performance: the collector concentration effect on the output variables.

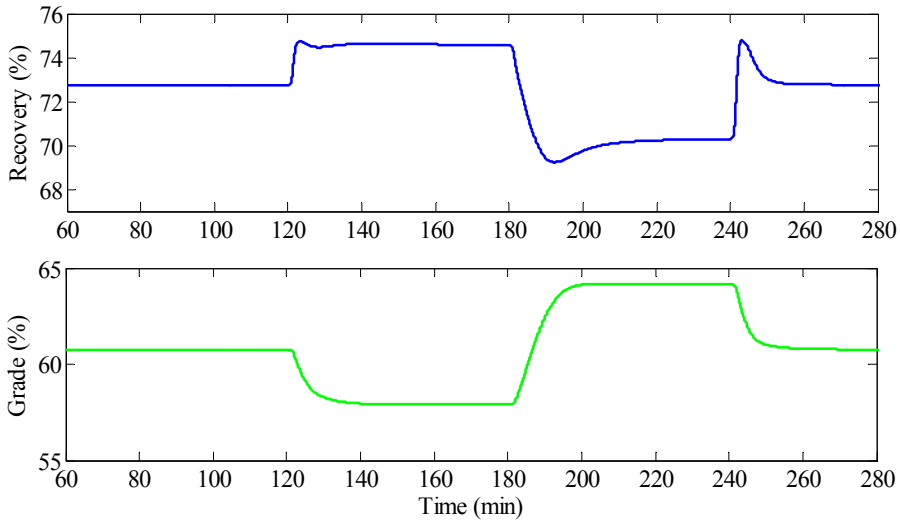

Fig. 7-43: Circuit performance: plant recovery-grade when the collector concentration varies.

7.8.2.2 Flotation circuit performance: changes of the rougher collection zone level

Increase of the level has two effects on the valuable mineral recovery: a) it increases the residence time inside collection zone, and b) it decreases residence time inside froth zone (Eq. 7-30). Both will increase the particles flotation while reducing Chalcopyrite grade in the concentrate stream. These explanations comply with what is observed in Figs. 7-44 and 7-45. Level of the rougher cell affects the plant recovery more than other cells level because of its size and chalcopyrite grade inside the tank. As seen in Fig. 7-45, ±0.2 m variation in the level causes about ±2% variation in the plant total recovery.

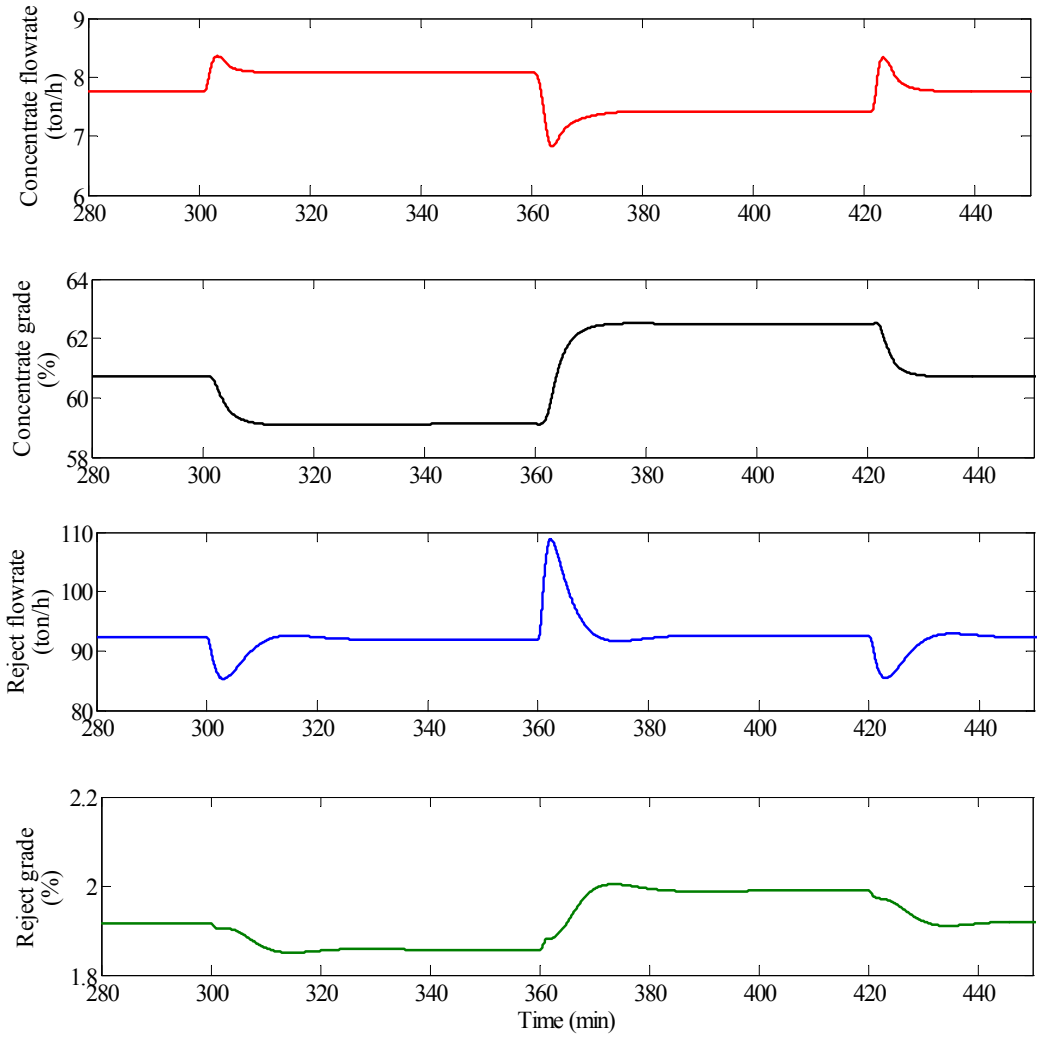

Fig. 7-44: Circuit performance: the rougher collection zone level changes effect on the output variables.

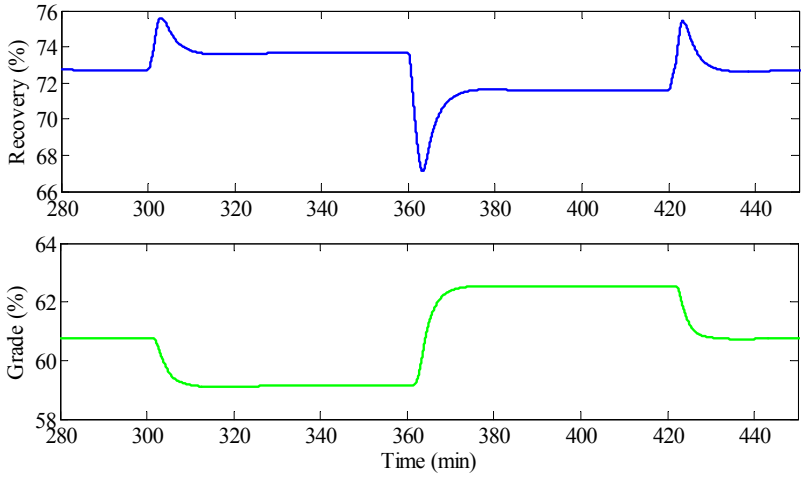

Fig. 7-45: Circuit performance: plant recovery-grade when rougher collection zone level changes.

7.8.2.3 Flotation circuit performance: changes of the cleaner collection zone level

Increase of the interface level in cleaner has almost the same effects on the output variables as the rougher cell level increase. However, transients and amplitudes are different. Variation of the cleaner level mostly affects the plant total grade. By increasing the level, again concentrate flowrate and recovery increase while grade decreases. Figs. 7-46 and 7-47 illustrate the simulation results.

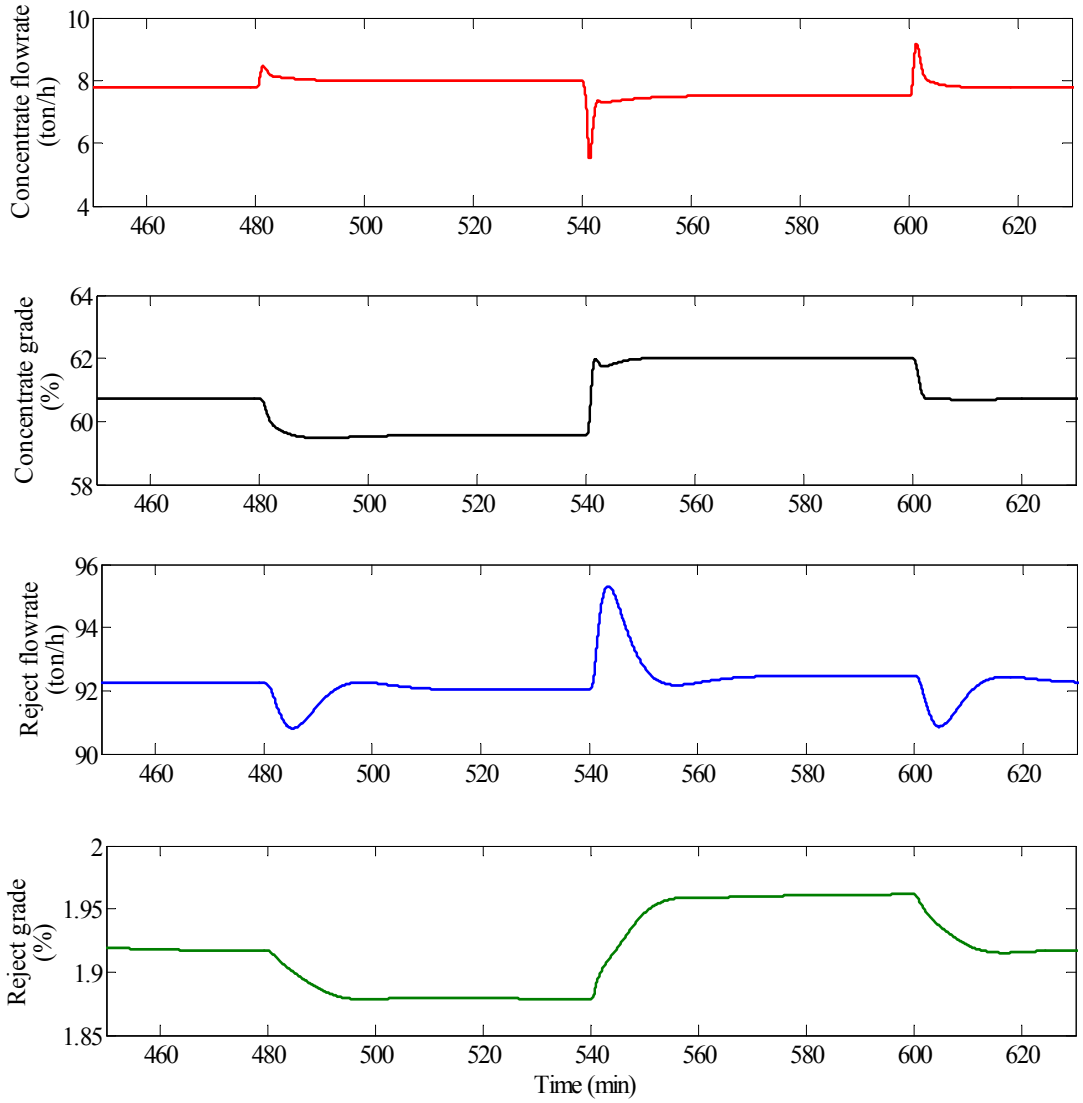

Fig. 7-46: Circuit performance: cleaner collection zone level changes effect on the output variables.

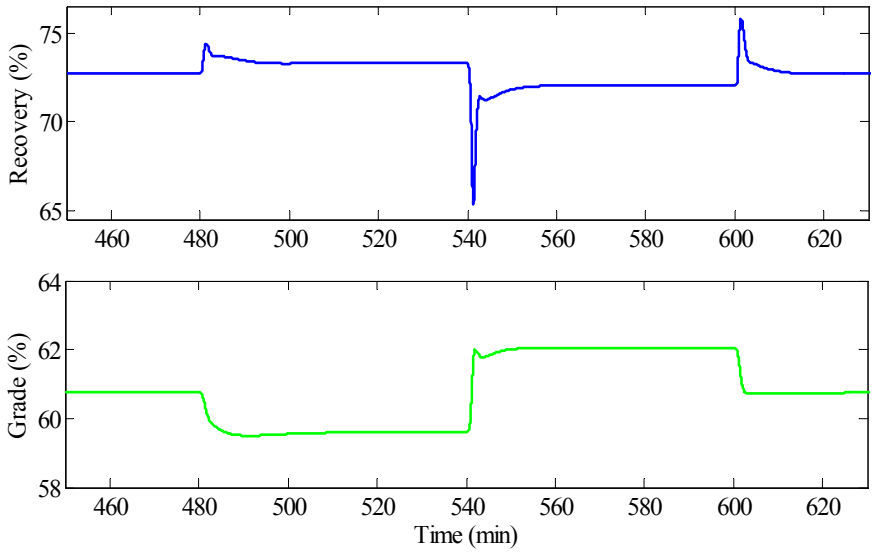

Fig. 7-47: Circuit performance: plant recovery-grade when cleaner collection zone level changes.

7.8.2.4 Flotation circuit performance: changes of the scavenger collection zone level

Similar to the rougher and cleaner, increase of the level in scavenger causes a rise in the concentrate flowrate and recovery while reducing the valuable mineral grade in the concentrate and solid flowrate in the reject. But magnitudes of the variations are smaller in comparison with rougher and cleaner. Moreover, because of the tank size, the transients are slower. Figs. 7-48 and 7-49 show the plant outputs and recovery-grade.

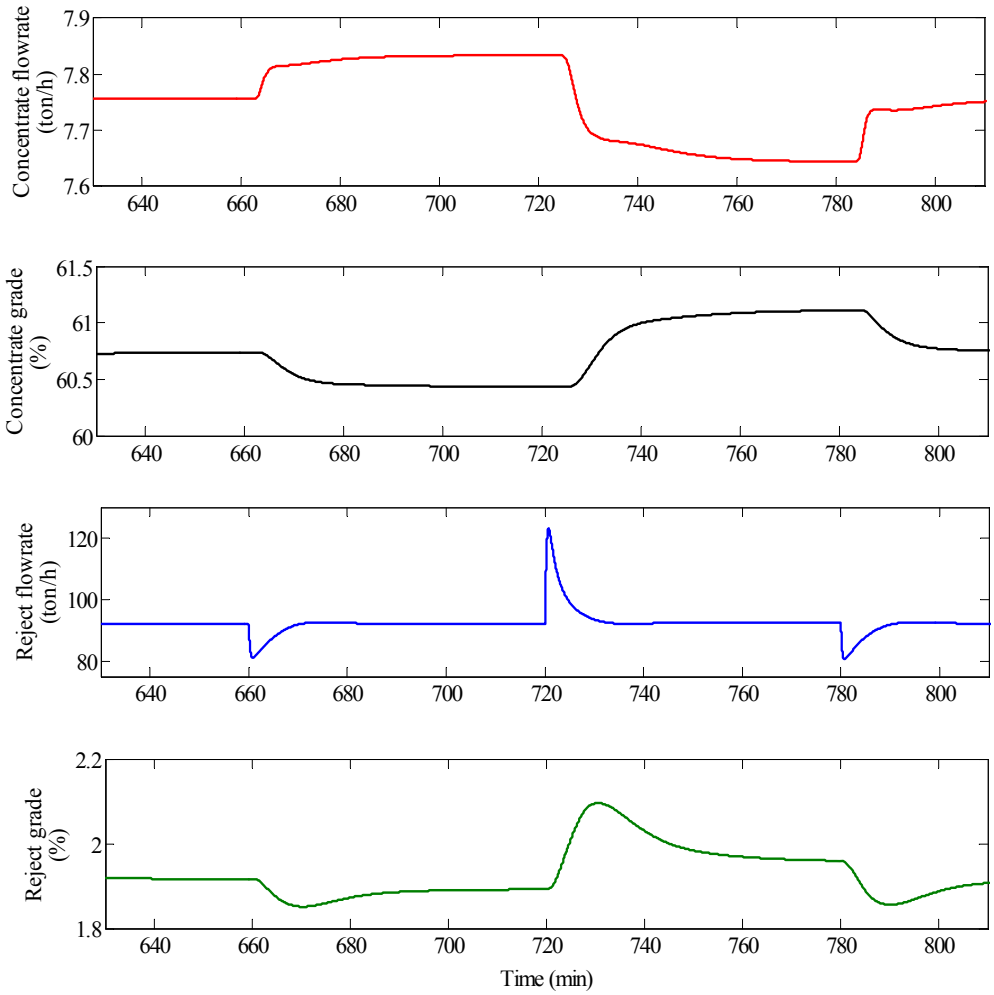

Fig. 7-48: Circuit performance: scavenger collection zone level changes effect on the output variables.

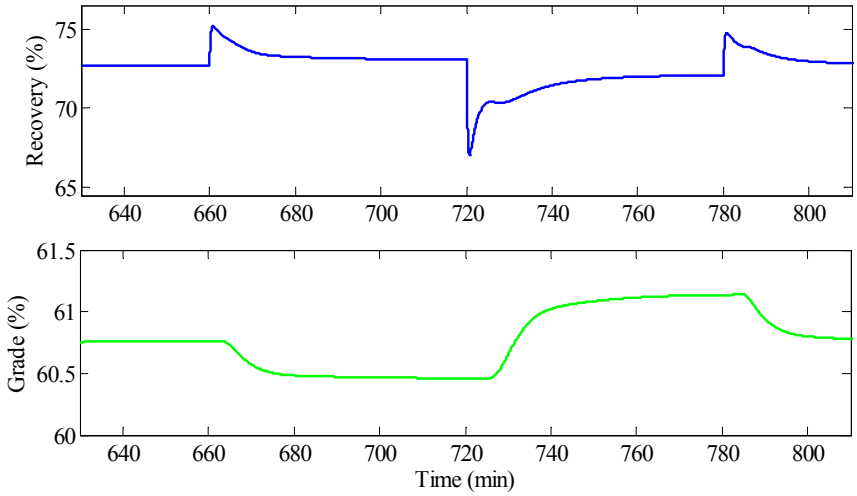

Fig. 7-49: Circuit performance: plant recovery-grade when scavenger collection zone level changes.

7.8.2.5 Flotation circuit performance: changes of the water addition in cleaner feed

Increase of water in the cleaner feed decreases the residence time inside the collection zone, so less material passes into the froth zone. Consequently, material residence time inside froth increases. Therefore, it is expected to have an increase in the grade while concentrate flowrate and recovery decrease. In Figs. 7-50 and 7-51, the output variables behavior and plant recovery-grade are shown. As seen, the effect of A_w on the plant recovery is marginal, but it significantly affects the plant concentrate grade showing that it could be a suitable candidate as the manipulated variable for the control application.

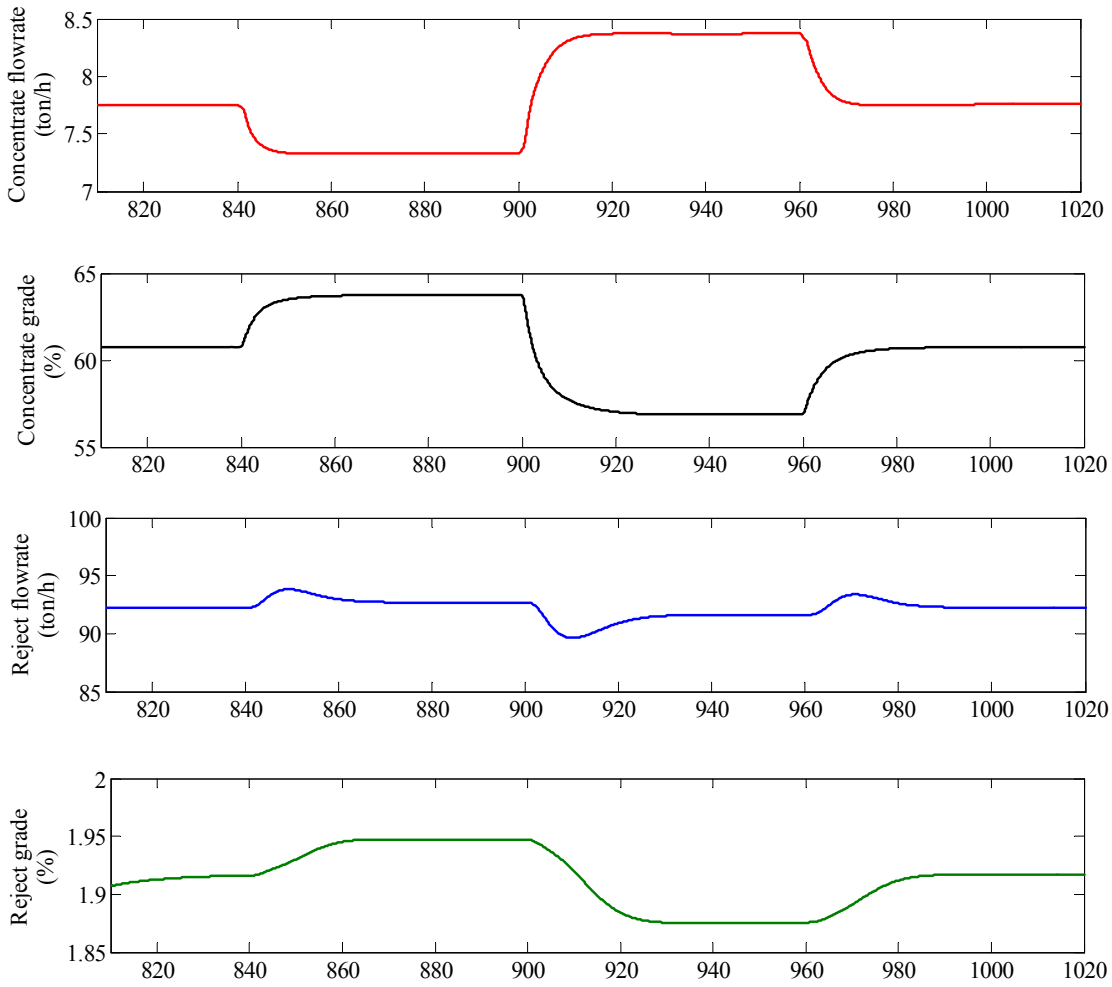

Fig. 7-50: Circuit performance: water addition changes effect on the output variables.

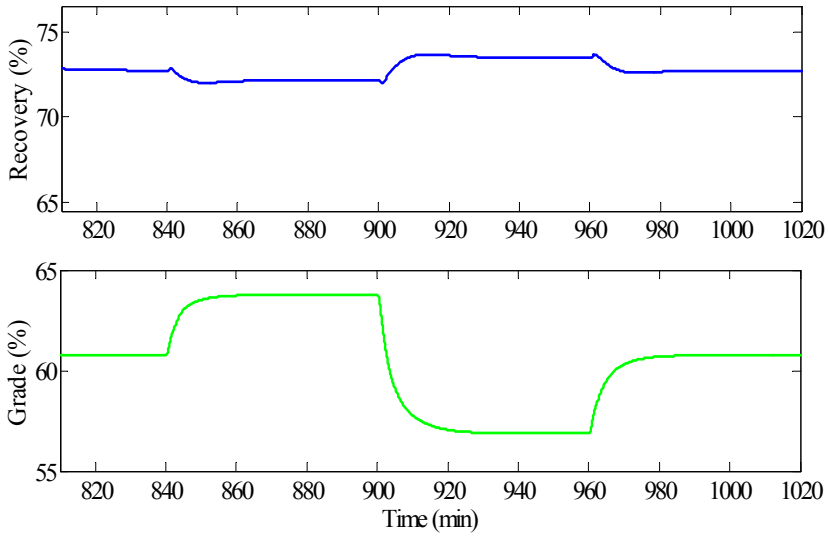

Fig. 7-51: Circuit performance: plant recovery-grade when water addition in cleaner feed changes.

7.9 Summary

This chapter has presented a dynamic simulator of froth flotation circuit. The simulator has been developed using dynamic mass balance equations and empirical relationships characterizing the kinetic phenomenon parameters. The aim of this work was to build a simulator for designing and testing data reconciliation observers and process control strategies. In the simulator, the collection and froth zones have been modeled as perfect mixter and plug flow reactor. Solid particles, water, and air interactions in the collection zone have been expressed using flotation and entrainment phenomena. Species drainage in the froth zone has been modeled by modifying the flotation rate constants. Dynamic mass conservation equations have been applied to water and twelve particle classes (three size and four composition classes). Collector and frother concentrations, collection zone level, and air flowrate have been considered as the manipulated variables. Several assumptions have been applied to simplify the models. Therefore, the simulator performance and model are not perfect, but its behavior is reasonable, at least for the objective of testing data reconciliation techniques and process control schemes.

First, a single cell has been modeled and its performance has been investigated using different tests cases. The tests have evaluated the model responses to the different disturbances applied to the plant feed and the manipulated variables. A detailed discussion

has been presented to justify the effect of disturbances on the output variables and cell behavior. Then, a flotation circuit simulator consisting of three cells has been considered, and its performance has been tested. For this purpose, the collector concentration, added water to the cleaner feed, and collection zone level in rougher, cleaner, and scavenger have been employed as the manipulated variables. Simulation results have revealed that increase of levels and collector concentrate improve the plant recovery while decreasing the grade. Water addition in cleaner feed significantly has increased the grade and slightly decreased recovery. In general, the simulator demonstrates a quite reasonable behavior and its performance is representative of flotation plants. Therefore the simulator is suitable for the study objective, and it can be applied as the case studies for data reconciliation observer and advanced controller design in Chapters 6 and 8, respectively. However, the simulator could be improved by: a) involving the bubble size distribution instead of using D_{32}, b) applying more detailed model for the froth zone, c) extending the model for more than two minerals, and d) including a grinding unit in the plant.

Chapter 8

Coupling Data Reconciliation with Process Control and Real Time Optimization

This chapter presents and evaluates the effect of data reconciliation when it is coupled with process control and real-time optimization strategies. In practice, estimating the benefits brought by data reconciliation to process control and optimization is a difficult task and not well addressed in the literature. The aim of this study is to illustrate that point at least for specific processes. For this purpose, two schemes are considered: a) Advanced Process Control (APC) and b) Real Time Optimization (RTO). For the first one, the objective is to reject the disturbances and track the set-points while the second scheme attempts to maximize the economic benefits of the plant over a period of time. To evaluate the performance of both schemes in the presence of data reconciliation, the flotation circuit simulator presented in Chapter 7 is used as a case-study, and statistical and economic performance indices are applied.

8.1 Data Reconciliation Application in Process Control and Optimization: A Review

High-quality data is essential to make suitable decisions, and consequently maximize the profits, deal with market changes, and achieve technical objectives. Moreover, to keep a plant around the optimum point, e.g. for advanced process control, real-time optimization, or plant supervision applications, quality of data plays a critical role. In practice, on the one hand, measured process variables are always corrupted by errors, either random or systematic. On the other hand, unmeasured key process variables and inconsistency between the process model and data cause major problems for auditing, control, and

optimization applications. To cope with the situation, data reconciliation is considered as an alternative providing more reliable data.

Before going through the related literature, it is worthwhile to recall the hierarchy of the plant monitoring, control, and optimization stages in a closed loop plant. To summarize all the information, the process control pyramid, composed of five stages, is presented in Fig. 8-1. Stage 1 stands for the measurement devices and actuators. Stage 2 consists of local control loops such as level, temperature, and pH controllers. In Stage 3, process key variables like valuable mineral grade and concentrate flowrates are controlled using advanced control strategies. In this step, manipulated variables are calculated to improve the plant behavior at each sampling time. In RTO stage, set-points of the lower stage are determined so that the plant performance, mainly economic performance, is improved for longer periods of time, e.g. days or weeks. In the final stage, plant performance is considered for even longer time windows, e.g. months and year, and based on desired performance of the plant and market changes, the plant model used in RTO is updated.

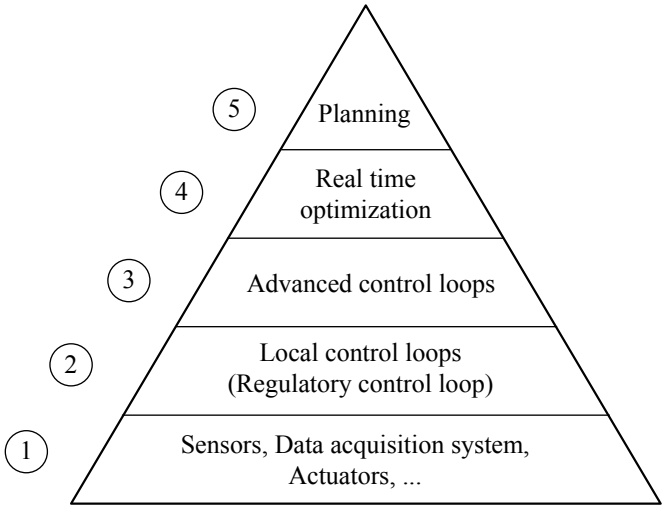

Fig. 8-1: Typical control hierarchy.

Based on the literature, DR can improve the performance of control strategies and RTO by attenuating the measurement noise and control action variations, estimating unmeasured variables, updating model parameters, and improving model and data coherency (Bai et al., 2005a). From an industrial point of view, these improvements can bring better products quality and more economic revenues. In the last decades, many studies have focused on the

data reconciliation topic mainly considering the optimal estimation of process states under open-loop conditions. On the contrary, few researchers have investigated the plant performance in the presence of controller and real-time optimizers, i.e. closed the loop, where reconciled data is applied instead of raw measurements.

For instance, Ramamurthi et al. (1993), Abu-el-zeet et al. (2002), Zhou and Forbes (2003), Bai et al. (2005a), Bai et al. (2005b), and Bai et al. (2007) involved data reconciliation in the process control level. Ramamurthi et al. (1993) proposed a new dynamic DR observer and investigated its effects on the closed-loop performance of a nonlinear predictive controller. They presented a successively linearized horizon-based estimator to estimate the process states and parameters. Ramamurthi applied a two-level estimation algorithm to reconcile the corrupted process inputs and outputs. Their study revealed that the integration of the DR observer to the controller provides smoother control actions allowing the use of more aggressive controllers.

In another attempt, Abu-el-zeet et al. (2002) introduced a dynamic DR observer, in conjunction with systematic bias detection, coupled with an MPC scheme. They used DR to improve the estimation of model parameters applied in MPC. They claimed that the overall performance of the model-based predictive controller considerably improves when the reconciled data is being fed to the controller. However, the degree of improvement in the controller performance was not specified.

Zhou and Forbes (2003) presented a systematic algorithm for quantifying the benefits of controller implementation in industrial plants. They proposed an optimization-based technique for calculating the expected economic performance of a given control system. This goal has been achieved in two steps: first, the performance estimation problem is posed in a stochastic optimization form. This optimization problem determines the controller operating conditions maximizing the economic benefits subject to some quality constraints. In the next stage, quantifying these economic benefits is discussed. The benefits were analyzed in analogy to the analysis of variance (ANOVA) technique. The paper did not explicitly consider DR but it presented some ideas that are applicable for integration of DR and process control.

Bai et al. (2005a) also introduced a dynamic DR algorithm embedded in a conventional PI control loop to reconcile noisy raw measurements before calculating the control actions. They illustrated that the application of DR can result in better feedback control performance. Filtering the measurements allows more aggressive controllers to be used, and, at the same time, prevents the manipulated variables from excessive variations. Bai et al. (2005b) investigated DR observer performance implemented in the conjunction with PID control system for a binary distillation column. They simulated the controller performance in 3 cases:

- Without measurement noise and DR.
- With measurement noise and without DR.
- With measurement noise and DR.

The results revealed that data reconciliation could reduce the propagation of measurement noise in control loops, so that the overall performance of the controller is enhanced. However, again, the degree of improvement in the controller performance was not specified. Furthermore, they did not discuss the effect of plant-model mismatch, it seems that they used the same model for the controller and plant simulator.

Bai et al. (2007) assessed the impact of model structure on the performance of dynamic data reconciliation coupled with process control. They first presented different DR observers based on different process models. Then observers were embedded inside the feedback loops, and finally DR observers were evaluated based on their performance in control procedure. For this purpose, they defined a plant overall cost function based on the distance between true and set-point values of controlled variables.

Souza et al. (2011) considered another aspect of DR, i.e. estimation of unmeasured variables and parameters, in the control loop of a polymer production plant. They concluded that estimated variables and parameters can be used to update the model implemented in the controller and to modify the optimum operation trajectory practiced at the plant site.

All above mentioned studies evaluated DR effectiveness using statistical properties of manipulated and controlled variables, and they did not investigate the associated economic gains. They only concluded that using DR in the process control layer allows more aggressive controllers to be used, and at the same time, prevents the manipulated variables from excessive manipulations.

Naysmith and Douglas (1995) presented a literature review on RTO applications in chemical industries. They used reconciled data in RTO procedure and assessed the performance of RTO with DR using an objective function derived from the plant model. This objective function represents the economic model of the process based on products value and associated costs. Finally, they concluded that application of RTO integrated with DR can make the following benefits for chemical industries:

- Improved product yields and/or quality.
- Reduced energy consumption and operating costs.
- Increased capacity of equipment, stream factors.
- Consistently holding the process at production targets.
- Decreased product variability.

Zhang and Forbes (2000) proposed a systematic and comprehensive procedure, called extended design cost, to evaluate the performance of different RTO designs. The design evaluation metric was defined as the total loss in the performance of RTO system due to design imperfections during a pre-specified evaluation period. Although, at the beginning, the paper claimed that DR is an important stage in RTO procedure, at the end it was neglected for simplicity purpose. However, the study presented a good systematic tool to evaluate the performance of RTO.

Faber et al. (2006) integrated a data reconciliation approach into an online optimization framework for a coke-oven-gas purification process. To increase the accuracy of the model, process parameters were estimated using a sequential parameter estimation approach. Using the parameter estimation based on the reconciled data, the average model deviations were significantly reduced. They did not present any quantitative analysis for this improvement.

Also, Forbes et al. (2006) introduced a general scheme for RTO integrated with data reconciliation and data validation. They proposed a five-step procedure for analyzing the results achieved from RTO. This procedure only checks the consistency of the results and does not evaluated the benefits of RTO from economic point of view. In another attempt, Jansky (2006) and Jansky (2007) investigated how data reconciliation can be economically beneficial to power plants. They determined three factors that using reconciled data can bring the financial benefits in power plants: a) increased efficiency (i.e. maximized output), b) time advantage in retrieving "lost" megawatts, and c) reduction of maintenance costs.

All above-discussed literature combined DR with RTO schemes, but they did not provide any economic analysis showing how much DR could be beneficial for a given plant. They only used some qualitative measures. Few studies have involved DR in both process control and optimization loops. Hodouin (2010) provided a general scheme for this purpose. In the scheme, stationary or dynamic observer is used for the control loop while a steady-state observer is applied for RTO level. Hallab (2010) employed Hodouin's scheme for a gold leaching circuit in mineral industry, and then it investigated the benefits of combining data reconciliation, control, and optimization from a technical and economic point of view. But for simplicity, it separately investigated DR effect on control and optimization loops. The effectiveness of DR in control loop was presented using variance reduction in the manipulated and controlled variables. For RTO layer, an economic criterion driven from plant model and operation condition was maximized. Solving the optimization problem revealed that DR can increase the economic revenues of RTO implementation.

The aim of this chapter is to illustrate the effect of data reconciliation in control and real-time optimization loops. Therefore, an advanced process control and a real time optimization schemes are considered. In APC, the objective is to reject the disturbances and follow the set-point changes while RTO attempts to maximize an objective function defined based on the economic revenue of plant. To implement both schemes, a mass conservation based system identification is applied and then a proper controller/RTO is designed. To evaluate the performance of both schemes in the presence of data reconciliation, statistical and economic performance indices are employed.

Section 8.2 is dedicated to introduce the controller structure used in the chapter. Process model identification and evaluation is presented in Section 8.3. Advanced process controller design and related issues are described in Section 8.4. Real-time optimization scheme based on economic features is design and discussed in Section 8.5. Section 8.6 is devoted to present the data reconciliation observer used for coupling with APC and RTO. In this section, observer model, test scenarios, and feed disturbances are illustrated. Sections 8.7 and 8.8 show APC and RTO performances respectively with and without data reconciliation observer under different feed disturbances.

8.2 Receding Horizon Internal Model Controller

Regardless of APC or RTO application, a general control scheme, called Internal Model Control (IMC), is applied in the current study. Designed RTO in this chapter is a direct scheme which couples both RTO and advanced control stages shown in Fig. 8-1, and it is different form the hierarchical one shown in Hodouin (2010). Roughly speaking, this RTO is a controller with an objective function maximizing economic benefits of the plant, and it does not use any set-point. In the literature, such an approach is often called economic MPC and mainly applied to improve the plant revenue over periods of time.

For control purpose, a receding horizon strategy is considered. The idea is to obtain the control actions that optimize and control the plant behavior for a long period of time. Therefore, standard MPC could be a good candidate but its closed loop observer, i.e. Kalman filter, can cause some problems for the study of data reconciliation effect in the closed loop plant. Having two observers (Kalman filter for MPC and DR observer) in the same loop can lead to some issues because the controller observer and DR observer do not necessarily share the same process states. For instance, sub-model based DR observers always use the states that have physical meaning while this is not the case for Kalman filter. Moreover, simultaneous use of KF (as the controller observer) and DR observer doubles the noise and disturbance filtering, and this point prevents the study to independently evaluate DR observer performance as the objective of the chapter. To isolate DR contribution from the other observers, instead of the standard MPC, a receding horizon IMC scheme that only benefits from a simple and open loop observer is employed in the

current study. In this open loop observer, process states are estimated using already identified models (i.e. transfer functions).

Schematic of the controller is shown in Fig. 8-2 where f_1, c_1, and D_E stand for the ore flowrate rate, chalcopyrite concentration, and water flowrate in the feed stream used to represent the feed characteristics and disturbances. Here, ore and chalcopyrite flowrates (f and f_c) in all streams are considered as the plant measured variables contaminated by random noises v and v_c. In the figure, there is also a block that extracts the controlled variables y, i.e. variable required for controller, form the plant measurements. $\hat{d}$ stands for the estimated disturbance containing the plant output disturbances and modeling errors. u_n and y_n are the nominal values of the manipulated and controlled variables, respectively. $\tilde{u}$ represents the variation of the manipulated variables around their nominal values (i.e. $u = u_n + \tilde{u}$) while $\hat{x}(k)$ is the current value of the process states obtained from identified transfer functions represented in state-space form.

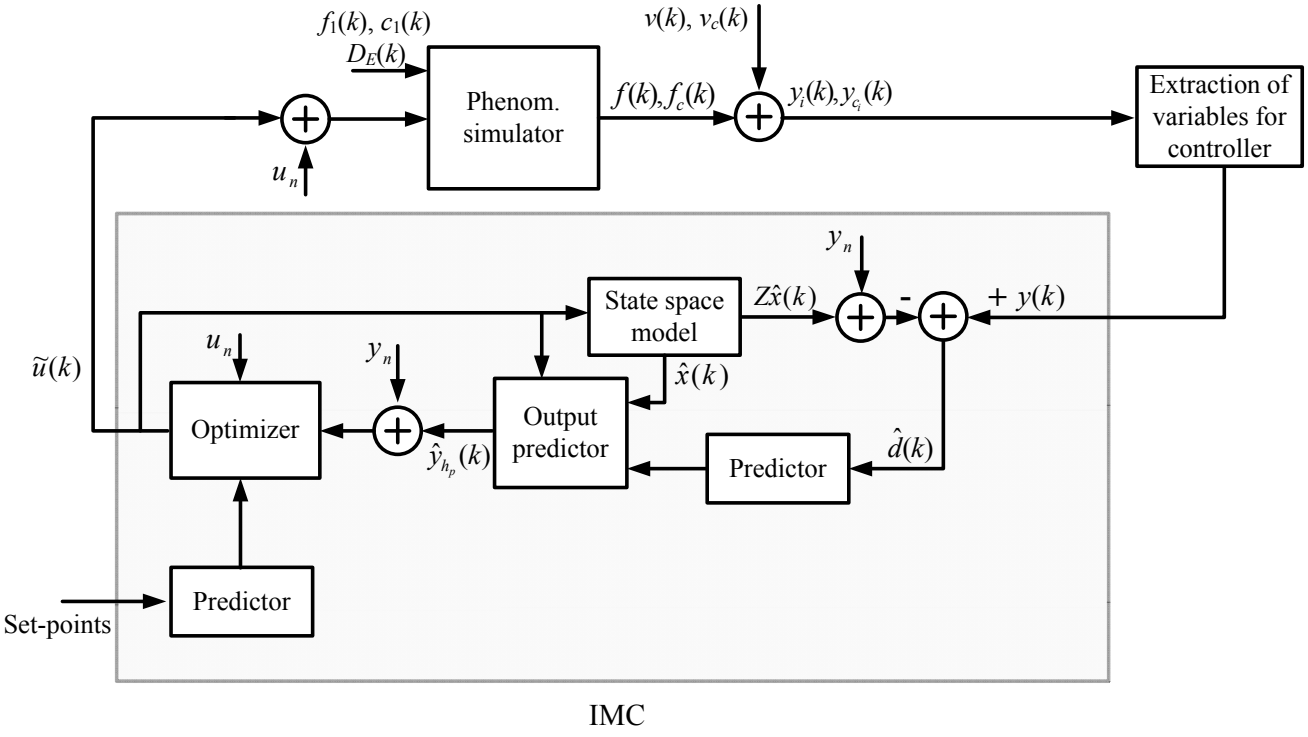

Fig. 8-2: General control scheme.

The process state-space model used for state estimation could be expressed by:

$$\begin{cases} \hat{x}(k+1) = A\hat{x}(k) + B\tilde{u}(k) \\ y^*(k) = Z\,\hat{x}(k) + y_n \end{cases} \tag{8-1}$$

where A, B, and Z stand for the process transition, input and observation matrices obtained from already identified transfer functions. The output disturbance $d(k)$ is estimated using:

$$\hat{d}(k) = y(k) - y^*(k) \tag{8-2}$$

For a given controller prediction horizon h_p, the output prediction equations could be written as:

$$\hat{y}_{h_p}(k) = M_{h_p}\hat{x}(k) + N_{h_p}\tilde{u}(k-1) + D_{h_p}(k) + P_{h_p}\Delta u_{h_p}(k) \tag{8-3}$$

where

$$\hat{y}_{h_p}(k) = \left[y^*(k+1\,|\,k) \quad y^*(k+2\,|\,k) \quad y^*(k+3\,|\,k) \quad \cdots \quad y^*(k+h_p\,|\,k)\right]^T \tag{8-4}$$

$$\begin{aligned} \Delta u_{h_p}(k) &= \left[\Delta u(k) \quad \Delta u(k+1) \quad \Delta u(k+2) \quad \cdots \quad \Delta u(k+h_p-1)\right]^T \\ \Delta u(k) &= \tilde{u}(k) - \tilde{u}(k-1) \end{aligned} \tag{8-5}$$

and

$$D_{h_p}(k) = E \otimes \hat{d}(k) \tag{8-6}$$

where E is a row vector of 1 with h_p length. In this implementation, it is assumed that disturbance $\hat{d}$ is constant over the h_p period. In Eq. 8-3,

$$M_{h_p} = \left[ZA \quad ZA^2 \quad ZA^3 \quad \cdots \quad ZA^{h_p}\right]^T \tag{8-7}$$

$$N_{h_p} = \left[ZB \quad Z(A+I)B \quad Z(A^2+A+I)B \quad \cdots \quad Z(A^{hp}+\cdots+A+I)B\right]^T \tag{8-8}$$

and

$$P_{h_p} = \begin{bmatrix} ZB & O & O & \cdots & O \\ Z(A+I)B & ZB & O & \cdots & O \\ Z(A^2+A+I)B & Z(A+I)B & ZB & \cdots & O \\ \vdots & \vdots & \vdots & \cdots & \vdots \\ Z(A^{hp}+\cdots+A+I)B & Z(A^{hp-1}+\cdots+A+I)B & Z(A^{hp-2}+\cdots+A+I)B & \cdots & ZB \end{bmatrix} \quad (8\text{-}9)$$

where I and O are identity and zero matrices with proper dimension, respectively. For a control horizon of h_c,

$$\Delta u(k+i) = 0 \qquad \text{for} \quad i \geq h_c \quad (8\text{-}10)$$

Therefore, the last term of Eq. 8-3 can be replaced by $P_{h_c}\Delta u_{h_c}(k)$ where

$$\Delta u_{h_c}(k) = \left[\Delta u(k) \quad \Delta u(k+1) \quad \Delta u(k+2) \quad \cdots \quad \Delta u(k+h_c-1)\right]^T \quad (8\text{-}11)$$

and P_{h_c} is the corresponding part of P_{h_p}.

8.3 Process Model Identification

The flotation circuit simulator developed in Chapter 7 is used as the case-study in this chapter. To implement the APC and RTO schemes, it is necessary to identify the suitable plant model. For this purpose, a set of manipulated and output variables should be selected. In the flotation simulator, there are a lot of possibilities for selecting the variables. Based on the availability of variables and economic value associated with them, variables listed in Table 8-1 are chosen. In practice, these variables are easily accessible and so they are widely applied for control applications. In Table 8-1, U_C stands for collector concentration and is defined as the amount of collector added to the plant feed per ton of ore feed. The plant diagram and variable locations are illustrated in Fig. 8-3. In the implemented schemes, the valuable mineral flowrates, i.e. C_n and R_n, instead of reject and concentrate grades are selected as the output variables for two reasons:

- In plant, when the solid flowrates and grades are measured, the valuable mineral flowrates can be easily calculated by multiplying them and applied in controller design instead of grades. So they do not need additional efforts to be measured.
- This chapter aims to identify an empirical process model conserving the mass in the steady-state situation. In such a model, gains of transfer functions for a given manipulated variable, i.e. SIMO case, are dependent, and they should respect the constraints induced by mass conservation law. To implement this idea, the reject and concentrate grades cannot be applied, instead of them, valuable mineral flowrates are selected as the output variables.

Table 8-1: Manipulated and output variables list selected for APC and RTO design.

Manipulated variables	Nominal value	Output variables	Nominal value
Collector concentrate (U_C)	0.5 l/t	Reject total flowrate (R)	92.25 t/h
Collection zone level: Rougher (L_R)	2.7 m	Reject valuable mineral flowrate (R_n)	1.77 t/h
Collection zone level: Cleaner (L_C)	0.7 m	Concentrate total flowrate (C)	7.75 t/h
Collection zone level: Scavenger (L_S)	2.7 m	Concentrate valuable mineral flowrate (C_n)	4.75 t/h
Water addition into cleaner feed (A_W)	4.5 t/h		

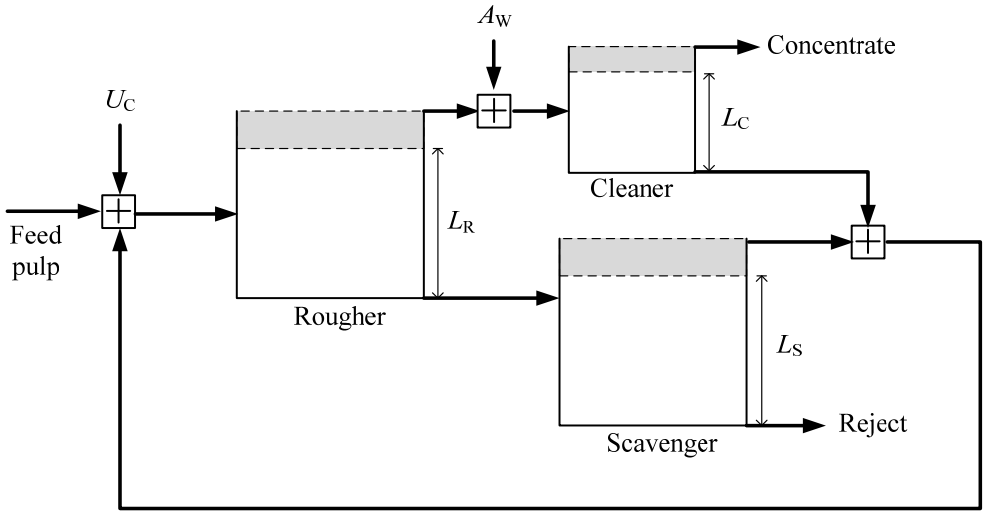

Fig. 8-3: Flotation circuit schematic and location of selected variables.

To identify the model, successive steps are applied to the manipulated variables around their nominal value shown in Table 8-1. Then a custom single-input multi-output identification technique is used. The identification algorithm has the following properties:

- A quadratic criterion based on the measurement and model output distance is minimized.
- Distances are uniformly weighted.
- The stochastic part of the model output is assumed to be a white noise implying that the transfer function of stochastic part is unitary.
- Constraints induced by mass conservation are applied for the estimation of transfer functions gains.

Identified transfer functions (TFs) are presented in Table 8-2. As seen, transfer functions gains conserve the mass; i.e. for a given manipulated variable *u*:

$$\begin{cases} G_{C,u}(0) = -G_{R,u}(0) \\ G_{C_n,u}(0) = -G_{R_n,u}(0) \end{cases} \tag{8-12}$$

where $G_{C,u}(0)$ is the gain of $G_{C,u}(s)$ which stands for transfer function between *C* and *u*. Listed transfer functions and variables in Table 8-2 are for the general case. For each of APC and RTO schemes, appropriate TFs and variables are selected from this table and applied. Identified transfer functions contain delays, right-hand side zero (non-minimum phase case), real and complex poles. Having poles with imaginary parts can result from the structure of plant where there are two circulating streams, i.e. cleaner reject and scavenger concentrate. These streams can cause some oscillations in the plant behavior. To illustrate the quality of identified models, fitted model compared to raw data is illustrated for the variables used in the following sections in Fig. 8-4. Although transfer functions show a good fit on a MSE basis and model parameters have acceptable estimation error, there is still nonlinearity especially in gains.

Table 8-2: Identified model transfer functions.

	U_C (l/t)	L_R (m)	L_C (m)	L_S (m)	A_W (t/h)
R (t/h)	$-2.16\frac{e^{-23s}}{(20810s^2+102.4s+1)}$	$-1.61\frac{(6860s+1)e^{-2s}}{(27690s^2+203s+1)}$	$-0.99\frac{(2350s+1)e^{-30s}}{(46230s^2+194s+1)}$	$-0.41\frac{(38500s+1)}{(199s+1)(25s+1)}$	$0.23\frac{(2800s+1)e^{-45s}}{(396s+1)^2}$
R_n (t/h)	$-0.433\frac{(1259s+1)e^{-20s}}{(808.5s+1)^2}$	$-0.336\frac{(464s+1)}{(136^2s^2+180s+1)}$	$-0.187\frac{(25s+1)e^{-20s}}{(11924s^2+110s+1)}$	$-0.13\frac{(3200s+1)}{(365s+1)(16s+1)}$	$0.02\frac{(740s+1)e^{-40s}}{(410s+1)^2}$
C (t/h)	$2.16\frac{(378s+1)e^{-20s}}{(173.2s+1)^2}$	$1.61\frac{(435s+1)e^{-60s}}{(114s+1)^2}$	$0.99\frac{(931s+1)e^{-20s}}{(348s+1)(24s+1)}$	$0.41\frac{e^{-160s}}{(260s+1)}$	$-0.23\frac{e^{-20s}}{(130s+1)(61s+1)}$
C_n (t/h)	$0.433\frac{(1181s+1)e^{-20s}}{(173s+1)^2}$	$0.336\frac{(1118s+1)e^{-60s}}{(109s+1)^2}$	$0.187\frac{(1659s+1)e^{-20s}}{(177s+1)(26s+1)}$	$0.13\frac{(1131s+1)e^{-160s}}{(1400s+1)(4356s^2+48s+1)}$	$-0.02\frac{(1-175s)}{(5685s^2+90s+1)}$

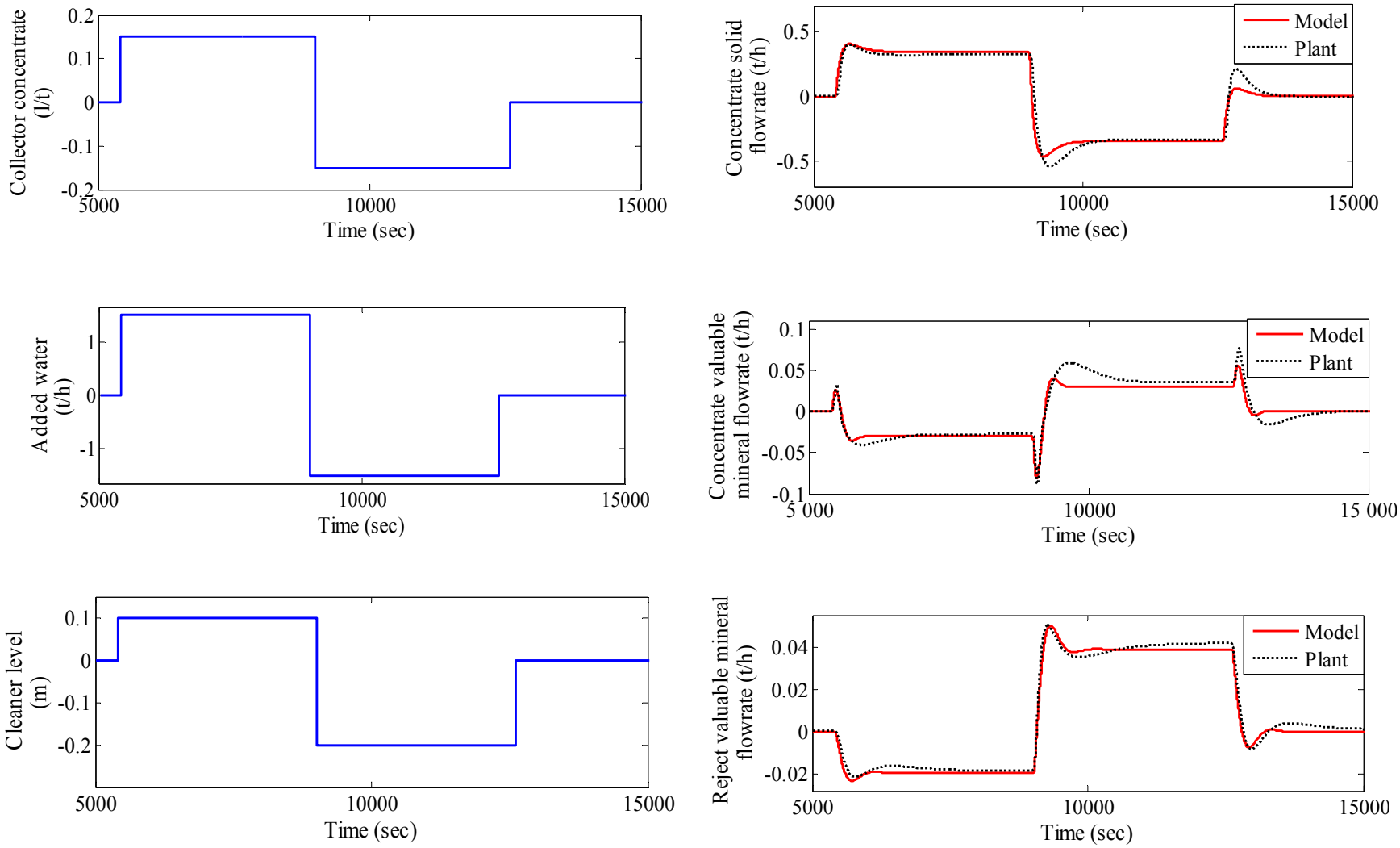

Fig. 8-4: Identified transfer functions and plant data comparison.

To show the mismatch between the identified model and the plant, an open loop test is used. In this test, collector concentration and added water, as the manipulated variables, change while output variables (i.e. reject and concentrate valuable mineral flowrates, and concentrate solid flowrates) are considered. This procedure is repeated for plant and model, and the results are compared (Fig. 8-5). As seen, the mismatch is mainly related to the gains while transient behaviors are adequately represented. Because of the mismatch, i.e. error, any control or RTO scheme designed in the following sections should be able to properly handle the modeling errors.

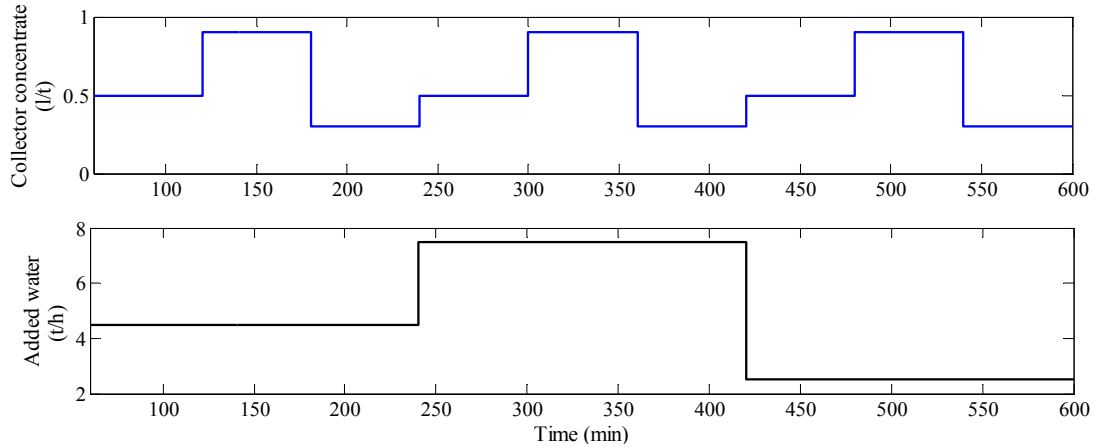

a) manipulated variables

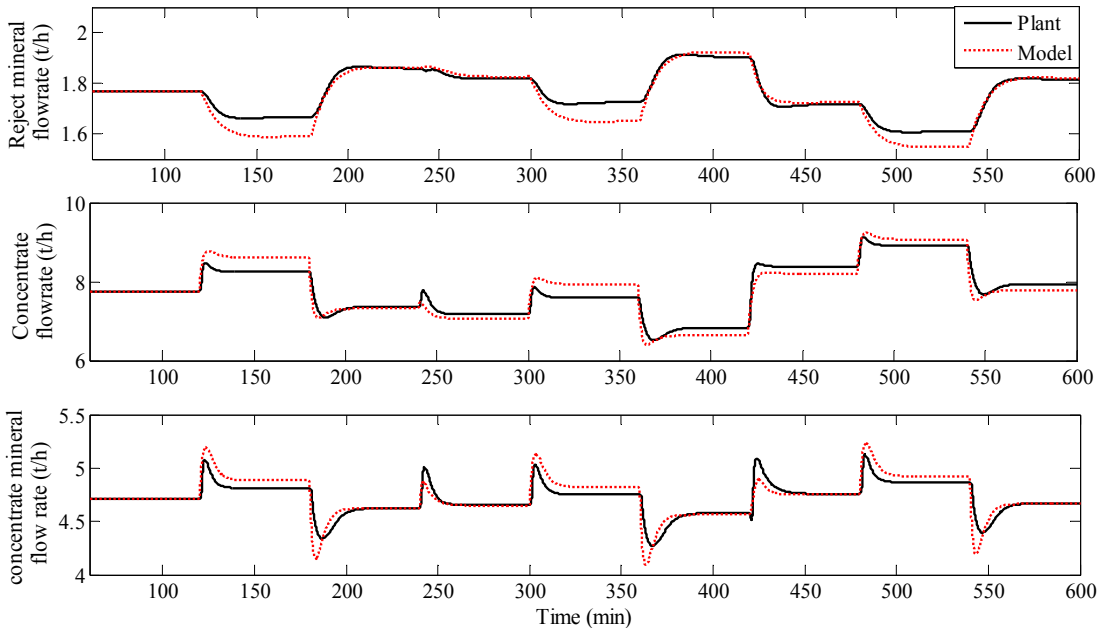

b) output variables

Fig. 8-5: Mismatch between plant and identified model.

8.4 Advanced Process Controller

As above mentioned, this study is interested to evaluate DR performance when it is coupled to an advanced control loop. Therefore, in this section, a control scheme keeping the plant recovery and grade at the predefined values in the presence of feed disturbances is designed. For this controller, a standard quadratic cost function is considered:

$$J_{APC}(k) = \alpha_{APC}\left(\rho_{h_p}(k) - \rho_{ref}\right)^2 + \beta_{APC}\left(c_{h_p}(k) - c_{ref}\right)^2 + \sum_{i=1}^{h_p} \Delta u^T(k+i) W_{u_{APC}} \Delta u(k+i) \qquad (8\text{-}13)$$

where $\Delta u(k)$ is defined as $u(k) - u(k-1)$, and ρ_{ref} and c_{ref} are the reference recovery and grade, respectively. c_{h_p} and ρ_{h_p} stand for the average grade and recovery over the prediction horizon calculated under the rectangular approximation of the integral using:

$$c_{h_p}(k) = \frac{\sum_{i=1}^{h_p} C_n(k+i) T_s}{\sum_{i=1}^{h_p} C(k+i) T_s} \qquad (8\text{-}14)$$

and

$$\rho_{h_p}(k) = \frac{\sum_{i=1}^{h_p} C_n(k+i) T_s}{\sum_{i=1}^{h_p} C_n(k+i) T_s + \sum_{i=1}^{h_p} R_n(k+i) T_s} \qquad (8\text{-}15)$$

where T_s is the sampling period. R_n, C and C_n as the output variables are used to calculate the controlled variables, i.e. c_{h_p} and ρ_{h_p}. In the current implementation, that is a 2×2 controller, the following manipulated variables are selected from Table 8-2:

$$u = \begin{bmatrix} U_C \\ A_W \end{bmatrix} \qquad (8\text{-}16)$$

From a practical point of view, U_C as a manipulated variable controls the particles hydrophobicity, and so directly acts on the physics and flotation kinetics of the particles.

On the other hand, A_W increases the degree of freedom to control the grade and is costless. To select the correct sampling time and prediction horizon, step responses of TFs are considered. Fig. 8-6 depicts the time response of measured variables for manipulated variables step change. As seen, the longest and shortest time responses correspond to G_{R_n,U_C} and G_{C_n,A_W}, respectively. The longest response time is chosen as h_p while the shortest one is used to select the sampling time T_s:

$$\begin{aligned} T_s &= 30\,\text{s} \\ h_p &= 120 \end{aligned} \tag{8-17}$$

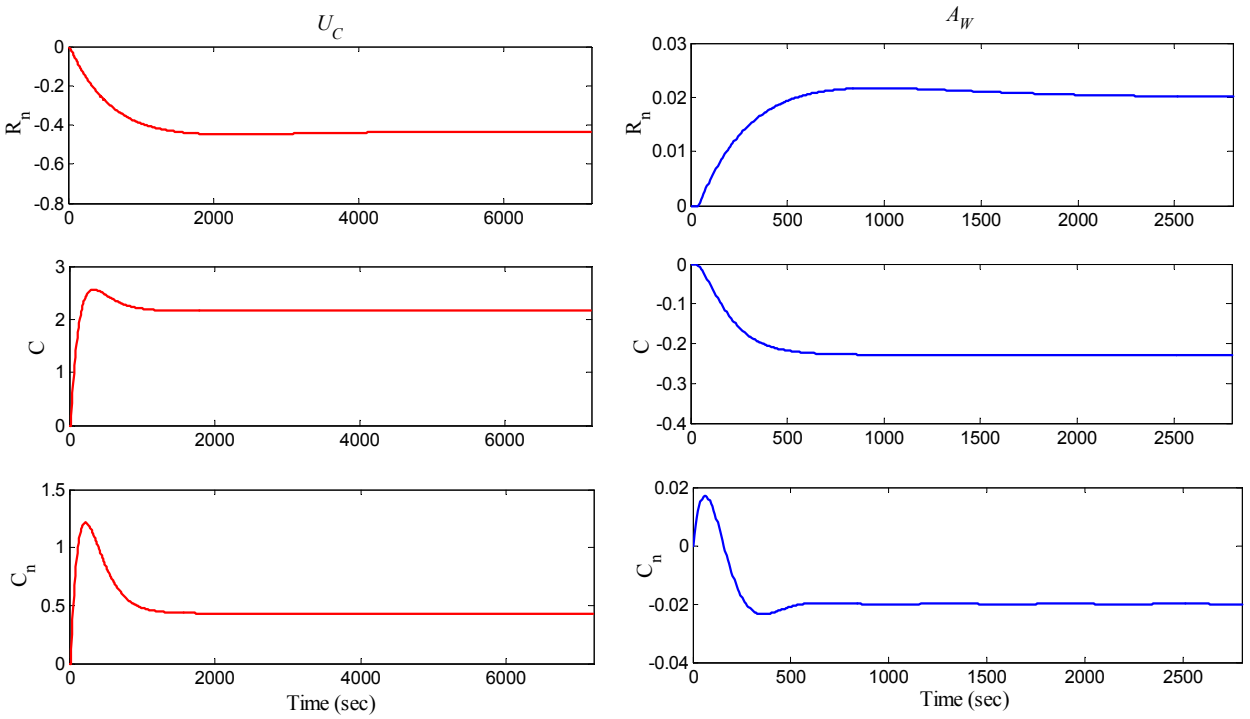

Fig. 8-6: Step response of model TFs (APC scheme).

Having a large control horizon h_c allows the controller to reach the set-points or reject the disturbances faster, and consequently leads to the large variations in the control actions. To have less aggressive control actions and a robust control, h_c is selected as:

$$h_c = 1 \tag{8-18}$$

However, larger values for h_c have also been tried to see whether they can improve the controller performance or not. But they did not much improved the closed loop plant performance. In Eq. 8-13, since recovery and grade have a similar importance for the plant performance evaluation and almost same magnitude, the corresponding coefficients, α_{APC} and β_{APC}, are equally assigned. Value of $W_{u_{APC}}$ is determined based on two facts:

- To improve the performance of the closed loop system, i.e. having a smooth behavior and avoiding any oscillation, a weighting value for the control actions should be assigned.
- $W_{u_{APC}}$ is able to filter the variations on the manipulated and output variables, and consequently it can attenuate the measurement noise. This point could affect the evaluation of DR performance. To reduce the filtering effect of $W_{u_{APC}}$, a very small value is chosen.

The value of the coefficients are illustrated in Table 8-3.

Table 8-3: APC objective function coefficients.

Coefficients	Value
α_{APC}	1
β_{APC}	1
$W_{u_{APC}}$	$\begin{bmatrix} 0.0005 & 0 \\ 0 & 0.0005 \end{bmatrix}$

In conclusion, the optimal controller comes down to:

$$\Delta u_{h_c} = \underset{\Delta u_{h_c}}{\arg\min}\left(J_{APC}\right) \qquad \text{s.t.} \quad g(u, y) \tag{8-19}$$

where $g(u, y)$ is the set of constraints including maximum and minimum values of manipulated variables u and the minimum value of output variables y. In fact, the manipulated variables are kept in the range where the model has been identified and is still valid. The output variables are always positive values, and this point should be considered in the optimization solver. In the current controller design, the limitation of manipulated variables rate is not considered. Therefore, the applied constraints are:

$$\begin{bmatrix} 0.2 \\ 1 \end{bmatrix} \leq \begin{bmatrix} U_c \\ A_w \end{bmatrix} \leq \begin{bmatrix} 1 \\ 10 \end{bmatrix} \tag{8-20}$$

and

$$\begin{bmatrix} R_n \\ C \\ C_n \end{bmatrix} \geq \begin{bmatrix} 0 \\ 0 \\ 0 \end{bmatrix} \tag{8-21}$$

To test the performance of the controller, a reference tracking test is designed. A set of step changes is applied to the references, i.e. ρ_{ref} and c_{ref}. These set-points are chosen so that they can be reachable for the closed loop plant considering the feed characteristics. Figs 8-7 and 8-8 show the plant behaviors, i.e. controlled and manipulated variables. All set-points are reached in steady-state, and there is no steady-state error. In the figures, the transient part of responses is not easy to be explained where they have non-minimum phase behaviors that might be caused by non-minimum phase TF between A_w and C_n, or the interaction between manipulated variables of the multi-input multi-output controller. However, general trends in the controlled and manipulated variables are reasonable and explainable. In Fig. 8-7, first a -2% step occurs in the grade while ρ_{ref} is constant. The grade has to track the new reference trajectory while disturbance in the recovery caused by grade change should be rejected and the recovery must be kept at the previous value. In this case, A_w is mainly reduced while U_C is almost constant (very small decrease). In the second point, both recovery and grade get +1% and +2.5% step changes, respectively. To reach the desired references, the controller largely increases A_w and U_C in point 2. Both

reference values for the controlled variables come down in the third point, and correspondingly both manipulated variables are reduced by the controller.

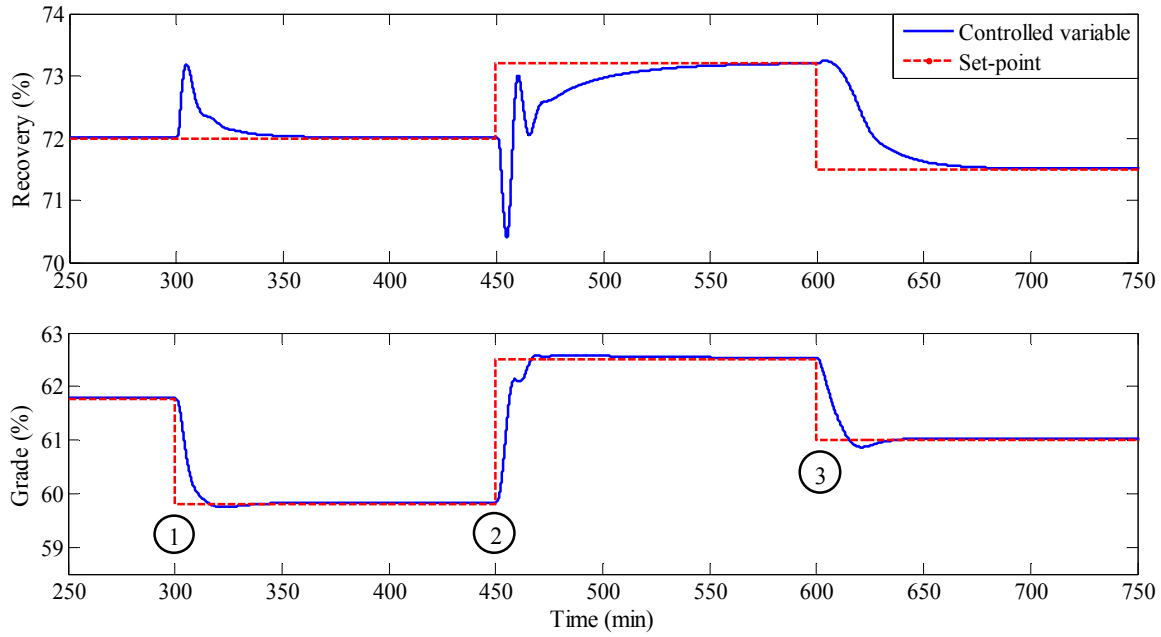

Fig. 8-7: APC performance test: controlled variables.

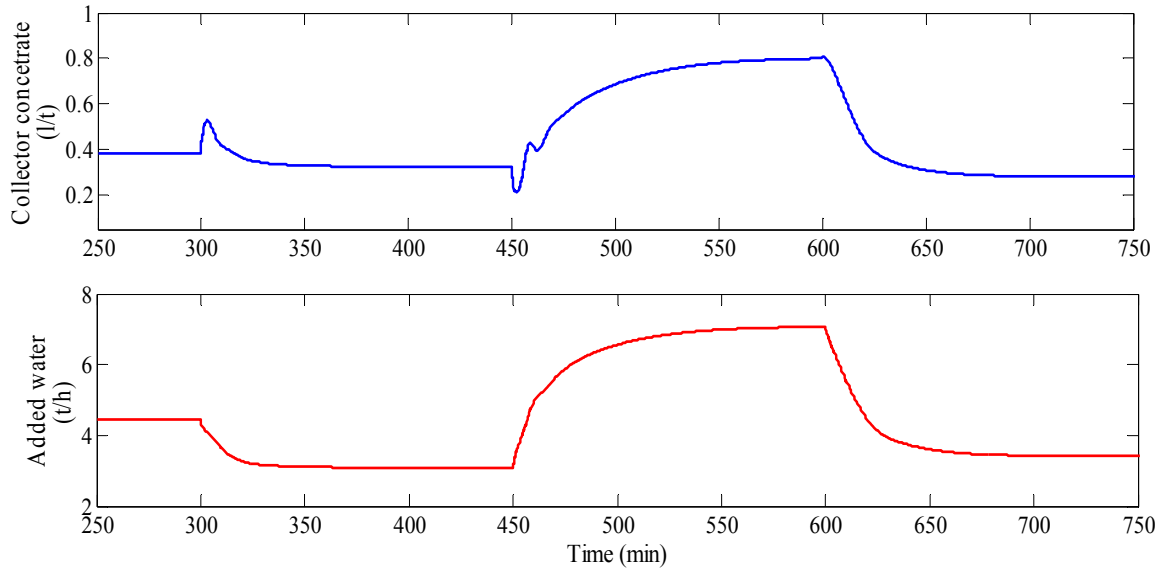

Fig. 8-8: APC performance test: manipulated variables.

8.5 Real-Time Optimization Scheme

This section develops a RTO scheme used for coupling with DR observer presented in the following sections. This RTO maximizes economic benefits of the plant. As previously mentioned, it is a direct RTO, not a hierarchical one as shown in Hodouin (2010). In such a RTO, both RTO and advanced control stages shown in Fig. 8-1 are merged. In fact, it is a receding horizon controller with economic objective function. Here, the objective function is defined based on the economic value of produced valuable minerals and associated cost for chemical reagents consumption. Moreover, a third term is considered to keep the concentrate grade close to the predefined value in the contract c_{con}. From a mathematical point of view, this term brings more curvature in the search space of the optimization problem and facilitates finding local minimums. The objective function is expressed by:

$$J_{RTO}(k) = \alpha_{RTO} \sum_{i=1}^{h_p} C_n(k+i)T_s - \beta_{RTO} \left(c_{h_p}(k) - c_{con}\right)^2 - \gamma_{RTO} \sum_{i=1}^{h_p} U_c(k+i)\, f_1(k+i)T_s \qquad (8\text{-}22)$$

where f_1 stands for plant feed rate ($\mathrm{t/h}$) and c_{h_p} is calculated from Eq. 8-14. To find the correct weights, the economic value of each term is considered. The first term represents the amount of valuable minerals produced in ton while the third integral stands for the amount of reagent consumed in liter. For a certain reagent on the market, the price of the reagent is almost twice of the chalcopyrite price in ton basis. So, from monetary point of view:

$$1\,\text{liter reagent price} = 2 \times 1\,\text{liter chalcopyri te price} = 0.002 \times 1\,\text{ton chalcopyri te price} \qquad (8\text{-}23)$$

This point is used to assign correct values to α_{RTO} and γ_{RTO}. In practice, large violations in the concentrate grade for a long period of time cannot be tolerated. In this regard, to give a reasonable value to β_{RTO}, it is assumed that any deviation in the grade up to 1% can be tolerated and its corresponding term in J_{RTO} should almost have same magnitude as other terms. Normalized values of coefficients are presented in Table 8-4. Here, again, value of the first and third terms of Eq. 8-22 grow with increasing prediction horizon but this is not the case for the second one. Therefore, the coefficients should be adjusted for the different value of h_p, correspondingly. As seen from Eq. 8-22, this scheme only has one manipulated

variable U_c. As mentioned before, U_C directly changes the physics and kinetics of particle and consequently affect the plant behavior. Also, it has an associated cost making it suitable as a manipulated variable for the economic objective function.

Table 8-4: RTO objective function coefficients.

Coefficients	Value
α_{RTO} [1/t]	1
β_{RTO} [ ]	16.66
γ_{RTO} [1/l]	0.002

In conclusion, RTO can be presented as:

$$\Delta U_{c\,h_c} = \underset{\Delta U_{c\,h_c}}{\arg\max}\left(J_{RTO}\right) \qquad \text{s.t.} \quad g(U_c, y) \tag{8-24}$$

where $g(U_c, y)$ is the set of constraints expressed by Eq. 8-21 and

$$0.2 \le U_c \le 1 \tag{8-25}$$

For RTO implementation again, sampling time and prediction horizon are selected using step responses of TFs taken from Table 8-2. The longest and shortest time responses stand for G_{R_n,U_C} and G_{C,U_C}, respectively. Using this information,

$$\begin{aligned} T_s &= 1\,\text{min} \\ h_p &= 60 \end{aligned} \tag{8-26}$$

As discussed in the APC section, larger control horizon h_c could lead to large variations in the control actions, so to have a less aggressive actions and robust control, h_c is selected as:

$$h_c = 1 \tag{8-27}$$

To test RTO performance, step disturbances are applied to the feed rate and grade (Fig. 8-9) where the flotation circuit simulator is used as the case-study. First, a +10% change in the plant feed rate is applied, and then the plant feed grade is disturbed by a -0.5% (out of 6.5%) step. In this case, c_{cont} is set to 0.618 (i.e. 1% more than the nominal grad). Fig. 8-10 illustrates the manipulated variable behavior. Although, in the current RTO implementation there is no explicit controlled variable, output variables could be useful to present the RTO performance (Fig. 8-11).

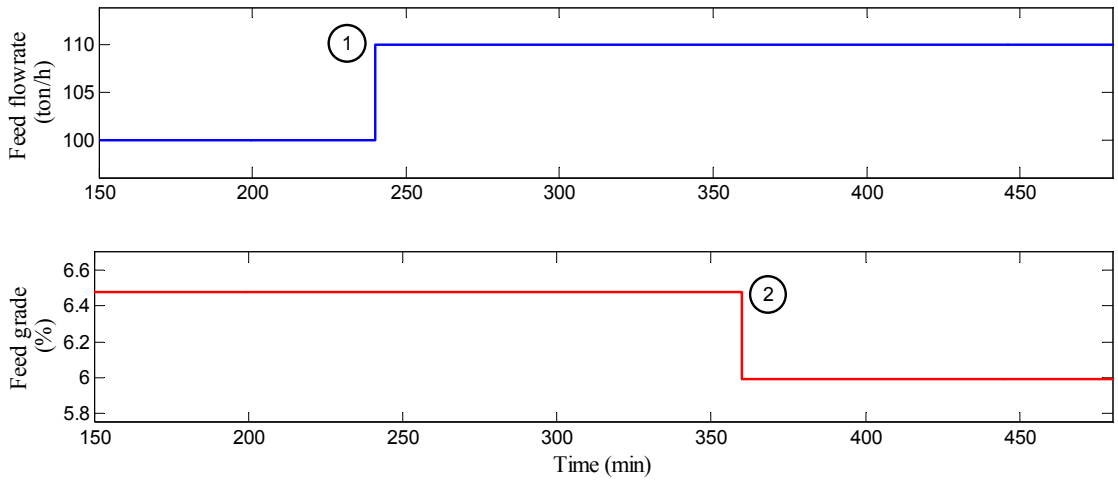

Fig. 8-9: RTO performance test: step disturbance in the feed rate and composition.

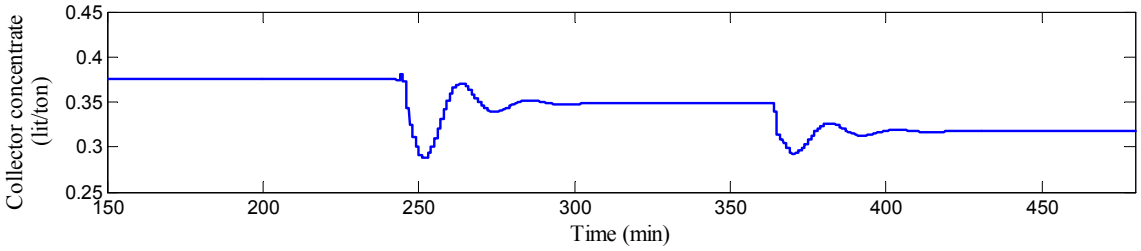

Fig. 8-10: RTO performance test: manipulated variable.

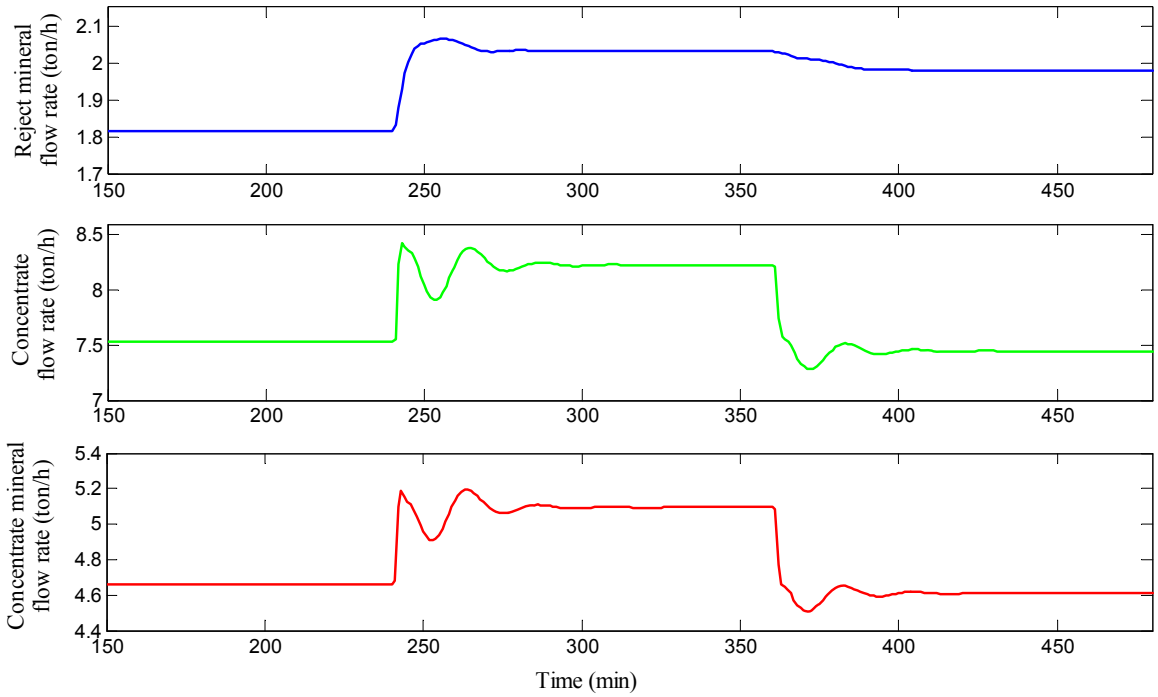

Fig. 8-11: RTO performance test: output variables.

From Figs. 8-10 and 8-11, it can be concluded that although there are some oscillations in the transient part of the manipulated and output variables, RTO still has an acceptable performance. These oscillations could be raised from the recycling streams of the plant. Also it could come from modeling errors resulting from the plant nonlinearity and/or the absence of an explicit term in the objective function to restrict ΔU_c.

8.6 Coupling DR with APC and RTO: Basics and Test Cases

In the following sections, above proposed APC and RTO schemes are applied to the situation that measurements are corrupted by random errors, and plant feed contains stationary disturbances. A DR block is added to the loop just before APC/RTO block (Fig. 8-12). In fact, DR block delivers the reconciled values of ore and chalcopyrite flowrates (noted by $\hat{y}_i, \hat{y}_{c_i}$) to the selection block of controlled variables.

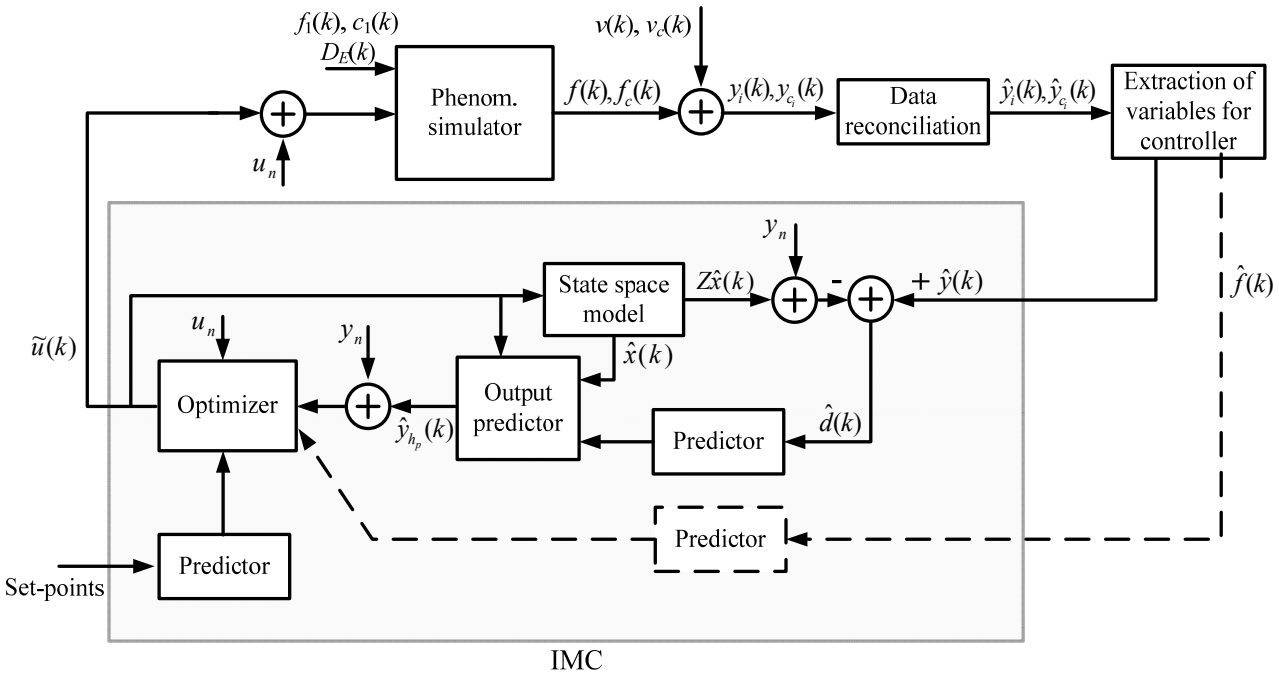

Fig. 8-12: Block diagram of DR coupled with APC and RTO loops.

8.6.1 Data reconciliation observer

Autocovariance Based Stationary observer (ABS) introduced in Chapter 5 is used to improve closed loop process performance. The time lag applied in ABS is selected based on plant information and node imbalance autocorrelation functions limited to the range where the values are significant according to the 95% confidence intervals. To tune the measurement noise variance Σ_v and node imbalance autocovariance matrices Σ_w, the flotation circuit simulator including control loops was run for 30 days while different disturbances were applied to the feed. Using this tuning procedure, the obtained autocovariance function contains the effect of both model uncertainty and controller behavior. More details about the tuning, time lag selection, and observer implementation are available in Chapter 5.

In this chapter, DR observer is applied in two cases: first all solid flowrates and valuable minerals flowrates are measured (called full measured case), and second all flowrates, i.e. solid and valuable minerals, are measured except for feed stream (named partial measured case). The plant flow sheet is illustrated in Fig. 8-13. In full measured case, solid flowrate

f_i and valuable mineral (chalcopyrite) flowrate f_{c_i} for all of 8 streams are measured while for partial measured case, f_1 and consequently f_{c_1} are not available. The measurement equations are expressed by:

$$\begin{cases} y = f + v \\ y_c = f_c + v_c \end{cases} \tag{8-28}$$

where y and y_c stand for measurements of solid flowrate and valuable mineral flowrate, respectively. v and v_c are random measurement errors. For full measured case, state vectors are:

$$\begin{cases} f = [f_1 \quad \cdots \quad f_8]^T \\ f_c = [f_{c_1} \quad \cdots \quad f_{c_8}]^T \end{cases} \tag{8-29}$$

and incidence matrices for the solid and valuable mineral flows, M_F and M_{c_F} respectively, are:

$$M_F = M_{c_F} = \begin{bmatrix} 1 & 0 & 0 & 0 & 1 & 1 & 0 & -1 \\ 0 & 0 & 0 & -1 & 0 & 0 & -1 & 1 \\ 0 & -1 & 0 & 1 & 0 & -1 & 0 & 0 \\ 0 & 0 & -1 & 0 & -1 & 0 & 1 & 0 \end{bmatrix} \tag{8-30}$$

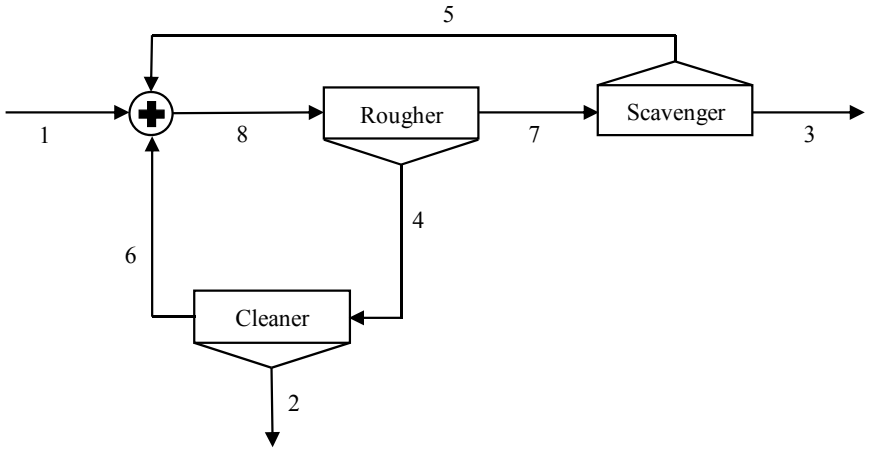

Fig. 8-13: Flow sheet of the flotation circuit simulator used as the plant.

For ABS observer implementation, in partial measured case, the reduced state vectors and reduced incidence matrices corresponding to the measured states are presented as:

$$\begin{cases} f = \begin{bmatrix} f_2 & \cdots & f_8 \end{bmatrix}^T \\ f_c = \begin{bmatrix} f_{c_2} & \cdots & f_{c_8} \end{bmatrix}^T \end{cases} \tag{8-31}$$

and

$$M_P = M_{c_P} = \begin{bmatrix} 0 & 0 & -1 & 0 & 0 & -1 & 1 \\ -1 & 0 & 1 & 0 & -1 & 0 & 0 \\ 0 & -1 & 0 & -1 & 0 & 1 & 0 \end{bmatrix} \tag{8-32}$$

8.6.2 Plant feed disturbances

To test the performance of DR coupled with APC/RTO, three different stationary disturbances are applied to the feed stream:

- *Disturbance* 1: stationary variation in feed rate and grade while liberation degree and middling grade are constant. Fig. 8-14 shows the corresponding feed grade, rate and solid percentage.
- *Disturbance* 2: stationary variation in feed rate and grade, while the particle population is not constant. Feed grade, rate and solid percentage are illustrated in Fig. 8-15.
- *Disturbance* 3: stationary variation in solid percentage of feed rate, while grade and particle population are constant (Fig. 8-16).

More information about feed characteristics is available in Table 7-8. Here, stationary variations in the plant feed including fluctuation in the particle population, grade, and feed rate are generated by filtering white noises with suitable time constants. For *Disturbance* 3, to create variation in the solid percentage, water flowrate is constant while solid flow is changing. This is why in Fig. 8-16, solid feed rate and percentage are strongly correlated. Although the original time duration of the disturbances is one day, for illustration purpose, only first twelve-hours is presented in Figs. 8-14 to Fig. 8-16.

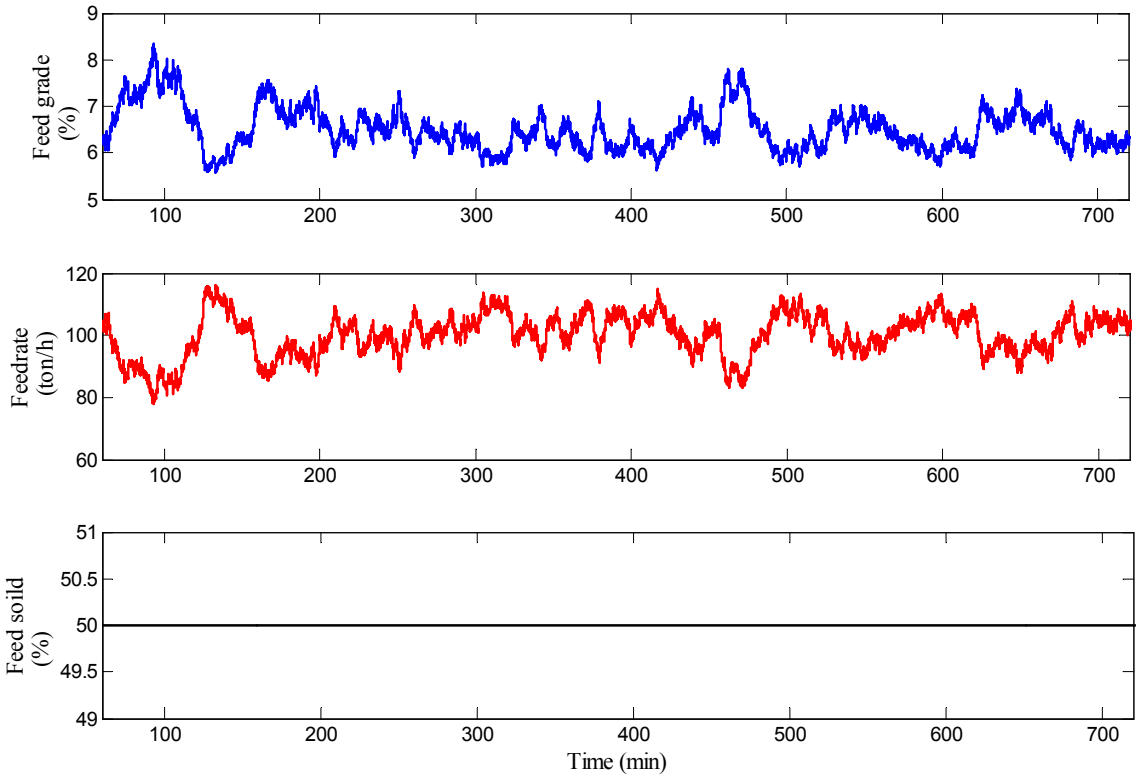

Fig. 8-14: *Disturbance* 1: variation in feed rate and grade (constant liberation & middling).

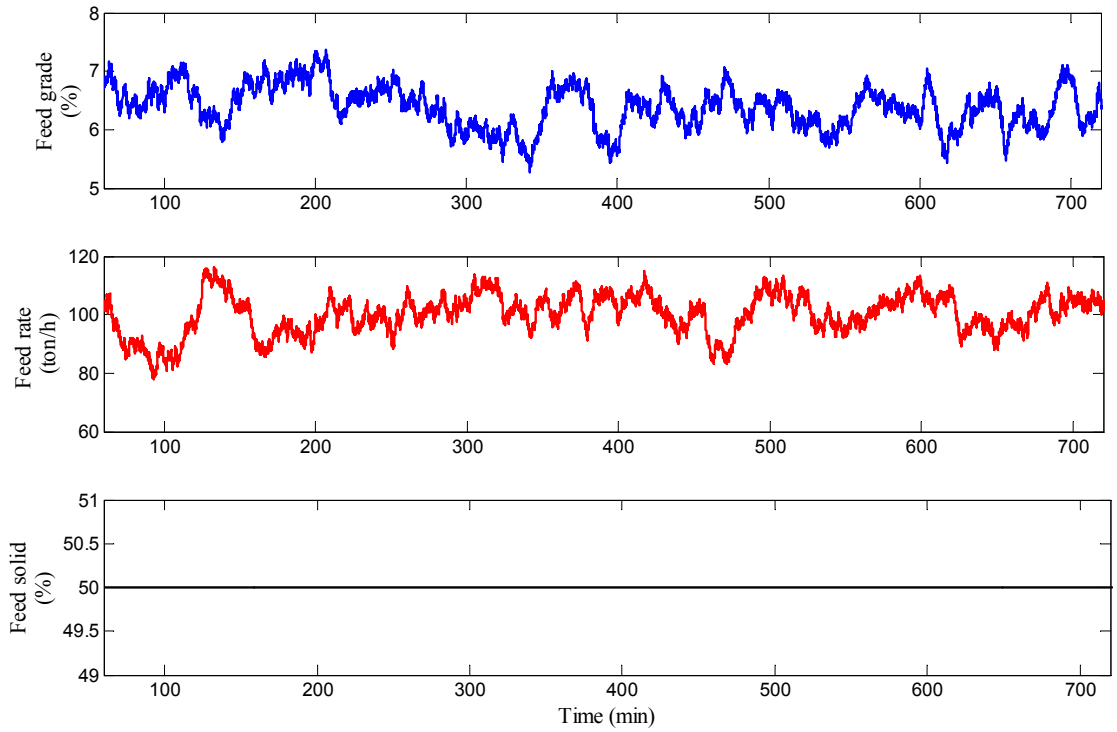

Fig. 8-15: *Disturbance* 2: variation in feed rate and grade (non-constant liberation & middling).

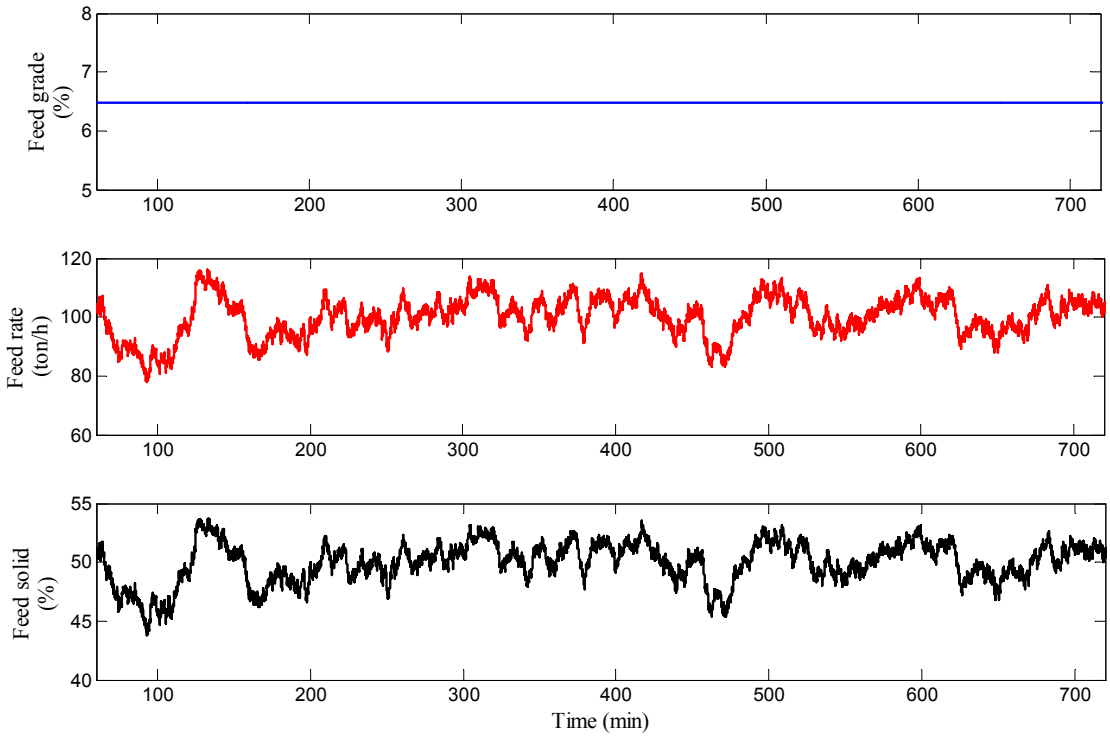

Fig. 8-16: *Disturbance* 3: variation in solid percentage (constant grade and particle population).

8.6.3 Simulation scenarios and evaluation indices

For APC and RTO schemes, i.e., four different scenarios are considered:

- *Scenario* 0: feed disturbance applied while APC and RTO are not involved (open loop case).
- *Scenario* 1: feed disturbance applied to the closed loop plant while there is no measurement error (benchmark case).
- *Scenario* 2: feed disturbance and measurement error (5%) applied to the closed loop plant while there is no DR observer.
- *Scenario* 3: in the closed loop plant, feed disturbance and measurement error (5%) applied while ABS observer is utilized for data reconciliation purpose.

In addition to full measured case, these scenarios are also repeated for the partial measured case, and in each scenario, all of three disturbances are examined.

For the performance evaluation of control schemes, different statistical and economic measures are employed, e.g. distribution and standard deviation of manipulated and output variables. As an economic index, the following gain function is calculated using true value of variables over a time window of one day:

$$J_{ECO} = \alpha_{ECO} \sum^{1\,\text{day}} C_n T_s - \gamma_{ECO} \sum^{1\,\text{day}} U_c f_1 T_s - \varphi_{ECO}\, \delta(\bar{c}) \sum^{1\,\text{day}} C T_s \tag{8-33}$$

This function is slightly different from J_{RTO}; two first terms of J_{ECO} are the same as the ones in J_{RTO} except for the calculation duration. But the last term is different, because in practice delivering products with a higher grade than the pre-specified value in contract c_{con} is not beneficial while a smaller grade is severely penalized. Averaged grade $\bar{c}$ and penalty function of grade violation are expressed using:

$$\bar{c} = \frac{\sum^{1\,\text{day}} C_n T_s}{\sum^{1\,\text{day}} C T_s} \tag{8-34}$$

and

$$\delta(\bar{c}) = \begin{cases} 100\left(c_{con} - \bar{c}\right)^2 + \left(c_{con} - \bar{c}\right) & \bar{c} < c_{con} \\ 0 & \bar{c} \geq c_{con} \end{cases} \tag{8-35}$$

In Eq. 8-35, $\bar{c}$ and c_{con} are in mass fraction unit. In this study, value of c_{con} is set to 0.618 which is 1% higher than the nominal plant concentrate grade. Fig. 8-17 gives visualization about the penalty function. Value of J_{ECO} coefficients are listed in Table 8-5. Here, to assign a reasonable value to φ_{ECO}, it is again assumed that any grade deviation up to 1% can be tolerated and its corresponding variation in J_{ECO} should almost have the same magnitude as other terms. Larger divergences should be harshly penalized.

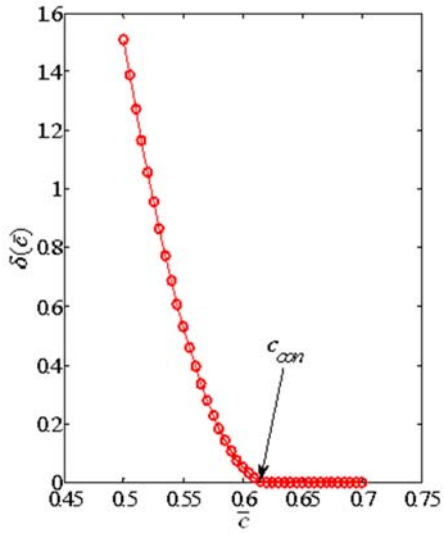

Fig. 8-17: Grade violation penalty function.

Table 8-5: Coefficients of economic gain function.

Coefficients	Value
α_{ECO} [$/t]	1
γ_{ECO} [$/l]	0.002
φ_{ECO} [$/t]	5000
c_{con} [ ]	0.618

To easily recall the different parts of J_{ECO} during the result presentations, its first, second, and third terms are named produced valuable mineral, consumed collector, and grade penalty, respectively.

8.7 Coupling DR with APC: Results and Discussion

In this section, APC scheme designed in Section 8.4 is involved with DR observer, and its performance is illustrated using different disturbance cases already presented. Here, an ABS observer with 10 time lags is applied where sampling time is 30 sec. Desired references in Eq. 8-13, c_{ref} and ρ_{ref} are set to 0.618 and 0.720, respectively. As a general

point, since results obtained for APC in the different disturbances are similar and coherent, a discussion is presented after showing all the results.

8.7.1 Results of applying disturbance 1

Table 8-6 illustrates the performance of APC for different scenarios using indices when all variables are measured and *disturbance* 1 is applied. As a recall, in *disturbance* 1, feed rate and grade stationary change and the liberation degree and middling grade are constant. In the table, Δ for each scenario presents the total benefit difference between *Scenario* 1 and that scenario, expressed in %. To give a sense about statistical properties of the controlled and manipulated variables, their histograms are illustrated in Figs. 8-18, 8-19 and 8-20 for *Scenarios* 1 to 3. The histograms were constructed by averaging the variables value over 10 min windows. As seen and expected, measurement noise leads to an increase in variables variances while DR reduces the variances. For open loop scenario, since manipulated variables are constant, so no histogram is presented. A deep discussion about the results is presented at the end of the section.

Table 8-6: APC performance: *disturbance* 1 (feed rate & grade variation with constant liberation and middling grade) and all variables measured.

Performance Indices		Scenarios			
		Open loop	No noise	With noise & without DR	With noise & DR
J_{ECO}	Earned mineral [k$]	112.5	112.2	112.6	112.4
	Consumed collector [k$]	-2.40	-2.14	-2.80	-2.38
	Grade penalty [k$]	-20.0	0	0	0
	Total benefit [k$]	90.10	110.06	109.80	110.02
	Δ [%]	-18.10	0.00	-0.23	0.00
Manipulated variables statistics	U_c [l/t]	0.50±0.00	0.44±0.164	0.51±0.22	0.49±0.19
	A_w [t/h]	4.50±0.00	4.74±1.22	4.92±1.42	4.88±1.31
Controlled variables statistics	c [%]	60.6±0.69	61.8±0.49	61.86±0.85	61.84±0.70
	ρ [%]	72.5±2.21	72±0.85	72.4±0.95	72.2±0.91
Output variables statistics	R_n [t/h]	1.77±0.10	1.81±0.10	1.79±0.11	1.79±0.10
	C [t/h]	7.75±0.63	7.56±0.22	7.59±0.25	7.58±0.23
	C_n [t/h]	4.69±0.39	4.67±0.15	4.69±0.18	4.69±0.15

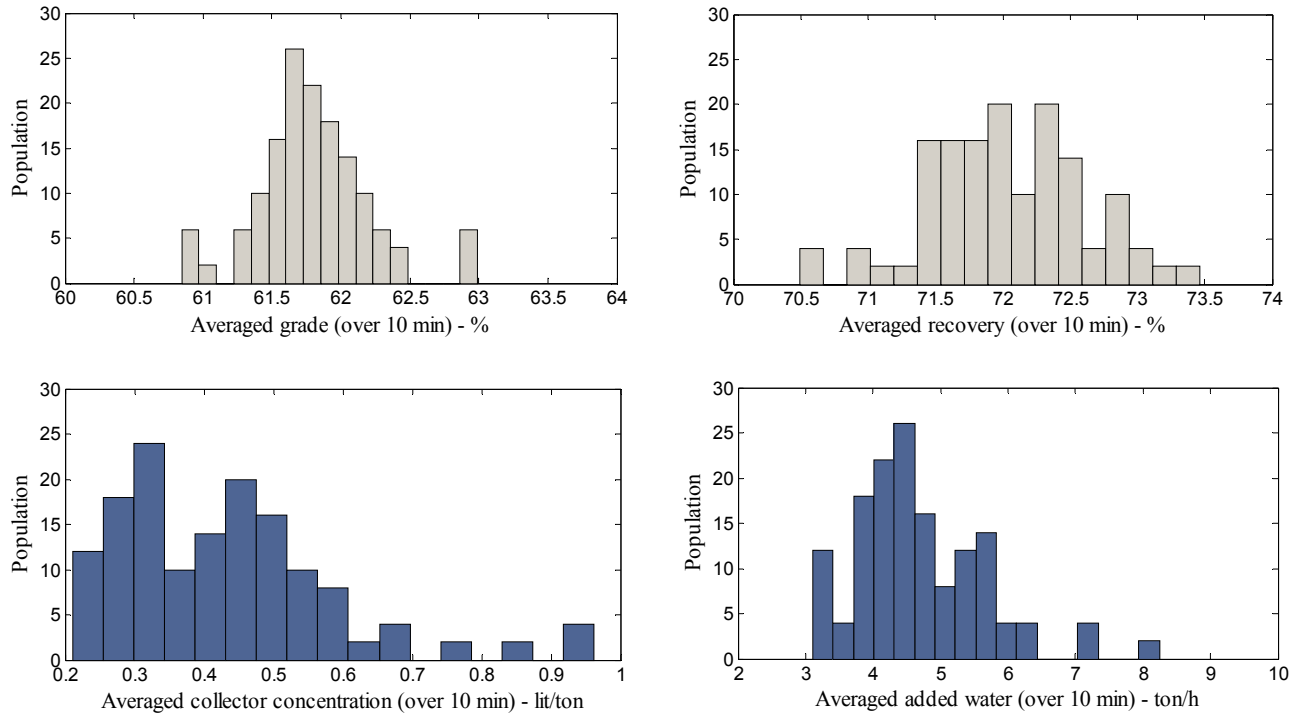

Fig. 8-18: APC: histogram of controlled and manipulated variables – *Scenario* 1 (without noise).

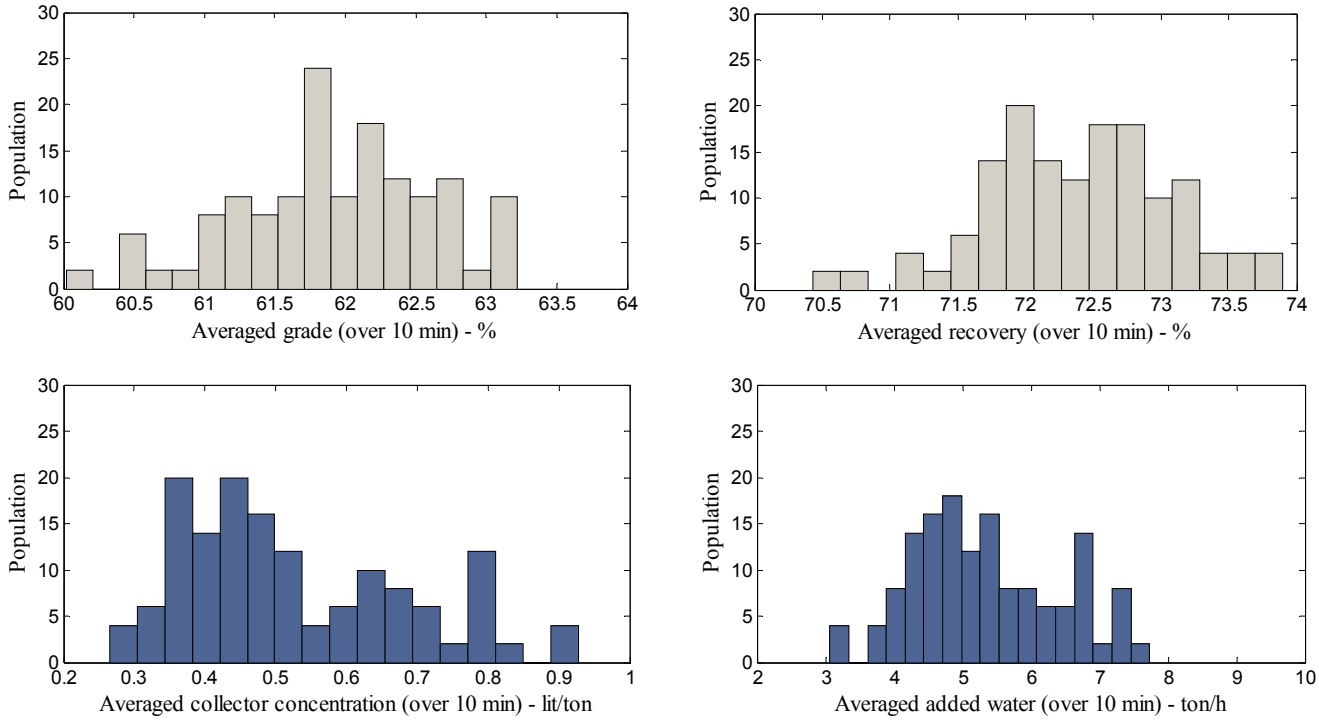

Fig. 8-19: Histogram of controlled and manipulated variables - *Scenario* 2 (with noise & without DR).

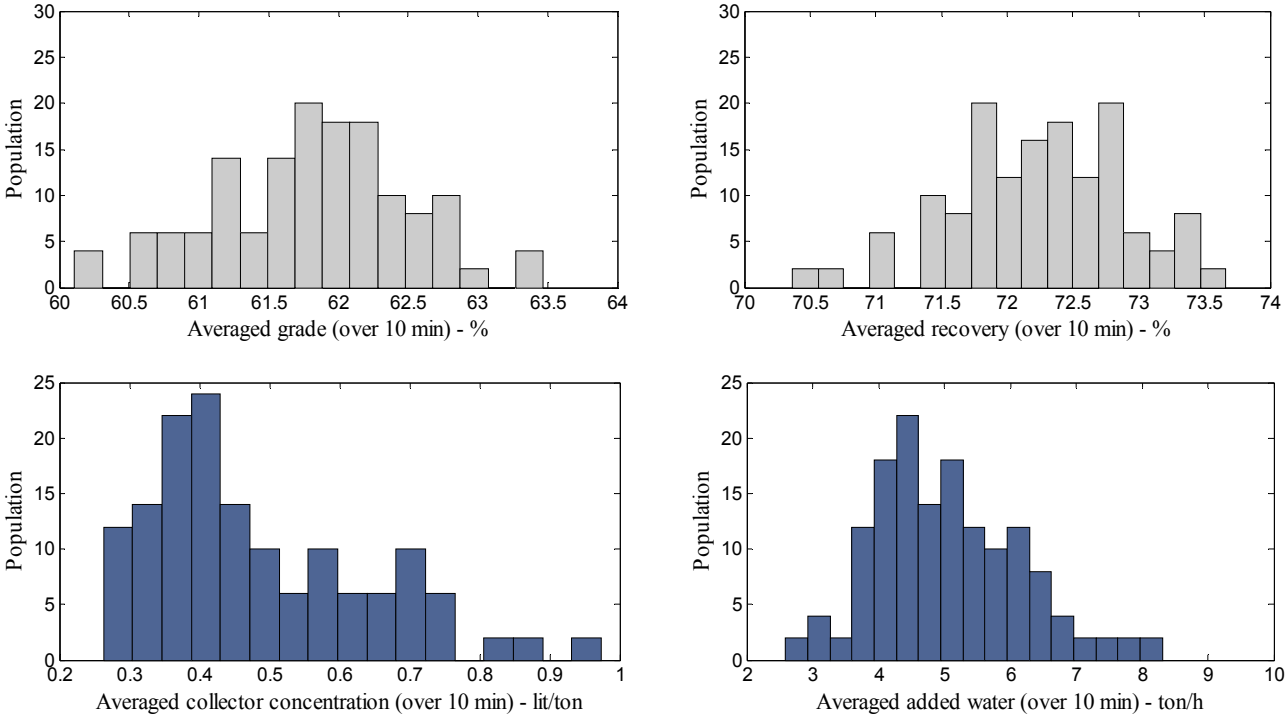

Fig. 8-20: APC: histogram of controlled and manipulated variables - *Scenario* 3 (with noise & with DR).

In the condition that feed rate f_1 is not measured, DR is able to estimate the value $\hat{f}_1$. This is another benefit that DR can bring to the process control. In *Scenario* 3, f_1 is estimated using DR while for other scenarios, under the assumption of stationary operating regime, nominal value of feed could be considered as a reasonable estimation. So for *Scenarios* 0, 1 and 2, $\hat{f}_1$ is set to 100 t/h. In the designed APC, f_1 is not involved in the control action calculation in J_{APC}, and it only participates in DR if applicable. Therefore, calculated control actions are independent of the feed rate variations, and consequently the closed loop performance is independent of measuring or not measuring the feed flowrate. Also the economic index J_{ECO} (Eq. 8-33) is calculated based on true variables values, so the feed rate measurement does not also affect J_{ECO} value in the current APC. In conclusion, measured or unmeasured f_1 does not have a direct effect on the plant performance and revenue in the current implementation (only through DR). In Table 8-7, the performance of APC in different scenarios, when the feed rate is not measured, and *disturbance* 1 is applied, is shown. For this simulation case, since the results have the same trend as

previous one, so the variable histograms are not presented to avoid any duplication. These results prove that in the current APC, measuring or not measuring f_1 does not change the plant revenue. However, DR is able to estimate the unmeasured variables if there is enough degree of redundancy, which could be used for feed forward control design or process model update.

Table 8-7: APC performance: *disturbance* 1 (feed rate & grade variation with constant liberation and middling grade) and feed rate not measured.

Performance Indices		Scenarios			
		Open loop	No noise	With noise & without DR	With noise & DR
J_{ECO}	Earned mineral [k$]	112.5	112.2	112.6	112.38
	Consumed collector [k$]	-2.41	-2.15	-2.82	-2.39
	Grade penalty [k$]	-20.0	0	0	0
	Total benefit [k$]	90.09	110.05	109.78	109.99
	Δ [%]	-18.10	0.00	-0.24	0.00
Manipulated variables statistics	U_c [l/t]	0.5±0.00	0.44±0.164	0.51±0.22	0.49±0.20
	A_w [t/h]	4.5±0.00	4.74±1.22	4.93±1.42	4.86±1.29
Controlled variables statistics	c [%]	60.6±0.69	61.8±0.49	61.86±0.85	61.82±0.72
	ρ [%]	72.5±2.21	72±0.85	72.4±0.95	72.3±0.92
Output variables statistics	R_n [t/h]	1.77±0.10	1.81±0.10	1.79±0.11	1.79±0.10
	C [t/h]	7.75±0.63	7.56±0.22	7.59±0.25	7.58±0.24
	C_n [t/h]	4.69±0.39	4.67±0.15	4.69±0.18	4.69±0.16

8.7.2 Results of applying disturbance 2

APC performance is evaluated using indices and presented in Table 8-8 when stationary variations occur in the feed rate and grade, and the liberation degree and middling grade are not constant, i.e. *disturbance* 2. Also it is assumed that all variables are measured. Again, the presence of measurement error reduces the economic benefits of plant and increases the variation range of variables; although the deterioration magnitude is marginal. Applying DR mainly compensates the benefit reduction and improves the statistical characteristics of variables. Table 8-9 shows the simulation results for unmeasured feed rate when *disturbance* 2 is applied. Here, since true values a used for economic benefits calculation, so measuring or not measuring f_1 does affect the plant revenue.

Table 8-8: APC performance: *disturbance* 2 (feed rate & grade variation with non-constant liberation and middling grade) and all variables measured.

Performance Indices		Scenarios			
		Open loop	No noise	With noise & without DR	With noise & DR
J_{ECO}	Earned mineral [k$]	111.90	112.00	112.10	112.06
	Consumed collector [k$]	-2.40	-2.70	-3.00	-2.80
	Grade penalty [k$]	-20.5	0	0	0
	Total benefit [k$]	89.00	109.30	109.10	109.26
	Δ [%]	-18.60	0.00	-0.18	0.00
Manipulated variables statistics	U_c [l/t]	0.5±0.00	0.54±0.24	0.58±0.26	0.56±0.25
	A_w [t/h]	4.5±0.00	4.96±1.61	5.20±1.72	5.10±1.68
Controlled variables statistics	c [%]	60.5±1.23	61.8±0.80	61.87±1.04	61.85±0.93
	ρ [%]	72.4±2.01	72.0±1.52	72.2±1.58	72.2±1.53
Output variables statistics	R_n [t/h]	1.78±0.16	1.79±0.13	1.78±0.16	1.78±0.13
	C [t/h]	7.71±0.66	7.52±0.64	7.53±0.67	7.53±0.64
	C_n [t/h]	4.67±0.40	4.66±0.39	4.67±0.40	4.67±0.39

Table 8-9: APC performance: *disturbance* 2 (feed rate & grade variation with non-constant liberation and middling grade) and feed rate not measured.

Performance Indices		Scenarios			
		Open loop	No noise	With noise & without DR	With noise & DR
J_{ECO}	Earned mineral [k$]	111.90	112.00	112.10	112.06
	Consumed collector [k$]	-2.41	-2.70	-3.01	-2.82
	Grade penalty [k$]	-20.5	0	0	0
	Total benefit [k$]	88.99	109.30	109.09	109.24
	Δ [%]	-18.60	0.00	-0.18	0.00
Manipulated variables statistics	U_c [l/t]	0.5±0.00	0.54±0.24	0.58±0.26	0.55±0.255
	A_w [t/h]	4.5±0.00	4.96±1.61	5.20±1.72	5.03±1.67
Controlled variables statistics	c [%]	60.5±1.23	61.8±0.80	61.87±1.04	61.86±0.94
	ρ [%]	72.4±2.01	72.0±1.52	72.2±1.58	72.2±1.53
Output variables statistics	R_n [t/h]	1.78±0.16	1.79±0.13	1.78±0.16	1.78±0.13
	C [t/h]	7.71±0.66	7.52±0.64	7.53±0.67	7.53±0.65
	C_n [t/h]	4.67±0.40	4.64±0.39	4.65±0.40	4.65±0.39

8.7.3 Results of applying disturbance 3

Here, above procedure is repeated for APC performance evaluation when solid percentage of feed is changing, *disturbance* 3. Tables 8-10 and 8-11 illustrate results for the measured and unmeasured feed rate, respectively. Again, similar conclusions can be derived: a) measurement noise increases variations on the variables and reduces the revenue of plant and, b) applying DR in the APC loop marginally improves the results, and c) measuring or not measuring f_1 does not have much effect on the plant revenue.

Table 8-10: APC performance: *disturbance* 3 (stationary variation in solid percentage of feed rate) and all variables measured.

Performance Indices		Scenarios			
		Open loop	No noise	With noise & without DR	With noise & DR
J_{ECO}	Earned mineral [k$]	113.8	113.4	113.8	113.7
	Consumed collector [k$]	-2.40	-2.00	-2.62	-2.36
	Grade penalty [k$]	-22.1	0.0	0.0	0.0
	Total benefit [k$]	89.30	111.40	111.18	111.34
	Δ [%]	-19.83	0.00	-0.20	0.00
Manipulated variables statistics	U_c [l/t]	0.5±0.00	0.415±0.12	0.498±0.19	0.489±0.16
	A_w [t/h]	4.5±0.00	4.83±1.06	4.93±1.36	4.90±1.35
Controlled variables statistics	c [%]	60.5±1.23	61.84±0.70	61.88±0.97	61.86±0.86
	ρ [%]	72.6±0.83	72.0±0.74	72.4±0.81	72.3±0.77
Output variables statistics	R_n [t/h]	1.78±0.10	1.82±0.12	1.79±0.13	1.80±0.12
	C [t/h]	7.81±0.68	7.58±0.48	7.61±0.53	7.61±0.52
	C_n [t/h]	4.72±0.33	4.68±0.29	4.71±0.32	4.71±0.30

Table 8-11: APC performance: *disturbance* 3 (stationary variation in solid percentage of feed rate) and feed rate not measured.

Performance Indices		Scenarios			
		Open loop	No noise	With noise & without DR	With noise & DR
J_{ECO}	Earned mineral [k$]	113.8	113.4	113.8	113.69
	Consumed collector [k$]	-2.40	-2.10	-2.63	-2.35
	Grade penalty [k$]	-22.1	0.0	0.0	0.0
	Total benefit [k$]	89.30	111.3	111.17	111.34
	Δ [%]	-19.83	0.00	-0.20	0.00
Manipulated variables statistics	U_c [l/t]	0.5±0.00	0.415±0.116	0.498±0.193	0.489±0.165
	A_w [t/h]	4.5±0.00	4.38±1.06	4.93±1.36	4.90±1.35
Controlled variables statistics	c [%]	60.5±1.23	61.84±0.70	61.88±0.97	61.87±0.86
	ρ [%]	72.6±0.83	72.0±0.74	72.4±0.81	72.3±0.78
Output variables statistics	R_n [t/h]	1.78±0.10	1.82±0.12	1.79±0.13	1.80±0.12
	C [t/h]	7.81±0.68	7.58±0.48	7.61±0.53	7.61±0.52
	C_n [t/h]	4.72±0.33	4.68±0.29	4.71±0.32	4.70±0.31

8.7.4 APC: Results analysis and discussion

This section discusses the results shown in the preceding tables and figures. It is noticeable that the presented conclusions here are case-based and they cannot be generalized to other case-studies. In the open loop scenario where no APC is involved, manipulated variables are set to the nominal values regardless of the feed disturbances. For this scenario, almost in all simulation cases, nominal value of U_c is larger than the optimum value. This point leads to more floated minerals and consequently having larger plant recovery then ρ_{ref}. For

A_w, the situation is inverse and therefore, the concentrate grade is less than c_{ref}. Therefore, economic benefits of this scenario were severely penalized and degraded.

For other scenarios involving APC, it can be summarized that measurement noise does not have much effect on the APC performance and plant revenue, and so DR cannot bring significant improvement. Therefore, the first and main question that should be addressed here is "why measurement noise does not adversely change the plant behavior and benefits?". To answer, it is important to clarify why grade penalty term in J_{ECO} is always zero. In the situation that the disturbances and measurement errors are stationary with zero mean, the averaged grade used in the economic index is calculated over a one-day period. The averaging over a long time window could be the source of this behavior. In the implemented APC, the grade is mainly adjusted using the added water while the collector concentration changes the plant recovery. Fig. 8-6 shows that A_w has a short response time effect on the grade compared to U_c, approximately four times shorter. It means that the water addition response time, which is about 8 minutes, is very short in comparison with the integration time. Therefore, for the stationary disturbances and random noises, averaged grade always stands around the optimal value. To reveal the effect of high frequency noises on the plant revenue, shorter integration window can be applied, but using shorter time window is faced with some difficulties. First, there are transfer functions related to recovery with longer time responses, about 1 hour, and second, calculating the plant benefits for periods shorter than one day is not acceptable from practical point of view. For these reasons, one-day integration duration has been kept in the current study.

Moreover, having two manipulated variables that can compensate adverse effects of each other could be one of the reasons. In APC scheme, the water addition acts as a free variable in J_{APC} and there is no cost associated to A_w in the economic gain function. So it can easily compensate any drops in the grade caused by increase of U_C. In other words, optimization problem always finds an A_w action, which is costless and covers major changes in U_C. By this way, APC is able to appropriately compensate the variations of manipulated and controlled variables caused by the measurement noise.

Another factor that can reduce the effect of the feed disturbances and measurement errors is the weighting of the manipulated variables rate $W_{u_{APC}}$. As mentioned, a very small value was assigned to make the time response of closed loop plant smoother. However, this small value limits and filters the control actions variations resulting from the disturbances and noises. For instance, using a very large $W_{u_{APC}}$ can keep the control actions at constant values and consequently almost makes the controller non-sensitive to feed disturbances. However, despite of its filtering effect, it is necessary to have smoother plant response. These reasons explain why the calculated economic index over one-day period almost has the same value with and without DR observers. DR reduces the energy of the control actions but might not significantly change the overall cumulated performance.

Another interesting point that needs clarification is "why DR does not bring any improvement when feed rate is unmeasured?". Eq. 8-13 shows that f_1 does not participate in the control action calculation, i.e. J_{APC}. This implies that, in the current implementation, measuring or not measuring f_1 does not have any direct effect through DR on the controller and plant performance. Moreover, for plant revenue calculation J_{ECO}, true value of variables are applied regardless of measuring or not measuring f_1. Therefore, measurement status of feed rate again does not affect the plant revenues. However, to take advantage of DR application, one may consider a feed-forward control based on the estimation of the unmeasured input disturbances. Estimated variables and parameters can be also utilized to update the parameters of process model used in the controller.

Although the disturbances and noises are centered, mean value of variables shows a small deviation from optimal values in some simulation cases. This point could be explained by the fact that the measurement noise increases the variations in the control actions. On the one hand, because of the plant nonlinearity, passing any symmetric noise or disturbance through such a plant could lead to unsymmetrical outcomes. On the other hand, since the optimal value of the manipulated variables may not exactly be located in the middle of the range, so one of the upper or lower bounds is touched more than another one resulting in an unsymmetrical distribution. For instance, Fig. 8-21 illustrates the collector concentration profile when the stationary disturbance occurs in the solid percentage of the feed. As seen,

without measurement noise, the lower bound has been not hit while it has been frequently touched in the presence of noise. Because of the statistical distribution dissymmetry, there is a small increase in the total collector consumption. From an economic point of view, it leads to a small increase in the profit associated with the valuable mineral production and, at the same time, a slight increase in the cost of collector consumption.

Finally, for the current APC implementation, it can be concluded that: a) measurement error increases variations on all variables and marginally reduces the economic revenue, and b) applying DR improves the results but the improvements are not significant. However, using DR in the control loop limits unnecessary variations in the control actions and consequently smooths the plant actuators actions reducing maintenance costs.

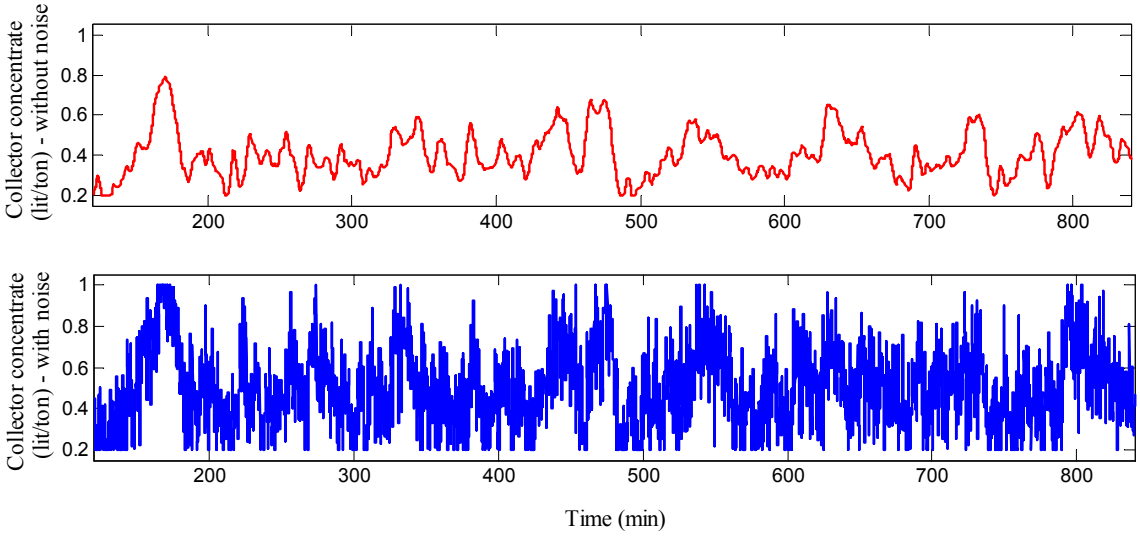

Fig. 8-21: APC: collector concentrate - without and with measurement noise.

8.8 Coupling DR with RTO: Results and Discussion

In this section, RTO proposed in Section 8.5 is coupled with DR observer, and its performance and economic benefits are presented using different disturbance cases for a period of one day. Here, an ABS observer with 5 time lags is applied where sampling time is 1 min. In Eq. 8-22, c_{con}, the grade value in contract, is set to 0.618. As a general point, similar to the preceding section, first all of the simulation results are presented and then a full section is devoted to analyze and discuss the results.

8.8.1 Results of applying disturbance 1

In Table 8-12, RTO performance for different simulation scenarios are shown when all variables are measured and *disturbance* 1 is applied. As a quick recall, scenarios here refer to four simulation cases: 0) process is open loop, 1) there is no measurement noise, 2) measurement errors exist but DR is not in the control loop, and 3) measurement noises exist and DR is involved.

Table 8-12: RTO performance: *disturbance* 1 (feed rate & grade variation with constant liberation and middling grade) and all variables measured.

Performance Indices		Scenarios			
		Open loop	No noise	With noise & without DR	With noise & DR
J_{ECO}	Earned mineral [k$]	113.04	112.00	112.35	112.20
	Consumed collector [k$]	-2.40	-1.87	-2.10	-2.00
	Grade penalty [k$]	-22.50	0.00	-5.40	-1.70
	Total benefit [k$]	88.14	110.12	104.85	108.50
	Δ [%]	-20.0	0.0	-4.8	-1.4
Manipulated variables statistics	U_c [l/t]	0.5±0.00	0.386±0.06	0.427±0.21	0.423±0.16
Metallurgical performance variables statistics	c [%]	60.54±0.83	61.91±0.37	61.40±0.88	61.65±0.67
	ρ [%]	72.15±2.21	71.83±1.32	72.07±1.73	72.01±1.59
Output variables statistics	R_n [t/h]	1.78±0.10	1.83±0.10	1.81±0.10	1.82±0.10
	C [t/h]	7.78±0.62	7.52±0.19	7.61±0.50	7.57±0.39
	C_n [t/h]	4.71±0.39	4.66±0.11	4.68±0.28	4.67±0.21

From Table 8-12, it is concluded that the measurement noise causes a violation in the averaged grade leading to a large penalty in the economic gain function. DR observer significantly improves the grade drop and increases the economic revenue. Valuable mineral flowrate in concentrate is slightly increased in the presence of noise in the cost of more collector consumption. To show statistical properties of the metallurgical performance indices and the manipulated variables, their histograms are illustrated in Figs. 8-22, 8-23 and 8-24 for *Scenarios* 1 to 3. The histograms were generated by averaging the variables over 10 min windows. As seen and expected, measurement noise increases the variance of variations on the variables while DR reduces the variances. For the open loop scenario, since manipulated variables are constant, no histogram is presented. A deep discussion about the results is presented at the end of the section.

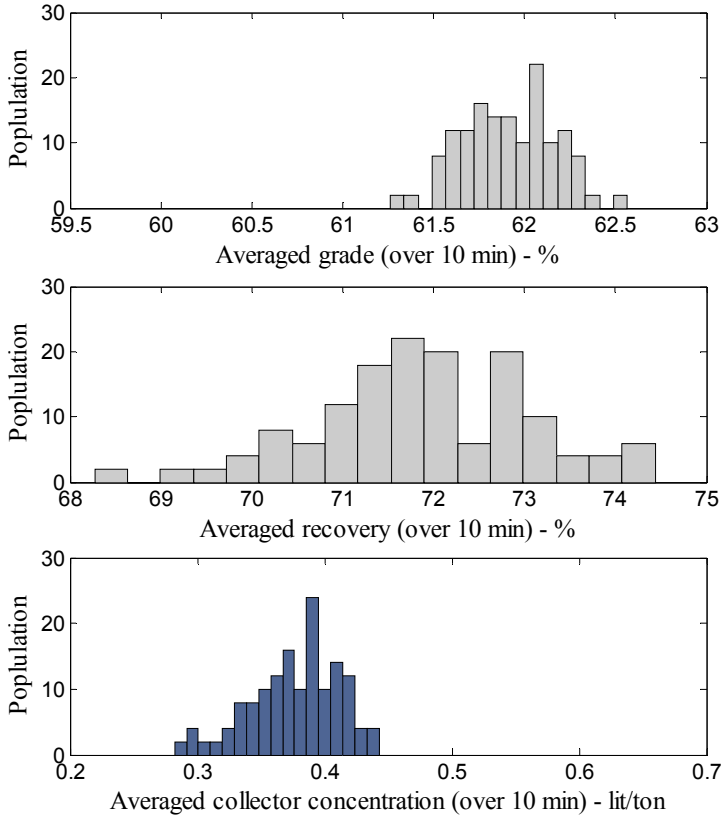

Fig. 8-22: RTO: histogram of controlled and manipulated variables – *Scenario* 1 (without noise).

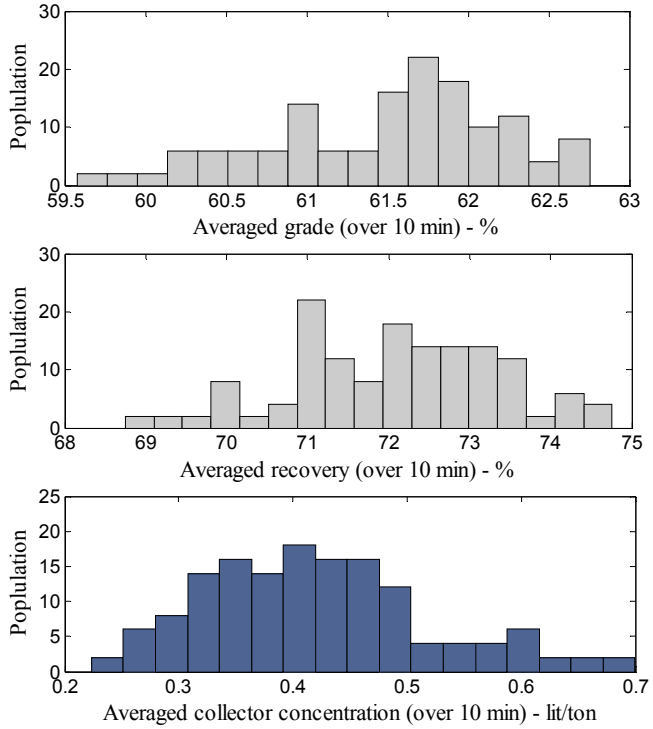

Fig. 8-23: RTO: histogram of controlled and manipulated variables - *Scenario* 2 (with noise & without DR).

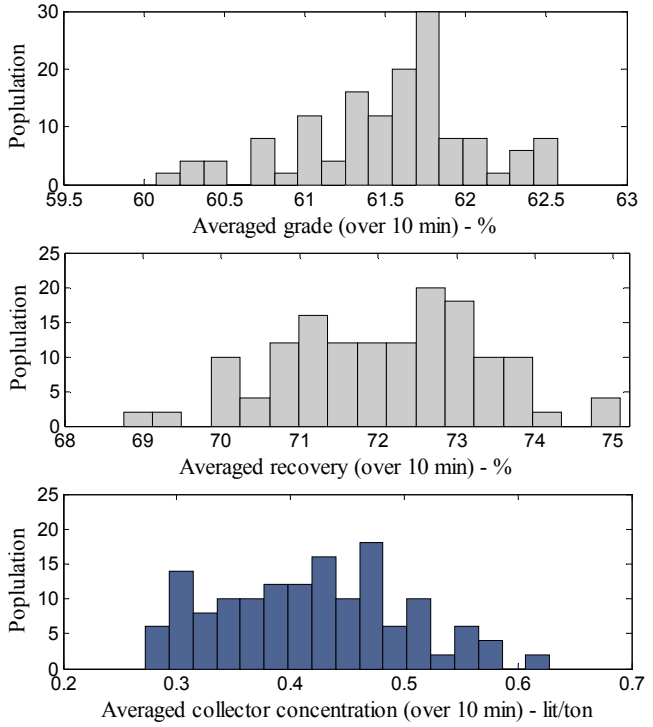

Fig. 8-24: RTO: histogram of controlled and manipulated variables - *Scenario* 3 (with noise & with DR).

For unmeasured feed rate f_1, $\hat{f}_1$ estimated by DR is applied in the control action calculation procedure. But other scenarios have to use nominal value of the feed rate. As a key point in this RTO, on the contrary to the APC, f_1 directly participates in the control action calculation, i.e. in J_{RTO}, and so it can considerably affect the plant closed loop behavior. Table 8-13 illustrates the performance of RTO in different scenarios when the feed rate is not measured and *disturbance* 1 is applied. For the current simulation, since results have the same trend as the previous one, so variable histograms are not presented. As a quick conclusion, having unmeasured variable increases the grade deviation and consequently decreases the economic benefits of RTO. However, estimating the unmeasured variables by DR mostly preserves the RTO performance.

Table 8-13: RTO performance: *disturbance* 1 (feed rate & grade variation with constant liberation and middling grade) and feed rate not measured.

Performance Indices		Scenarios			
		Open loop	No noise	With noise & without DR	With noise & DR
J_{ECO}	Earned mineral [k$]	113.08	111.7	112.05	112.17
	Consumed collector [k$]	-2.42	-1.85	-2.05	-2.00
	Grade penalty [k$]	-22.50	0	-6.50	-2.10
	Total benefit [k$]	88.16	109.85	103.5	108.07
	Δ [%]	-20.0	0	-5.7	-1.6
Manipulated variables statistics	U_c [l/t]	0.5±0.00	0.385±0.07	0.423±0.22	0.419±0.18
Metallurgical performance variables statistics	c [%]	60.54±0.83	61.9±0.38	61.3±0.88	61.6±0.70
	ρ [%]	72.15±2.21	71.8±1.32	72.04±1.74	72.00±1.63
Output variables statistics	R_n [t/h]	1.78±0.10	1.83±0.10	1.82±0.10	1.82±0.10
	C [t/h]	7.78±0.62	7.52±0.19	7.615±0.50	7.56±0.42
	C_n [t/h]	4.71±0.39	4.65±0.11	4.67±0.28	4.67±0.23

8.8.2 Results of applying disturbance 2

The simulation procedure applied in Section 8.8.1 is repeated here when stationary variations occur in the feed rate and grade while the liberation degree and middling grade are not constant, i.e. *disturbance* 2. Again, two simulation cases (measured and unmeasured f_1) are considered, and simulation results are presented in Tables 8-14 and 8-15, respectively. Since obtained results are consistent with the previous ones, any discussion is postponed to the final part of this section.

Table 8-14: RTO performance: *disturbance* 2 (feed rate & grade variation with non-constant liberation and middling grade) and all variables measured.

Performance Indices		Scenarios			
		Open loop	No noise	With noise & without DR	With noise & DR
J_{ECO}	Earned mineral [k$]	112.50	111.14	111.56	111.38
	Consumed collector [k$]	-2.40	-1.93	-2.15	-2.07
	Grade penalty [k$]	-22.11	0.00	-6.07	-2.40
	Total benefit [k$]	87.99	109.21	103.3	106.91
	Δ [%]	-19.4	0.0	-5.5	-2.1
Manipulated variables statistics	U_c [l/t]	0.5±0.00	0.392±0.07	0.435±0.20	0.430±0.16
Metallurgical performance variables statistics	c [%]	60.5±1.32	61.93±0.71	61.35±1.02	61.7±0.81
	ρ [%]	72.3±2.51	71.40±2.30	71.62±2.52	71.55±2.43
Output variables statistics	R_n [t/h]	1.79±0.14	1.85±0.13	1.83±0.14	1.84±0.13
	C [t/h]	7.76±0.76	7.48±0.71	7.57±0.84	7.52±0.81
	C_n [t/h]	4.69±0.54	4.63±0.43	4.65±0.50	4.64±0.48

Table 8-15: RTO performance: *disturbance* 2 (feed rate & grade variation with non-constant liberation and middling grade) and feed rate not measured.

Performance Indices		Scenarios			
		Open loop	No noise	With noise & without DR	With noise & DR
J_{ECO}	Earned mineral [k$]	112.24	111.00	111.32	111.30
	Consumed collector [k$]	-2.37	-1.90	-2.08	-2.06
	Grade penalty [k$]	-22.11	0	-6.91	-2.50
	Total benefit [k$]	87.76	109.10	102.33	106.74
	Δ [%]	-19.6	0	-6.2	-2.2
Manipulated variables statistics	U_c [l/t]	0.5±0.00	0.389±0.10	0.430±0.25	0.429±0.18
Metallurgical performance variables statistics	c [%]	60.5±1.32	61.90±0.72	61.30±1.03	61.68±0.84
	ρ [%]	72.3±2.51	71.38±2.30	71.61±2.52	71.53±2.45
Output variables statistics	R_n [t/h]	1.79±0.14	1.845±0.13	1.835±0.14	1.84±0.13
	C [t/h]	7.76±0.76	7.47±0.72	7.57±0.85	7.52±0.81
	C_n [t/h]	4.69±0.54	4.625±0.44	4.64±0.50	4.64±0.50

8.8.3 Results of applying disturbance 3

Here, the performance of RTO is evaluated when solid percentage of feed is changing, *disturbance* 3. Simulation results for the different scenarios are shown in Tables 8-16 and 8-17 for the measured and unmeasured feed rate, respectively.

Table 8-16: RTO performance: *disturbance* 3 (stationary variation in solid percentage of feed rate) and all variables measured.

Performance Indices		Scenarios			
		Open loop	No noise	With noise & without DR	With noise & DR
J_{ECO}	Earned mineral [k$]	114.18	113.1	113.4	113.3
	Consumed collector [k$]	-2.40	-1.80	-2.06	-2.04
	Grade penalty [k$]	-21.00	0	-6.9	-3.1
	Total benefit [k$]	90.78	111.3	104.44	108.16
	Δ [%]	-18.4	0	-6.2	-2.8
Manipulated variables statistics	U_c [l/t]	0.5±0.00	0.390±0.12	0.437±0.22	0.436±0.18
Metallurgical performance variables statistics	c [%]	60.59±1.21	61.90±0.84	61.30±1.12	61.55±1.02
	ρ [%]	72.6±1.81	71.75±1.30	72.10±1.56	72.00±1.48
Output variables statistics	R_n [t/h]	1.80±0.10	1.85±0.11	1.83±0.12	1.84±0.11
	C [t/h]	7.85±0.71	7.61±0.48	7.72±0.67	7.68±0.60
	C_n [t/h]	4.76±0.43	4.71±0.27	4.73±0.38	4.72±0.34

Table 8-17: RTO performance: *disturbance* 3 (stationary variation in solid percentage of feed rate) and feed rate not measured.

Performance Indices		Scenarios			
		Open loop	No noise	With noise & without DR	With noise & DR
J_{ECO}	Earned mineral [k$]	114.00	112.95	113.3	113.2
	Consumed collector [k$]	-2.37	-1.78	-2.05	-2.00
	Grade penalty [k$]	-21.00	0	-8.30	-3.30
	Total benefit [k$]	90.63	111.17	103.00	107.90
	Δ [%]	-18.5	0	-7.3	-2.9
Manipulated variables statistics	U_c [l/t]	0.5±0.00	0.389±0.12	0.433±0.25	0.435±0.20
Metallurgical performance variables statistics	c [%]	60.59±1.21	61.89±0.84	61.20±1.12	61.52±1.04
	ρ [%]	72.6±1.81	71.73±1.30	72.00±1.56	71.90±1.50
Output variables statistics	R_n [t/h]	1.80±0.10	1.854±0.11	1.84±0.12	1.843±0.11
	C [t/h]	7.85±0.71	7.60±0.48	7.71±0.68	7.67±0.63
	C_n [t/h]	4.76±0.43	4.706±0.27	4.72±0.38	4.717±0.35

8.8.4 RTO: Results analysis and discussion

In this section, first a general conclusion taken from simulation results is presented and then the results are discussed in more details. In the open loop scenario where no RTO is involved, U_c as the manipulated variable is set to 0.5 l/t (i.e. nominal value) regardless of the feed disturbances. For this scenario, in all simulation cases, nominal value of U_c is larger than the optimum value calculated by RTO. It implies that more valuable minerals

are floated and consequently plant recovery is increased. For a constant A_w, which is the case here, it leads to less grade and consequently more grade deviation from c_{con}. Because of this deviation, the economic gain of the scenario has been significantly degraded.

For other simulation scenarios, it can be summarized that measurement noise deteriorates the RTO performance and the plant revenue. More precisely, it increases the variations in the manipulated and output variables and leads to a deviation in the plant grade. Although the valuable mineral flowrate is increased in the presence of noise, the cost associated with the collector consumption and grade deviation also increases at the same time. The major drop in J_{ECO} comes from the grade penalty part. So it would be useful to investigate why the noise causes such deviation in the grade. In the current RTO implementation, since the controller objective function has been defined based on the economic aspects, it only contains one manipulated variable. Therefore, U_C is only responsible to maximize the chalcopyrite production, and, at the same time, it has to keep the grade in the certain range. In other words, there is a strong compromise in J_{RTO}.

In the RTO, the control action severely fluctuates to respond the variation caused by the stationary disturbance in the feed and the noise in the measurements. Consequently, one of the upper or lower bounds of U_C is hit more frequently than another one resulting to an unsymmetrical distribution of variables. This could be caused by the plant nonlinear nature and/or location of the optimal point that may not exactly be in the middle of the range. For instance, Fig. 8-25 illustrates the collector concentration profile when solid percentage disturbance occurs in the feed. As seen, without measurement noise, the lower bound has been hit few times while it has been frequently touched in the presence of noise. This implies that mean value of U_C in the presence of the noise should be larger than optimal one, so more valuable minerals are floated, i.e. more valuable mineral in the cost of larger grade deviation.

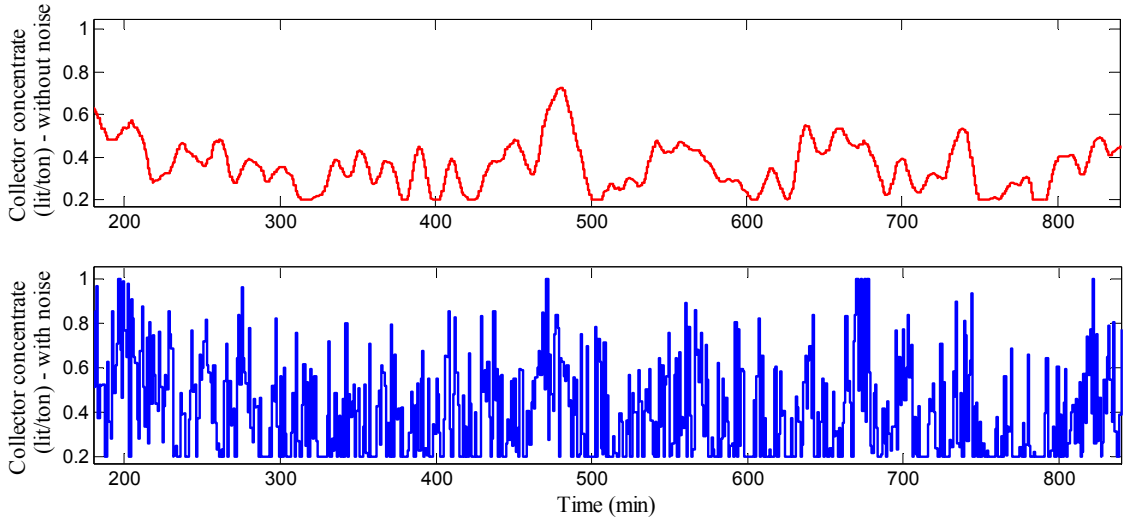

Fig. 8-25: RTO: collector concentrate - without and with measurement noise.

Applying data reconciliation partially removes the measurement noises and so leads to less variations in the collector concentration. Therefore, the lower bound is less touched in comparison to the case without DR leading to a smaller mean value of U_C, and so less deviation in the grade. Obviously, smaller grade deviation causes smaller penalties in J_{ECO}. From a statistical point of view, DR reduces the variance of output variables and improves their distributions.

One question that could raise here is "why measurement noise has a significant impact on the RTO, but not in APC scheme?". In RTO objective function, which is an economic based function, only U_C is used as the manipulated variable because of its associated cost. In fact, in the RTO, U_C is the only variable that makes a balance between the amount of produced chalcopyrite and the grade while for APC there are two manipulated variables. The water addition, that acts as a free variable in J_{APC}, can easily compensate any drop in the grade. In other words, in the APC, the effect of an increase in U_C is compensated by an increase of A_w leading to the compensation of the grade deviation in J_{ECO}.

For unmeasured feed rate, $\hat{f}_1$ is estimated by DR and used in the RTO. Since the redundancy degree is reduced, so the RTO performance is slightly become worse, but not far from full measured case. For the scenarios that have not been coupled with DR,

degradation in the RTO performance is much larger. In these cases, nominal value of f_1 is employed. Since the feed disturbances are stationary, nominal value of feed rate is still a reasonable alternative. This is why degradation in the RTO performance is not huge with and without feed rate measurement. Again, using the estimation of the unmeasured input disturbances for designing a feed-forward controller and updating the process model could emphasize the benefits of the data reconciliation.

8.9 Summary

In this chapter, two advanced process control and real-time optimization schemes based on receding horizon internal model control have been designed. The flotation circuit simulator developed in Chapter 7 has been employed as the benchmark plant. A process model conserving masses has been identified and applied for the control purpose. The APC and RTO performances using step changes in the set-points and plant feed characteristics have been tested. Then they have been coupled with an autocovariance based stationary data reconciliation observer proposed in Chapter 5. To assess the effect of involving DR in closed loop process, several test cases and disturbances have been defined and applied. The APC and RTO performance and economic benefits with and without DR observer have been investigated using the statistical measures and economic gain function.

For the implemented APC, it has been concluded that: a) measurement error increases variations in all variables and marginally reduces the economic revenue, b) applying DR improves the results but the improvements are not significant. In fact, the simulation results have revealed that measurement noise does not have much effect on the APC performance and the plant revenue, and consequently DR cannot bring significant improvement. This slight improvement is far away from what was expected. Many factors are candidate to reduce and eliminate the noise effect in the implemented APC such as: 1) having two manipulated variables so that the second one A_w is costless and can freely compensate the grade drops, 2) short response time of A_w on the grade in comparison with the time duration of economic benefit calculation, 3) the filtering effect of weighting factor of manipulated variables changes $W_{u_{APC}}$ in the controller objective function, and 4) using a

very small sampling time in comparison with the grade averaging and economic benefit calculation durations.

From the simulation results of the developed RTO, it can be summarized that measurement noise deteriorates the RTO performance and the plant revenue. It increases the variations in the manipulated and output variables, and deviation in the concentrate grade. The later one leads to a large decrease in economic revenue of the plant. The deviation in the grade comes from the fact that in the RTO U_C is the only variable that maximizes the chalcopyrite production and, at the same time, it should keep the grade in the certain range showing a strong compromise in J_{RTO}. In the implemented RTO, since A_w is no longer involved, the grade drop cannot be compensated.

As the final conclusion, first it should be noted that the presented results and discussions are case-based, and they cannot be generalized to other control schemes and case-studies. Second, in the implemented APC, data reconciliation and noise filtering techniques did not bring significant improvement. Third, coupling DR with RTO loop here considerably increased the plant revenue. Moreover, the performance of APC and RTO can be improved by designing feed forward controller using feed estimates, and updating process model by reconciled data.

Chapter 9

Thesis Conclusion and Recommendations for Future Work

The aim of this section is to summarize and unify the conclusions presented in each chapter and also give a general conclusion for the thesis. Moreover, it provides suggestions for future work.

9.1 Thesis Conclusion

In mineral and metal processing plants, accurate and reliable process data is crucial for optimum and safe plant operation. Measurements of process variables are always influenced by errors, either random or systematic. Furthermore, unmeasured key variables and inconsistency between the process model and data can cause major problems for auditing, control, and optimization applications. To cope with the situation, data reconciliation is considered as an alternative. Therefore, it has been involved in many applications like process monitoring, plant simulation, process control, and real-time optimization. In mineral processing industries, data reconciliation has been widely applied for production accounting, survey analysis, sensor network design, and fault detection.

Data reconciliation observers are developed based on a trade-off between modeling efforts and estimation precision. More detailed and sophisticated process models provide better estimations than simple models. Obtaining and calibrating such complex models are a challenging task in practice. Meanwhile, characterization of measurements and models errors is another issue that should be carefully addressed. The literature has reported that data reconciliation can improve the performance of advanced process control and real-time optimization loops by attenuating measurement noises and control action variations, estimating unmeasured variables, updating model parameters, and improving the model and

data coherency. But there are limited efforts to show how much data reconciliation is economically beneficial for a given plant. Based on these needs, the following objectives were defined for this thesis:

- Investigating the effect of correctly selecting uncertainty covariance matrices, used for characterizing the modeling and measurement errors, on the data reconciliation performance.
- Developing new dynamic data reconciliation observers based on limited modeling efforts.
- Determining a dynamic model for mineral processing plants to support the implementation of a Kalman filter for data reconciliation purpose.
- Developing a simulator of the mineral processing plants for design and test of data reconciliation observers and process control strategies.
- Coupling data reconciliation observers with advanced process control and real-time optimization schemes, and consequently investigating the benefits of using data reconciliation in closed loop plants.

In the first step, the thesis has presented the importance of correctly tuning the statistical properties of the modeling and measurement uncertainties. Chapter 3 has revealed that neglecting the covariance terms, as a common industrial practice, and also incorrect tuning of variance terms of the uncertainties matrices can deteriorate the observer performance. Using five case-studies taken from mineral and metallurgical industries the following topics have been studied in the chapter:

- The importance of considering the model parameter errors and their correlation terms.
- The impact of taking into account the correlation of the measurement errors.
- The effect of involving process dynamic fluctuations in the data reconciliation procedure.
- Correct tuning of measurement error covariance matrix when constraint linearization is used for the bilinear data reconciliation.
- The impact of uncertainties of variance terms on the data reconciliation performance.

Chapter 3 has concluded that the weighting strategies of the data reconciliation objective function used in commercial packages may result in poor performance of data reconciliation. Regardless of the mass and energy balance calculation applications, a careful analysis of the uncertainty structure is a key factor for data reconciliation success.

As the second step, Chapter 4 has illustrated how steady-state data reconciliation commercial software packages can be adjusted to deal with process dynamics. It proposed three solutions. First, when inventories are measured, a sub-optimal implementation of data reconciliation with dynamic mass/energy conservation methods can be used. In the second technique, plant input variables are pre-filtered for synchronization with other plant variables, in such a way that steady-state reconciliation can be applied. In the third solution, fictitious streams representing the accumulation rate variables are added to the plant network. When the variance of these variables is correctly evaluated, the steady-state implementation leads to the same optimal results as the ones obtained via stationary data reconciliation method.

For dynamic data reconciliation purpose, Chapter 5 has proposed a new observer based on a mass conservation sub-model. The observer uses the autocovariance function of node imbalances as the additional information improving the estimation precision. For evaluation purpose, two simulated benchmark plants operating in a stationary regime have used, and its performance has been compared with sub-model based observers and Kalman filter. The proposed observer has provided more precise estimates than steady-state and standard stationary observers, particularly when the process dynamic regime becomes important compared to measurement errors. Moreover, it has exhibited more robust performance against modeling errors compared to Kalman filter. Although Kalman filter has led to optimal performances when perfectly tuned, it is more sensitive to modeling errors than the proposed observer. It has been concluded that using limited modeling efforts, like involving the node imbalance autocovariance function, can largely improve the estimates precision and makes the observer able to cope with process dynamics.

Many powerful observers have been developed in the literature, but they have not been frequently applied in the mineral processing industries for data reconciliation purpose. These observers need detailed models that are not available or difficult to build in practice. Therefore, Chapter 6 has proposed a procedure to obtain a simple model for a flotation circuit to support the implementation of Kalman filter for dynamic data reconciliation. Simplifying assumptions, empirical first-order transfer functions obtained from the plant topology, nominal operating conditions, and historical data, have been used to build the model. The flotation circuit simulator introduced in Chapter 7 has been applied as a case-study. To obtain the model parameters and corresponding uncertainties, practical guidelines have been provided. Kalman filter performance has been compared with two sub-model based observers using the estimation error reduction index and robustness test. Kalman filter with the empirical model has provided more precise estimates than standard and autocovariance based stationary observers. In the robustness test, sub-model based observers have shown slightly better performance than the implemented Kalman filter. The chapter has concluded that for data reconciliation purpose using dynamic empirical models with correctly tuned uncertainty matrices is extremely beneficial, although these simple models do not represent all dynamic behaviors of complex plants like flotation circuits.

Therefore, doing limited modeling efforts can facilitate the application of advanced observers like Kalman filter in the mineral processing industries.

Chapter 7 has presented a dynamic simulator of flotation circuit for designing and testing data reconciliation observers and process control strategies. This simulator is based on dynamic mass balance equations and empirical relationships. For this purpose, the collection and froth zones have been modeled as a perfect mixer and plug flow reactor. In the collection zone, flotation and entrainment phenomena have been considered. Species return from the froth zone into the collection zone has been also modeled by modifying flotation rate constants. Collector and frother concentrations, collection zone level, and air flowrate were considered as the process manipulated variables. A single cell has been first simulated and tested using different disturbance scenarios. Then a flotation circuit simulator consisting of three cells has been considered and assessed. Based on simulation results, the simulator has demonstrated quite reasonable behavior, compatible with plant behavior. Therefore, the simulator has been applied as a case-study for data reconciliation observer and advanced controller design in Chapters 6 and 8, respectively.

As the last part of the thesis, two advanced process control and real-time optimization schemes based on receding horizon internal model control have been designed. In Chapter 8, the aim was coupling dynamic data reconciliation with the advanced controller and real-time optimizer and illustrating its impact in a closed loop plant. The flotation circuit simulator developed in Chapter 7 has been employed as a case-study. For the controller design, an empirical process model conserving mass has been identified and applied. For advanced controller, a standard quadratic reference tracking objective function has been defined while real-time optimizer has used an economic cost function. Then they have been coupled to autocovariance based stationary observer presented in Chapter 5. To assess the effect of involving data reconciliation in the closed loop plant, several test cases and disturbances have been applied. Performance and economic benefits of advanced control and real-time optimization schemes with and without data reconciliation have been investigated using statistical measures and economic gain function.

For the implemented advanced controller, simulation results revealed that: a) random measurement errors increase variations in all variables and slightly reduces the economic

revenue, b) using data reconciliation improves the results but the improvements are marginal. However, coupling data reconciliation to the control loop could limit variations in the manipulated variables and smooths the plant actuator actions reducing maintenance costs. For the real-time optimization scheme, it has been summarized that measurement noise deteriorates the performance and revenue of the plant. It increases the variations in the manipulated and output variables, and also deviation in the concentrate grade leading to a large decrease in economic revenue of the plant. Involving data reconciliation with the real-time optimization scheme mainly compensates these effects and significantly improves the plant revenue. However, these conclusions are case-based, and they cannot be generalized to other control schemes and case-studies.

As a general summary, the thesis has presented how inappropriate use of steady-state data reconciliation without considering process dynamics and measurement correlation could deteriorate the data quality, and consequently it has provided several recommendations and solutions. Moreover, with minimum modeling efforts, it has proposed a dynamic observer that gives better estimates than other sub-model based observers. To facilitate the implementation of Kalman filter, a guideline has been provided to build a suitable dynamic model for complex flotation circuit plants. As a huge effort, it has developed a phenomena-based simulator that behaves reasonably close to the plant, and it can be easily used for the control and data reconciliation practices. Finally, it has coupled the data reconciliation with advanced process control and real-time optimization schemes to answer the questions about the economic value of using data reconciliation, and it has concluded that data reconciliation brings significant economic revenue in some cases, while the benefits are marginal in other cases depending on the implementation of schemes. As a general statement, the study has revealed that data reconciliation observers with appropriate process models and correctly tuned uncertainty matrices can improve the open and closed loop performance of the plant by: a) estimating the measured and unmeasured process variables, b) increasing data and model coherency, c) attenuating the variations in the output and manipulated variables, and d) consequently increasing the plant profitability.

9.2 Recommendations for Future Work

The following issues should be addressed in future works:

- In Chapter 5, the autocovariance based stationary observer has been developed for linear data reconciliation problem. However, it could be extended to bilinear cases by developing corresponding uncertainty matrices. Moreover, time lags selection procedure for the autocovariance function can be improved by introducing a systematic procedure.

- Chapter 6 has provided a procedure to obtain an empirical model of a flotation circuit for Kalman filter implementation. Proposing such modeling procedures for other mineral processing units like grinding circuits would also be interesting.

- The flotation circuit simulator in Chapter 7 can be improved by involving the bubble size distribution in the modeling and using detailed models for the froth zone.

- The economic evaluation of data reconciliation in closed loop process can be emphasized by applying reconciled data for process model updating and involving plant feed estimates in the controller design, i.e. feed forward controller.

- In Chapter 8, the autocovariance based stationary observer has been coupled with control schemes. Based on obtained model in Chapter 6, Kalman filter can be also involved in the advanced process control and real-time optimization loops.

- Also, a strong study about the impact of sampling time and prediction horizon selection on the final benefits of the plant is recommended.

- It would be interesting to validate the different methods developed in the thesis with industrial data. For instance using plant data for validation of proposed observer, calibration of the simulator, and implementation of Kalman filter.

- Furthermore, proposing a general and systematic procedure for evaluation of data reconciliation integration in the closed loop plant would be a valuable contribution.

- Finally and most importantly, coupling data reconciliation with bias detection techniques is more realistic and extremely beneficial from the technical and economic point of view. Therefore, for any future work in the data reconciliation field, introducing bias detection and identification methods are highly recommended.

References

Abu-el-zeet, Z.H. & Roberts, P.D. (2002), Enhancing Model Predictive Control Using Dynamic Data Reconciliation. *American Institute of Chemical Engineers Journal*, 48, p. 324–333.

Akesson, B.M., Jorgensen, J.B., Poulsen, N.K. & Jorgensen, S.B. (2008) A generalized autocovariance least-squares method for Kalman filter tuning. *Journal of Process Control*, 18, p. 769–779.

Almasy, G.A. & Mah, R.S.H. (1984), Estimation of Measurement Error Variances from Process Data. *Industrial and Engineering Chemistry Research*, 23, p. 779–784.

Almasy, G.A. (1990), Principles of dynamic balancing. *American Institute of Chemical Engineers Journal*, 36, p. 1321–1330.

Arbiter, N. & Harris, C.C. (1962), Flotation kinetics. In: Fuerstenau, D.W. (ed.), Froth Flotation. AIME, New York, p. 215–262.

Bagajewicz M.J. & Jiang Q. (1998), Gross error modeling and detection in plant linear dynamic reconciliation. *Computers and Chemical Engineering*, 22, p. 1789–1809.

Bagajewicz, M.J. & Jiang, Q. (1997), Integral approach to plant linear dynamic reconciliation. *American Institute of Chemical Engineers Journal*, 43, pp. 2546–2558.

Bagajewicz, M.J. & Jiang, Q. (2000), Comparison of steady-state and integral dynamic data reconciliation. *Computers and Chemical Engineering*, 24, p. 2367–2383.

Bagajewicz, M.J. (2010), Smart process plants: Software and hardware solutions for accurate data and profitable operations. McGraw-Hill.

Bai, S. & Thibault, J. (2009), Dynamic data reconciliation. Verlag press.

Bai, S., McLean, D.D. & Thibault, J. (2005b), Enhancing Controller Performance via Dynamic Data Reconciliation, *The Canadian Journal of Chemical Engineering*, 83, p. 515–526.

Bai, S., McLean, D.D. & Thibault, J. (2007). Impact of model structure on the performance of dynamic data reconciliation. *Computers and Chemical Engineering*, 31, p. 127–135.

Bai, S., Thibault, J. & McLean, D.D. (2005a), Closed-Loop Data Reconciliation for the Control of a Binary Distillation Column, *Chemical Engineering Communications*, 192, p. 1444–1467.

Bai, S., Thibault, J. & McLean, D.D. (2006), Dynamic data reconciliation: Alternative to Kalman filter. *Journal of Process Control*, 16, p. 485–498.

Ballantine, C.S. (1968), On the Hadamard product. *Mathematische Zeitschrift*, 106, p. 365–366.

Bascur, O.A. (2000), An interactive dynamic flotation model framework. *In: Proceedings of the XXI International Mineral Processing Congress*, Rome, Italy, p. C8a-21–C8a-31.

Bascur, O.A., & Hebst, J.A. (1982), Dynamic modeling of a flotation cell with a view toward automatic control. *In: Proceedings of XIV International Mineral Processing Congress*, CIM, Toronto, Canada, p. 11.1–11.22.

Basseville, M. & Nikiforov, I.V. (1993), Detection of abrupt changes: theory and application. New Jersey, Prentice-Hall.

Bavdekar,V.A., Deshpande, A.P. & Patwardhan S.C. (2011), Identification of process and measurement noise covariance for state and parameter estimation using extended Kalman filter. *Journal of Process Control*, 21, p. 585–601.

Bazin, C. & Hodouin, D. (2001), Importance of covariance in mass balancing of particle size distribution data. *Minerals Engineering*, 14, p. 851–860.

Bellec, S., Hodouin, D., Bazin, C., & Duchesne, C. (2007), Multi-level data reconciliation – application to a gold ore processing plant. *Proceedings of IFAC MMM07 Symposium*, p. 39–44.

Benqlilou, C. (2004), Data Reconciliation as a Framework for Chemical Processes Optimization and Control, Thesis for the Doctor of Science degree at the Universitat Politècnica de Catalunya.

Bergh, L, & Yianatos, J. (2013), Control of Rougher Flotation Circuits Aided By Industrial Simulator. *Journal of Process Control*, 23, p. 140–147.

Berton A., Hodouin D. (2007), Synchronized Node Imbalances for Fault Detection and Isolation in Plant Networks Involving Material Recirculation. *Computers and Chemical Engineering*, 31, p. 815–832.

Berton, A. & Hodouin, D. (2003), Linear and bilinear fault detection and diagnosis based on mass and energy balance equations. *Control Engineering Practice*, 11, p. 103–113.

Bohrnstedt, G.W. & Goldberger, A.S. (1967), On the exact covariance of products of random variables. *Journal of the American Statistical Association*, 64, p. 1439–1442.

Casali, A., Gonzalez, G., Agusto, H. & Vallebuona, G. (2002), Dynamic simulator of a rougher flotation circuit for a copper sulphide ore. *Minerals Engineering*, 15, p. 253–262.

Chen, J., Bandoni, A. & Romagnoli, J. (1997), Robust estimation of measurements error variance/covariance from process sampling data. *Computers and Chemical Engineering*, 21, p. 593–600.

Crowe, C.M. (1989), Reconciliation of process flowrates by matrix projection II: the nonlinear case. *American Institute of Chemical Engineers Journal*, 32, p. 616–623.

Crowe, C.M. (1996), Formulation of linear data reconciliation using information theory. *Chemical Engineering Science*, 51, p. 3359–3366.

Darouach, M. & Zasadzinski, M. (1991), Data reconciliation in generalized linear dynamic systems. *American Institute of Chemical Engineers Journal*, 37, p. 193–201.

Darouach, M., Ragot, J., Zasadzinski, M. & Krzakala, G. (1989), Maximum likelihood estimator of measurement error variances in data reconciliation. *IFAC Advanced Information Processing in Automatic Control*, Nancy, France, p. 109–112.

Dochain, D. (2003), State and parameter estimation in chemical and biochemical processes: A tutorial. *Journal of Process Control*, 13, p. 801–818.

Dunik, J. & Simandl, M. (2008), Estimation of state and measurement noise covariance matrices by multi-step prediction. *In Proceeding of the 17th IFAC World Congress*, Seoul, Korea, p. 171–176.

Dunik, J., Simandl, M. & Straka, O. (2009), Methods for estimating state and measurement noise covariance matrices: aspects and comparison. *IFAC Symposium on System Identification*, Saint-Malo, France, p. 372–377.

Eldar, Y.C. (2007), Rethinking Biased Estimation: Improving Maximum Likelihood and the Cramér–Rao Bound. *Foundations and Trends in Signal Processing*, 1, p. 305–449.

Faber, R., Li, B., Li, P. & Wozny, G. (2006), Data reconciliation for real-time optimization of an industrial coke-oven-gas purification process, *Simulation Modelling Practice and Theory*, 14, p. 1121–1134.

Finch J. A., Gomez C. O., Hardie C., Leichtle G., Filippone R. & Leroux D. (1999), Bubble Surface Area Flux: a Parameter to Characterise Flotation Cells. *Proceedings of the 31st Canadian Mineral Processors Conference*, Ottawa, Canada, p. 199–210.

Finch, J.A. & Dobby, G.S. (1990), Flotation column. Pergamon Press.

Finch, J.A., Gomez, C.O. & Xiao, J. (2000) Gas dispersion properties: bubble surface area flux and gas holdup. *Minerals Engineering*, 13, p. 365–372.

Finch, J.A., Nesset, J.A. & Acuna, C. (2008), Role of frother on bubble production and behaviour in flotation. *Minerals Engineering*, 21, p. 949–957.

Forbes, J.F., Marlin, T.E. & Yip, W.S. (2006), Real-Time Optimization: Status, Issues, and Opportunities. *Encyclopedia of Chemical Processing*, 12, p. 2585–2598.

Goodman, L.A. (1960), On the exact variance of products. *Journal of the American Statistical Association*, 55, p. 708–713.

Gorain, B.K., Harris, M.C., Franzidis, J.P. & Manlapig, E.V. (1998b), The effect of froth residence time on the kinetics of flotation. *Minerals Engineering*, 11, p. 627–638.

Gorain, B.K., Napier-Munn, T.J., Franzidis, J.P. & Manlapig, E.V. (1998a), Studies on impeller type, impeller speed and air flow rate in an industrial scale flotation cell- part 5: validation of k-S_b relationship and effect of froth depth. *Minerals Engineering*, 11, pp. 615–626.

Gy, P. (1982), Sampling of Particulate Materials Theory and Practice. 2nd edition, Amsterdam: Elsevier.

Hallab, S. (2010), Utilisation de sous-modèles comme filtres utilisés pour la commande et l'optimisation d'un atelier de lixiviation de l'or. Master of Science degree thesis, Université Laval, Québec, Canada.

Harris, C.C. (1978), Multiphase models of flotation machine behaviour. *International Journal of Mineral Processing*, 5, p. 107–129.

Hlavacek, V. (1977), Analysis of a complex plant steady state and transient behavior. *Computers and Chemical Engineering*, 1, p. 75–100.

Hodouin, D. & Flament, F. (1989), New developments in material balance calculations for the mineral processing industry. *Proceedings of the SME annual meeting*, Las Vegas, USA, p. 89–147.

Hodouin, D. & Flament, F. (1991), Influence of data collection and conditioning strategies on the significancy of performance indices in mineral processing plants. *Int. Symp. Evaluation and Optimization of Metallurgical Performance*, Littleton, USA, p. 195–208.

Hodouin, D. & Ketata, C. (1994), Variance of average stream compositions obtained by automatic incremental sampling. *International Journal of Mineral Processing*, 40, p. 199–223.

Hodouin, D. (2010), Process Observers and Data Reconciliation Using Mass and Energy Balance Equations. In: Sbarbaro, D. & del Villar, R. (eds.). Advanced Control and Supervision of Mineral Processing Plants. Springer, p. 15–83.

Hodouin, D. (2011), Methods for automatic control, observation, and optimization in mineral processing plants. *Journal of Process Control*, 21, p. 211–225.

Hodouin, D., Lachance, L., & Desbiens, A. (2007), Dynamic data reconciliation: From the full model observer to the stationary on-line mass conservation filter – The flotation case. *IFAC Symposium on Automation in Mining, Mineral and Metal Processing*, Québec, Canada, p. 87–92.

Hodouin, D., Mirabedini, A., Makni, S. & Bazin, C. (1998), Reconciliation of mineral processing data containing correlated measurement errors. *International Journal of Mineral Processing*, 54, p. 201–215.

Holmes, R.J. (2004), Correct sampling and measurement – the foundation of accurate metallurgical accounting. *Chemometrics and Intelligent Laboratory Systems*, 74, p. 71–83.

Jamsa-Jounela, S.L., & Lattila, T. (1995), A methodology for computer aided process study at mineral processing plants. *Proceedings of Copper '95*, Santiago, Chile, p. 89–98.

Jansky, A. (2006), Financial Benefits of Process Data Reconciliation in Power Generating Plants. *14th International Conference on Nuclear Engineering*, Miami, USA, p. 49–57.

Jansky, A. (2007), Increasing Plant Efficiency and Safety with Online Process Data Reconciliation. *15th International Conference on Nuclear Engineering*, Nagoya, Japan, p. 49–57.

Kalman, R.E. (1960), A new approach to linear filtering and prediction problems. *Journal of Basic Engineering*, 82, p. 35–45.

Kay, S.M. (1993), Fundamentals of Statistical Signal Processing: Estimation Theory. Prentice-Hall.

Keller, J.Y., Zasadzinski, M. & Darouach, M. (1992), Analytical estimator of measurement error variances in data reconciliation. *Computers and Chemical Engineering*, 16, p.185–188.

Kuehn, D.R. & Davidson, H. (1961), Computer control II: mathematics of control. *Chemical Engineering Progress*, 57, p. 44–47.

Lachance, L. (2007), Observation de procédés basée sur des sous-modèles: Applications au traitement et au transport de la matière. Ph.D. Thesis, Université Laval, Québec, Canada.

Lachance, L., Desbiens, A. & Hodouin, D. (2006a), Using sub-models for dynamic data reconciliation. *International Symposium on Advanced Control of Chemical Processes*, Gramado, Brazil, p. 711–716.

Lachance, L., Poulin, É., Hodouin, D. & Desbiens, A. (2006b), Performance of steady-state and stationary data reconciliation as a function of process and disturbance dynamics. *In Mineral process modeling, simulation and control conference*, Sudbury, Canada, p. 393–408.

Lachance, L., Poulin, E., Hodouin, D. & Desbiens, A. (2007), Tuning stationary observers: Application to a flotation unit simulator. *12th IFAC Symposium on Automation in Mining, Mineral and Metal Processing*. p. 357–362.

Madron, F. (1985), A new approach to the identification of gross errors in chemical engineering measurements. *Chemical Engineering Science*, 40, p. 1855–1860.

Mah, R.S.H. (1990), Chemical Process Structures and Information Flows. Butterworth.

Makni, S., Hodouin, D. & Bazin, C. (1995a), A recursive node imbalance method incorporating a model of flowrate dynamics for on-line material balance of complex flowsheets. *Journal of Minerals Engineering*, 8, p. 753–766.

Makni, S., Hodouin, D., & Bazin, C. (1995b), On-line data reconciliation by minimization of a weighted sum of squared residuals and node imbalances. *Proceedings of XIXth international mineral processing congress,* Colorado, USA, p. 233–237.

Maldonado, M.A. (2010), Estimation and control on a laboratory flotation column. Ph.D. Thesis, Université Laval, Québec, Canada.

Manenti, F., Grottoli, M.G. & Pierucci, S. (2011), Online data reconciliation with poor redundancy systems. *Industrial and Engineering Chemistry Research*, 50, p. 14105–14114.

Maronna, R. & Arcas, J. (2009), Data reconciliation and gross error diagnosis based on regression. *Computers and Chemical Engineering*, 33, p. 65–71.

Martini, A., Sorce, A., Traverso, A. & Massardo, A. (2013), Data reconciliation for power systems monitoring: Application to a microturbine-based test rig. *Applied Energy*, 111, p. 1152–1161.

Mazzour, E.H., & Hodouin, D. (2008), Measurement accuracy selection for designing observers of metallurgical plant performances. *Mediterranean Conference on Control and Automation*, Ajaccio-Corsica, France, p. 1478–1483.

Mika, T.S., & Fuerstenau, D.W. (1969), A microscopic model of the flotation process. *Proceedings of the VIII International Mineral Processing Congress*, Leningrad, USSR, p. 246–269.

Miller, R.W. (1983), Flow measurement engineering handbook. McGraw-Hill.

Mirabedini, A. & Hodouin, D. (1998), Calculation of variance and covariance of sampling errors in complex mineral processing systems, using state–space dynamic models. *International Journal of Mineral Processing*, 55, p.1–20.

Mitsas, C. (2010), Data reconciliation and variable classification by null space methods. Measurement, 43, p. 702–707.

Morad, K., Svrcek, W.Y. & McKay, I. (1999), A robust direct approach for calculating measurement error covariance matrix. *Computers and Chemical Engineering*, 23, p. 889–897.

Moreno, R.P. (2010), Steady-State Detection, Data Reconciliation, and Gross Error Detection: Development for Industrial Processes. Master of Science degree Thesis at University of New Brunswick.

Narasimhan, S. & Jordache, C. (2000), Data reconciliation & gross error detection: an intelligent use of process data. Gulf Publisher.

Narasimhan, S. & Shah, S.L. (2008), Model identification and error covariance matrix estimation from noisy data using PCA. *Control Engineering Practices*, 16, p. 146–155.

Narasimhan, S. (2012), Data reconciliation and its application in mineral processing industries. *International Mineral Processing Congress*, New Delhi, India, p. 217–222.

Naysmith, M.R. & Douglas, P. L. (1995), Review of Real Time Optimization in the Chemical Process Industries. *Developments in Chemical Engineering and Mineral Processing*, 3, p. 67–87.

Nesset, J.A., Hernandez, J.R., Acuna, C., Gomez, C.O. & Finch, J.A. (2006), Some gas dispersion characteristics of mechanical flotation machines. *Minerals Engineering*, 19, p. 807–815.

Ofori, P., O'Brien, G., Hapugoda, P. & Firth, B. (2014), Distributed flotation kinetics models – A new implementation approach for coal flotation. *Minerals Engineering*, 66, p. 77–83.

Özyurt, D.B. & Pike, R.W. (2004), Theory and practice of simultaneous data reconciliation and gross error detection for chemical processes. *Computers and Chemical Engineering*, 28, p. 381–402.

Patil G.P. (1995), Composite sampling. *Environmental and Ecological Statistics*, 2, p. 169–179.

Pérez-Correa, R., Gonzalez, G., Casali, A., Cipriano, A., Barrera, R. & Zavala, E. (1998), Dynamic modelling and advanced multivariable control of conventional flotation circuits. *Minerals Engineering*, 11, p. 333–346.

Pietilä, J., Remes, A., Kaartinen, J., Torttila, S., Huuskonen, J., Lähteenmäki, S. & Zenger, K. (2015), On-Line Flotation Simulator at Pyhäsalmi Mine. *47th Annual Canadian Mineral Processors Operators Conference*, Ottawa, Canada, p. 173–184.

Pitard, F.F. (1993), Pierre Gy's sampling theory and sampling practice. CRC Press.

Poulin, É., Hodouin, D. & Lachance, L. (2009), Estimation of measurement error variances in data reconciliation using a flow distribution model. *IFAC System Identification*, Saint-Malo, France.

Poulin, É., Hodouin, D. & Lachance, L. (2010), Impact of plant dynamics on the performance of steady-state data reconciliation. *Computers and Chemical Engineering*, 34, p.354–360.

Puigjaner, L. & Heyen, G. (Eds) (2006), Computer aided process and product engineering. Wiley.

Ramamurthi, Y., Sistu, P.B. & Bequette, B.W. (1993), Control-Relevant Dynamic Data Reconciliation and Parameter Estimation. *Computers and Chemical Engineering*, 17, p. 41–59.

Reimers, C., Werther, J. & Gruhn, G. (2008), Flowsheet Simulation of Solids Processes: Data Reconciliation and Adjustment of Model Parameters. *Chemical Engineering and Processing: Process Intensification*, 47, p. 138–158.

Rollins, D.K. & Devanathan, S. (1993), Unbiased estimation in dynamic data reconciliation. *American Institute of Chemical Engineers Journal*, 39, p. 1330–1334.

Romagnoli, J. & Sanchez, M. (2000), Data Processing and Reconciliation for Chemical Process Operations, Academic Press.

Ruel, J., 2010. Développement de Simulateurs de Procédés Pour la Commande Automatique ET L'optimisation - Approche de Conception Hybride avec Modelica et Matlab/Simulink, Master thesis, Université Laval, Québec, Canada.

Shean, B.J. & Cilliers, J.J. (2011), A review of froth flotation control. *International Journal of Mineral Processing*, 100, p. 57–71.

Song, S., Lopez-Valdiviesco, A., Reyes-Bahena, J.L. & Lara-Valenzuela, C. (2001), Floc flotation of galena and sphalerite fines. *Minerals Engineering,* 14, p. 87–98.

Song, S., Lopez-Valdiviesco, A., Reyes-Bahena, J.L., Bermejo-Perez, R.I. & Trass, O. (2000), Hydrophobic flocculation of galena fines in aqueous suspensions. *Journal of Colloid and Interface Science,* 227, p. 272–281.

Souza, P.N., Soares, M., Amaral, M.M., Lima, E.L. & Pinto, J.C. (2011), Data Reconciliation and Control in Styrene-Butadiene Emulsion Polymerizations. *Macromolecular Symposia, Special Issue: Polymer Reaction Engineering – 10th International Workshop*, 302, p. 80–89.

Stanley, G.M. & Mah, R.S.H. (1977), Estimation of flows and temperatures in process networks. *American Institute of Chemical Engineers Journal*, 23, p. 642–650.

Tamhane, A.C. & Mah R.S.H. (1985), Data reconciliation and gross error detection in chemical process networks. *Technometrics*, 27, p. 409–422.

Tona, R.V., Benqlilou, C., Espuña, A. & Puigjaner, L. (2005), Dynamic data reconciliation based on wavelet trend analysis. *Industrial and Engineering Chemistry Research*, 44, p. 4323–4335.

Vasebi, A., Poulin, É. & Hodouin, D. (2011), Observers for mass and energy balance calculation in metallurgical plants. *IFAC World Congress*, Milan, Italy, p. 9935–9940.

Vasebi, A., Poulin, É. & Hodouin, D. (2012a), Dynamic data reconciliation based on node imbalance autocovariance functions. *Computers and Chemical Engineering*, 43, p. 81–90.

Vasebi, A., Poulin, É. & Hodouin, D. (2012b), Dynamic data reconciliation in mineral and metallurgical plants. *Annual Reviews in Control*, 36, p.235–243.

Vasebi, A., Poulin, É. & Hodouin, D. (2014), Selecting proper uncertainty model for steady–state data reconciliation – Application to mineral and metal processing industries. *Minerals Engineering*, 65, p. 130–144.

Willems, J.L. & Callier, F.M. (1992), Divergence of the stationary Kalman filter for correct and for incorrect noise variances. *IMA Journal of Mathematical Control & Information*, 9, p. 47–54.

Williams, M.C. & Meloy, T.P. (1983), Dynamic model of flotation cell banks – circuit analysis. *International Journal of Mineral Processing*, 10, p. 141–160.

Xu, H. & Rong, G. (2010), A new framework for data reconciliation and measurement bias identification in generalized linear dynamic systems. *American Institute of Chemical Engineers Journal*, 56, p. 1787–1800.

Xu, M., Finch, J. A. & Uribe-Salas, A. (1991), Maximum Gas and Bubble Surface Area Rates in Flotation Columns. *International Journal of Mineral Processing*, 32, p. 233–250.

Yianatos, J., Carrasco, C., Bergh, L., Vinnett, L. & Torres, C. (2012), Modelling and Simulation of Rougher Flotation Circuits. *International Journal of Mineral Processing*, 112, p. 63–70.

Zhang, Y. & Forbes, J.F. (2000), Extended design cost: a performance criterion for real-time optimization systems. *Computers and Chemical Engineering*, 24, p. 1829–1841.

Zhou, Y. & Forbes, J.F. (2003), Determining controller benefits via probabilistic optimization. *International Journal of Adaptive Control and Signal Processing*, 17, p. 553–568.

Appendix A

This section provides complementary information about the case-studies used in Chapter 3.

A.1 Coefficients of energy and mass balance equations presented in Section 3.5.1

This part gives the expressions of the coefficients of the heat balance equation (Eq. 3-18) and mass conservation equations (Eqs. 3-21 to 3-24) discussed in Section 3.5.1. The following equations give the heat balance coefficients:

$$e_1 = \Delta H_g(T_r) + T_r(\overline{C}_g - \overline{C}_{ch} + \overline{C}_o) \tag{A-1}$$

$$e_2 = -\overline{C}_g \tag{A-2}$$

$$e_3 = \overline{C}_{ch} - \gamma \overline{C}'_o \tag{A-3}$$

$$e_4 = -\overline{C}_o + \gamma \overline{C}'_o \tag{A-4}$$

$$e_5 = \overline{C}_a \tag{A.5}$$

$$e_6 = -\overline{C}_a \tag{A-6}$$

$$e_7 = -\overline{C}'_o \tag{A-7}$$

$$e_8 = \overline{C}'_o \tag{A-8}$$

where $\Delta H_g(T_r)$ is the combustion enthalpy (Jg^{-1}) of the fuel gas at the reference temperature T_r, and γ is the mass of oxygen consumed per unit mass of fuel. At the nominal operating regime, the averaged mass specific heats $\overline{C}$ ($\mathrm{Jg}^{-1}\mathrm{K}^{-1}$) are calculated using integration in the selected temperature period. They are defined as:

- $\overline{C}_g$: averaged mass specific heat for fuel gas in the temperature range of T_g to T_r
- $\overline{C}_o$: averaged mass specific heat for oxygen in the temperature range of T_o to T_r

- $\overline{C}_o'$: averaged mass specific heat for oxygen in the temperature range of T_o to T
- $\overline{C}_a$: averaged mass specific heat for the air in the temperature range of T_a to T
- $\overline{C}_{ch}$: averaged mass specific heat for the combustion products (CO_2 and H_2O) in the temperature range of T_r to T.

The m_i coefficients in mass conservation Eqs. 3-21 to 3-24 have the following definitions, and are calculated for the nominal regime of operation.

- m_1: mass of water produced per unit mass of fuel gas combustion
- m_2: mass of carbon dioxide produced per unit mass of fuel gas combustion
- m_3: mass fraction of oxygen in the air
- m_4: mass of oxygen consumed per unit mass of fuel gas combustion
- m_5: mass fraction of nitrogen in the air

A.2 Measurements correlation matrix applied in Section 3.5.2

The correlation r_v among measured variables in the hydrocyclone case-study II (Section 3.5.2) is presented below.

$$r_v = \begin{array}{c} \begin{matrix} f_1 & f_2 & f_3 & f_4 & f_5 & u_1 & u_2 & u_3 & u_4 & u_5 & o_1 & o_2 & o_3 & o_4 & o_5 \end{matrix} \\ \begin{bmatrix} 1.00 & -0.23 & 0.03 & -0.04 & 0.00 & 0.01 & 0.02 & 0.00 & -0.02 & -0.01 & -0.01 & 0.01 & 0.00 & -0.01 & 0.01 \\ -0.23 & 1.00 & -0.59 & -0.02 & 0.01 & 0.00 & -0.03 & 0.04 & -0.03 & 0.03 & 0.01 & 0.00 & 0.00 & 0.03 & -0.04 \\ 0.03 & -0.59 & 1.00 & -0.63 & -0.02 & 0.02 & 0.02 & -0.05 & 0.04 & 0.01 & 0.00 & 0.00 & -0.01 & 0.01 & -0.01 \\ -0.04 & -0.02 & -0.63 & 1.00 & -0.58 & -0.04 & 0.00 & 0.03 & -0.01 & -0.02 & 0.02 & 0.03 & -0.01 & -0.02 & -0.01 \\ 0.00 & 0.01 & -0.02 & -0.58 & 1.00 & 0.03 & -0.01 & 0.00 & 0.01 & -0.04 & -0.05 & -0.03 & 0.03 & -0.03 & 0.03 \\ 0.01 & 0.00 & 0.02 & -0.04 & 0.03 & 1.00 & -0.30 & 0.01 & 0.02 & -0.02 & 0.03 & 0.00 & 0.01 & 0.00 & -0.01 \\ 0.02 & -0.03 & 0.02 & 0.00 & -0.01 & -0.30 & 1.00 & -0.67 & -0.01 & -0.03 & 0.00 & 0.00 & -0.03 & 0.00 & 0.02 \\ 0.00 & 0.04 & -0.05 & 0.03 & 0.00 & 0.01 & -0.67 & 1.00 & -0.67 & 0.05 & 0.01 & 0.01 & 0.02 & -0.01 & -0.01 \\ -0.02 & -0.03 & 0.04 & -0.01 & 0.01 & 0.02 & -0.01 & -0.67 & 1.00 & -0.39 & -0.01 & -0.02 & -0.01 & 0.03 & -0.02 \\ -0.01 & 0.03 & 0.01 & -0.02 & -0.04 & -0.02 & -0.03 & 0.05 & -0.39 & 1.00 & -0.02 & 0.02 & 0.03 & -0.04 & 0.02 \\ -0.01 & 0.01 & 0.00 & 0.02 & -0.03 & 0.03 & 0.00 & 0.01 & -0.01 & -0.02 & 1.00 & -0.09 & 0.02 & 0.03 & -0.05 \\ 0.01 & 0.00 & 0.00 & 0.03 & -0.05 & 0.00 & 0.00 & 0.01 & -0.02 & 0.02 & -0.09 & 1.00 & -0.43 & 0.02 & -0.03 \\ 0.00 & 0.00 & -0.01 & -0.01 & 0.03 & 0.01 & -0.03 & 0.02 & -0.01 & 0.03 & 0.02 & -0.43 & 1.00 & -0.52 & -0.04 \\ -0.01 & 0.03 & 0.01 & -0.02 & -0.03 & 0.00 & 0.00 & -0.01 & 0.03 & -0.04 & 0.03 & 0.02 & -0.52 & 1.00 & -0.79 \\ 0.01 & -0.04 & -0.04 & -0.01 & 0.03 & -0.01 & 0.02 & -0.01 & -0.02 & 0.02 & -0.05 & -0.03 & -0.04 & -0.79 & 1.00 \end{bmatrix} \end{array} \quad \text{(A-9)}$$

A.3 Uncertainty covariance matrix calculation for the variable change technique (Section 3.5.4)

This section presents how to calculate the covariance matrix of the pseudo-measurements Y used in the variable change technique for linearizing the constraints of a data reconciliation problem. As discussed in Section 3.5.4, in bilinear data reconciliation context, the state vector contains ore flowrates F and concentrations z. Assuming steady-state regime implies that V is diagonal in this case. After the variable change, the state vector and its measured values contains F and component flowrates $N = F \circ z$. As a consequence of the presence of F in all the measured values, the new measurement covariance matrix V_N inherently has off-diagonal terms. For a given plant with m streams and n species, V_N has four main parts:

- Measurement noise variance of F_i that is known ($\sigma^2_{F_i}$), where i is stream index.
- Variance of measurement noise of component flowrate $N_{i,j} = F_i \times z_{i,j}$,

$$\sigma^2_{N_{i,j}} = \left(\bar{z}_{i,j}\right)^2 \times \sigma^2_{F_i} + \left(\overline{F_i}\right)^2 \times \sigma^2_{z_{i,j}} + \sigma^2_{F_i} \times \sigma^2_{z_{i,j}} \tag{A-10}$$

  where $\bar{z}_{i,j}$ and $\overline{F_i}$ are mean value of concentration and ore flowrate, and $\sigma^2_{z_{i,j}}$ represents the concentration measurement error variance.

- Covariance between component flowrate measurement noise and corresponding flowrate measurement error,

$$\mathrm{cov}(F_i, N_{i,j}) = \left(\bar{z}_{i,j}\right) \times \sigma^2_{F_i} \tag{A-11}$$

- Covariance between measurement errors of two component flowrates with shared ore flowrate,

$$\mathrm{cov}(N_{i,k}, N_{i,j}) = \left(\bar{z}_{i,k}\right) \times \left(\bar{z}_{i,j}\right) \times \sigma^2_{F_i} \tag{A-12}$$

Appendix B

This appendix shows the mathematical calculations used in Chapter 5 to build Autocovariance Based Stationary (ABS) observer, and it consists of four parts. Each one proves an expression or a property of the ABS observer.

B.1 State estimation equation

The optimization criterion for the ABS observer is expressed as:

$$J(k) = \left(\underline{y}(k) - \underline{C}^f \underline{x}^f(k) \right)^T \underline{\Sigma}_v^{-1} \left(\underline{y}(k) - \underline{C}^f \underline{x}^f(k) \right) + \underline{\varepsilon}^T(k) \underline{\Sigma}_\varepsilon^{-1} \underline{\varepsilon}(k) \tag{B-1}$$

The derivative of $J(k)$ with respect to $\underline{x}^f(k)$ is

$$\frac{dJ(k)}{dx^f(k)} = \left(-2(\underline{C}^f)^T \underline{\Sigma}_v^{-1} \left(\underline{y}(k) - \underline{C}^f \underline{x}^f(k) \right) + 2\underline{M}^T \underline{\Sigma}_\varepsilon^{-1} (\underline{M}\, \underline{x}^f(k)) \right) \tag{B-2}$$

Setting Eq. B-2 equal to zero, the estimation expression is obtained as:

$$\hat{\underline{x}}^f(k) = \left((\underline{C}^f)^T \underline{\Sigma}_v^{-1} \underline{C}^f + \underline{M}^T \underline{\Sigma}_\varepsilon^{-1} \underline{M} \right)^{-1} (\underline{C}^f)^T \underline{\Sigma}_v^{-1} \underline{y}(k) \tag{B-3}$$

Additional manipulations lead to:

$$\hat{\underline{x}}^f(k) = \left(\underline{\alpha} - \underline{\alpha}\, \underline{M}^T (\underline{\Sigma}_\varepsilon + \underline{M}\, \underline{\alpha}\, \underline{M}^T)^{-1} \underline{M}\, \underline{\alpha} \right) (\underline{C}^f)^T \underline{\Sigma}_v^{-1}\, \underline{y}(k) \tag{B-4}$$

where

$$\underline{\alpha} = \left((\underline{C}^f)^T \underline{\Sigma}_v^{-1} \underline{C}^f \right)^{-1} \tag{B-5}$$

B.2 Confirmation that the solution corresponds to a minimum

To confirm that the solution given by Eq. B-4 is a minimum, the second derivative of the criterion expressed by Eq. B-1 must be positive-definite. It is given by:

$$\frac{d^2 J(k)}{d(x^f(k))^2} = \left((\underline{C}^f)^T \underline{\Sigma}_v^{-1} \underline{C}^f + \underline{M}^T \underline{\Sigma}_\varepsilon^{-1} \underline{M}\right) \tag{B-6}$$

Since matrices $\underline{\Sigma}_v^{-1}$ and $\underline{\Sigma}_\varepsilon^{-1}$ are positive-definite, the first and second quadratic forms of Eq. B-6 are positive-definite. Consequently, the second derivative of the criterion is positive-definite.

B.3 Proof that the estimate is not biased

For this purpose, the mathematical expectation of estimates must be equal to the true process states. The expected value of the estimate is:

$$\begin{aligned} E\left\{\underline{\hat{x}}^f(k)\right\} &= E\left\{\left((\underline{C}^f)^T \underline{\Sigma}_v^{-1} \underline{C}^f + \underline{M}^T \underline{\Sigma}_\varepsilon^{-1} \underline{M}\right)^{-1} (\underline{C}^f)^T \underline{\Sigma}_v^{-1} \underline{y}(k)\right\} \\ &= \left(\left((\underline{C}^f)^T \underline{\Sigma}_v^{-1} \underline{C}^f + \underline{M}^T \underline{\Sigma}_\varepsilon^{-1} \underline{M}\right)^{-1} (\underline{C}^f)^T \underline{\Sigma}_v^{-1}\right)\left(\underline{C}^f E\left\{\underline{x}^f(k)\right\} + E\left\{\underline{v}(k)\right\}\right) \end{aligned} \tag{B-7}$$

By using measurement error properties and after mathematical manipulations, Eq. B-7 becomes:

$$E\left\{\underline{\hat{x}}^f(k)\right\} = \left\{\left(\underline{\alpha} - \underline{\alpha}\underline{M}^T (\underline{\Sigma}_\varepsilon + \underline{M}\underline{\alpha}\underline{M}^T)^{-1} \underline{M}\,\underline{\alpha}\right) \times \underline{\alpha}^{-1}\right\} \times E\left\{\underline{x}^f(k)\right\} \tag{B-8}$$

Using the definition of node imbalances given by Eq. 5-15 gives:

$$E\left\{\underline{\hat{x}}^f(k)\right\} = E\left\{\underline{x}^f(k)\right\} - \underline{\alpha}\,\underline{M}^T (\underline{\Sigma}_\varepsilon + \underline{M}\,\underline{\alpha}\,\underline{M}^T)^{-1} \times E\left\{\underline{\varepsilon}(k)\right\} \tag{B-9}$$

Finally,

$$E\left\{\underline{\hat{x}}^f(k)\right\} = E\left\{\underline{x}^f(k)\right\} = \underline{x}^f(k) \tag{B-10}$$

B.4 Covariance matrix of the estimation error

The estimation error can be expressed as:

$$\begin{aligned}\underline{\hat{x}}^f(k)-\underline{x}^f(k) &= \left(\underline{\alpha}-\underline{\alpha}\,\underline{M}^T(\underline{\Sigma}_\varepsilon+\underline{M}\,\underline{\alpha}\,\underline{M}^T)^{-1}\underline{M}\,\underline{\alpha}\right)(\underline{C}^f)^T\underline{\Sigma}_v^{-1}\,\underline{y}(k)-\underline{x}^f(k)\\ &= \left(\underline{\alpha}\,\underline{M}^T(\underline{\Sigma}_\varepsilon+\underline{M}\,\underline{\alpha}\,\underline{M}^T)^{-1}\right)\underline{M}\,\underline{x}^f(k)+\left(I-\underline{\alpha}\,\underline{M}^T(\underline{\Sigma}_\varepsilon+\underline{M}\,\underline{\alpha}\,\underline{M}^T)^{-1}\underline{M}\right)\underline{\alpha}\,(\underline{C}^f)^T\underline{\Sigma}_v^{-1}\underline{v}(k)\end{aligned} \tag{B-11}$$

The covariance of estimation error is given by

$$\operatorname{cov}\left(\underline{\hat{x}}^f(k)-\underline{x}^f(k)\right)=\left\{\begin{array}{l}\left(-\underline{\alpha}\,\underline{M}^T(\underline{\Sigma}_\varepsilon+\underline{M}\,\underline{\alpha}\,\underline{M}^T)^{-1}\right)\underline{\Sigma}_\varepsilon\left(-\underline{\alpha}\,\underline{M}^T(\underline{\Sigma}_\varepsilon+\underline{M}\,\underline{\alpha}\,\underline{M}^T)^{-1}\right)^T\\ +\left(I-\underline{\alpha}\,\underline{M}^T(\underline{\Sigma}_\varepsilon+\underline{M}\,\underline{\alpha}\,\underline{M}^T)^{-1}\underline{M}\right)\underline{\alpha}\left(I-\underline{\alpha}\,\underline{M}^T(\underline{\Sigma}_\varepsilon+\underline{M}\,\underline{\alpha}\,\underline{M}^T)^{-1}\underline{M}\right)^T\end{array}\right\} \tag{B-12}$$

Finally, after some algebraic manipulations, the covariance matrix of the estimation error is obtained as:

$$\operatorname{cov}\left(\underline{\hat{x}}^f(k)-\underline{x}^f(k)\right)=\underline{\alpha}-\underline{\alpha}\,\underline{M}^T(\underline{\Sigma}_\varepsilon+\underline{M}\,\underline{\alpha}\,\underline{M}^T)^{-1}\underline{M}\,\underline{\alpha} \tag{B-13}$$